

---

# Resolution of the Direct Containment Heating Issue for All Westinghouse Plants With Large Dry Containments or Subatmospheric Containments

---

Prepared by  
M. M. Pilch, M. D. Allen, E. W. Klamerus

**Sandia National Laboratories**  
Operated by  
Sandia Corporation

Prepared for  
U.S. Nuclear Regulatory Commission

9603260307 960229  
PDR NUREG  
CR-6338 R PDR

DFD<sup>D</sup>/<sub>1</sub>

## AVAILABILITY NOTICE

### Availability of Reference Materials Cited in NRC Publications

Most documents cited in NRC publications will be available from one of the following sources:

1. The NRC Public Document Room, 2120 L Street, NW., Lower Level, Washington, DC 20555-0001
2. The Superintendent of Documents, U. S. Government Printing Office, P. O. Box 37082, Washington, DC 20402-9328
3. The National Technical Information Service, Springfield, VA 22161-0002

Although the listing that follows represents the majority of documents cited in NRC publications, it is not intended to be exhaustive.

Referenced documents available for inspection and copying for a fee from the NRC Public Document Room include NRC correspondence and internal NRC memoranda; NRC bulletins, circulars, information notices, inspection and investigation notices; licensee event reports; vendor reports and correspondence; Commission papers; and applicant and licensee documents and correspondence.

The following documents in the NUREG series are available for purchase from the Government Printing Office: formal NRC staff and contractor reports, NRC-sponsored conference proceedings, international agreement reports, grantee reports, and NRC booklets and brochures. Also available are regulatory guides, NRC regulations in the *Code of Federal Regulations*, and *Nuclear Regulatory Commission Issuances*.

Documents available from the National Technical Information Service include NUREG-series reports and technical reports prepared by other Federal agencies and reports prepared by the Atomic Energy Commission forerunner agency to the Nuclear Regulatory Commission.

Documents available from public and special technical libraries include all open literature items, such as books, journal articles, and transactions. *Federal Register* notices, Federal and State legislation, and congressional reports can usually be obtained from these libraries.

Documents such as theses, dissertations, foreign reports and translations, and non-NRC conference proceedings are available for purchase from the organization sponsoring the publication cited.

Single copies of NRC draft reports are available free, to the extent of supply, upon written request to the Office of Administration, Distribution and Mail Services Section, U. S. Nuclear Regulatory Commission, Washington, DC 20555-0001.

Copies of industry codes and standards used in a substantive manner in the NRC regulatory process are maintained at the NRC Library, Two White Flint North, 11545 Rockville Pike, Rockville, MD 20852-2738, for use by the public. Codes and standards are usually copyrighted and may be purchased from the originating organization or, if they are American National Standards, from the American National Standards Institute, 1430 Broadway, New York, NY 10018-3308.

## DISCLAIMER NOTICE

This report was prepared as an account of work sponsored by an agency of the United States Government. Neither the United States Government nor any agency thereof, nor any of their employees, makes any warranty, expressed or implied, or assumes any legal liability or responsibility for any third party's use, or the results of such use, of any information, apparatus, product, or process disclosed in this report, or represents that its use by such third party would not infringe privately owned rights.



---

---

# Resolution of the Direct Containment Heating Issue for All Westinghouse Plants With Large Dry Containments or Subatmospheric Containments

---

---

Manuscript Completed: January 1996  
Date Published: February 1996

Prepared by  
M. M. Pilch, M. D. Allen, E. W. Klamerus

Sandia National Laboratories  
Albuquerque, NM 87185

R. Y. Lee, NRC Project Manager

Prepared for  
Division of Systems Technology  
Office of Nuclear Regulatory Research  
U.S. Nuclear Regulatory Commission  
Washington, DC 20555-0001  
NRC Job Code J6027

## ABSTRACT

This report uses the scenarios described in NUREG/CR-6075 and NUREG/CR-6075, Supplement 1, to address the direct containment heating (DCH) issue for all Westinghouse plants with large dry or subatmospheric containments. DCH is considered resolved if the conditional containment failure probability (CCFP) is less than 0.1. Loads versus strength evaluations of the CCFP were performed for each plant using plant-specific information. The DCH issue is considered resolved for a plant if a screening phase results in a CCFP less than 0.01, which is more stringent than the overall success criterion. If the screening phase CCFP for a plant is greater than 0.01, then refined containment loads evaluations must be performed and/or the probability of high pressure at vessel breach must be analyzed. These analyses could be used separately or could be integrated together to recalculate the CCFP for an individual plant to reduce the CCFP to meet the overall success criterion of less than 0.1. The CCFPs for all of the Westinghouse plants with dry containments were less than 0.01 at the screening phase, and thus, the DCH issue is resolved for these plants based on containment loads alone. No additional analyses are required.

## CONTENTS

	<u>Page</u>
Abstract .....	iii
Preface .....	xiii
Acknowledgments .....	xv
Acronyms.....	xvii
Executive Summary.....	xix
1.0 Introduction.....	1
2.0 Resolution Methodology.....	5
3.0 Probabilistic Framework.....	10
3.1 Nomenclature .....	11
4.0 Quantification of Initial Conditions.....	14
4.1 Introduction.....	14
4.2 Splinter Scenarios .....	15
4.3 Summary of SCDAP/RELAP5 and CONTAIN Insights.....	17
4.4 Definition of Probability Levels .....	21
4.5 TCE/LHS Summary Quantifications.....	22
4.6 Scenario V - SBLOCA with Repressurization of the RCS by Operator Intervention .....	22
4.7 Scenario VI - SBLOCA under Wet Core Conditions.....	27
4.8 Nomenclature .....	29
5.0 Quantification of the DCH Phenomena.....	43
5.1 Nomenclature .....	52
6.0 Quantification of Containment Fragility.....	63
7.0 Results and Sensitivities.....	67
8.0 Conclusions and Recommendations .....	79
9.0 References.....	81

CONTENTS (concluded)

Page

Appendix A Peer Review of NUREG/CR-6338.....	A-1
Appendix B Melt Mass/Composition Distributions.....	B-1
Appendix C Plant Geometry.....	C-1
Appendix D Catalog of IPE Containment Fragility Curves for Operating Pressurized Water Reactors (PWRs).....	D-1

## LIST OF FIGURES

<u>Figure</u>		<u>Page</u>
2.1	Methodology for resolution of the DCH issue for all PWRs.....	9
3.1	The probabilistic framework for containment failure under direct containment heating scenarios.....	12
3.2	Illustration of the probabilistic framework in terms of schematic depiction of its components.....	13
4.1	Splinter DCH scenarios used in NUREG/CR-6075.....	36
4.2	Splinter DCH scenarios reflecting working group recommendations.....	37
4.3	Distribution for fraction of Zr oxidized (core-wide) in Scenarios V and VI.....	38
4.4	Crucible formation in a flooded RPV - Scenario V and Va.....	39
4.5	Distribution of molten UO <sub>2</sub> in the lower plenum at the time of vessel rupture for Scenarios V and Va.....	40
4.6	Crucible formation in wet core scenarios with partial operator intervention- Scenarios VI and VIa.....	41
4.7	Distribution for molten UO <sub>2</sub> in the lower plenum at the time of vessel rupture for Scenarios VI and VIa.....	42
5.1	Validation of the two-cell equilibrium model against all experiments with compartmentalized geometry.....	59
5.2	Potential impact of codispersed water on DCH loads.....	60
5.3	Validation of the coherence ratio for scenarios without coejected water.....	61
5.4	Validation of the hole ablation model.....	62
B.1	Crucible formation in a flooded RPV for Scenario V and Va.....	B-15
B.2	Distribution for molten UO <sub>2</sub> mass at the time of melt relocation to the lower plenum for Scenarios V and Va.....	B-16
B.3	Distribution for molten UO <sub>2</sub> mass at the time of vessel breach for Scenarios V and Va.....	B-17



## LIST OF FIGURES (continued)

<u>Figure</u>	<u>Page</u>
B.4	Crucible formation in wet core scenarios with partial operator intervention- Scenario VI.....B-18
B.5	Distribution for molten UO <sub>2</sub> mass at the time of melt relocation to the lower plenum for Scenario VI.....B-19
B.6	Distribution of molten UO <sub>2</sub> mass at the time of vessel breach for Scenario VI.....B-20
C.1	Schematic drawings of the IDCOR cavity groups.....C-40
C.2	Schematic drawing of all Westinghouse cavities (excluding plants with ice condenser containments).....C-43
C.3	Reactor cavity and lower compartments of South Texas 1 and 2 .....C-48
D.1	Comparison of steel containment fragility curves (non-Ice Condenser type) .....D-31
D.2	Comparison of steel containment fragility curves (Ice Condenser type).....D-32
D.3	Comparison of normalized steel containment fragility curves .....D-33
D.4	Comparison of reinforced concrete containment fragility curves (higher pressure).....D-34
D.5	Seabrook containment fragility curve.....D-35
D.6	Comparison of reinforced concrete containment fragility curves (medium pressure).....D-36
D.7	Comparison of reinforced concrete containment fragility curves (lower pressure).....D-37
D.8	Comparison of reinforced concrete containment fragility curves (Ice Condenser type) .....D-38
D.9	Comparison of normalized reinforced concrete containment fragility curves (larger) .....D-39
D.10	Comparison of normalized reinforced concrete containment fragility curves (smaller) .....D-40
D.11	Comparison of prestressed concrete containment fragility curves (higher pressure, larger).....D-41
D.12	Comparison of prestressed concrete containment fragility curves (higher pressure, smaller) .....D-42

## LIST OF FIGURES (concluded)

<u>Figure</u>		<u>Page</u>
D.13	Comparison of prestressed concrete containment fragility curves (medium pressure) .....	D-43
D.14	Comparison of prestressed concrete containment fragility curves (lower pressure).....	D-44
D.15	Comparison of normalized prestressed concrete containment fragility curves (larger).....	D-45
D.16	Comparison of normalized prestressed concrete containment fragility curves (medium) ...	D-46
D.17	Comparison of normalized prestressed concrete containment fragility curves (smaller)....	D-47

## LIST OF TABLES

<u>Table</u>	<u>Page</u>
4.1 Definition of probability levels.....	30
4.2 Description of TCE/LHS summary quantifications.....	31
4.3 Summary of TCE/LHS input .....	33
5.1 Survey of DCH-relevant experiments .....	54
5.2 Quantification of the coherence ratio .....	56
5.3 Applicability of the database to reactors.....	57
5.4 Validation of melt retention by freezing during cavity dispersal .....	58
6.1 Similarity of containment fragility .....	66
7.1 CCFP results .....	70
7.2 Loads-to-strength results for Scenario V .....	71
7.3 Loads-to-strength results for Scenario Va .....	72
7.4 Loads-to-strength results for Scenario VI.....	73
7.5 Loads-to-strength results for Scenario VIa.....	74
7.6 Safety margin results for Scenario V.....	75
7.7 Safety margin results for Scenario Va.....	76
7.8 Safety margin results for Scenario VI .....	77
7.9 Safety margin results for Scenario VIa.....	78
B.1 Calculation of UO <sub>2</sub> melt relocation for Scenarios V and Va .....	B-7
B.2 Distribution for molten UO <sub>2</sub> mass at the time of melt relocation to the lower plenum for Scenarios V and Va.....	B-8
B.3 Distribution for molten UO <sub>2</sub> mass at the time of vessel breach for Scenarios V and Va .....	B-9

## LIST OF TABLES (concluded)

<u>Table</u>	<u>Page</u>
B.4	Calculation of UO <sub>2</sub> melt relocation for Scenario VI.....B-10
B.5	Distribution for molten UO <sub>2</sub> mass at the time of melt relocation to the lower plenum for Scenarios VI and VIa .....B-11
B.6	Distribution of molten UO <sub>2</sub> mass at the time of vessel breach for Scenarios VI and VIa .....B-12
B.7	Comparison with prior work for Zion.....B-13
B.8	Comparison with prior work for Surry .....B-13
B.9	Comparison with prior work for ANO-2 .....B-14
B.10	Comparison with prior work for Calvert Cliffs .....B-14
C.1.	Cavity dispersal summary for Westinghouse plants.....C-36
C.2.	Validation of melt retention by freezing during cavity dispersal .....C-37
C.3.	Input for coherence ratio correlation.....C-37
C.4.	Cavity water summary for Westinghouse plants .....C-38
C.5	Dome transport comparison table.....C-39
D.1	Comparison of PWR containments.....D-17
D.2	Cumulative containment failure probabilities.....D-19

## PREFACE

The direct containment heating (DCH) issue has been identified in the Nuclear Regulatory Commission's (NRC) Revised Severe Accident Research Plan as a important issue for resolution because of its potential for early containment failure. The NRC has asked Sandia National Laboratories (SNL) to develop the methodology to resolve the DCH issue for all Pressurized Water Reactors (PWRs). NUREG/CR-6075 and NUREG/CR-6075, Supplement 1, were the first steps in this process. They addressed the DCH issue for the Zion nuclear power plant (NPP) by performing loads versus strength evaluations to calculate the conditional containment failure probability (CCFP) for Zion. No intersections of the loads and strength distributions were predicted, and thus, the DCH issue for Zion was resolved. In addition, these reports established the methodology and conditions that would be used in future efforts, e.g., the enveloping accident scenarios (splinters) that would be analyzed, the initial conditions, the model to predict loads, the use of fragility curves from the IPEs, and the probabilistic framework that would be used to compute the loads distribution and the conditional containment failure probabilities, i.e., the TCE/LHS code.

NUREG/CR-6109 used the methodology and scenarios described in NUREG/CR-6075 and its supplement to address the DCH for the Surry NPP. There were no intersections of the loads and strength distributions for Surry, and thus, the DCH issue was resolved based on containment loads alone. However, the likelihood of high reactor coolant system pressure at vessel breach was also evaluated for Surry and was shown to be low for all station blackout scenarios without operator intervention. This probability could have been factored into the CCFP if there had been intersections of the loads and strength distributions.

NRC's plan for resolving the direct containment heating (DCH) issue for Pressurized Water Reactors (PWRs) is to address groups of plants in separate reports. This report, NUREG/CR-6338, addresses the DCH issue for all Westinghouse plants with large dry or subatmospheric containments (a total of 41 plants) using the methodology and assumptions consistent with those developed in NUREG/CR-6075 and NUREG/CR-6075, Supplement 1, for the Zion NPP. In addition, the NRC has asked Sandia to prepare reports for three other groups of plants: Westinghouse plants with ice condenser containments, Combustion Engineering plants, and Babcock & Wilcox plants. The purpose of these reports is to apply the extrapolation methodology described in this report to these other plant types to provide a technically defensible resolution for all PWRs.



## ACKNOWLEDGMENTS

The authors would like to thank J.E. Kelly, K.D. Bergeron, F.T. Harper, A.L. Camp, M.P. Bohn, and D.C. Williams for their contributions in the development of the DCH issue resolution process. C.M. Erickson and A.W. Reed developed the software to allow the TCE/LHS code to run multiple plant evaluations. T.K. Blanchat and T.D. Brown reviewed the report, providing numerous helpful comments. R. Hickman (Ktech) gathered most of the plant-specific data given in Appendix C from FSARs and IPEs. M.L. Garcia typed, compiled, and edited the manuscript.

Much of the successful resolution of the DCH issue is the result of an extensive experimental program. The DCH experiments were reviewed as part of a Nuclear Regulatory Commission (NRC)-sponsored effort known as the Severe Accident Scaling Methodology (SASM) Program that was chaired by N. Zuber (NRC). As a result of SASM recommendations, the NRC-sponsored experimental programs were redirected toward performing integral counterpart experiments at two different physical scales at Sandia National Laboratories and Argonne National Laboratory. These experiments included detailed (geometrically scaled) simulations of the Zion and Surry subcompartment structures and had initial conditions closely tied to postulated accident scenarios.

Additional guidance for the experiment programs was provided by a five-member DCH Experiment Technical Review Group (TRG) who were all members of the original SASM program. They included R.E. Henry, M. Ishii, F.J. Moody, B.R. Sehgal, and T.G. Theofanous. The DCH working group for the experimental program consisted of representatives of the sponsor (NRC), universities and industry (TRG), and the national laboratories (SNL and ANL), and met periodically to discuss new results and decide future directions.

NUREG/CR-6075 ("The Probability of Containment Failure by Direct Containment Heating in Zion") and NUREG/CR-6109 ("The Probability of Containment Failure by Direct Containment Heating in Surry") were reviewed by a panel of 13 experts representing national laboratories, universities, and industry. The reviewers identified two areas of unresolved concerns: initial conditions and model validity. Two working groups were formed to address these concerns. The first meeting, on initial conditions, included R.E. Henry, S. Levy, and M. Modarres. The second meeting, on model validity, included J. Shepherd, M. Ishii, S. Levy, F.J. Moody, and R.E. Henry. The authors would like to thank these reviewers for their guidance and input on these reports which established the basis for extrapolation to other plants.

The authors would like to acknowledge representatives of Zion, Surry, Point Beach, H.B. Robinson, and Vogtle who provided additional input for this report. This work was sponsored by the Accident Evaluation Branch of the Office of Research of the U.S. Nuclear Regulatory Commission. Input and valuable guidance were supplied by C.G. Tinkler and R.Y. Lee.

## ACRONYMS

ANL	Argonne National Laboratory
ANS	American Nuclear Society
B&W	Babcock & Wilcox
CCFP	Conditional containment failure probability
CDF	Core damage frequency
CE	Combustion Engineering
CLCH	Convection limited containment heating
COV	Coefficient of variation
CR1	Causal relation
CWTI	Corium/water thermal interaction
DCH	Direct containment heating
DPD	Discrete probability distribution
ECCS	Emergency core cooling system
EPRI	Electric Power Research Institute
FAI	Fauske and Associates, Inc.
FSAR	Final safety analysis report
GPM	Gallons per minute
HIPS	High pressure streaming
HPME	High-pressure melt ejection
IET	Integral effects test
INEL	Idaho National Engineering Laboratory
IPE	Individual plant examination
LFP	Limited flight path
LHS	Latin hypercube sampling
LOCA	Loss of coolant accident
NPP	Nuclear power plant
NRC	Nuclear Regulatory Commission
PDF	Probability density function
PORV	Power-operated relief valve
PRA	Probabilistic risk assessment
PSAR	Preliminary safety analysis report
PWR	Pressurized water reactor
QS	Quench spray
RCB	Reactor containment building
RCDT	Reactor coolant drain tank
RCP	Reactor coolant pump
RCS	Reactor coolant system
RHR	Residual heat removal
RPV	Reactor pressure vessel
RWST	Refueling water storage tank
SASM	Severe accident scaling methodology
SBLOCA	Small break loss-of-coolant accident

## ACRONYMS (concluded)

SBO	Station blackout accident
SG	Steam generator
SNL	Sandia National Laboratories
TCE	Two-cell equilibrium
TDS	Technology development tests
TPG	Technical Program Group
<u>W</u>	Westinghouse

## EXECUTIVE SUMMARY

In a light-water reactor core melt accident, if the reactor pressure vessel (RPV) fails while the reactor coolant system (RCS) is at high pressure, the expulsion of molten core debris may pressurize the reactor containment building (RCB) beyond its failure pressure. A failure in the bottom head of the RPV, followed by melt expulsion and blowdown of the RCS, will entrain molten core debris in the high-velocity steam blowdown gas. This chain of events is called a high-pressure melt ejection (HPME). Four mechanisms may cause a rapid increase in pressure and temperature in the reactor containment: (1) blowdown of the RCS, (2) efficient debris-to-gas heat transfer, (3) exothermic metal/steam and metal/oxygen reactions, and (4) hydrogen combustion. These processes, which lead to increased loads on the containment building, are collectively referred to as direct containment heating (DCH). It is necessary to understand factors that enhance or mitigate DCH because the pressure load imposed on the RCB may lead to early failure of the containment.

NUREG/CR-6075, "The Probability of Containment Failure by Direct Containment Heating in Zion," was the first step in resolving the DCH issue. It assessed the probability of containment failure by DCH for the Zion nuclear power plant (NPP). It underwent an extensive review by a panel of 13 experts representing national laboratories, universities, and industry. The reviewers provided written comments; the authors responded to these comments; and finally, the reviewers wrote rebuttals to the authors' responses. From the peer review process, two areas of residual concern were identified: initial conditions and the validity of the model. Two working group meetings addressed these unresolved issues. A supplement to NUREG/CR-6075 was written to document the peer review process, address residual concerns about initial conditions and model validity, and document modeling enhancements.

Four new splinter scenarios were proposed for Zion in the working group meetings. The new scenarios either bound the scenarios in NUREG/CR-6075 or stress greater consistency in the conditions at vessel breach. Two high-pressure scenarios resulting from operator intervention were defined. Scenario V is characterized by coejection of large quantities of water (75 mt) at 16 MPa, and Scenario VI is characterized by coejection of 10 mt of water at 8 MPa. The expected melt composition is predominantly oxidic. Two low-pressure scenarios were also defined. These are characterized by melts with a larger metallic component and small amounts of coejected water.

In order to ensure consistent initial conditions for each scenario, the working group members stressed the use of insights from system-level codes, specifically SCDAP/RELAP5 and CONTAIN. Existing SCDAP/RELAP5 calculations for short-term station blackout scenarios for Zion, Surry, Calvert Cliffs, and Arkansas Nuclear One Unit 2 all indicate that failure of the hot leg or surge line and resulting depressurization of the primary system occur well before core relocation and lower head failure in all cases analyzed. Calculations were continued until lower head failure and showed that only a small amount of metallic debris relocates to the lower plenum. Little or no melting of upper plenum steel was observed, and there was very little relocation of metallic core blockages into the lower plenum. In addition, these analyses showed that RCS pressure could remain high only if the vessel was reflooded. These insights were used to develop the distributions for the four new scenarios defined in the supplement to NUREG/CR-6075.

## Executive Summary

NUREG/CR-6109 used the methodology, which was based on comparisons of containment loads with containment strength, developed for NUREG/CR-6075 and its supplement to assess the conditional containment failure probability for the Surry NPP. The scenarios described in NUREG/CR-6075, Supplement 1, were considered in NUREG/CR-6109. The methodology used for NUREG/CR-6075 to quantify initial conditions was repeated with specific input from Surry and with the insights gained from existing SCDAP/RELAP5 calculations for the Surry NPP.

There are several tools for calculating DCH loads. In NUREG/CR-6075, the two-cell equilibrium (TCE) model and the convection-limited containment heating (CLCH) model were used. These models were validated against the extensive DCH experimental database and gave similar results because the basic modeling assumptions are the same. Only the TCE model was used to compute containment loads in NUREG/CR-6109 and in NUREG/CR-6338. In addition, the CONTAIN code has also been used to calculate DCH loads. For comparison, load calculations were performed for specific sets of input parameters with the CONTAIN code and with the TCE model in NUREG/CR-6109. The calculations were performed for Scenarios V, Va, and VI at the upper end of the mass distributions and with likely hydrogen concentrations. The loads computed with CONTAIN were comparable to or less than the loads calculated with the TCE model for comparable DCH scenarios.

The conditional (on core damage) containment failure probability (CCFP) can be divided into two components: (1) the likelihood of being at high pressure at vessel failure, and (2) the probability that the containment will fail given DCH. NUREG/CR-6075 and its supplement resolved the DCH issue for Zion based on containment loads only, i.e., the load distributions were convoluted with the containment strength distribution to calculate containment failure probabilities without regard to the likelihood of being at high pressure at vessel breach. The conclusion in NUREG/CR-6075 for Zion was that there were no intersections of the load distributions and the containment strength distributions, and thus the DCH issue was resolved for the Zion NPP. The results of the load evaluations for Surry were similar to those for Zion: there were no intersections of the load distributions with the containment strength distribution, and thus the DCH issue for Surry can also be resolved on containment loads alone. Furthermore, the likelihood of high RCS pressures at vessel breach was evaluated for Surry for a limited number of sequences. The probability of RCS pressures greater than 1.38 MPa for all station blackout scenarios without power recovery or operator intervention was found to be low ( $p \sim 0.077$ ). This probability could have been factored into the containment failure probability for Surry if there had been substantial intersections of the load and strength distributions.

NUREG/CR-6338 addresses the DCH issue for all Westinghouse plants with dry containments, which include 34 plants with large dry containments and 7 plants with subatmospheric containments. Westinghouse plants with ice condenser containments are excluded. The methodology developed in NUREG/CR-6075 and NUREG/CR-6075, Supplement 1, was used to perform a load versus strength evaluation for each of these plants using plant-specific data gathered from IPEs, FSARs, and when necessary, direct contacts with plant personnel. The same enveloping accident scenarios (splinters) that were used in NUREG/CR-6075, Supplement 1, and NUREG/CR-6109 were used for these plant evaluations; these scenarios establish important input parameters for the loads calculations, e.g. the RCS pressure at vessel breach, the RPV breach size, the containment pressure and composition at



vessel breach, etc. The melt mass and composition distributions developed for Zion (a four-loop plant) in NUREG/CR-6075, Supplement 1, were used for all of the four-loop plants. For all of the three-loop plants, the melt mass and composition developed for Surry (a three-loop plant) in NUREG/CR-6109 were used. For two-loop plants, the prescription given in NUREG/CR-6075, Supplement 1, was used to develop the melt mass and composition distributions. These quantifications are given in this report.

Plant-specific data were gathered for each of the Westinghouse plants with dry containments for the loads versus strength evaluations. As much as possible, similar plants were grouped to facilitate the DCH quantifications. Drawings from all 41 Westinghouse plants were reviewed so that cavities could be grouped for cavity dispersal and coherence quantifications and so that lower compartment configurations could be grouped to facilitate the quantifications of the debris transport through the subcompartments to the containment dome. The likelihood of water being present in the cavity at vessel breach is also assessed because cavity water may have an impact on DCH loads. Cavities are grouped according to whether they are dry, wet, or deeply flooded and are categorized as either excavated or free standing.

The containment fragility curve was extracted and digitized from the IPE for each plant and the fragility quantifications are summarized in NUREG/CR-6338. The TCE/LHS code was used to perform a load versus strength evaluation using a Monte Carlo simulation to determine the CCFP for each of the Westinghouse plants with dry containments. The results of these calculations show that the CCFP based on the mean fragility curves is less than 0.01 for each splinter scenario and for each plant analyzed in this study. Consequently, there was no need to integrate sequence or HPME probabilities with conditional containment failure probabilities for each splinter. Thus, DCH is considered resolved for all Westinghouse plants, excluding only plants with ice condenser containments, and no additional analyses are required.

We contacted all of the Westinghouse two-loop plants (Ginna, Kewaunee, Prairie Island 1 & 2, and Point Beach 1 & 2) for additional plant information to allow more accurate estimates of the subcompartment debris transport fractions. The utilities provided the necessary information and their data were factored into the assessments for two-loop plants. Westinghouse plants with ice condenser containments, all Combustion Engineering plants, and all Babcock and Wilcox plants will be addressed in future resolution efforts.

## 1.0 INTRODUCTION

In a light-water reactor core melt accident, if the reactor pressure vessel (RPV) fails while the reactor coolant system (RCS) is at high pressure, the expulsion of molten core debris may pressurize the reactor containment building (RCB) beyond its failure pressure. A failure in the bottom head of the RPV, followed by melt expulsion and blowdown of the RCS, will entrain molten core debris in the high-velocity steam blowdown gas. This chain of events is called a high-pressure melt ejection (HPME). Four mechanisms may cause a rapid increase in pressure and temperature in the reactor containment: (1) blowdown of the RCS, (2) efficient debris-to-gas heat transfer, (3) exothermic metal-steam and metal-oxygen reactions, and (4) hydrogen combustion. These processes, which lead to increased loads on the containment building, are collectively referred to as direct containment heating (DCH) when they have the potential to occur simultaneously. It is necessary to understand factors that enhance or mitigate DCH because the pressure load imposed on the RCB may lead to early failure of the containment.

DCH is a prominent severe accident issue because of its potential for early containment failure. The Nuclear Regulatory Commission (NRC) has identified DCH as a major issue for resolution in the Revised Severe Accident Research Plan (NRC, 1992) and has sponsored programs at Sandia National Laboratories (SNL) to resolve the DCH issue.

NUREG-1150 was the first attempt to treat DCH from a PRA perspective that integrates sequence probabilities with uncertainties associated with initial/boundary conditions and phenomenological uncertainties associated with predicting containment loads. NUREG-1150 addressed only a small number of reference plants and the DCH database was largely nonexistent at the time, so there was no way to validate these early attempts to predict DCH loads. More recently, the IPEs have also addressed the DCH issue from a PRA perspective. Their strength is that plant-specific sequence information is fully integrated into the assessment for every plant. On the other hand, the approaches taken to assess containment loads are inconsistent and poorly tied to the existing database.

This report (NUREG/CR-6338) performs loads/strength evaluations in a consistent manner for all plants. The phenomenological modeling is closely tied to a now substantial database. Plant-specific analyses are performed, but sequence uncertainties are enveloped by a small number of splinter scenarios without assignment of probabilities.

The NRC-sponsored experimental program has played a major role in developing an understanding of the key physical processes in DCH. The technical basis for these scaled experiments was developed by the Severe Accident Scaling Methodology Technical Program Group (SASM-TPG) (Zuber et al., 1991) and by Pilch et al. (1992). The extensive database from counterpart experiments by Sandia National Laboratories and Argonne National Laboratory (ANL) has allowed the development and validation of simple analytical models for predicting the containment loads. In particular, the two-cell equilibrium (TCE) model is based on insights from the experimental program and is used in the analyses presented here. The TCE model takes into account the coherence between the entrained debris and the RCS blowdown steam. Any noncoherence in the entrainment process potentially limits the interactions that result in debris-to-gas heat transfer and in chemical reactions that produce hydrogen.

## Introduction

The first step in the DCH issue resolution process was writing NUREG/CR-6075 (Pilch et al., 1994a): "The Probability of Containment Failure by Direct Containment Heating in Zion." NUREG/CR-6075 assesses the probability of containment failure by DCH for the Zion nuclear power plant (NPP) and establishes the basic methodology that will be used to address DCH for all NPPs. The report was extensively reviewed by a panel of 13 experts representing national laboratories, universities, and industry (see Appendix A, Pilch et al., 1994b). The review process included written comments by the reviewers, responses by the authors, and rebuttals by the reviewers. Following this process, two working group meetings of selected members of the original peer review group were held to resolve two residual concerns: initial conditions and validity of the model.

Supplement 1 of NUREG/CR-6075 (Pilch et al., 1994b) was written in response to the peer review process to close the DCH issue for the Zion plant. It contains the additional analyses that the working groups indicated were necessary to strengthen the original conclusions. The working groups defined four new scenarios for analysis using the methodology in NUREG/CR-6075 and suggested using system-level codes to ensure consistency of the DCH initial conditions. They recommended using insights from core melt progression analyses performed by the Idaho National Engineering Laboratory (INEL) with SCDAP/RELAP5 in order to achieve consistency in quantifying initial conditions. These analyses indicated that failure of the hot leg or surge line resulting in depressurization of the primary system was observed well before core relocation and lower head failure. However, the calculations were continued until the lower head failed in order to gain insights about conditions at lower head failure, such as the melt mass and composition, reactor coolant system pressure, melting of upper plenum steel, and relocation of metallic core blockages into the lower plenum. These insights were applied in developing the distributions for the new scenarios. The CONTAIN code, using sources from SCDAP/RELAP5, was used to ensure consistency in containment initial conditions prior to vessel failure. Load versus strength evaluations were performed using the TCE/LHS code, which uses the two-cell equilibrium model to calculate containment loads and Monte Carlo sampling to compute the load distribution (Pilch et al., 1994b). The containment strength was described in probabilistic terms using a fragility curve taken from the Individual Plant Examination (IPE). The conditional (on core damage) containment failure probabilities (CCFPs) for each of the new scenarios was determined. There were no intersections of the loads and strength distributions, and thus the probability of containment failure by DCH is low enough so that the issue is resolved for the Zion plant.

NUREG/CR-6109 (Pilch et al., 1995) used the methodology and scenarios described in NUREG/CR-6075 and NUREG/CR-6075, Supplement 1, to address the DCH issue for the Surry plant. Consistency of the initial condition distributions was again ensured by using insights from systems-level codes, specifically SCDAP/RELAP5 and CONTAIN. The most useful insights are that the RCS pressure is low at vessel breach, metallic blockages in the core region do not melt and relocate into the lower plenum, and melting of upper plenum steel is correlated with hot leg failure. The SCDAP/RELAP5 output was used as input to CONTAIN to assess the containment conditions at vessel breach.

The loads evaluations for Surry in NUREG/CR-6109 (Pilch et al., 1995) showed no intersections of the loads distributions with the containment strength distribution, and thus the DCH issue for Surry

was resolved based on containment loads alone. However, the likelihood of high RCS pressures at vessel breach was evaluated for Surry. The probability of RCS pressures greater than 1.38 MPa for all station blackout scenarios without power recovery or operator intervention was found to be low ( $\approx 0.077$ ). This probability could have been factored into the containment failure probability for Surry if there had been significant intersections of the loads and strength distributions.

SCDAP/RELAP5 is the NRC's more mechanistic tool for performing integrated analyses of core melt progression. However, the peer review of SCDAP/RELAP5 noted that models and the existing database for late-phase core melt progression are often inadequate. Consequently, we anticipate that continued research will improve our understanding and capabilities in this area. Nonetheless, an integrated perspective of core melt progression was recommended by previous working groups to guide the selection of melt mass and composition distributions for DCH analyses.

Extrapolation of the DCH issue resolution beyond the Zion plant was first envisioned in NUREG/CR-6075 (Pilch et al., 1994a) where it was argued that most plants would have load distributions similar to Zion. Similarity of containment loads coupled with an anticipation that there would not be any significant deviations from the Zion fragility curve for containments of a similar class led to the tentative conclusion that DCH could be resolved for most PWRs. Two concerns were expressed in the peer review (by a 13 member NRC appointed panel) of this work. First, peer reviewers recommended that consensus be achieved on the Zion resolution before proceeding with extrapolation to other plants. This recommendation has been satisfied by the establishment of two working groups to resolve residual concerns for Zion and the publication of NUREG/CR-6075, Supplement 1, which documents modifications in the methodology arising from working group recommendations.

The peer reviewers of NUREG/CR-6075 also expressed concern that plant-specific differences in nuclear steam supply systems or plant geometry were not adequately addressed. In response to this concern, the NRC has instructed INEL to perform best estimate calculations of core melt progression using SCDAP/RELAP5. When complete, SCDAP/RELAP5 calculations will be available for representative plants from each supplier of nuclear steam supply systems. Insights from the calculations performed to date are factored into the current analyses. Concerns arising from differences in plant size, plant parameters, or plant geometry are addressed in this report by performing analyses for each individual plant or site using plant-specific input.

This NUREG report addresses the DCH issue for all Westinghouse plants with dry containments, which include 34 plants with large dry containments and 7 plants with subatmospheric containments. Westinghouse plants with ice condenser containments are excluded. The methodology developed in NUREG/CR-6075 and NUREG/CR-6075, Supplement 1, was used to perform a load versus strength evaluation for each of these plants using plant-specific data gathered from IPEs, Final Safety Analysis Reports (FSARs), and when necessary, direct contacts with plant personnel. The same enveloping accident scenarios (splinters) that were used in NUREG/CR-6075, Supplement 1, and NUREG/CR-6109 were used for these plant evaluations; these scenarios establish important input parameters for the loads calculations, e.g. the RCS pressure at vessel breach, the RPV breach size, the containment pressure and composition at vessel breach, etc. The melt mass and composition distributions developed for



## Introduction

Zion (a four-loop plant) in NUREG/CR-6075, Supplement 1, were used for all of the four-loop plants. For all of the three-loop plants, the melt mass and composition developed for Surry (a three-loop plant) in NUREG/CR-6109 were used. For two-loop plants, the prescription given in NUREG/CR-6075, Supplement 1, was used to develop the melt mass and composition distributions. These assessments are summarized in Section 4 for all Westinghouse plants and a more complete description for all PWRs (including Combustion Engineering and Babcock & Wilcox plants) is given in Appendix B.

Plant-specific data were gathered for each of the Westinghouse plants with dry containments for the loads versus strength evaluations. As much as possible, similar plants were grouped to facilitate the DCH assessments. For example, cavity drawings from all 41 Westinghouse plants were reviewed, along with the IDCOR (1985) categorization, and it was decided for coherence purposes that the cavities could be grouped into three types: Zion-like, Surry-like, and other. Only South Texas 1 and 2 fall into the "other" category. The cavity dispersal and coherence assessments are summarized in Section 4 and a more detailed description is given in Appendix C. The likelihood of water being present in the cavity at vessel breach is also assessed in Appendix C. Cavities are grouped according to whether they are dry, wet, or deeply flooded. Furthermore, review of the drawings of the lower compartment configurations of all 41 Westinghouse plants indicated that they could be grouped into four types (Zion-like, Surry-like, two-loop plants, and other). The only plants that fall into the "other" category are H.B. Robinson and South Texas 1 and 2. This grouping facilitated the assessment of the debris transport through the subcompartments to the containment dome. These assessments are also summarized in Section 4 and a more complete description is given in Appendix C. Quantification of DCH phenomena is addressed in Section 5.

The containment fragility curve was extracted from the IPE for each plant. The fragility assessments are summarized in Section 6 and are compiled in Appendix D. The TCE/LHS code was used to perform a load versus strength evaluation to determine the CCFP for each of the Westinghouse plants with dry containments. The results of these calculations are presented in Section 7. The conclusions and recommendations are given in Section 8.



## 2.0 RESOLUTION METHODOLOGY

The methodology is aimed at grouping each PWR into one of two categories:

1. PWRs in which the threat of early containment failure is shown to be  $\leq 0.1$ , and
2. PWRs in which the threat is  $> 0.1$ .

We consider DCH "resolved" for those plants that fall into the first category. The figure of merit by which resolution is judged is the mean conditional containment failure probability (CCFP). We emphasize that the containment failure probability is ultimately conditional on core damage. Based on NRC recommendations, the DCH issue for any PWR will be considered resolved if a CCFP  $\leq 0.1$  is reasonably demonstrated. We recognize that DCH must be considered in the plant-specific context of all early containment modes when this success criterion is applied; however, DCH is thought to dominate early containment failure for most plants. The DCH issue for plants falling into category 2 (CCFP  $> 0.1$ ) may ultimately be considered resolved if the NRC chooses to view resolution from a broader perspective that convolutes the CCFP with the core damage frequency (CDF), or if the NRC chooses to perform a cost/benefit analysis.

Figure 2.1 provides an overview of the DCH resolution methodology. Consistent with peer review recommendations on NUREG/CR-6075, the first step in the methodology was to work through the key issues for Zion. When consensus was reasonably achieved through the peer review process and follow-on activities, the process was demonstrated a second time for Surry. In both cases, containment loads were calculated using simplified models<sup>1</sup> and distributions on the dominant initial condition parameters. Three splinter scenarios were analyzed with the intent to envelop the expected range of initial conditions. The CCFP was calculated by convoluting the predicted loads distribution with a structural response distribution obtained from the IPEs. We note here that the CCFP was conditional on the splinter scenario since no attempt was made to assign probabilities to the various splinter scenarios. The analyses are documented in NUREG/CR-6075 and NUREG/CR-6075, Supplement 1, for Zion (Pilch et al., 1994a,b) and in NUREG/CR-6109 for Surry (Pilch et al., 1995). For both Zion and Surry, there were no intersections (CCFP  $\ll 0.1$ ) of the load distribution with the strength distribution.

The second step in the methodology is to repeat the process quantitatively used for Zion and Surry to all remaining PWRs using plant-specific input. This report executes this step for all Westinghouse plants with large dry or subatmospheric containments. Two additional efforts are scheduled: the first will focus on all Westinghouse plants with ice condenser containments. We expect that CONTAIN will be used to calculate loads in this effort because it has models for the ice beds. The second will include all Combustion Engineering (CE) plants and all Babcock & Wilcox (B&W) plants.

---

<sup>1</sup> Two-Cell Equilibrium (TCE) model for Zion and Surry, and the Convection Limited Containment Heating (CLCH) model for Zion.

## Resolution Methodology

Convolution of the containment load distribution with the containment fragility is performed for each plant using plant-specific information. The key plant-specific information used in these analyses are listed below with a brief description of how extrapolation is performed.

1. **RCS Initial Conditions:** Two splinter scenarios are analyzed based on the Zion/Surry resolution efforts. RCS pressures and temperatures were specified for the splinter scenarios in the Zion/Surry resolution documents. Plant-specific RPV geometry and core compositions are employed and tabulated in Table 4.3.
2. **Melt Mass Distributions:** A simple prescription for determining melt mass based on core size was developed as part of the Zion/Surry resolution effort. The bounding nature of this prescription was validated by SCDAP/RELAP5 for Zion, Surry, Calvert Cliffs, and ANO-2. The core size for Westinghouse plants can be grouped according to whether the plant has four, three, or two-loops. Existing melt mass distributions for Zion and Surry are applied to all four and three-loop plants, respectively. The same prescription used to develop melt mass distributions for Zion/Surry is used (Appendix B) to develop a melt mass distribution for all two-loop plants.
3. **Plant Geometry:** Plant-specific geometry is used in these analyses and tabulated in Table 4.3. The coherence ratio and dome transport are two geometry specific phenomenological parameters that receive special attention in their assignments in Sections C.2.2 and C.3, respectively. Reactor cavities are grouped into three categories: Zion-like, Surry-like, and other. Existing coherence correlations for Zion and Surry are applied to all Zion-like and Surry-like cavities, respectively. A biased coherence correlation is applied to cavities that are neither Zion-like or Surry-like. Dome transport is calculated using plant-specific areas for flow around the RPV and for line-of-sight flow paths from the cavity exit.
4. **Fragility:** Plant-specific fragility curves are cataloged from the IPEs as part of Appendix D.

We refer to the initial attempt at extrapolation as screening because the models are tied to the Zion and Surry database and other plants have different geometries and flow paths, which necessitate some judgment in application of the models. In addition, Zion and Surry were very well characterized. Complete plant drawings were available and SNL staff who were knowledgeable about DCH issues participated in tours of the plants. The primary sources for plant information are PSARs, FSARs, IPEs, and other PSAs. Of these, the IPEs proved most useful, but they do not carry the same level of detail that was available for Zion and Surry. In general, the plant data employed here has not been reviewed by the plant owners, except in a few cases where uncertainties were judged significant. To allow for any potential nonconservatisms or possible residual modeling concerns in the screening stage, we recommend a tighter resolution criterion,  $CCFP \leq 0.01$ . Like the Zion and Surry efforts, the screening process will focus on a small number of splinter scenarios; consequently, the computed CCFPs will be conditional on the splinter scenario since no attempt will be made to assign probabilities to the splinters. Utilities may wish to employ some of the methods or results of this report when revising their PSAs to provide a more integrated perspective on this issue; however, this is beyond the scope or needs of the current effort.

Plants that do not pass the initial screening will then be examined more carefully to determine whether they can meet the  $CCFP \leq 0.1$  criterion with more detailed analyses, and therefore be considered resolved. This can be accomplished by one of three processes: refined load/strength analyses, consideration of HPME probabilities given core damage (i.e., assign probabilities to the splinters), or some integration of load/strength analyses and HPME probabilities. Additional analyses for plants that do not meet the success criterion for the initial screening phase (i.e.,  $CCFP \leq 0.01$ ) will be formally documented in a separate report to the NRC. This step will ensure that any plant that does not pass the initial screening test will receive close scrutiny that will be publicly documented. The best course of action must be judged for each individual plant. Some potentially fruitful options are discussed below.

Several options exist for refined load/strength analyses. They are listed here in order (roughly) of increasing effort.

1. The CCFP may not be very sensitive to potential uncertainties in the containment fragility. It is possible that the  $CCFP \geq 0.01$  in the screening study (using mean fragility curves) while the use of a high confidence fragility curve could still meet the resolution criterion,  $CCFP \leq 0.1$ . This may occur if the plant has a long flat tail at the low end of the fragility curve.
2. Refine the accuracy of the TCE/LHS input. This can be accomplished by obtaining detailed plant drawings or by consulting with knowledgeable plant personnel.
3. Best estimate CONTAIN calculations could be performed that may result in lower predicted loads than those calculated using the TCE model. Lower loads were generally predicted in CONTAIN/TCE comparisons that were performed for NUREG/CR-6109 (Pilch et al. 1995) for Surry.
4. Side failure of the RPV could retain ~25 - 50 percent of the melt in the RPV. Credit was taken for this in NUREG-1150 for Sequoyah. The likelihood of side failure, however, has yet to be resolved in a definitive way.

Demonstrating that the probability of HPME events is sufficiently low offers an independent path to resolving the DCH issue. Integration of sequence or HPME probabilities with conditional failure probabilities (for each splinter) was not performed or needed in this study. The plant's accident management procedures can be examined to determine if the operators will depressurize the RCS. We note that many plants can depressurize even in station blackout accidents because the PORVs have DC power. Recent SCDAP/RELAP5 calculations for Zion, Surry, ANO-2, and Calvert Cliffs support a body of evidence indicating that natural circulation processes will result in hot leg or surge line failure long before melt relocation to the lower plenum and bottom head failure. These natural circulation processes will lead to spontaneous and complete depressurization of the RCS for core melt accidents that involve no operator intervention. Thus, in station blackout accidents and in recovered accidents there is a high likelihood that the RCS will be depressurized at the time of vessel breach.

Recovery attempts without depressurization could have various consequences. Recovery at TMI-II did not immediately arrest the core melt progression, but it was instrumental in preventing lower

## Resolution Methodology

head failure. On the other hand, the margin to failure seems to have been small and recovery actions disrupted energy transport to the hot legs and surge line, thus preventing their failure. Consequently, attempts to demonstrate low HPME probabilities must address both spontaneous depressurization and the consequences of recovery. The necessary plant-specific information may be summarized from the IPEs, but the basis for the utilities quantifications should be reviewed. For perspective, the NUREG-1150 study for Sequoyah showed that ~40 percent of the core damage accidents involved accident recovery in sufficient time to preclude vessel failure. Resolution can be achieved solely on HPME probabilities if their likelihood is shown to be  $\leq 0.1$ . If independent resolution is not achieved, then HPME probabilities can be combined with the CCFPs to complete an integrated approach to resolution.

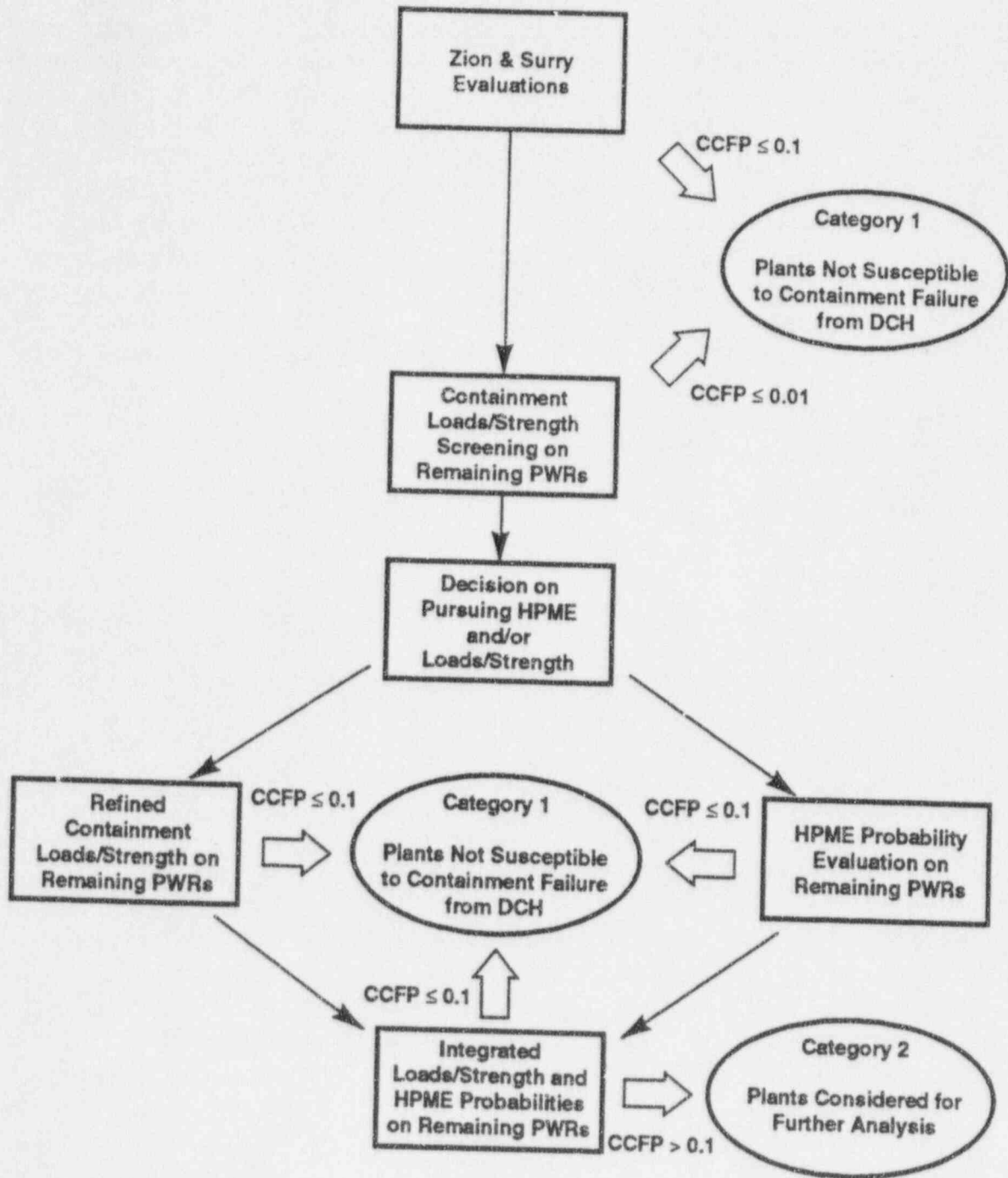


Figure 2.1. Methodology for resolution of the DCH issue for all PWRs.



### 3.0 PROBABILISTIC FRAMEWORK

The basic understanding upon which this approach to resolving the DCH issue is based (and confirmed in repeated experiments) is that the intermediate (or steam generator) compartment traps most of the debris dispersed from the reactor cavity and that the thermal-chemical interactions during this dispersal process are limited by the incoherence in the steam blowdown and melt entrainment processes. To put it simply, for blowdowns that are sufficient to cause entrainment and significant thermal-chemical interactions, the entrainment time is short compared with the blowdown time so that the molten debris is exposed to only a small fraction of the steam from the primary system. Because this steam is the principal medium for carrying the melt energy and the hydrogen produced by steam-metal interactions to the main containment volume, this incoherence is a crucial mitigating factor. With this understanding, it is possible to reduce most of the complexity of the DCH phenomena to a single parameter: the ratio of the melt entrainment time constant to the system blowdown time constant ( $R_t = \tau_e/\tau_b$  in the TCE model). For simplicity,  $R_t$  is referred to as a coherence ratio.

Besides these modeling factors, the DCH loads depend on parameters that characterize the system initial conditions; that is, primary system pressure, temperature and composition (i.e., hydrogen mole fraction), melt quantity and composition (zirconium and stainless steel mass fractions), initial containment pressure and composition (hydrogen mole fraction), and geometry (containment volume and the size of the breach). The key component of the framework, therefore, is the causal relation (CR1) between these parameters and the resulting containment pressure (and temperature) under the influence of the uncertainty in the coherence ratio,  $R_t$ . Of these parameters, some are fixed, some vary only over a narrow range, and some are so uncertain that they can be approached only in a very bounding sense. The following features were considered in coming up with the final choice of a framework:

1. *Geometry.* The specific geometry is fixed for a given plant; however, the basic features are an intermediate compartment between the cavity and the main containment volume and a lower head that fails by rupture in a local (rather than global) manner. In addition, the geometry is characterized by the free volume of the containment and the primary system volume.
2. *Containment Conditions.* Typically, high-pressure scenarios evolve with significant primary system venting prior to vessel breach (see Section 4); this venting increases the containment pressure to ~0.25 MPa with temperatures near saturation. This pressure is somewhat lower for a subatmospheric plant (~0.15 MPa) such as Surry and can be considerably lower if any of the active containment heat removal systems are operational. The containment atmosphere will also contain hydrogen at a concentration of a few mole percent. Preexisting hydrogen is limited by the quantity of zirconium available to react in the core; thus, there is a constrained relationship between preexisting hydrogen in the containment and the hydrogen produced by steam-zirconium reactions in the DCH event.
3. *Primary System Conditions.* We emphasize here the reasonable consistency between reactor coolant system pressure (and temperature) and melt mass and composition. Model predictions indicate that DCH loadings are insensitive to the temperature of the primary system (see Appendix D, NUREG/CR-6075, Pilch et al., 1994a), and accident analyses indicate that the primary system

pressure can be enveloped rather than predicted (Section 4). This leaves only the expelled melt parameters in need of quantification. These are melt quantity, composition, and temperature and are the variables that drive the DCH process; however, they are highly uncertain. They depend on the complex interactions and the scenario variations in the core meltdown, relocation, and lower head failure processes and are hence in need of very careful quantification. This is done in Section 5.

The probabilistic framework can be structured in the manner illustrated in Figures 3.1 and 3.2. As shown in these figures, the initial melt parameters are to be quantified as independent probability density functions, representing modeling uncertainty in the parameters. Variations from stochastic processes are assessed as insignificant relative to modeling uncertainty. These functions are formed into a joint probability density function and then combined with CR1, under the parameter distribution function that represents model uncertainty for the DCH processes, coherence ratio ( $R_c$ ), to obtain a probability density function for the peak containment pressure. This distribution function for peak containment pressure is combined (CR2) with the set of containment fragility curves (probabilistically distributed themselves<sup>2</sup>) to obtain a probability distribution of containment failure frequency.<sup>3</sup>

Sandia has developed software to perform either traditional Monte Carlo sampling or stratified Monte Carlo sampling. The software, called LHS, is user friendly and has an established quality assurance pedigree, including code assessment and verification. Sandia chose to use this numerical tool based on LHS to propagate distributions through the probabilistic framework. The resulting software was applied in NUREG/CR-6075, Supplement 1 (Pilch et al. 1994b), where it is described more fully in Appendix B. The same software was used in NUREG/CR-6109 (Pilch et al., 1995), and it is used here without modification.

### 3.1 Nomenclature

$F_f$	=	failure frequency
$M_{st}$	=	mass of steel
$M_{UO_2}$	=	mass of $UO_2$
$P_f$	=	failure probability
$R_c$	=	coherence ratio
$\tau_b$	=	characteristic blowdown time
$\tau_e$	=	characteristic entrainment interval
$X_{Zr}$	=	mass fraction Zr

<sup>2</sup> In the current assessments, only a single fragility curve is available, but the discussion here has been generalized to accommodate desired improvements in information.

<sup>3</sup> Each fragility curve is expressed in terms of failure frequency, and this frequency expresses the statistically meaningful variations (based on actual experience) in containment strength. These containment strength variations are due to variations in material and workmanship and are characterized by the fraction that failed in a nominally similar population of structures subjected to the same load. On the other hand, the probability assigned to each fragility curve expresses a subjective degree of belief as to the appropriateness of it in meeting the intended task.



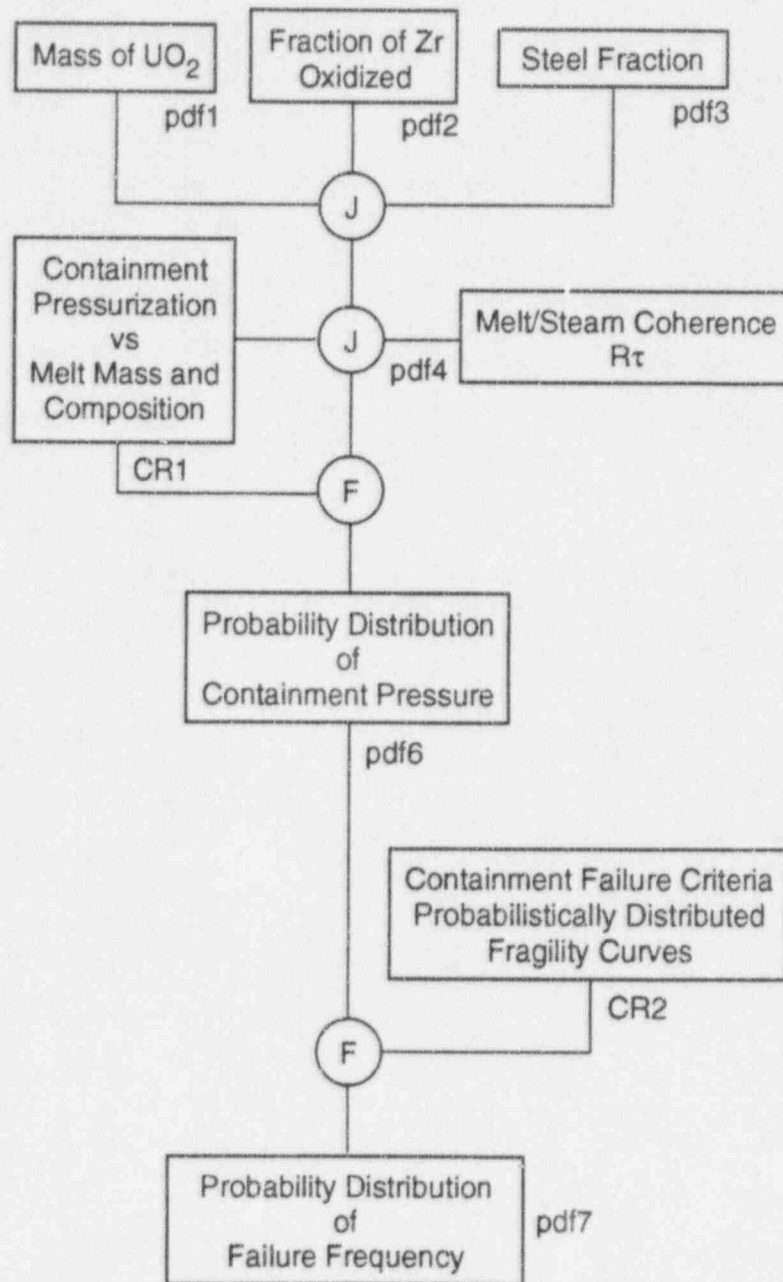


Figure 3.1. The probabilistic framework for containment failure under direct containment heating scenarios. The (J) and (F) are the "joint" and "function" operations, respectively, as described in the text.

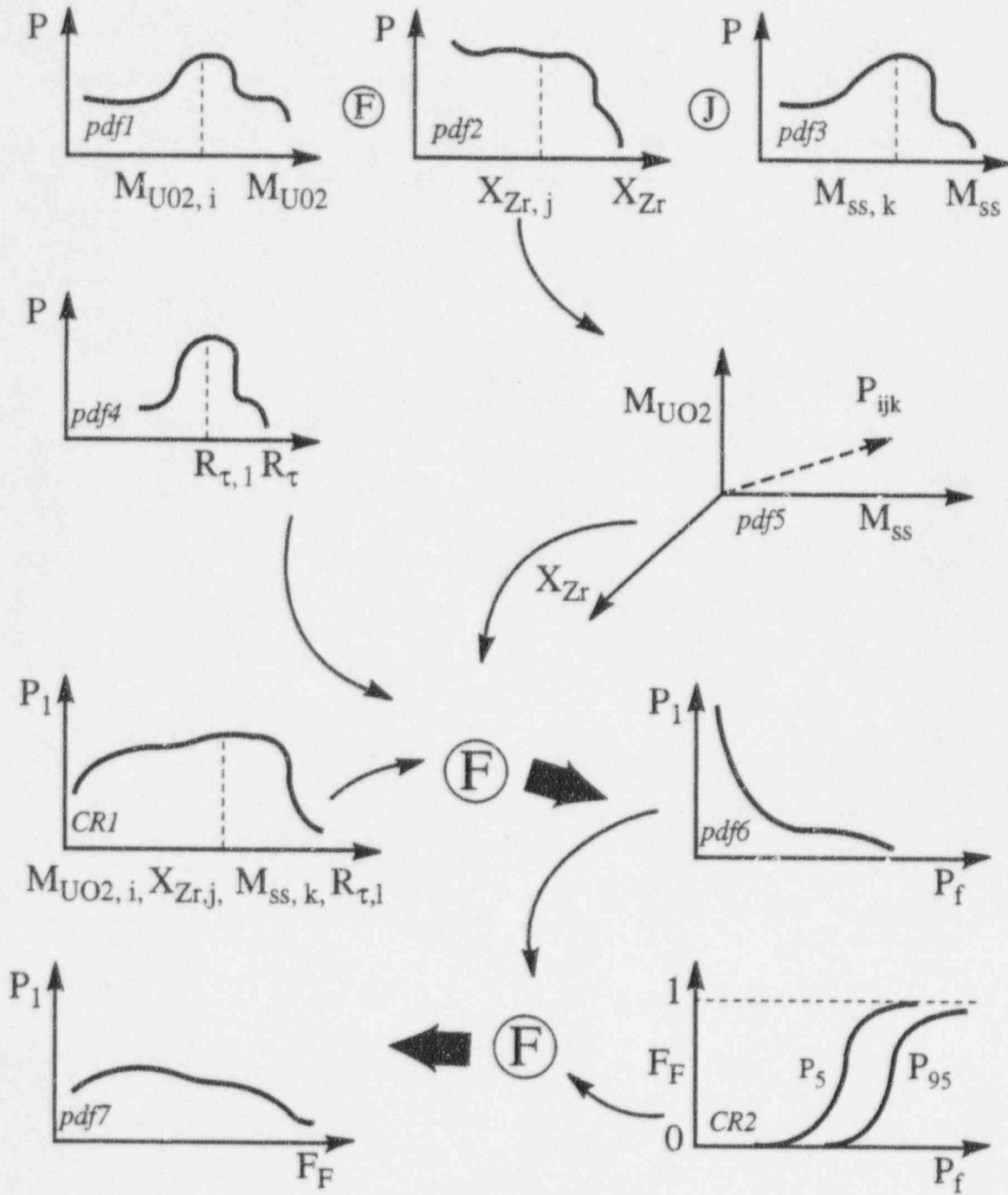


Figure 3.2. Illustration of the probabilistic framework in terms of schematic depiction of its components.

## 4.0 QUANTIFICATION OF INITIAL CONDITIONS

### 4.1 Introduction

DCH has traditionally been examined for a rather narrow range of hypothesized severe accident conditions: unmitigated station blackout at full system pressure; formation of a metallic blockage with an overlying ceramic crust in the core that contains a large fraction of core in a molten state; sudden failure of this blockage and crust, resulting in a massive relocation of the melt into the lower plenum; failure of a penetration passing through the lower head of the reactor pressure vessel; rapid ablation of the resulting hole in the RPV from 5 to about 40 cm (Pilch and Tarbell, 1985); and high-pressure melt ejection from the single hole followed by high-pressure steam blowdown. In attempts to address the DCH issue from either a systems point of view or an accident management point of view, intentional depressurization of the primary system has been examined (Hanson et al., 1990). Experiments have shown that the pressure must be very low (less than 1 MPa) to preclude the onset of dispersal from the cavity and to prevent the possibility of DCH (Tutu et al., 1988). Bounding calculations (Pilch and Tarbell, 1986) suggest that as little as 20 percent of the core (participating in DCH) could pose a threat for the containment. With this traditional understanding, containment-threatening loads from DCH can only be precluded if the RCS is almost fully depressurized. However, based on early CONTAIN calculations (Williams and Louie, 1988) the understanding developed in NUREG/CR-6075 (Pilch et al. 1994a, b), a substantial reduction of DCH loads is achieved without having to rely upon nearly complete depressurization of the RCS.

Quantification of melt release conditions was developed by attempting to envelop physically possible behavior in a comprehensive and systematic manner. This means that we needed to examine all reasonably conceivable severe accident scenarios, identify key aspects of their phenomena and respective ranges of behavior, and establish the few scenarios that envelop the DCH challenge to the containment.

Reviewers raised the following questions (Appendix A in Pilch et al. 1994b) regarding the completeness of the splinter scenarios considered in NUREG/CR-6075 (Pilch et al. 1994a) for the Zion application:

1. Can full-system pressure cases be ruled out?
2. Should operator intervention scenarios be analyzed?
3. Can dry core scenarios lead to melting and relocation of the metal (Zr) blockage from the core to the lower plenum?

Generally, the reviewers characterized initial condition quantifications in NUREG/CR-6075 (Pilch et al. 1994a) for Zion as "optimistic." Specifically, they expressed concern that ~8 MPa RCS pressure might not be adequately bounding, that the melt mass distributions were too narrow, and that the melt composition did not contain sufficient metallics (Zr and steel). The reviewers also stressed that SCDAP/RELAP5 analyses should be performed and used in a consistent manner in establishing initial conditions.

The NRC convened a working group to make recommendations on how to resolve these concerns for Zion. Their minutes are included in Appendix A of Pilch et al. (1994b) and summarized here in Section 4.2, where additional splinter scenarios are defined. Residual concerns were fully resolved for Zion (Appendix A in Pilch et al. 1994b) and it is our intent to follow the prescription for quantifying initial conditions for all Westinghouse plants. SCDAP/RELAP5 calculations were performed to provide confirmatory insight into the working group recommendations for Zion (Knudson, Appendix E in Pilch et al. 1994b) and for Surry (Knudson and Dobbe, 1993; Quick and Knudson, Appendix E in Pilch et al. 1995). The relevant insights are summarized in Section 4.3. Quantifications for the new scenarios are presented in Sections 4.5, 4.6, and 4.7.

## 4.2 Splinter Scenarios

DCH is only of concern if the RPV fails while the RCS is still at elevated pressure. Figure 4.1 depicts the four splinter scenarios analyzed in NUREG/CR-6075 (Pilch et al., 1994a). The complex phenomena of severe accidents lead to the possibility of two divergent scenarios: one concerned with the quantity of melt that accumulates in the core region prior to its release and relocation into the lower plenum, and the other concerned with the mode and timing of lower head failure. Analysis of the first considers crucible formation or failure versus gradual relocation (no crucible) as the mechanism for melt relocation into the lower plenum. Analysis of the second considers a localized penetration failure of the lower head versus rupture.

Working group recommendations focused on four new splinter scenarios as shown in Figure 4.2. The intent was to place greater reliance on systems-level codes (SCDAP/RELAP5) in order to achieve better consistency between RCS pressure at vessel breach with melt mass and composition. Specifically, the working group emphasized that there were correlations between RCS pressure and melt composition; high RCS pressures and oxidic melts are correlated predominantly with operator intervention; metallic melts are correlated with reduced RCS pressures associated with pump seal leaks of sufficient magnitude that hot leg failure does not occur. The working group minutes (Appendix A in Pilch et al., 1994b) refer to the new splinters as Scenarios II, IIa, IIb, and III; however, to avoid confusion with the scenarios already analyzed in NUREG/CR-6075, we refer to the new splinters in this report as Scenarios V, VI, VII, and VIII. The new scenarios either bound the scenarios in NUREG/CR-6075 or stress greater consistency in the conditions at vessel breach; thus, the new scenarios are intended to replace those in NUREG/CR-6075. The rationale leading to these new splinter scenarios is discussed next.

The working group felt that there was no compelling need to further analyze scenarios with penetration failures. The INEL lower head failure analysis (Rempe et al., 1993) and the OECD-NEA-TMI-2 vessel investigation project (Stickler et al., 1993) both concluded that rupture was much more likely than a penetration-type failure. Marshall (1988) performed some scoping experiments on tube ejection. Specifically, he confirmed that binding caused by differential thermal expansion could prevent ejection of a penetration from the lower head (for the conditions and materials tested); however, ballooning of the lower head, which could induce ejection of a penetration as a precursor to rupture, was not modeled in these experiments. Fauske and Associates, Inc. (FAI) (Hammersley et al., 1993), under the sponsorship of the Electric Power Research Institute (EPRI), has examined melt penetration

into in-core instrument guide tubes. Pressure-driven melt was observed to travel approximately 2 m, which is far enough to carry it well beyond the lower head. However, the melt mass is too small to threaten the integrity of the guide tube. These limited experiments confirm INEL and OECD conclusions that penetration-type failures are unlikely. NUREG/CR-6075 (Pilch et al., 1994a) showed that a penetration failure followed by ablation of the lower head would produce a hole about the same size as would be expected for a local rupture of the lower head. Finally, work reported in NUREG/CR-6075 (Pilch et al., 1994a) showed that predicted loads for rupture scenarios bound predicted loads for penetration failure scenarios; consequently, penetration failures need not be considered further in the extrapolation activities.

Scenario VI is very similar to Scenario II in NUREG/CR-6075. Here, the working group wanted to emphasize the presence of water in the lower head. They recommended the addition of a new TMI-like scenario (Scenario V) characterized by reflooding and repressurization (~16 MPa) of the RCS as a result of operator actions. Scenarios V and VI were envisioned as having water in the core (at least covering the bottom) during much of the core melt progression; consequently, slumping core material would form a crucible which could fail only locally. The melt composition would be largely oxidic, with most unoxidized Zr permanently retained as a metal blockage in the core. Scenarios V and VI envelop those scenarios in which operators attempt to manage or recover an accident but fail to prevent severe core damage, which then leads to failure of the RPV lower head.

The working group then recommended consideration of scenarios (VII and VIII) in which core melting would proceed without water in the core region and largely without water in the lower plenum. It was their expectation that these scenarios would evolve to much lower RCS pressures (< 4 MPa) at vessel failure for typical small break loss-of-coolant accidents (SBLOCAs). Confirmatory calculations (Section 4.3) using SCDAP/RELAP5 indicate that complete depressurization of the RCS can be expected. At the lower pressures, the possibility of the upper plenum steel melting without also failing the hot leg becomes possible; thus, both scenarios VII and VIII augment the oxidic melt with large quantities of upper plenum steel. Scenario VIII is distinguished from Scenario VII in that the metal blockage is also assumed to remelt, allowing large quantities of unoxidized Zr to relocate to the lower plenum.

NUREG/CR-6075 (Scenario IV) considered a gradual relocation that progressed under high pressure (~8 MPa) with complete melting of upper plenum steel. Working group discussions pointed out that this scenario is overly conservative and that melting of upper plenum steel is strongly correlated with hot leg failure. In fact, gradual relocation has been predicted in only one MELPROG calculation for the Surry plant (Heames and Smith, 1987); and even here, hot leg failure was predicted to occur before core relocation into the lower plenum. Should a gradual relocation occur, working group members believed that it would look like Scenario VIII at the time of vessel failure.

SCDAP/RELAP5 calculations have been performed (based on working group recommendations) to confirm the basic features of Scenarios VII and VIII for Zion (Appendix C in Pilch et al. 1994b) and for Surry (Quick and Knudson, Appendix E in Pilch et al. 1995). Three cases (representing short-term station blackout accidents) were run for Zion with SCDAP/RELAP5 representing the full spectrum of expected pump seal LOCAs: no leaks, 250 gpm/pump, and 480 gpm/pump. The key conclusion for Zion, however, is that hot leg failure will occur before core relocation for all pump seal LOCAs,



leading to complete depressurization of the RCS before lower head failure. Earlier SCDAP/RELAP5 calculations for Surry (Knudson and Dobbe, 1993) also predicted that hot leg failure would occur before core relocation for these cases except for the 480-gpm/pump RCP leak. The earlier Surry calculations, however, were intentionally biased to accelerate core melt progression and lower head failure. Consequently, the NRC asked INEL to perform a best-estimate SCDAP/RELAP5 calculation for a 480-gpm/pump RCP leak at Surry. This best-estimate calculation also led to hot leg failure and complete depressurization of the RCS before lower head failure. Appendix E in Pilch et al. (1995) presents these calculations in detail. Depressurized events such as this are of no interest to DCH. Consequently, Scenarios VII and VIII are not further analyzed in this report. Should the vessel fail, gravity drainage of melt into the cavity could pose risks that are beyond the scope of the current work.

In addition to RCS conditions, we must also envelop the range of containment conditions that can exist at vessel breach. Short-term station blackout accidents lead to the highest containment pressures (and steam concentrations) prior to vessel breach. These conditions are ascribed to Scenarios V and VI directly. Most DCH relevant accidents involve operator intervention and the associated possibility that active containment cooling (i.e., fan coolers or sprays) could be operational. Such was the case at TMI-II. We analyze these splinters with no steam in the atmosphere (as an extreme), as Scenarios Va and VIa depending on whether the RCS pressure is high or at intermediate levels. Limited sensitivities were performed for containment pressures midway between the extremes noted above. The predicted loads were lower than the extremes, thus supporting the enveloping nature of the splinter scenarios.

In summary, DCH is only of concern if the reactor pressure fails while the RCS is still at elevated RCS pressure. Consequently, we exclude here from further analysis any scenarios with low RCS pressure at the onset of core damage, scenarios where the RCS is intentionally depressurized in compliance with accident management procedures or other forms of operator intervention, and sequences where the RCS unintentionally depressurizes as a natural consequence of core melt progression. SCDAP/RELAP5 calculations show that hot leg failure and RCS depressurization is likely unless the operators intervene in the accident. We envelop the RCS pressure with high pressure (16 MPa) and intermediate pressure (8 MPa) splinter scenarios, which are noted as Scenarios V and VI, respectively. We envelop containment conditions by considering splinters with and without active cooling in the containment; these are noted as Scenarios Va and VIa, respectively, depending on whether the RCS is at high or intermediate pressure. These four splinter scenarios adequately envelop the full range of RCS and containment conditions for the few DCH relevant scenarios.

#### 4.3 Summary of SCDAP/RELAP5 and CONTAIN Insights

The initial and boundary conditions for the scenarios analyzed in this report are based in part on insights from SCDAP/RELAP5 and CONTAIN calculations. These system code calculations are used to better quantify a consistent set of initial and boundary conditions for the splinter scenarios discussed in Section 4.2. In this regard, we do not blindly use the results of system-level code calculations; rather, we use the codes as one form of input when forming our expert judgments. For example, we include zirconium in our melts when SCDAP/RELAP5 predicts essentially none.

SCDAP/RELAP5 calculations have been performed for Zion (W 4-loop plant), Surry (W 3-loop plant), Calvert Cliffs (CE lowest power density), and ANO-2 (CE highest power density). The

## Quantification of Initial Conditions

credible range of pump seal leaks have been examined for each plant and sensitivity studies have been performed. SCDAP/RELAP5 will also analyze B&W plants in a similar fashion as part of the DCH issue resolution effort for those plants. When complete, SCDAP/RELAP5 will have analyzed each of the major reactor types from each supplier of PWR nuclear steam supply systems in the U.S. All of the cases analyzed so far produced "dry core" conditions, so the potential existed for metallic blockages to relocate to the lower plenum.

Zion is a four-loop Westinghouse nuclear steam supply system. Three dry core cases were run with SCDAP/RELAP5 for Zion at different leak rates: (1) no leaks, (2) 250 gpm per pump leaks, and (3) 480 gpm per pump leaks. The results of these calculations are discussed in Appendix C of Pilch et al. (1994b). The goal of these calculations was to develop a better understanding of the melt mass, melt composition, and RCS pressure at the time of lower head failure for dry scenarios. In each case, hot leg failure was allowed to occur, if predicted during the calculation. This failure would lead to depressurization and complete accumulator discharge.

The SCDAP/RELAP5 calculations for Zion predicted that hot leg failure occurred prior to melt relocation into the lower plenum in all cases. The failure resulted in depressurization and accumulator discharge. In all cases, the RCS pressure was at containment pressure at the time of lower head failure. Owing to the significant amount of time between hot leg failure and lower head failure, we conclude that the sequences, as calculated by SCDAP/RELAP5, will not result in a DCH threat. This supports the assessment in NUREG/CR-6075 that full system pressure scenarios can be excluded (except operator intervention accidents such as TMI-II). The SCDAP/RELAP5 calculations also confirm that the ~8 MPa bound in NUREG/CR-6075 is not only conservative, but perhaps excessively so unless the operator intervenes in the accident. This assumes, of course, that water injection does not arrest melt progression.

Surry is a three-loop Westinghouse nuclear steam supply system that does not have the core bypass feature found in Zion. Existing SCDAP/RELAP5 calculations (Knudson and Dobbe, 1993), which were intentionally biased to accelerate core melt progression and lower head failure, were examined for insights on core melt progression. Three different RCP leak rates were examined: (1) no leaks, (2) 250-gpm/pump leaks, and (3) 480-gpm/pump leaks. In addition, a best-estimate calculation for the 480-gpm/pump case was performed for the NUREG/CR-6109 study (Pilch et al., 1995). These calculations provide additional insight into melt mass, melt composition, and RCS pressure at the time of lower head failure.

The existing SCDAP/RELAP5 calculations for Surry indicated that hot leg or surge line failure occurred prior to melt relocation into the lower plenum in all but the 480-gpm/pump case. The existing calculations were intentionally biased to accelerate core melt progression and lower head failure in order to bound the likelihood that lower head failure could occur while the RCS was still at elevated pressure. Consequently, the NRC asked INEL to perform a best-estimate calculation of the 480-gpm/pump case. This best estimate also led to hot leg failure. These conclusions are fully consistent with those reached for Zion.

Sensitivity studies were performed for the biased SCDAP/RELAP5 calculations (Appendix F in Pilch et al., 1995) in order to assess the potential impact of uncertainties on these conclusions. The



probability that the RCS pressure would exceed 1.38 MPa (200 psig) is ~1.1 percent conditional on a short-term station blackout accident. This insensitivity occurs because of the significant amount of time between hot leg failure and lower head failure. As a result, we conclude that the probability of an HPME is small for a station blackout accident, without operator intervention or recovery. We note best estimate calculations and sensitivity studies have also been performed for CE plants. Consistent with results for Westinghouse plants, hot leg failure is predicted before melt relocation (assuming the operator does not intervene and recovery is not attempted).

A second insight is related to the amount of metallic debris present in the melt in the lower plenum. We noted that the degree of upper plenum steel melting is limited in all cases and is strongly correlated with hot leg failure. The maximum amount of upper plenum steel that was predicted to melt was much less than 1 mt for Surry and ~3 mt for Zion. We also noted that lower plenum steel was assumed to melt in all cases, representing an additional ~5 mt of steel. Melting of lower plenum steel occurs only to the extent that thin lower plenum steel is submerged in the relocated core material. Lower plenum water always existed in the SCDAP/RELAP5 calculations, even in the absence of operator interaction; consequently, radiative melting of lower plenum steel is not expected.

With respect to zirconium in the melt, SCDAP/RELAP5 indicates that very little zirconium is predicted to relocate into the lower plenum for Zion and Surry. The maximum amount of zirconium in the lower plenum melt is ~0.13 mt for Surry and ~0.5 mt for Zion. This implies that meltout of the metallic blockage in the core region is not predicted, even in dry core scenarios. SCDAP/RELAP5 calculations for CE plants lead to similar conclusions.

The reason for this behavior can be seen by a careful review of the calculations. In all cases, the melt that relocated into the lower plenum is predicted to quench, but not all of the available water is vaporized. This is most likely due to displacement of water from the lower plenum as the melt relocates. The water eventually settles back into the lower plenum, but a stratified condition exists, i.e., the water overlies the debris residing on the lower head. Owing to inefficient heat transfer between the debris and the water, the water is vaporized slowly and, in all cases, water remains in the lower plenum at the time of lower head failure. The presence of water and its slow vaporization appears to be sufficient to prevent meltout of the in-core blockages. Hence, we conclude that the amount of zirconium in the melt in the lower plenum will be very limited. We acknowledge uncertainties in modeling of late-phase core melt progression; consequently, additional Zr will be treated in our melt composition quantifications as discussed in Sections 4.6 and 4.7.

A third insight is related to the amount of hydrogen generated for Zion and Surry, which corresponds to from ~20 to 60 percent oxidation of the initial zirconium inventory in the core. Similar results were obtained for the CE plants. Our expectation is that the 60 percent level is a likely upper bound since much of the remaining zirconium is contained in metallic blockages that are difficult to oxidize.

The fourth insight is related to the amount of molten material at the time of lower head failure. We noted that the amount of oxide material that was available to relocate into the lower plenum for Zion varies from approximately 77 mt to 104 mt for the three Zion cases, but the amount of molten oxide varies from 55 mt to 66 mt. Hence, while the amount of oxide material in the lower plenum

## Quantification of Initial Conditions

shows some variation, the amount of *molten* oxide at vessel breach is limited to a rather narrow range. We noted that the maximum amount of oxide material available to relocate into the lower plenum was ~75 mt for Surry. The biased SCDAP/RELAP5 calculations for Surry indicate that virtually all of the core debris relocated in the lower plenum is solid at the time of lower head failure. This is a consequence of attempts to accelerate lower head rupture. The Surry best estimate calculation indicates that ~13 mt of relocated material will be solidified leaving ~62 mt molten at the time of lower head failure. Our prescription for quantifying molten oxide masses conservatively envelops available SCDAP/RELAP5 predictions for Westinghouse and CE plants. Regardless of core power, plant calculations and sensitivity studies with SCDAP/RELAP5 show that plants with lower power densities will have lower melt masses at vessel breach. Our approach to quantifying melt masses takes no credit for this fact in plants with low power densities.

The flow of steam, water, hydrogen, and nitrogen (from accumulator discharge) into the containment for Zion and Surry was provided to Sandia by INEL for use in CONTAIN to determine the containment conditions at the time of lower head failure. The hydrogen flow into the containment was assessed to determine if the hydrogen would burn as it entered the containment. A number of important insights were obtained from these calculations.

The CONTAIN calculations for Zion showed that the containment pressure at the time of lower head failure was in the range of 0.23 to 0.26 MPa for the full spectrum of credible pump seal leaks. The CONTAIN calculations for Surry showed that the containment pressure at the time of lower head failure was ~0.15 MPa for the best-estimate 480-gpm/pump case. The Surry values are somewhat lower than similar assessments for Zion primarily because Surry is a subatmospheric plant. Condensation on internal structures and containment walls had a significant influence on the steam concentration in the containment atmosphere prior to vessel breach. It was predicted that the gases would not accumulate in the steam generator compartments or in the containment annulus for Zion or Surry.

During the time hydrogen was injected into the Zion containment, the global mixtures were nonflammable for the full spectrum of pump seal leaks. In the dome, for example, the steam concentration varied between approximately 40 - 60 percent as the hydrogen was injected while the hydrogen concentration was typically below 5 percent.

Insights were obtained on non DCH-induced hydrogen combustion in Zion using both the SCDAP/RELAP5 and CONTAIN calculations. The SCDAP/RELAP5 predictions were analyzed to determine what fraction, if any, of the hydrogen injected into the Zion containment would be consumed as an autoigniting jet. Furthermore, since the scenarios analyzed were station blackout scenarios, the autoigniting jets were considered to be the only possible ignition source for deflagrations in the containment. Therefore, CONTAIN predictions of the source compartments were analyzed to determine if mixtures were flammable at the time the jets autoignited. It was determined that the only possibility of jet autoignition in Zion would occur at the hot leg break in the case of no pump seal leak or in the case of a 480 gpm/pump leak, and these cases would depressurize so quickly that they would not be a DCH threat. Otherwise, the temperatures of the gases (~600 K) released from the power-operated relief valves (PORVs) were too low for autoignition for all cases, and the hydrogen concentration in the jet never exceeded ~5 percent and usually was zero. Likewise, gases released

from the RCPs likely would not autoignite in all of the cases analyzed because hydrogen concentrations in the jets were very low (~5 - 15 percent) during periods of high gas temperatures. Thus, the hydrogen concentration in the Zion containment just prior to vessel failure can be simply determined by summing all hydrogen released from the RCS.

Hydrogen combustion during venting from the RCS or combustion of hydrogen in the atmosphere prior to the DCH event was evaluated only for the best-estimate 480 gpm case in Surry. The SCDAP/RELAP5 predictions were analyzed to determine what fraction, if any, of the hydrogen injected into the containment would be consumed as an autoigniting jet. Furthermore, since the scenario analyzed was a station blackout scenario, the autoigniting jets were considered to be the only possible ignition source for deflagrations in the containment. The analyses indicated that autoignition would occur in the hot leg for a 480 gpm/pump leak, but that this case would depressurize so quickly that it would not be a DCH threat. The analyses also indicate the gases venting from the third RCP might also autoignite, but that only a negligible amount (~6 kg) of jet hydrogen would be consumed if the jet did autoignite. The atmosphere composition in the steam generator rooms were flammable at the time when the RCP pump might autoignite; however, only ~6 percent of the premixed hydrogen in the containment at that time would be consumed. We conclude that global mixtures in the dome were nonflammable during the period when hydrogen was injected into the Surry containment. Lastly, the possibility of autoigniting jets does little to alter the composition of the containment atmosphere prior to vessel breach for Westinghouse subatmospheric plants.

#### 4.4 Definition of Probability Levels

Our approach here recognizes that variability (i.e., statistical variations for nominally similar conditions) will probably be smaller than uncertainties in the phenomena themselves. We chose to use artificial probabilities as a tool to demonstrate relative variations in the probabilities of different outcomes. The numbers themselves have no quantitative value; they are important only in a relative sense. We used a physically based probability scale (Table 4.1) to quantify inputs and used the same scale to convert bottom-line results to a physical interpretation. The physical interpretations have been selected for the case of DCH within the context of the entire risk picture. We recognize that a probability of 0.01 might be considered very high in another context.

Empirically, it can be shown that the physical interpretation of the probability calculation is invariant relative to the numbers assigned to the judgmental degrees of belief, as long as the same geometrical progression is preserved. With our recommended assignment, the product of two "edge of spectrum" events ( $p \sim 10^{-1}$ ) is  $10^{-2}$ , which should be interpreted as an "upper bound." The interpretations in Table 4.1 might be given the alternative assignments: 1, 1/3, 1/9. Once again, the product of two "edge of spectrum" events ( $p \sim 1/3$ ) is 1/9, which should be interpreted physically as an "upper bound" with the new assignments. Therefore, the specific value of a judgmental degree of belief has no intrinsic meaning; it is only meaningful when measured against the physical assignment.

Our judgmental degree of belief for any process can be characterized as likely ( $p \sim 1$ ), as unlikely ( $p \sim 10^{-2}$ ), or as something in between ( $p \sim 10^{-1}$ ). As a practical matter, we assign  $p \sim 1$  to our best estimate and  $p \sim 10^{-2}$  to our estimate of a reasonable upper bound (assuming we have a reasonable

expectation that the upper bound is unlikely). The working group for NUREG/CR-6075, Supplement 1 concurred with this interpretation (Pilch et al., 1994b).

### 4.5 TCE/LHS Summary Quantifications

Table 4.2 provides a description of the TCE/LHS data input. Table 4.3 provides a concise summary of the TCE/LHS quantifications for every plant. Multiple entries for crmm, prcs, trcs, fdisp, and UO2m exist. The first entry corresponds to Scenarios V and Va and the second entry corresponds to Scenarios VI and VIa, as defined below. Multiple entries also exist for prcb and trcb. The first applies to Scenarios V and VI while the second applies to Scenarios Va and VIa.

### 4.6 Scenario V - SBLOCA with Repressurization of the RCS by Operator Intervention

Scenario V represents a core melt accident that progresses with water still present in the lower portions of the core. Such conditions lead to formation of a crust within the core followed by a massive release of melt when the crust fails. Accumulation of core material on the lower head of the RPV causes the lower head to heat up, eventually to the point where its structural strength is so degraded it can no longer withstand the stresses induced in the lower head by elevated RCS pressures. Thus, creep rupture of the lower head is the expected failure mechanism. The distinguishing feature of Scenario V is that operator actions are assumed to refill the RPV with water and to fully repressurize the RCS. Analysis of DCH for a repressurized RCS is deemed conservative because we expect operators to depressurize the RCS in a core damage accident.

Operator actions are assumed to repressurize the RCS to 16 MPa. Operator intervention refills the RPV with water to the hot leg nozzles and quenches any steam remaining in the RCS to near saturation (~700 K). Recall that at TMI-II a noncondensable gas bubble prevented operators from refilling the entire RCS. The RPV lower head must be heated by accumulated core material to the point that steel loses its strength (~1000 K), which leads to rupture of the lower head. The initial hole diameter is ~0.40 m (Pilch et al., 1994a) because of the likely presence of hot spots and because of stress concentrations associated with the existence and spacing of lower head penetrations. This rupture size is in accordance with working group recommendations (Appendix A in Pilch et al., 1994b) for Zion; experiments (Allen et al., 1991) at ~4 MPa driving pressures and the TCE model do not show a strong sensitivity to the initial hole size. The final hole size is computed with the ablation model, Eq. (5.3) for each plant, scenario, and Monte Carlo sampling; however, ablation is not important for the large initial hole sizes associated with rupture of the lower head.

Oxidation of Zr occurs predominantly before significant core degradation, as demonstrated in various calculations. In earlier two-dimensional MELPROG calculations performed by Kelly et al. (1987), 80 percent of the Zr oxidation occurred prior to formation of a molten pool. SCDAP/RELAP5 calculations (Appendix C in Pilch et al., 1994b) performed for Zion confirm these early assessments and show that nearly 100 percent of the hydrogen is produced before core slump. SCDAP/RELAP5 predicts similar behavior for Surry (Appendix E and Knudson and Dobbe, 1993). A dramatic reduction in oxidation is expected after clad relocation and freezing in the lower portions of the core as qualitatively observed in the DF-4 experiment (Gauntt et al., 1989). To a first order then, Zr oxidation is independent of the core melt progression that follows the main oxidation event; and



since oxidation occurs predominantly before formation of the molten pool, existing system-level computer codes are technically adequate to assess the range of possible oxidation.

Referring then to SCDAP/RELAP5 calculations (Knudson and Dobbe, 1993; Knudson, 1993; Appendix C in Pilch et al., 1994b; and Appendix E in Pilch et al., 1995), MELPROG/PWR-MOD1 calculations (Kelly et al., 1987), and CORMLT calculations (Denny and Sehgal, 1983), we find that the fraction of Zr oxidized ranges from 20 to 60 percent, with a mean around 40 percent. Observations from TMI-II fall into this range. Consistent with NUREG-1150 expert elicitations, the extremes of the distributions are considered unlikely ( $p \sim 0.01$ ). The distribution is shown in Figure 4.3. The calculations cited were chosen because of their explicit treatment of recirculating flow patterns in the core.

Consistent with TMI-II, the potential release of molten material to the lower head is controlled by the formation of a hemispherical crucible that excludes only the outer assemblies of the core (Figure 4.4). The outer assemblies are generally not expected to be in a severely degraded state because the RPV is flooded. We note that SCDAP/RELAP5 does predict melting of the outer assemblies in the region of the incore crucible. It is an imposed code requirement that the crucible grow to the core edge before relocation is allowed. We feel that asymmetries in crucible growth ensure that localized penetration of the outer assembly and the core barrel would most likely occur when the crucible has grown (on average) to the outer assembly. This is consistent with the observed end state at TMI-II.

We expect the melt mass to be a function of the core size for each plant; fortunately, there are only a limited number of core sizes for all Westinghouse plants. We note that the core size strongly correlates with the number of loops for Westinghouse plants. South Texas is an exception among four-loop plants in that its core is  $\sim 15\%$  taller. This has an impact on our quantifications for Scenario VI but not for Scenario V, being considered here, because the mass contained in a hemispherical crucible depends only on core diameter and not core height. The distribution for molten  $\text{UO}_2$  at vessel breach has been quantified previously for Westinghouse 4-loop (Zion) and 3-loop (Surry) plants in NUREG/CR-6075, Supplement 1 (Pilch et al., 1994b) and NUREG/CR-6109 (Pilch et al., 1995), respectively. The quantifications are repeated in Appendix B where core sizes for all PWRs (including Westinghouse 2-loop plants) are grouped and  $\text{UO}_2$  (molten) distributions quantified for Scenarios V and Va.

Figure 4.5 shows the distribution of molten  $\text{UO}_2$  in the lower plenum at the time of vessel rupture for Scenarios V and Va. As expected, the melt mass decreases with decreasing core size. The upper ends of the distributions correspond to a bottom failure of the crucible with the best estimate corresponding to a side failure of the crucible as observed in TMI-II. The quantifications recognize that  $\sim 15$  percent of the material contained in the crucible is  $\text{ZrO}_2$ . Furthermore, the quantifications take nominal credit for relocating melt that freezes ( $\sim 10$  mt) as a necessary condition to heat the lower head to rupture.

We conservatively assume bottom failure of the RPV so that all molten material is available for ejection into the cavity. Side peaked at fluxes could cause the lower head to fail near the pool surface if convecting molten pools are established in the lower plenum. For the same hole size ( $\sim 0.4$  m), scoping analyses based on published hydrodynamic entrainment criteria indicate that  $\sim 25$ -50

## Quantification of Initial Conditions

percent of the melt in the lower plenum cannot be entrained out the hole. The presence of an oxidic crust overlying the melt pool would likely enhance melt retention in the RPV. We note that credit was taken in NUREG-1150 for side failure of the RPV for Sequoyah as part of its DCH assessment.

The amount of molten  $ZrO_2$  in the melt is controlled by the amount of clad oxidation that occurs prior to core melt. The amount of molten  $ZrO_2$  can be estimated from

$$M_{ZrO_2} = \frac{M_{UO_2}(melt)}{M_{UO_2}(core)} M_{Zr}^0 f_{Zr} \frac{123}{91} \quad (4.1)$$

This expression assumes that  $ZrO_2$  is contained in the melt in the same fraction to which the core is degraded  $M_{UO_2}(degraded)/M_{UO_2}(core)$  and that  $ZrO_2$  relocates to the lower plenum in the same manner as the  $UO_2$ , that is,  $M_{UO_2}(melt)/M_{UO_2}(degraded)$ .

The relocation of Zr metal within the core plays a key role in the ultimate formation of core blockages. Upon melting, most of the Zr metal and  $(U,Zr)O_2$  relocates downward until it freezes in cooler portions of the core, forming partial or complete blockages, depending on the amount of relocating material. The subsequent melting of  $UO_2$  and  $ZrO_2$  allows molten oxides (at least initially) to settle and refreeze on top of the metallic blockages. In this way, the accumulating melt forms a crucible on top of the metallic blockage. This picture is consistent with SCDAP/RELAP5 calculations and TMI-II observations. This separation of molten oxides from the blockage, which consists of unoxidized clad and dissolution products, ensures that little metal enters the melt, except possibly through some additional formation of  $(U,Zr)O_2$  eutectics, dripping of Zr from fuel stubs above the degraded region, or when the crust fails. However, SCDAP/RELAP5 predicts only negligible additional formation of eutectics, and dripping is not predicted even in scenarios in which the core is completely dry. As observed in TMI-II, the crust is expected to fail locally (from inhomogeneities in the crust and asymmetries in crucible growth), carrying only small quantities of metal from the blockage into the lower plenum. The flooded core scenario precludes melting out of the blockage. Thus, little or no Zr is expected in the melt.

We note that SCDAP/RELAP5 calculations predict little or no Zr in the melt. However, to account for uncertainties in eutectic formation and crucible failure (and consistent with the working group recommendations), we assume that the molten Zr mass is proportional to the mass of molten  $UO_2$ . Thus, the amount of molten Zr can be computed from

$$M_{Zr} = 0.029 M_{UO_2} \quad (4.2)$$

The constant of proportionality (0.029), as estimated for Zion (Pilch et al., 1994b), is assumed to be applicable to all plants. We conservatively assume that any Zr that relocates with the melt does not oxidize as it falls through the water pool. Additional perspectives on this formulation are discussed in Section 4.7.

In a wet core scenario such as this, the control rod material will be an initial contributor to the metal blockage in the core and the flooded core scenario precludes melting out of the blockage.



Consequently, only trivial quantities (~0 mt) of control rod will be present in the melt at the time of vessel breach.

Melting of upper plenum steel is strongly correlated with failure of the surge line or hot leg nozzle at high system pressures (~8 MPa). Specifically, gas temperatures that are hot enough to melt upper plenum steel (~1700 K) are also hot enough to induce rupture (under pressure) of the hot leg or surge line. Upper plenum steel is a potential contributor to melt mass and composition only in those scenarios (Scenarios VII and VIII) that proceed to relatively low pressures at the time of vessel breach; and even then, SCDAP/RELAP5 predicts failure of the hot leg. In any case, melting of upper plenum steel cannot be important when operators reflood the RPV as they did in TMI-II. The small amount of steel initially in the core, like cladding and control rod material, is largely retained in core blockages, which cannot melt out in a flooded core scenario.

The melting of lower plenum steel by relocated core material is the only source of molten steel of potential importance in a DCH event. SCDAP/RELAP5 calculations show that some water is always present in the lower plenum, so the core debris cannot radiate to structures. Only thin lower plenum steel (e.g., nozzles) that is submerged in the accumulating core material is assumed to melt. The quantity of submerged steel depends on the volume of core material in the lower plenum and can be computed from

$$M_s = M_{s,LP} \frac{\frac{M_{UO_2}}{\rho_{UO_2}} + \frac{M_{ZrO_2}}{\rho_{ZrO_2}} + \frac{10 \times 10^3}{\rho_{UO_2/ZrO_2}} + \frac{M_{Zr}}{\rho_{Zr}} + \frac{M_{CRM}}{\rho_{CRM}}}{V_{LP}} \quad (4.3)$$

where the densities ( $\text{kg/m}^3$ ) are  $\rho_{UO_2} = 10,400$ ,  $\rho_{ZrO_2} = 5,900$ ,  $\rho_{UO_2/ZrO_2} = 9,660$ ,  $\rho_{Zr} = 6,500$ , and  $\rho_{CRM} = 9,250$ . Note that the quenched 10 mt must be taken into account because it is part of the volume of core material. We note that submerged nozzles at TMI-II did not all melt; consequently, Eq. (4.3) gives a conservative result.

Consideration of natural convection in volumetrically heated pools (Theofanous, 1988; Epstein and Fauske, 1989) indicates that the melt superheat cannot exceed ~200 K under steady-state conditions. These assessments are also consistent with SCDAP/RELAP5 analyses. The  $UO_2/ZrO_2$  eutectic melts at about 2800 K, so the maximum temperature on relocation is about 3000 K (~2900 K has been estimated for TMI-II), but some cooling on relocation is expected. Thus, we believe that a conservative bounding value of ~2800 K is appropriate for Scenario V.

Westinghouse containments can be classified as large dry, subatmospheric, or ice condenser. DCH resolution for plants with ice condenser containments is deferred to a future activity. Zion and Surry are representative of plants with large dry containments and subatmospheric containments, respectively. Our quantifications of containment conditions prior to vessel breach for Zion are taken as representative of all Westinghouse plants with large dry containments. A similar procedure is followed for plants with subatmospheric containments like Surry.

MAAP calculations for the Zion plant indicate that the containment pressure at vessel breach is about ~0.25 MPa and the conditions are saturated (~380 K). CONTAIN calculations (Tutu et al.,

1990) for the Zion plant produced 0.3 MPa at vessel breach. The most recent CONTAIN calculations (Appendix D in Pilch et al., 1994b), using sources from SCDAP/RELAP5, show containment pressures in excess of ~0.25 MPa up to and through the period of accumulator discharge. As a result, ~0.25 MPa is chosen as representative for our purposes, which is consistent with NUREG/CR-6075 (Pilch et al., 1994a). Appendix D in NUREG/CR-6075 (Pilch et al., 1994a) concludes that DCH loads are insensitive to reasonable choices of initial containment pressure (assuming fan coolers or sprays are not operational). The Zion containment is initially at atmospheric pressure, so approximately  $0.1 \text{ MPa} \times (400 \text{ K}/314 \text{ K}) \approx 0.13 \text{ MPa}$  of the pressure at vessel breach is air. Consequently, the initial steam concentration is ~48 percent.

Surry is a subatmospheric plant so the containment pressure at vessel breach could be somewhat lower than the ~0.25 MPa estimate for Zion (Pilch et al. 1994b). Supporting documentation for NUREG-1150 (NUREG/CR-4551) lists the containment pressure as ~0.18 MPa. MAAP calculations in support of the Surry IPE range from ~0.19 MPa to ~0.25 MPa, depending on the sequence. The most recent CONTAIN calculations, using sources from SCDAP/RELAP5 for a 480-gpm/pump RCP leak case, yield ~0.15 MPa at the time of vessel breach. As a result, ~0.18 MPa was chosen as representative of cases where active containment cooling is not operational. Appendix D in NUREG/CR-6075 (Pilch et al., 1994a) concludes that DCH loads are insensitive to reasonable choices of initial containment pressure (assuming fan coolers or sprays are not operational). The Surry containment is initially subatmospheric, so approximately  $0.069 \text{ MPa} \times (360 \text{ K}/314 \text{ K}) = 0.079 \text{ MPa}$  of the pressure at vessel breach is air. Consequently, the initial steam concentration is ~56 percent.

The containment conditions discussed above assume that active containment cooling systems (i.e., fan coolers or sprays) are not operational. We note that fan coolers were operational at TMI-II and that containment conditions were  $P \sim 0.11 \text{ MPa}$ ,  $T \sim 326 \text{ K}$ ,  $X_{\text{STM}} \sim 0.035$ , and  $X_{\text{H}_2} \sim 0.079$ . Thus, there was little steam in the containment. This situation will also be analyzed as Scenario Va in this report to better envelop the range of containment conditions.

The core-wide oxidation of Zr also controls the amount of preexisting hydrogen that can exist in the containment building at the time of vessel breach. The RCS retains very little of this hydrogen because it is produced early in the accident and most is vented to the containment. This is supported by earlier SCDAP/RELAP5 calculations (Knudson, 1993) where more than 90 percent of the  $\text{H}_2$  was released to the containment. Recent SCDAP/RELAP5 calculations performed for Zion (Appendix C in Pilch et al., 1994b) indicate that essentially all the hydrogen produced in-vessel will be released to the containment. Steam and  $\text{H}_2$  sources from SCDAP/RELAP5 are sometimes very hot (Appendix D in Pilch et al., 1994b) and there is a possibility that hydrogen will burn as it enters the containment. However, recent CONTAIN assessments for Zion (Pilch et al., 1994b) and Surry (Pilch et al., 1995) using SCDAP/RELAP5 sources suggest that this effect is minimal except possibly in the event of a hot leg failure, which precludes a DCH event. Consequently, we assume that all hydrogen produced in-vessel will be released to containment, where it will not burn prior to vessel breach. The moles of preexisting hydrogen in the containment are given by

$$N_{\text{H}_2} (\text{g} \cdot \text{mole}) = \frac{2}{0.091} f_{\text{Zr}} M_{\text{Zr}}^0 (\text{core}), \quad (4.4)$$

or alternatively, a concentration can be specified

$$X_{H_2} = \frac{N_{H_2}}{N_{ATM}^0} \quad (4.5)$$

We note that at TMI-II there was ~7.9 percent  $H_2$  in the atmosphere and essentially no steam. Even though these conditions are in the flammable regime, we cannot guarantee that a random ignition source (unless intentional) will burn off the hydrogen prior to vessel failure if the flammability limits are exceeded.

#### 4.7 Scenario VI - SBLOCA under Wet Core Conditions

In the absence of any RCS leaks, SCDAP/RELAP5 (Pilch et al., 1994b, 1995) predicts surge line failure long before bottom head failure. These cases fully depressurize and are of no interest for DCH. We then sought SBLOCAs of just the right size to depressurize sufficiently that natural circulation degrades to the point that surge line or hot leg failure is not assured. Such an intermediate state was not found. In fact, SCDAP/RELAP5 predicts hot leg failure before core relocation for the full spectrum of SBLOCAs; consequently, Scenario VI can only exist as the consequence of partial operator intervention. Owing to the similarity in Scenarios V and VI, we emphasize only the differences in RCS temperature, melt mass, and composition, with all other parameters developed in a manner similar to that for Scenario V.

The RCS gas at the time of vessel breach clearly must be superheated. In conjunction with the pressure and volume, the moles of gas in the RCS can be computed with the RCS temperature. The gas temperatures in each region of the RCS are estimated from SCDAP/RELAP5 output for Zion (Pilch et al., 1994b). Given this assessment, a lower bound of ~1000 K is assigned to this scenario.

The potential release of molten material to the lower head is again controlled by the formation and failure of a crucible in the core region. Water occupies only the lowest regions of the core, so radial cooling of a growing crucible is reduced in this situation, and consistent with SCDAP/RELAP5 predictions, the crucible could take on the bounding shape of an upright cylinder as depicted in Figure 4.6. We note that SCDAP/RELAP5 conservatively assumes that the melt pool must grow to the core boundary as a condition for core relocation, thus SCDAP/RELAP5 shows some localized involvement of the outer assemblies. We expect, however, that asymmetries in crucible growth ensure that localized penetration of the outer assembly and core barrel would likely occur when the crucible has grown (on average) to the outer assembly. Consequently, the outer assemblies are excluded from our assessments.

The distribution for molten  $UO_2$  at vessel breach has been quantified previously for Westinghouse 4-loop and 3-loop plants in NUREG/CR-6075, Supplement 1 (Pilch et al., 1994b) and NUREG/CR-6109 (Pilch et al., 1995), respectively. The quantifications are repeated in Appendix B where core sizes for all PWRs (including Westinghouse 2-loop plants) are grouped and  $UO_2$  (molten) distributions quantified for Scenario VI. South Texas is treated separately as its core is ~15% taller than other four-loop plants.

## Quantification of Initial Conditions

Figure 4.7 shows the distribution of molten  $\text{UO}_2$  in the lower plenum at the time of vessel rupture for Scenario VI. As expected, the melt mass decreases with decreasing core size. The upper ends of the distributions correspond to a bottom failure of the crucible with the best estimate corresponding to a side failure of the crucible as observed in TMI-II. The quantifications recognize that some of the material contained in the crucible is  $\text{ZrO}_2$ . Furthermore, the quantifications take nominal credit for relocating melt that freezes ( $\sim 10$  mt) as a necessary condition to heat the lower head to rupture.

Scenario VI is envisioned as having water in the lower plenum, but not to the extent that it submerges the bottom of the core. Under such circumstances, it is possible for low melting point control rod material to relocate to the lower plenum. SCDAP/RELAP5 calculations for Surry (Knudson and Dobbe, 1993; Quick and Knudson, Appendix E in Pilch et al., 1995) suggest that  $\sim 2$  mt of control rod material may relocate into the lower plenum when the core is not submerged. Although this material will quench in lower plenum water or on the lower head, we conservatively assume that the subsequent relocation of large quantities of oxide material will remelt all the control rod material and heat it to the oxide temperature ( $\sim 2800\text{K}$ ). The amount of molten control rod material for other plants is obtained from the Surry value by scaling on the square of the core diameter.

We note that SCDAP/RELAP5 calculations predict little or no Zr in the melt. However, to account for uncertainties in eutectic formation and crucible failure, we assume that the molten Zr mass is 2.9 percent of the molten  $\text{UO}_2$  mass (Eq. 4.2). Although SCDAP/RELAP5 does not predict relocation of the metallic blockage, we acknowledge that scenarios where the bottom of the core is not submerged in water have an increased potential for partial melting and relocation of the metallic blockage into the lower plenum. We note, however, that complete oxidation of the Zr in prototypic core melts was observed in a FARO experiment involving melt drainage into a pressurized water pool. More importantly, however, are SCDAP/RELAP5 predictions that the RCS will be depressurized in those scenarios that have the greatest potential for relocation of the metallic blockage.

It is useful to examine the recommended Zr content of the melt from alternative perspectives. The recommended formulation is equivalent to a hypostoichiometry of urania, which can be expressed as  $\text{UO}_{2-x}$ , where  $x \sim 0.17$ . One can also perform a mass balance on the Zr inventory. For instance, the core contains 16.5 mt of Zr in Surry. On a core-wide basis,  $\sim 40$  percent of Zr is oxidized, so  $\sim 9.9$  mt of Zr metal remains. About 26 percent of the initial Zr inventory resides in the cooler outer assemblies, which are not part of the degraded core debris. Assuming only 20 percent oxidation in the outer assemblies, about 3.4 mt of Zr will remain in the outer assemblies and the remaining 6.5 mt will be retained in the core blockage. At the upper end of the Scenario VI  $\text{UO}_2$  distribution,  $\sim 1.6$  mt of Zr will relocate to the lower plenum. This represents  $\sim 25$  percent of the Zr inventory in the metal blockage. These perspectives on possible Zr relocation coupled with the likelihood of complete oxidation on relocation and low RCS pressures, support the bounding nature of our assessments, even in scenarios where the core is not submerged in water.

The fraction of Zr oxidized envelops the range of expected behavior here also. In fact, the code calculations cited previously are more closely analogous to this scenario. This, in conjunction with the causal relations (Eqs. 4.1 - 4.4) developed in Section 4.6, defines the remaining melt constituents and atmosphere compositions. We acknowledge that active containment cooling could produce conditions



in the containment atmosphere with little or no steam as occurred at TMI-II. This situation will also be analyzed as Scenario VIa in this report to better envelop the range of containment conditions.

#### 4.8 Nomenclature

$f_{Zr}$	=	fraction of Zr oxidized core-wide
$M_{CRM}$	=	mass of control rod material in melt at vessel failure
$M_{Zr}^0$	=	mass of Zr initially in core
$M_s$	=	mass of steel in melt at vessel failure
$M_{s,LP}$	=	mass of steel in lower plenum
$M_{UO_2}$	=	mass of $UO_2$ in melt at vessel failure
$M_{Zr}$	=	mass of Zr in melt at vessel failure
$M_{ZrO_2}$	=	mass of $ZrO_2$ in melt at vessel failure
$N_{ATM}^0$	=	atmosphere moles in containment just prior to vessel failure
$N_{H_2}$	=	mole of hydrogen produced from Zr oxidation
$P$	=	initial containment pressure
$T$	=	initial containment temperature
$V_{LP}$	=	volume of lower plenum
$X_{H_2}$	=	hydrogen concentration in the containment atmosphere
$X_{stm}$	=	steam concentration in the containment atmosphere

#### Greek

$\rho_{CRM}$	=	mass density of control rod material
$\rho_{UO_2}$	=	mass density of $UO_2$
$\rho_{UO_2/ZrO_2}$	=	mass density of $UO_2/ZrO_2$ eutectic
$\rho_{Zr}$	=	mass density of Zr
$\rho_{ZrO_2}$	=	mass density of $ZrO_2$



**Table 4.1 Definition of probability levels**

Process Likelihood	Process Characteristics
~1	Behavior is within known trends - best estimate.
$10^{-1}$	Behavior is within known trends but obtainable only at the edge of spectrum parameter.
$10^{-2}$	Behavior cannot be positively excluded - upper bound.

Table 4.2 Description of TCE/LHS summary quantifications

Variable	Units	Description
tthead	m	Thickness of RPV lower head. Used in hole ablation calculations.
vlp	m <sup>3</sup>	Volume of RPV lower plenum, which is defined as that portion of the RPV volume located below the core. Determines how much thin lower plenum steel is submerged by melt.
dh0	m	Initial diameter of lower head failure site before hole ablation occurs. Used in hole ablation calculations.
tw0	K	Outside surface temperature of lower head at vessel breach. Used in hole ablation calculations.
crmm	kg	Mass of control rod material in the melt.
uo2m0	kg	Total inventory of UO <sub>2</sub> in the core prior to core damage.
zrm0	kg	Total mass of zircaloy in the core prior to core damage.
stlmp	kg	Total mass of thin (meltable) steel in the lower plenum.
cohmul	----	Plant-specific constant in coherence ratio correlation.
prcs	Pa	RCS pressure at vessel breach.
vracs	m <sup>3</sup>	RCS volume.
trcs	K	Average RCS gas temperature at vessel breach.
proboc	Pa	Pressure in the reactor containment building at operating conditions.
trboc	K	Atmosphere temperature in the reactor containment building at operating conditions.
prcb	Pa	Pressure in the reactor containment building at vessel breach.
trcb	K	Atmosphere temperature in the reactor containment building at vessel breach.
vrcb	m <sup>3</sup>	Volume of the reactor containment building.
vcav	m <sup>3</sup>	Volume of the reactor cavity.
fasub	----	Fraction of dispersed debris retained in the subcompartments (vs. bypass plus carryover to the dome).
fsub	----	Volume of the subcompartment region that predominantly traps debris normalized by the containment volume. Set to an arbitrarily small value in this study.
tautoig	K	Autoignition temperature for sudden volumetric combustion of hydrogen in the dome.
tdeb	K	Temperature of molten debris as it is ejected from the RPV.
fzrel	----	Fraction of Zr blockage relocated to lower head. This parameter is disabled and is no longer used. The default of 0.0 should always be used.
fh2rcs	----	Fraction of all hydrogen production by Zr/steam reactions in the RPV that remains in the RCS at the time of vessel breach.
feject	----	Fraction of melt in the lower head of the RPV that is ejected into the reactor cavity.
fdisp	----	Fraction of melt ejected from RPV into the cavity that is then dispersed from the reactor cavity.

**Table 4.2 Description of TCE/LHS summary quantifications**

Variable	Units	Description
zro2ml	----	Multiplier on calculation of $ZrO_2$ . This parameter is no longer used and the default value of 1.0 should always be used.
stimul	----	Multiplier on steel mass. This parameter is no longer used and the default value of 0.0 should always be used.
uo2m	kg	Piecewise linear, cumulative distribution of $UO_2$ mass.
stlmi	----	Piecewise linear, cumulative distribution of molten steel in addition to lower plenum steel that is submerged. Set to an arbitrarily small value in this study.
fzrox	----	Piecewise, linear, cumulative distribution of core zirconium oxidized prior to vessel breach.
cohdis	----	Distribution of the coherence ratio.
subdis	----	Distribution for fraction of dispersed melt trapped in subcompartment (fasub). The distribution is normal with a default mean of 0.0. Any other value would represent a relative bias. The relative standard deviation must also be input. Set to an arbitrarily small value in this study.
zdist	----	Distribution on the Kg-Zr per Kg- $UO_2$ in the melt. The distribution is normal with a default mean of 0.0. Any other value would represent a relative bias. The relative standard deviation must also be input. Set to an arbitrarily small value in this study.
tcedist	----	Distribution for modeling uncertainty in TCE pressure rise predictions. The distribution is normal with a default mean of 0.0. Any other value would represent a relative bias. The relative standard deviation must also be input. Set to an arbitrarily small value in this study.
pfail	----	Piecewise linear, cumulative distribution for the containment fragility.

Table 4.3 Summary of TCE/LHS input

	BV1,2	Byron1,2,	Braidwood 1,2	Callaway	Comanche 1,2	Diablo Can.1,2	Farley 1,2	Ginna	HB Robinson 2
tthead	0.13	0.14	0.14	0.14	0.15	0.14	0.13	0.11	0.13
vlp	24.5	28.1	28.1	28.1	25.8	28.1	20.8	12.6	24.5
dh0	0.4	0.4	0.4	0.4	0.4	0.4	0.4	0.4	0.4
tw0	1000	1000	1000	1000	1000	1000	1000	1000	1000
crmm	0/2000	0/2120	0/2120	0/2120	0/2120	0/2280	0/1800	0/1240	0/2000
uo2m0	80091	101245	101245	101245	101202	101202	80909	47955	79727
zrm0	16500	23142	23142	23142	21360	21360	16364	11785	18909
stlmlp	10000	10000	10000	10000	10000	10000	7800	5800	7800
cohmul	12.2	9.661	9.661	12.2	9.661	9.661	12.2	12.2	12.2
prcs	16e6/8e6	16e6/8e6	16e6/8e6	16e6/8e6	16e6/8e6	16e6/8e6	16e6/8e6	16e6/8e6	16e6/8e6
racs	274	347	347	347	340	318	282	192	271
trcs	700/1000	700/1000	700/1000	700/1000	700/1000	700/1000	700/1000	700/1000	700/1000
prcboc	6.90e+04	1.00e+05	1.00e+05	1.00e+05	1.00e+05	1.00e+05	1.00e+05	1.00e+05	1.00e+05
trcboc	316	316	316	316	316	316	316	316	316
prcb	1.5E5/6.9e4	2.5e5/1.0e5	2.5e5/1.0e5	2.5e5/1.0e5	2.5e5/1.0e5	2.5e5/1.0e5	2.5e5/1.0e5	2.5e5/1.0e5	2.5e5/1.0e5
trcb	360/316	400/316	400/316	400/316	400/316	400/316	400/316	400/316	400/316
vrcb	4.99e+04	8.21e+04	8.21e+04	7.07e+04	8.43e+04	7.44e+04	5.49e+04	2.82e+04	5.95e+04
vcav	251	339	339	488	385	377	300	278	248
fasub	0.762	0.821	0.821	0.826	0.782	0.794	0.801	0.815	0.379
fvsb	0.01	0.01	0.01	0.01	0.01	0.01	0.01	0.01	0.01
tautoig	950	950	950	950	950	950	950	950	950
tdeb	2800	2800	2800	2800	2800	2800	2800	2800	2800
fzrel	0	0	0	0	0	0	0	0	0
fh2rcs	0	0	0	0	0	0	0	0	0
fejec	1	1	1	1	1	1	1	1	1
fdisp	0.91/0.92	0.93/0.93	0.93/0.93	0.90/0.90	0.91/0.91	0.91/0.91	0.91/0.91	0.77/0.87	0.91/0.92
zro2ml	1	1	1	1	1	1	1	1	1
stlmul	0	0	0	0	0	0	0	0	0
uo2m	Tbl B3,B6, 3-L	Tbl B3,B6, 4-L	Tbl B3,B6, 4-L	Tbl B3,B6, 4-L	Tbl B3,B6, 4-L	Tbl B3,B6, 4-L	Tbl B3,B6, 3-L	Tbl B3,B6, 2-L	Tbl B3,B6, 3-L
stlmi	1.00e-06	1.00e-06	1.00e-06	1.00e-06	1.00e-06	1.00e-06	1.00e-06	1.00e-06	1.00e-06
fzrox	Figure 4.3	Figure 4.3	Figure 4.3	Figure 4.3	Figure 4.3	Figure 4.3	Figure 4.3	Figure 4.3	Figure 4.3
cohdist	0.18	0.29	0.29	0.18	0.29	0.29	0.18	0.18	0.18
subdis	0,1.0e-3	0,1.0e-3	0,1.0e-3	0,1.0e-3	0,1.0e-3	0,1.0e-3	0,1.0e-3	0,1.0e-3	0,1.0e-3
zdist	0,1.0e-3	0,1.0e-3	0,1.0e-3	0,1.0e-3	0,1.0e-3	0,1.0e-3	0,1.0e-3	0,1.0e-3	0,1.0e-3
lcedist	0,1.0e-3	0,1.0e-3	0,1.0e-3	0,1.0e-3	0,1.0e-3	0,1.0e-3	0,1.0e-3	0,1.0e-3	0,1.0e-3
pfail	Table D.2	Table D.2	Table D.2	Table D.2	Table D.2	Table D.2	Table D.2	Table D.2	Table D.2

**Table 4.3 Summary of TCE/LHS input (continued)**

	Indian Point 2,3	Kewaunee	Millstone 3	N. Anna 1,2	Point Beach 1,2	Prairie Island 1,2	Salem 1,2	Seabrook 1
tlhead	0.14	0.11	0.14	0.13	0.11	0.11	0.14	0.14
vlp	28.1	12.6	28.1	24	12.6	12.6	28.4	28.1
dh0	0.4	0.4	0.4	0.4	0.4	0.4	0.4	0.4
tw0	1000	1000	1000	1000	1000	1000	1000	1000
crmm	0/2280	0/1320	0/2280	0/1920	0/1480	0/1240	0/2120	0/2120
uo2m0	100909	54232	101245	80909	54604	54936	97369	101245
zrm0	19088	11110	23142	16364	11027	11095	20320	23142
stlmlp	10000	5800	10000	7800	5800	5800	10000	10000
cohmul	9.661	12.2	12.2	12.2	12.2	12.2	9.661	9.661
prcs	16e6/8e6	16e6/8e6	16e6/8e6	16e6/8e6	16e6/8e6	16e6/8e6	16e6/8e6	16e6/8e6
vrcs	355	177	338	282	187	194	376	347
trcs	700/1000	700/1000	700/1000	700/1000	700/1000	700/1000	700/1000	700/1000
prcboc	1.00e+05	1.00e+05	6.90e+04	6.90e+04	1.00e+05	1.00e+05	1.00e+05	1.00e+05
trcboc	316	316	316	316	316	316	316	316
prcb	2.5e5/1.0e5	2.5e5/1.0e5	1.5e5/6.9e4	1.5e5/6.9e5	2.5e5/1.0e5	2.5e5/1.0e5	2.5e5/1.0e5	2.5e5/1.0e5
trcb	400/316	400/316	360/316	360/316	400/316	400/316	400/316	400/316
vrcb	7.39e+04	3.83e+04	6.51e+04	5.16e+04	2.83e+04	3.83e+04	7.41e+04	7.64e+04
vcav	286	136	232	252	157	143	251	491
fasub	0.825	0.068	0.915	0.844	0.411	0.068	0.770	0.827
fvsb	0.01	0.01	0.01	0.01	0.01	0.01	0.01	0.01
tautoig	950	950	950	950	950	950	950	950
tdeb	2800	2800	2800	2800	2800	2800	2800	2800
fzrel	0	0	0	0	0	0	0	0
fh2rcs	0	0	0	0	0	0	0	0
fejec	1	1	1	1	1	1	1	1
fdisp	0.94/0.94	0.87/0.93	0.94/0.94	0.91/0.92	0.85/0.92	0.86/0.92	0.94/0.94	0.91/0.91
zro2ml	1	1	1	1	1	1	1	1
stlmul	0	0	0	0	0	0	0	0
uo2m	Tbl B3,B6, 4-L	Tbl B3,B6, 2-L	Tbl B3,B6, 4-L	Tbl B3,B6, 3-L	Tbl B3,B6, 2-L	Tbl B3,B6, 2-L	Tbl B3,B6, 4-L	Tbl B3,B6, 4-L
stlmi	1.00e-06	1.00e-06	1.00e-06	1.00e-06	1.00e-06	1.00e-06	1.00e-06	1.00e-06
fzrox	Figure 4.3	Figure 4.3	Figure 4.3	Figure 4.3	Figure 4.3	Figure 4.3	Figure 4.3	Figure 4.3
cohdist	0.29	0.18	0.18	0.18	0.18	0.18	0.29	0.29
subdis	0,1.0e-3	0,1.0e-3	0,1.0e-3	0,1.0e-3	0,1.0e-3	0,1.0e-3	0,1.0e-3	0,1.0e-3
zdist	0,1.0e-3	0,1.0e-3	0,1.0e-3	0,1.0e-3	0,1.0e-3	0,1.0e-3	0,1.0e-3	0,1.0e-3
tcedist	0,1.0e-3	0,1.0e-3	0,1.0e-3	0,1.0e-3	0,1.0e-3	0,1.0e-3	0,1.0e-3	0,1.0e-3
pfail	Table D.2	Table D.2	Table D.2	Table D.2	Table D.2	Table D.2	Table D.2	Table D.2



Table 4.3 Summary of TCE/LHS input (concluded)

	S. Harris 1	S. Texas 1,2	Summer	Surry 1,2	Turkey Pt. 3,4	Vogtle 1,2	Wolf Creek	Zion 1,2
lthead	0.13	0.14	0.13	0.13	0.13	0.14	0.14	0.14
vlp	24.5	18.9	24.5	25.9	24.5	28.1	28.1	28.1
dh0	0.4	0.4	0.4	0.4	0.4	0.4	0.4	0.4
tw0	1000	1000	1000	1000	1000	1000	1000	1000
crmm	0/2080	0/2660	0/1920	0/2000	0/2000	0/2280	0/2280	0/2280
uo2m0	80636	118636	82366	80091	81364	101245	101245	98455
zrm0	17729	24927	17377	16500	16181	23142	23142	20249
stlmlp	7800	10000	7800	7800	7800	10000	10000	10000
cohmui	12.2	14.6	12.2	12.2	12.2	9.661	12.2	9.661
prcs	16e6/8e6	16e6/8e6	16e6/8e6	16e6/8e6	16e6/8e6	16e6/8e6	16e6/8e6	16e6/8e6
vrsc	274	401	273	274	284	347	347	369
trcs	700/1000	700/1000	700/1000	700/1000	700/1000	700/1000	700/1000	700/1000
prcboc	1.00e+05	1.00e+05	1.00e+05	6.90e+04	1.00e+05	1.00e+05	1.00e+05	1.00e+05
trcboc	316	316	316	316	316	316	316	316
prcb	2.5e5/1.0e5	2.5e5/1.0e5	2.5e5/1.0e5	1.5e5/6.9e4	2.5e5/1.0e5	2.5e5/1.0e5	2.5e5/1.0e5	2.5e5/1.0e5
trcb	400/316	400/316	400/316	360/316	400/316	400/316	400/316	400/316
vrcb	7.07e+04	9.34e+04	5.34e+04	5.09e+04	4.39e+04	7.64e+04	7.07e+04	8.09e+04
vcav	256	304	284	360	303	275	275	230
fasub	0.917	0.838	0.902	0.835	0.819	0.881	0.831	0.875
fvsb	0.01	0.01	0.01	0.01	0.01	0.01	0.01	0.01
tautoig	950	950	950	950	950	950	950	950
tdeb	2800	2800	2800	2800	2800	2800	2800	2800
fzrrel	0	0	0	0	0	0	0	0
fh2rcs	0	0	0	0	0	0	0	0
fejec	1	1	1	1	1	1	1	1
fdisp	0.91/0.92	0.92/0.92	0.90/0.92	0.88/0.90	0.89/0.91	0.93/0.93	0.93/0.93	0.95/0.95
zro2ml	1	1	1	1	1	1	1	1
stlmui	0	0	0	0	0	0	0	0
uo2m	Tbl B3,B6, 3-L	Tbl ,B3,B6, 4-L	Tbl B3,B6, 3-L	Tbl B3,B6, 3-L	Tbl B3,B6, 3-L	Tbl B3,B6, 4-L	Tbl B3,B6, 4-L	Tbl B3,B6, 4-L
stlmi	1.00e-06	1.00e-06	1.00e-06	1.00e-06	1.00e-06	1.00e-06	1.00e-06	1.00e-06
fzrox	Figure 4.3	Figure 4.3	Figure 4.3	Figure 4.3	Figure 4.3	Figure 4.3	Figure 4.3	Figure 4.3
cohdist	0.18	0.33	0.18	0.18	0.18	0.29	0.18	0.29
subdis	0,1.0e-3	0,1.0e-3	0,1.0e-3	0,1.0e-3	0,1.0e-3	0,1.0e-3	0,1.0e-3	0,1.0e-3
zdist	0,1.0e-3	0,1.0e-3	0,1.0e-3	0,1.0e-3	0,1.0e-3	0,1.0e-3	0,1.0e-3	0,1.0e-3
tcedist	0,1.0e-3	0,1.0e-3	0,1.0e-3	0,1.0e-3	0,1.0e-3	0,1.0e-3	0,1.0e-3	0,1.0e-3
pfail	Table D.2	Table D.2	Table D.2	Table D.2	Table D.2	Table D.2	Table D.2	Table D.2

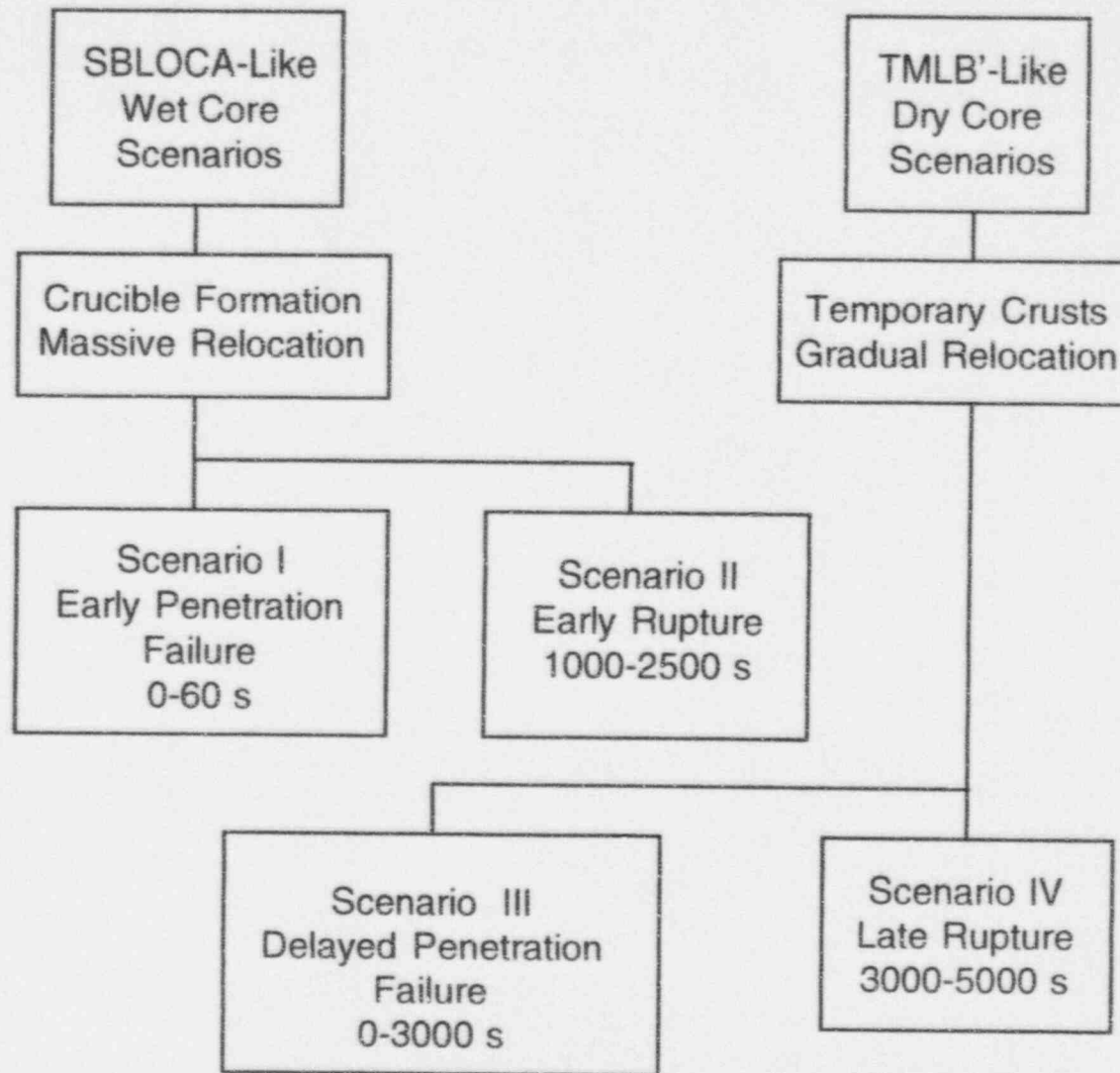


Figure 4.1. Splinter DCH scenarios used in NUREG/CR-6075.

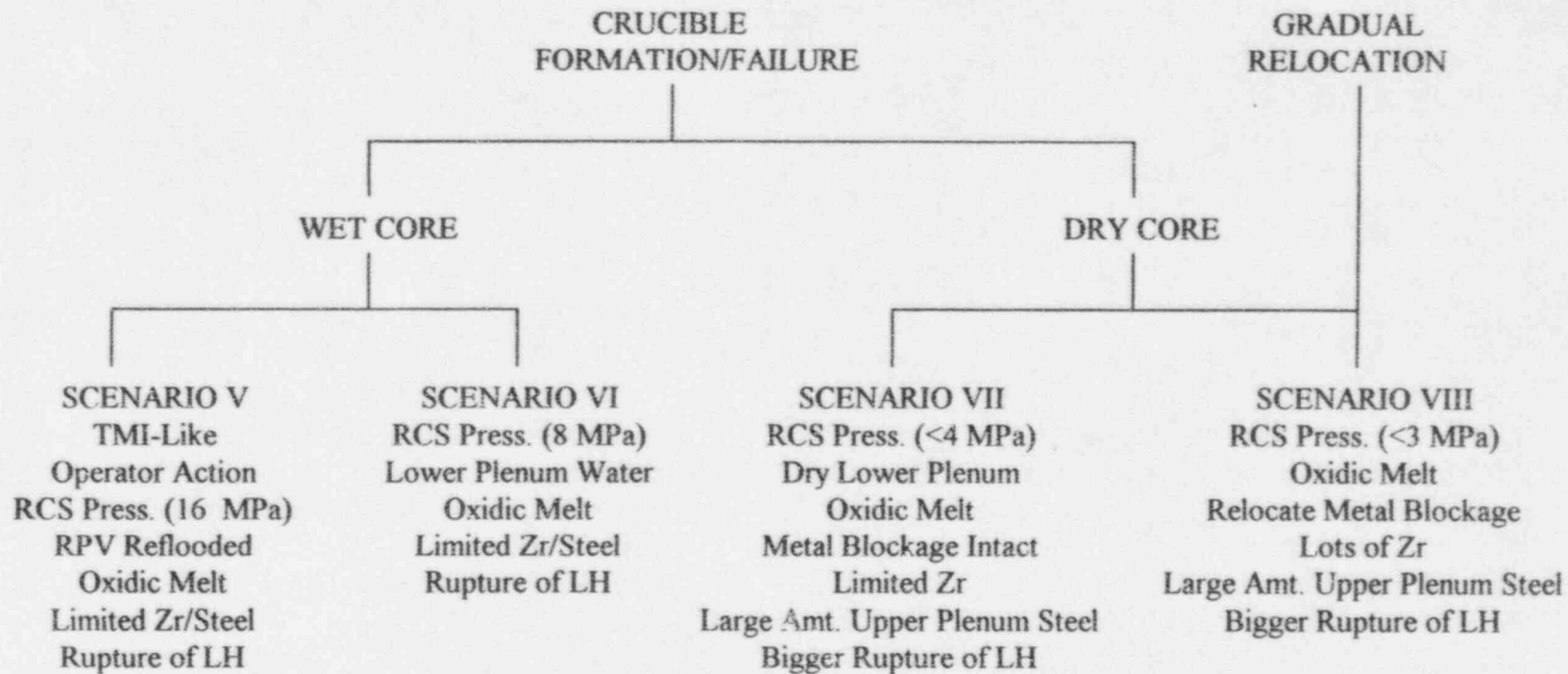


Figure 4.2. Splinter DCH scenarios reflecting working group recommendations.

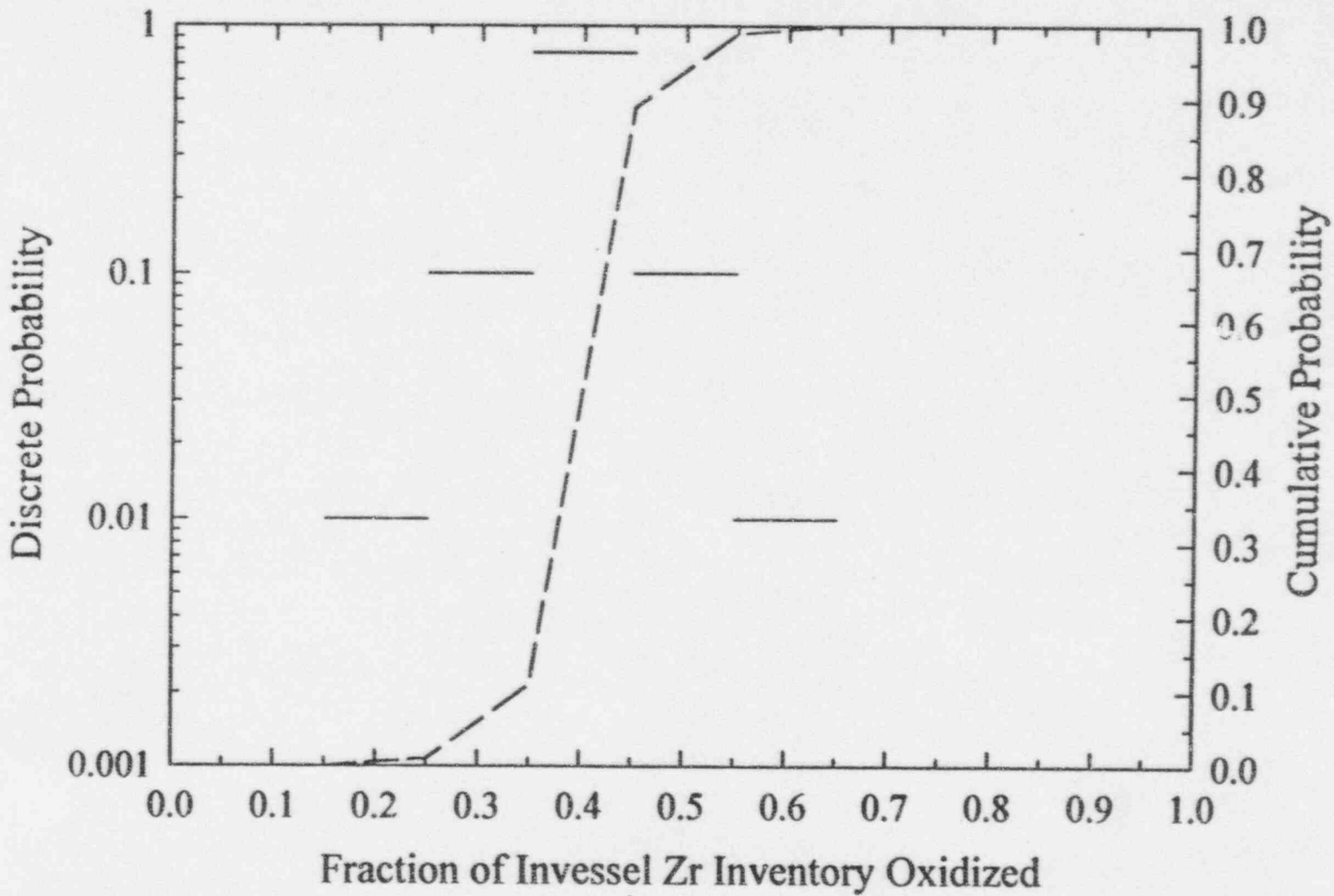


Figure 4.3. Distribution for fraction of Zr oxidized (core-wide) in Scenarios V and VI.

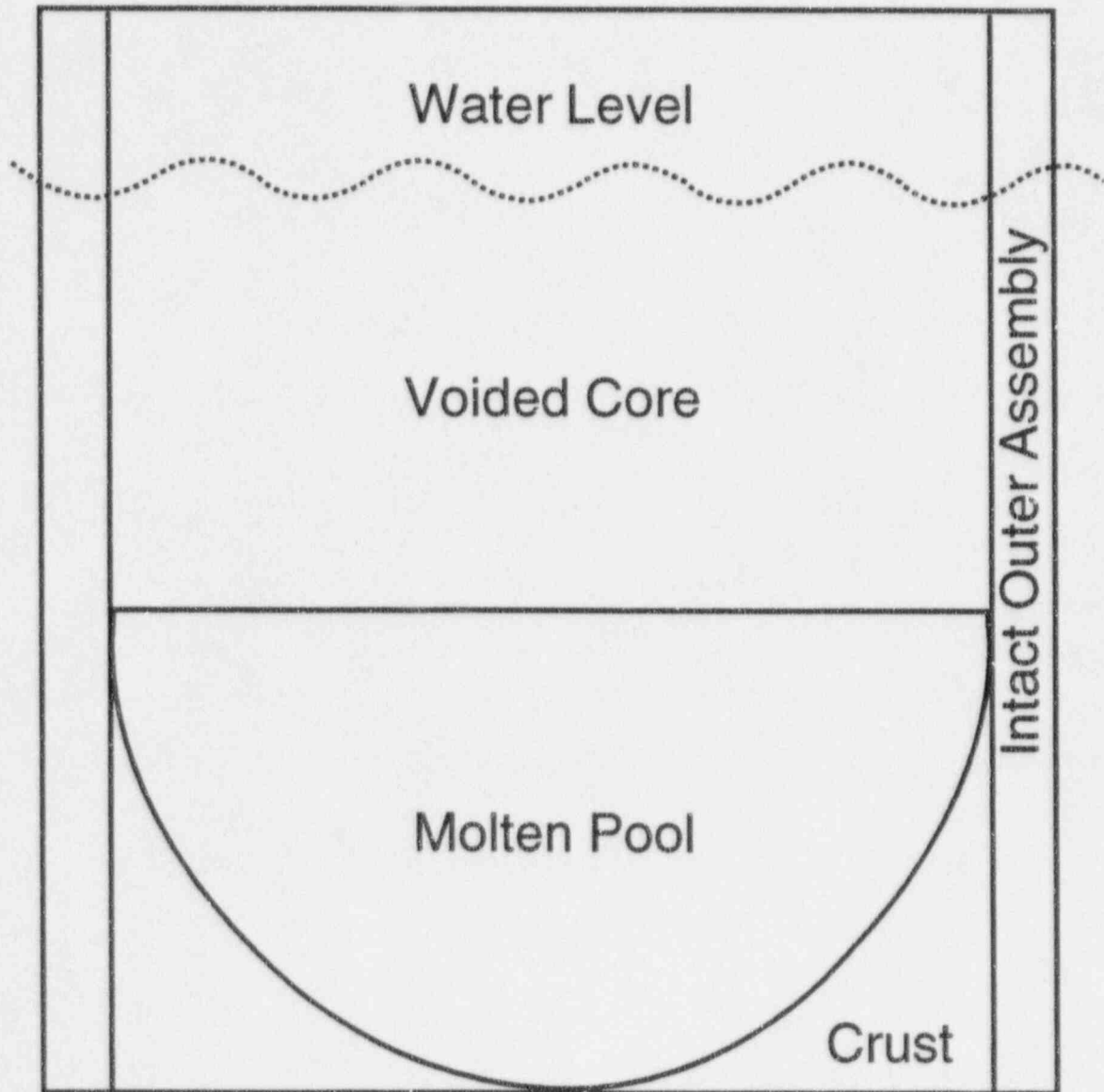


Figure 4.4. Crucible formation in a flooded RPV - Scenarios V and Va.



# Quantification of Initial Conditions

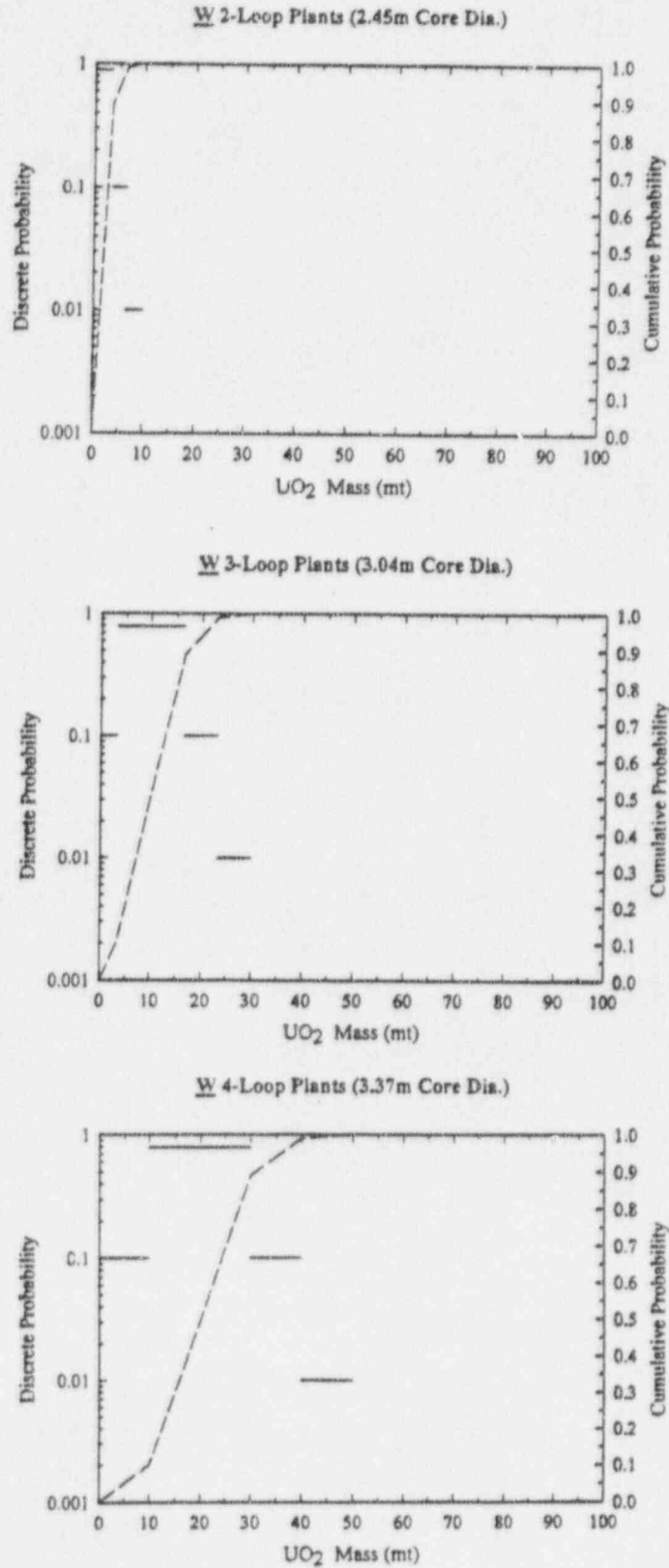


Figure 4.5. Distribution of molten  $UO_2$  in the lower plenum at the time of vessel rupture for Scenarios V and Va.

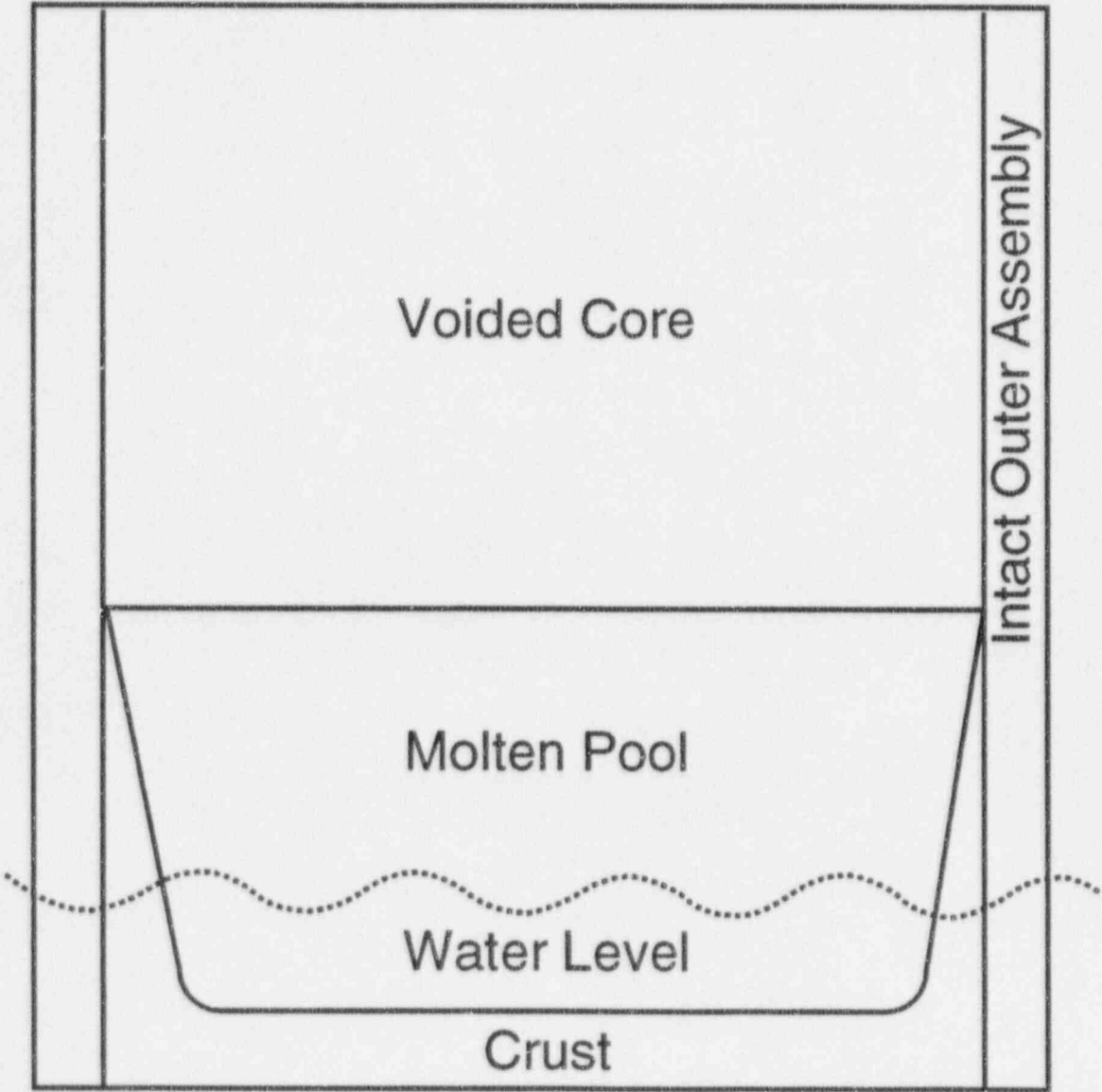


Figure 4.6. Crucible formation in wet core scenarios with partial operator intervention - Scenarios VI and VIa.

Quantification of Initial Conditions

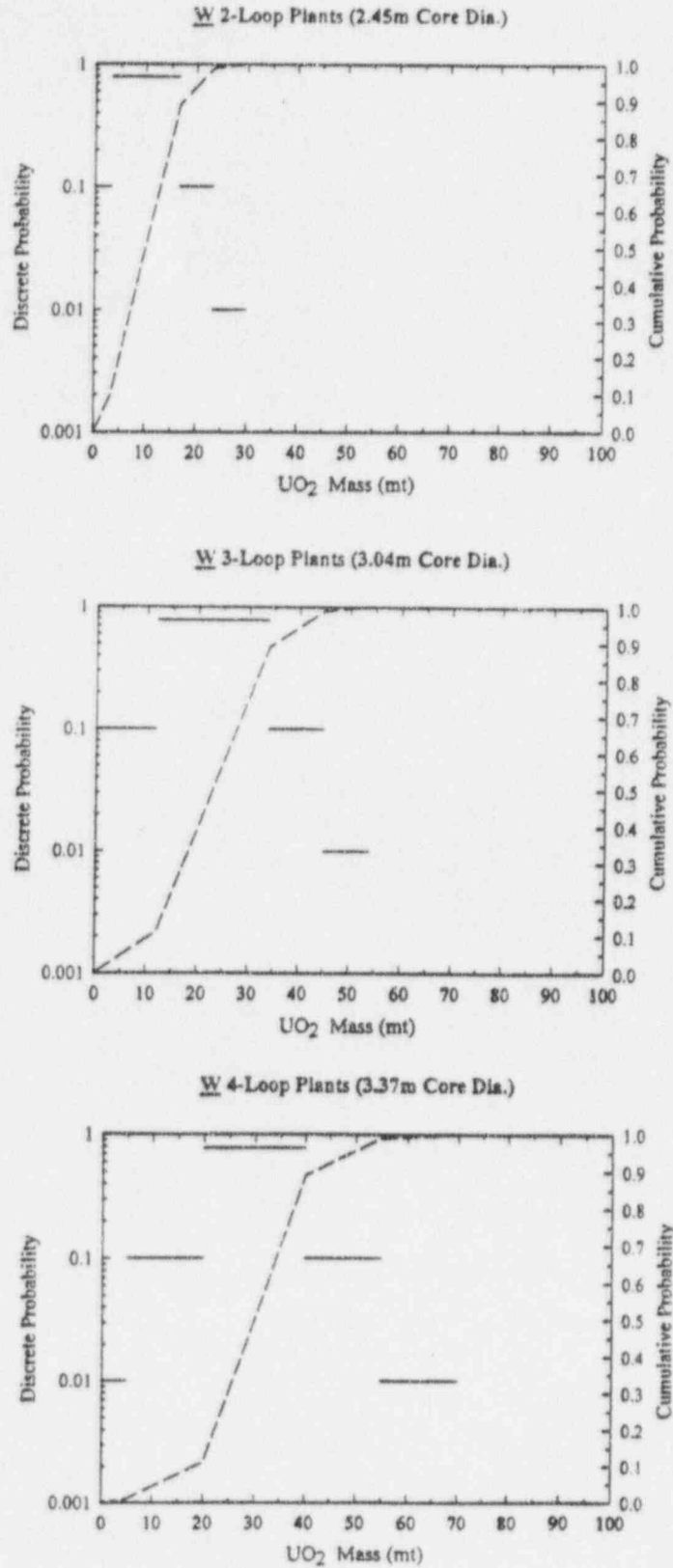


Figure 4.7. Distribution for molten UO<sub>2</sub> in the lower plenum at the time of vessel rupture for Scenarios VI and VIa.

## 5.0 QUANTIFICATION OF THE DCH PHENOMENA

The quantification of the DCH phenomenon is carried out by means of a causal relation (CR1) for the containment load. CR1 is fulfilled here by the two-cell equilibrium model, which is developed in Appendix E of NUREG/CR-6075 (Pilch et al., 1994a). Refinements to the hydrogen combustion models are documented in Appendix E of NUREG/CR-6075, Supplement 1 (Pilch et al., 1994b). In the TCE model, the containment pressurization can be written in terms of the various energy sources (blowdown, latent and sensible heat of debris, oxidation of metallic debris constituents, and hydrogen combustion) that can contribute to DCH,

$$\frac{\Delta P}{P_c^0} = \eta \frac{\sum \Delta E_i}{U^0(1 + \psi)}, \quad (5.1)$$

where  $\eta$  is an efficiency of containment pressurization due to the combined processes of blowdown, heating of the atmosphere, and hydrogen combustion. The efficiency accounts for compartmentalized geometry of the containment and accounts for mitigation that is due to the noncoherence of debris dispersal and blowdown processes. The TCE model has been validated against the extensive database that is summarized in Table 5.1. Figure 5.1 compares model predictions with the relevant database. The TCE model attempts to represent the dominant processes contributing to DCH loads using a fast running code that meets the needs of the issue resolution effort; there is no claim that it captures every detail of DCH phenomenology.

Appendix C of NUREG/CR-6109 (Pilch et al., 1995) gives an overview of other available models that have been used to predict DCH loads. In particular, the convection limited containment heating (CLCH) model (Yan and Theofanous, Appendix D in Pilch et al., 1994a) has been used (along with TCE) in resolution of the DCH issue for Zion, where TCE and CLCH gave similar results. The CONTAIN code has also been used extensively in DCH analysis of containment loads. Appendix G in NUREG/CR-6109 (Pilch et al., 1995) compares CONTAIN and TCE predictions for conditions near the upper end of our distributions. CONTAIN predicts loads comparable to or less than the TCE model. Consequently, we do not expect different modeling approaches to yield significantly different loads for comparable conditions.

In support of a detailed independent peer review of the CONTAIN code (Boyack et al., 1985), extensive analyses of recent DCH experiment were performed using the CONTAIN code (Williams et al., 1995). This work was performed in parallel with the issue resolution effort and its results were not available to the NUREG/CR-6075 peer review process; however, the results of the CONTAIN analyses were presented to the CONTAIN peer review group and the major findings were accepted by that group. Principal findings of interest here are as follows:

1. Atmosphere-structure heat transfer combined with hydrogen hold-up in oxygen-starved subcompartments can constitute an important DCH mitigation process that is not modeled in TCE.
2. Interaction of blowdown steam with nonairborne debris, which is not modeled in TCE, can augment DCH hydrogen production and containment loads.

3. Codispersed cavity water can augment DCH loads, rather than mitigate loads, under some circumstances. Codispersed water contributions to DCH were judged to be significant in the Zion geometry IET experimental analyses.

In the experimental analyses using CONTAIN, the mitigating effects tended to compensate for the augmenting effects, but it was not considered likely that this would always be the case. For present purposes, a crucial point is that the most important reason that the CONTAIN analyses were sensitive to these issues is that, in the experiments, hydrogen production was steam-limited rather than metal-limited. Hence, hydrogen production and DCH loads were sensitive to uncertainties in the amount of steam available to interact with the metal. With the highly oxidic melts assumed here, hydrogen production is metal-limited and sensitivity to these issues is expected to be considerably less.

We believe, therefore, that the net effect of these uncertainties is within the margin allowed for by using a CCFP success criterion of 0.01 in the screening study, and these issues are unlikely to compromise the present results. However, these issues should be studied in more detail (e.g., using the CONTAIN code) should it become necessary to consider melts with a high metallic content in the future.

NUREG/CR-6075 (Pilch et al., 1994a) identified the need to catalog the extent of cavity flooding prior to vessel breach. This is accomplished in Section C.2.3, where assessments are taken from the IPEs under two limiting cases: with/without injection of the RWST into the containment. The assessments are quite plant-specific, but cavities are predominantly dry (26 dry, 11 wet, 4 unknown) if the RWST is not injected, and predominantly flooded (21 flooded, 11 wet, 7 dry, 2 unknown) if the RWST discharges fully. A deeply flooded cavity usually, but not always, means that the lower head of the RPV is at least partially submerged in water increasing the potential for in-vessel retention.

Figure 5.2 explores the potential impact of cavity water on containment loads. Three experiments with cavity water from the DCH database have counterparts with essentially dry cavities: FAI/DCH-2, 3 (Henry et al., 1991), SNL/WC-1,2 (Allen et al., 1992), and SNL/IET-7,8B (Allen et al., 1993). The WC tests were conducted in an open vessel, while the FAI/DCH tests and the SNL/IET tests were conducted in a Zion-like compartmentalized geometry. We note that only SNL/IET-8B had a reactive atmosphere. The data suggest that DCH loads are insensitive to water mass. In the IET-8B experiment, the containment atmosphere exceeded the saturation temperature only slightly indicating that DCH energies (including hydrogen combustion) went into vaporizing water, so that most of the resulting pressurization came from added moles. No systematic attempt has been made to validate models predicting the impact of cavity water on DCH, but computer models sometimes predict enhanced loads for optimal quantities of water. The CONTAIN peer review (Boyack et al., 1995) concluded that CONTAIN was inadequate for predicting the impact of water on DCH. Consistent with the limited data, we ignore the potential impact of cavity water in our analyses.

We further categorize reactor cavities as *excavated* (29 plants) or *free standing* (12 plants). Free standing cavities are potentially vulnerable to damage in the event of high cavity pressures resulting from explosive or non-explosive FCIs in the cavity. The failure pressure for each free standing cavity is not known; but should cavity failure occur, the debris will be dispersed onto the containment floor thus



minimizing DCH interactions. Structural damage has the potential to enhance dome transport also in some unquantifiable manner; however, containment loads are insensitive to dome carryover in plants with high compartmentalized geometry. Excavated cavities are not vulnerable to damage from high cavity pressures. Detailed assessments of FCIs and their impact on cavity structures is outside the scope of this report.

The working group discussions from NUREG/CR-6075, Supplement 1 (Appendix A in Pilch et al., 1994b) defined two new scenarios (V and VI) which involve significant quantities (~10-75 mt) of water that would be coejected with the melt into the reactor cavity. This is a situation that has not been addressed by the existing database; however, the working group (Appendix A in Pilch et al., 1994b) expressed an opinion that water in the primary system at vessel breach is expected to mitigate the impact of DCH. We note that a related experiment involving large quantities of cavity water (Allen et al., 1993; 1994) suggests that DCH energies went entirely into vaporizing water, pressurizing the containment to levels comparable to containment pressures observed in (essentially) dry DCH tests. RPV water (unlike cavity water) will partially flash to steam during isentropic blowdown. The contribution to containment pressure from this mechanism is less than ~0.075 MPa for ~75 mt of water in Zion. The calculations and results presented here are performed by ignoring any impact of coejected water. The margins to a significant DCH threat are high enough for Westinghouse plants so that the impact of coejected water can be ignored in these analyses. However, there are substantial uncertainties concerning the amounts and enthalpies of RPV water present at vessel breach, and additional study of the effects of coejected water would be warranted if future work indicates that large amounts of near-saturated water could be present. Towards this end, the NRC is sponsoring a 1:10th scale experiment in Calvert Cliffs geometry (CE) that will address the issue of coejected water. These experiments are scheduled for completion in the winter of 1995.

Most inputs to the TCE model are related to initial conditions and material properties. Four supplemental phenomenological models are required to complete evaluation of the TCE model:

1. a model for the coherence ratio as a function of hole size and cavity geometry,
2. a model for the hole size,
3. a model for the amount of preexisting hydrogen burned on DCH time scales, and
4. a model for the amount of debris transported to the dome.

A key modeling parameter in the TCE model is the melt-to-steam coherence ratio. Because the entrainment time is short compared with the blowdown time, molten debris is exposed to a small fraction of the primary system steam during the dispersal process. Since this steam is the medium oxidizing metal and carries the melt energy and the hydrogen produced by steam-metal interactions to the main containment volume, this incoherence can be an important mitigating factor, particularly if the metal content is high. We note, however, that only limited sensitivity to  $R_r$  is observed for the melt compositions identified in our study. With this understanding, it is possible to reduce most of the complexity of cavity phenomena to the coherence ratio ( $R_r = \tau_d/\tau_b$  in the TCE model). We now focus on the coherence ratio and its quantitative representation in the calculations (i.e., *pdf4*, see Figures 3.1 and 3.2).

Appendix E in NUREG/CR-6075 (Pilch et al., 1994a) develops a correlation for the coherence ratio based on experiment values obtained by a procedure best suited to the TCE model. The correlation can be expressed as

$$R_r = \frac{\tau_e}{\tau_b} = C_{Rr} f_d \left( \frac{T_{RCS}^0}{T_d^0} \right)^{1/4} \left( C_d \frac{M_d^0}{M_g^0} \frac{A_h V_{can}^{1/3}}{V_{RCS}} \right)^{1/2}, \quad (5.2)$$

where  $C_{Rr}$  is a cavity-specific (weakly) multiplier that is determined from experiment data.

The database on which the coherence ratio correlation is based contains Zion-like geometries and Surry-like geometries, and the lead constant on the correlation is a weak function of the cavity type. Figure 5.3 compares the coherence ratio with the Zion, Surry, and combined Zion/Surry database. For the purpose of quantifying the coherence constant and a relative standard deviation for each plant, we have categorized all Westinghouse cavities into one of three groups: Zion-like, Surry-like, and other. We have consulted the IDCOR descriptions of reactor cavities and applied our own subjective assessments when making the assignments. Our basis is described more fully in Appendix C.

We define Zion-like cavities as having a U-tube layout with a slanted riser section, and we define Surry-like cavities as having a U-tube layout with a vertical riser section. Only two plants, South Texas 1 & 2, can not be characterized as Zion-like or Surry-like. Our assessments are summarized in Table C.1. Westinghouse cavities (41 total) are 27 percent Zion-like, 68 percent Surry-like, and 5 percent neither. There are variations within these groupings, so it is useful to explore how sensitive loads are to variations in the coherence ratio that could potentially arise due to variations in cavity geometry. Towards this end, sensitivities were run for Zion, Surry, and South Texas. A 30% increase in the recommended coherence produced only ~ 1% increase in containment loads.

Having further grouped the cavity designs, we assign the lead constant and relative standard deviation appropriate to Zion to all Zion-like cavities. A similar procedure is followed for Surry. Only two plants, South Texas 1 & 2, can not be characterized as Zion-like or Surry-like. In the case of South Texas 1 & 2, we biased (in the conservative direction) the lead constant for the combined Zion/Surry database by one standard deviation and then assigned the relative standard deviation appropriate to the combined database to the biased correlation. Uncertainties resulting from a geometry significantly outside the current database are bounded in this fashion while still maintaining a generous uncertainty distribution. The coherence constant and relative standard deviation for each cavity group are tabulated in Table 5.2.

The Zion and Surry database for the coherence ratio largely overlaps the range of individual parameters that are of interest to reactor applications (Table 5.3). However, the database does not include all possible combinations of parameters for each of the potential applications; consequently, the correlation for the coherence ratio is required to fill gaps in the database. It is significant that this process is one of interpolation rather than extrapolation for Zion and Surry. This argument is based upon recognized *nondimensional* parameters. We do not imply that the database includes full scale reactor cavities.

Rapid ejection of hot melt through a breach in the RPV leads to ablation, which increases the initial hole size. Appendix J in NUREG/CR-6075 (Pilch et al., 1994a) develops a model for hole ablation. The final hole size can be computed from

$$\frac{\Delta D_h}{D_h^0} = \frac{\frac{\tau_M}{\tau_D}}{1 + 0.6934 \left( \frac{\tau_M}{\tau_D} \right)^{2/3}} \quad (5.3)$$

where

$$\tau_M = \frac{M_d^0}{\dot{M}_d} = \frac{M_d^0}{\rho_d C_d \frac{\pi (D_h^0)^2}{4} \left( \frac{2}{\rho_d} (P_{RCS}^0 - P_c^0) \right)^{1/2}} \quad (5.4)$$

is the characteristic time to eject all the melt from the RPV in the absence of ablation and where

$$\tau_D = \frac{D_h^0}{\dot{D}_h} = \frac{D_h^0}{\left( \frac{2 h_{d,w} (T_d^0 - T_{mp,w})}{\rho_w [C_{p,w} (T_{mp,w} - T_w) + h_{f,w}] } \right)} \quad (5.5)$$

is the characteristic time to double the initial hole size by ablation. Figure 5.4 validates the model against the existing database. This figure also illustrates that ablation increases the hole size only slightly for initial hole sizes characteristic of lower head rupture; consequently, ablation will not have a strong influence on the calculations performed for this report. Although a point estimate of the initial hole size is specified in this report, a distribution of final hole sizes results because the causal relation (Equation 5.3) is evaluated for a distribution of melt masses.

A second phenomenological uncertainty concerns hydrogen combustion during DCH. The working group for Zion resolution (Appendix A in Pilch et al., 1994a) emphasized that hydrogen combustion should be treated in a manner consistent with the expected conditions in the containment. Appendix E (Pilch et al., 1994b) addresses the issue of jet combustion, entrainment into a jet, stratification, global mixing, and volumetric combustion phenomenology in more detail. Our conclusions regarding hydrogen combustion during DCH events can be summarized as follows:

1. DCH-produced hydrogen (plus some entrainment of H<sub>2</sub> from the preexisting atmosphere) can burn as a jet in the dome and contribute to peak containment pressures. These burning jets would represent an adequate ignition source for deflagrations if flammable conditions exist in the containment.

2. Stratification of hot jet combustion products will occur in the dome if sprays are not operational, thus impeding the mixing of combustion products with the cooler preexisting atmosphere. Thus, we picture hot nonflammable gases accumulating in the upper dome and the cooler, potentially flammable, preexisting atmosphere displaced downward in the lower dome regions.
3. Flame propagation is difficult to achieve in stratified containment atmospheres with ~50 percent steam, and the burning process is too slow and inefficient to contribute to peak loads except possibly at the upper end of H<sub>2</sub> distribution. Explicit treatment of deflagrations to better define and bound uncertainties in hydrogen combustion (Pilch et al., 1995; Pilch, 1995) was included in the Zion supplement (Pilch et al., 1994b) and our current analyses. The fraction of the preexisting hydrogen that can burn on DCH time scales and contribute to peak loads is given by

$$f_{pre} = \eta_c \left( 1 - \frac{\dot{E}_{HT}}{\dot{E}_{H_2}} \right). \quad (5.6)$$

Even for finite combustion completeness ( $\eta_c$ ), heat transfer to structures can exceed the energy release rate that is due to the deflagration so that the deflagration does not contribute to peak DCH loads. The deflagration model also handles the continuum of cases where deflagrations can contribute to peak DCH loads depending on atmosphere composition and temperatures induced by the DCH event itself. Deflagration-enhanced DCH loads are predicted for a TMI-like scenario with essentially no steam in the atmosphere, but the increased pressure is offset by the lower initial pressure in the containment.

4. Slow volumetric combustion of preexisting hydrogen can occur in parallel with potential deflagrations, but slow volumetric combustion does not contribute to peak loads.
5. Sudden volumetric combustion (autoignition) of preexisting hydrogen is essentially impossible in a stratified atmosphere because heating of the containment atmosphere is limited by mixing. However, to better bound uncertainties in hydrogen combustion phenomena, we recommend a bulk averaged autoignition temperature of 950 K based on separate effects data.
6. Combustion initiated by passive mixing (i.e., sprays are not operational) of hot gases with the preexisting atmosphere is too slow to contribute to peak pressure. This is because the mixing time scale of the atmosphere is long compared with the time scale for structure heat transfer. Here, we refer to global mixing of the atmosphere, not entrainment into a burning jet, which is already accounted for in item 1 above. This mixing limited combustion occurs in parallel with potential deflagrations and volumetric combustion.

These insights and recommendations are consistent with peer review comments for NUREG/CR-6075 (Pilch et al., 1994a) concerning the autoignition temperature and the need to consider partial combustion of the preexisting hydrogen. These recommendations have been factored into the



calculated results presented in Section 7. We note that some of the plants considered here have significantly higher dome transport fractions than the existing database. The potential impact of high dome transport fractions on combustion of preexisting hydrogen will be addressed in upcoming tests to be conducted in Combustion Engineering geometry.

The IET-11 experiment (Blanchat et al., 1994) showed that stainless steel insulation around the RPV was largely dispersed with the molten debris. Little of the intact insulation was recovered posttest. The interaction of steam with the insulation has the potential to be a source of additional hydrogen that could burn and contribute to peak containment loads. High hydrogen production values reported in IET-11 compared to IET-9 and IET-10 can be partially explained in terms of differences in initial conditions or the stochastic range of possible hydrogen production. The Cr content of the insulation is the most likely source of any additional hydrogen because of thermodynamic limitations to Fe oxidation and because of coherent steam limitations in the annulus. In the Surry plant, oxidation of the Cr content of the insulation would produce  $\sim 1.45 \times 10^4$  additional moles of hydrogen resulting in an additional load of  $\sim 0.023$  MPa if all the hydrogen burns. In addition, melting of the insulation comes at the expense of quenching the molten core materials. Lastly, significant quantities of cavity water or water coejected from the RCS may reduce the tendency of the insulation to melt and thus mitigate the production of additional hydrogen. The analyses do not model this potential source of additional hydrogen.

The amount of material participating in DCH is typically less than the melt mass on the lower head at the time of bottom head failure. Experiments show melt retention in both the crucible (scaled to the bottom head of the RPV) and the reactor cavity below the RPV. On average,  $\sim 93$  percent of the melt in the Zion experiments (Allen et al., 1994; Binder et al., 1994) and 99 percent of the melt in the Surry experiments (Blanchat et al., 1994) was ejected into the cavity. A conservative upper bound of 100 percent is used for all the scenarios in this report.

Section C.2.1 provides a comprehensive review of debris dispersal phenomena. To summarize, we expect that debris dispersal will be complete for RCS conditions of most interest to DCH, except for some retention by freezing on cavity surfaces, for all cavity designs representative of Westinghouse plants. We also expect that dispersal will be dominated by surface entrainment and that the melt will be fragmented to sizes  $\sim 1$  mm.

The DCH database indicates that melt retention occurs predominantly as a thin crust ( $\sim 1$  mm) of frozen material plated out on all cavity surfaces. A first order correction to the dispersal fraction, which accounts for surface freezing

$$f_{disp} = 1 - \frac{\delta(t) A_s \rho_d}{M_d^o} \sim 1 - \frac{2\lambda_c (\alpha_c R_r \tau_b)^{1/2} 6V_c^{2/3} \rho_d}{M_d^o}, \quad (5.7)$$

is developed in Section C.2.1. This simple model is validated against the database in Table 5.4.

Reactor applications are both plant-specific and scenario-specific. The former is true because of geometric differences and the latter is true because of the scenario dependent melt masses and RCS pressures. Section C.2.1 computes the fraction dispersed for each plant and for each scenario, with the



evaluation being performed for the upper end of the mass distributions. Freezing on cavity surfaces retains only ~10 percent of the melt for each plant and scenario.

There are two primary debris transport pathways from the reactor to the containment dome in Westinghouse plants: (1) through the annular gap between the RPV and the biological shield wall, and (2) from the in-core instrument tunnel through the lower compartments. We express the dome transport fraction as

$$f_{dome} = f_{gap} (1 - f_{noz/shld}) + f_{sub} (1 - f_{gap}). \quad (5.8)$$

Section C.3 quantifies the various contributions to dome transport for each Westinghouse plant; however, we briefly summarize our approach. The gap contribution is determined primarily by available flow areas, and the subcompartment contribution is determined by inertially dominated flow through the seal table room. Thus, to first order, we expect dome transport to be independent of RCS pressure. The gap contribution is determined primarily by available flow areas, and the subcompartment contribution is determined by inertially dominated flow through the seal table room. Thus, to first order, we expect dome transport to be independent of RCS pressure and constant for all scenarios. Although it is within the capabilities of the existing methodology and coding, uncertainty distributions on dome transport were not considered in the belief that the current quantifications are adequately bounding. We performed an arbitrary sensitivity study for the most sensitive plant (H.B. Robinson) and for the most sensitive scenario (VIa). The dome carryover fraction was increased by 30 percent from 0.621 to 0.807, and this resulted in only a 3 percent increase in the loads at the upper end of the loads distribution.

Transport of debris through the gap is calculated from a simple area ratio,

$$f_{gap} = \frac{A_{gap}}{A_{gap} + A_{cavity}}. \quad (5.9)$$

This simple model was developed and validated against the DCH database in Appendix I of NUREG/CR-6075 (Pilch et al., 1994a). Based on experiments conducted by Bertodano (1993), we take nominal credit ( $f_{noz/shld} \sim 0.10$ ) for the missile shield and diversion of gap flow back into the subcompartments through the nozzle cutouts in the biological shield wall.

After reviewing the IPE drawings of all 41 Westinghouse plants, we were able to categorize the lower compartment geometries into four distinct types (1) Zion-like (17 plants); (2) Surry-like (15 plants); (3) two-loop plants (6 plants); and (4) others (3 plants). For all of the plants that are Zion or Surry-like, a transport fraction ( $f_{sub}$ ) from the cavity exit to the upper dome of 0.05 will be used in the extrapolation calculations, which is consistent with NUREG/CR-6075 and NUREG/CR-6109. In all of these plants, there are at least two floors between the cavity exit and the upper dome (usually the seal table room floor and ceiling, which is the operating deck level) and there are no significant line-of-sight debris transport pathways to the upper dome.

We note that the Zion and Surry experiments typically showed ~9 percent dome transport, which contains an unspecified amount of contaminants such as concrete. The quantification used here (0.05) is deemed conservative:

- a) because the experiments did not model the vast array of in-core instrument guide tubes that may be dispersed from the cavity with the debris (Allen et al., 1990),
- b) because the experiments did not model the steel hatches or "penthouses" (which restrict personnel access to the cavity) that will be blown upward into the seal table opening,
- c) because most of the experiments did not model the seal table and because the seal table did not fail or fail completely in those experiments (Blanchat et al., 1994) that did model the seal table,
- d) because the experiments did not model any of the equipment in the seal table room, and
- e) because most of the experiments did not model the "plug" in the roof of the seal table room and because the plug was not always dislodged in the experiments (Allen et al., 1994a) that did model the plug.

We note that more recent separate effects experiments for Zion (Wu, 1995) conducted at Purdue show dome carryover fractions of ~3 - 5% for the conditions of interest here. The enhanced carryover in the SNL/ANL IET tests could have resulted from the distorted cavity exit which was 2.7 times longer than prototypic. Wu's experiment show that dome carryover is comprised of a line-of-sight contribution that passes through the seal table room and very fine particles (~60  $\mu\text{m}$ ) that are carried by gas through the subcompartments and through vents into the dome. These very small particles are not fully effective when they reach the dome because oxidation is likely complete and some heat transfer has occurred prior to their arrival in the dome. We note that the TCE model is conservative in this regard because all debris transported to the dome is considered to be fresh, carrying its full undiluted energy content.

Enhanced dome transport (~35 percent) was observed in IET-8B resulting from FCIs in a cavity half full of water. The structure was not scaled for strength and structural damage was observed. Enhanced dome transport in the presence of large quantities of water is not expected to have the same impact on containment loads as dry transport because of significant quenching effects.

The two-loop plants have two floors between the cavity exit and the upper dome, i.e., the seal table room floor and the operating deck floor. However, there is a direct line-of-sight debris transport pathway that will allow some debris dispersal directly to the dome should the seal table fail. There are three plants (H.B. Robinson and South Texas 1 & 2) that are categorized as "other" in Table C.5. These plants do not look either like Zion or Surry and do not appear to meet the criteria for using the debris transport fractions used for Zion in NUREG/CR-6075 and for Surry in NUREG/CR-6109. The H.B. Robinson plant has two floors but appears to have significant direct line-of-sight debris transport pathways to the upper dome. In South Texas 1 & 2, the instrument guide tubes are sealed by 2 feet of concrete and the only debris transport pathway out of the cavity besides the RPV annular gap is through a manway that leads to a tortuous path to the upper compartments in the containment. There

## Quantification of the DCH Phenomena

is no direct vertical debris transport pathway from the cavity except through the annular gap between the RPV and biological shield wall, so for South Texas 1 & 2 the fraction of debris that can be transported through the lower compartments is assumed to be zero.

Debris transport through line-of-sight flow paths to the dome is controlled by flow into and out of the seal table room,

$$f_{sub} = \min \left\{ \frac{A_{str}}{\frac{1}{2} A_{cav\ exit}} ; 1 \right\} \min \left\{ \frac{A_{op\ deck}}{A_{str}} ; 1 \right\} - 0.05, \quad (5.10)$$

where nominal credit (0.05) is taken for the last array of equipment and structures that could impede flow into or out of the seal table room. These include: steel hatches or "penthouses" which restrict personnel access to the cavity, partial failure or nonfailure of the seal table, the array of in-core instrument guide tubes and their support structures that will be dispersed from the cavity with the debris, and equipment in the seal table room. A factor of  $\frac{1}{2}$  is multiplied by the area of the cavity exit ( $A_{cav\ exit}$ ) because DCH experiments indicate that virtually all of the debris is ejected from the half of the opening furthest from the RPV.

### 5.1 Nomenclature

$A_{cav\ exit}$	=	area of instrument tunnel exit
$A_{cavity}$	=	minimum flow area through the reactor cavity
$A_{gap}$	=	minimum flow area through the annular gap around the RPV
$A_h$	=	breach area in RPV
$A_{op\ deck}$	=	area of the opening in the operating deck that is directly above the seal table
$A_e$	=	surface area of the reactor cavity
$A_{str}$	=	area of the seal table room opening
$C_d$	=	discharge coefficient (0.6)
$C_{p,w}$	=	heat capacity of RPV steel
$C_{R\tau}$	=	constant in coherence correlation
$D_h^0$	=	initial hole diameter
$D_h$	=	characteristic ablation rate
$E_{HT}$	=	characteristic heat transfer rate to structure
$E_{HD}$	=	energy release rate from combustion of preexisting hydrogen
$f_d$	=	fraction dispersed
$f_{disp}$	=	fraction of debris dispersed from cavity
$f_{dome}$	=	fraction of dispersed debris that enters dome
$f_{gap}$	=	fraction of dispersed debris that enters the annular gap around the RPV
$f_{noz/shld}$	=	fraction of dispersed debris that enters the RPV gap that flows back into the subcompartments through nozzle cutouts in the biological shield wall or that gets knocked down by the missile shield

$f_{pre}$	=	fraction of preexisting hydrogen burned on DCH timescales
$f_{sub}$	=	fraction of dispersed debris that enters the subcompartment and subsequently passes through to the dome
$h_{d,w}$	=	debris/wall heat transfer coefficient during ablation (see Appendix J, NUREG/CR-6075)
$h_{f,w}$	=	heat of fusion for RPV steel
$M_d$	=	melt ejection rate from RPV
$M_d^0$	=	initial melt mass
$M_g^0$	=	initial RCS gas mass
$P_c^0$	=	initial containment pressure
$P_{RCS}^0$	=	initial RCS pressure
$R_c$	=	coherence ratio
$T_d^0$	=	debris temperature
$T_{RCS}^0$	=	RCS gas temperature
$T_{mp,w}$	=	melting temperature of RPV steel
$T_w$	=	temperature of RPV lower head at vessel failure
$U^0$	=	total internal energy of containment atmosphere
$V_c$	=	cavity volume
$V_{cav}$	=	cavity volume
$V_{RCS}$	=	RCS volume

## Greek

$\alpha_c$	=	thermal diffusivity of frozen core material
$\delta$	=	thickness of frozen core debris on cavity walls
$\Delta D_h$	=	change in hole diameter
$\Delta E_i$	=	energy contribution of DCH process
$\Delta P$	=	pressure increase in containment due to DCH
$\rho_d$	=	mass density of debris
$\rho_w$	=	mass density of RPV steel
$\sigma_{bias}$	=	relative bias
$\sigma_{rms}$	=	relative (root mean squared) standard deviation
$\tau_b$	=	characteristic blowdown time
$\tau_c$	=	characteristic entrainment interval
$\tau_D$	=	characteristic time to double the initial hole size by ablation
$\tau_M$	=	characteristic time to eject melt from RPV in the absence of ablation
$\gamma$	=	total heat capacity of dispersed debris divided by total heat capacity of the atmosphere
$\lambda_c$	=	growth rate constant for conduction limited freezing of a superheated liquid on an infinite substrate
$\eta$	=	pressurization efficiency
$\eta_c$	=	combustion efficiency

Table 5.1 Survey of DCH-relevant experiments

Experiment Series	Number of Tests	Nominal Scale	Cavity Type	Water
SNL/DCH	4	1:10	Zion	None
SNL/TDS	7	1:10	Surry	None
SNL/LFP	6	1:10	Surry	None
SNL/WC	3	1:10	Zion	None Cavity
SNL/IET-Zion	9	1:10	Zion	Cavity Cavity/basement
SNL/IET-Surry	3	1:5.75	Surry	None Cavity/basement
ANL/CWTI	2	1:30	Zion-like	Cavity/basement
ANL/IET	6	1:40	Zion	None Cavity
ANL/U	3	1:40	Zion	None
FAI/DCH	4	1:20	Zion	Basement Cavity/basement



Table 5.1 (continued)  
Survey of DCH-relevant experiments

Experiment Series	Driving Gas	Driving Pressure (MPa)	Melt Mass (kg)	Melt Composition	Hole Size
SNL/DCH	N <sub>2</sub>	2.6 - 6.7	20, 80	Fe/Al <sub>2</sub> O <sub>3</sub>	0.06
SNL/TDS	H <sub>2</sub> O	3.7 - 4.0	80	Fe/Al <sub>2</sub> O <sub>3</sub> /Cr	0.065
SNL/LFP	H <sub>2</sub> O	2.5 - 3.6	50, 80	Fe/Al <sub>2</sub> O <sub>3</sub> /Cr	0.04 - 0.09
SNL/WC	H <sub>2</sub> O	3.8 - 4.6	50	Fe/Al <sub>2</sub> O <sub>3</sub> /Cr	0.04 - 0.10
SNL/IET Zion	H <sub>2</sub> O	5.9 - 7.1	43	Fe/Al <sub>2</sub> O <sub>3</sub> /Cr	0.04
SNL/IET Surry	H <sub>2</sub> O	12	158	Fe/Al <sub>2</sub> O <sub>3</sub> /Cr	0.072-0.098
ANL/CWTI	N <sub>2</sub>	4.7 - 5.0	4.1	UO <sub>2</sub> /ZrO <sub>2</sub> /SS	0.13
ANL/IET	H <sub>2</sub> O	5.7 - 6.7	0.72, 0.82	Fe/Al <sub>2</sub> O <sub>3</sub> /Cr	0.011
ANL/U	H <sub>2</sub> O	3.0 - 6.0	1.13	UO <sub>2</sub> /Zr/ZrO <sub>2</sub> /SS	0.011
FAI/DCH	N <sub>2</sub> , H <sub>2</sub> O	2.4 - 3.2	20	Fe/Al <sub>2</sub> O <sub>3</sub>	0.025

**Table 5.1 (concluded)**  
**Survey of DCH-relevant experiments**

Experiment Series	Containment Pressure (MPa)	Annular Gap Around RPV	Atmosphere Composition	Containment Structures
SNL/DCH	0.08	No	Air, Ar	Open containment
SNL/TDS	0.09 - 0.23	No	Air, Ar	Open containment
SNL/LFP	0.16	No	Ar	Compartmentalized by slab
SNL/WC	0.16	No	Ar	Essentially open
SNL/IET Zion	0.2	No	N <sub>2</sub> , N <sub>2</sub> /Air, N <sub>2</sub> /Air/H <sub>2</sub> , CO <sub>2</sub> /Air/H <sub>2</sub>	Zion subcompartment structures
SNL/IET Surry	0.13-0.19	No partial insulation	Air/H <sub>2</sub> O/H <sub>2</sub>	Surry subcompartment structures
ANL/CWTI	0.1	No	Ar	Compartmentalized by baffle
ANL/IET	0.2	No	N <sub>2</sub> , N <sub>2</sub> /Air, N <sub>2</sub> /Air/H <sub>2</sub> , H <sub>2</sub> O/Air/H <sub>2</sub>	Zion subcompartment structures
ANL/U	0.2	No	N <sub>2</sub> /Air/H <sub>2</sub>	Zion subcompartment structures
FAI/DCH	0.1	No	N <sub>2</sub>	Zion (Like) subcompartment structures

**Table 5.2 Quantification of the coherence ratio**

Cavity	C <sub>Rt</sub>	σ
Zion	9.661	0.29
Surry	12.2	0.18
Other	14.6	0.33

Table 5.3 Applicability of the database to reactors

	CAVITY	$f_{disp}$	$T_d^0/T_{RCS}^0$	$M_d^0/M_g^0$	$A_h V^{1/3} / V_{RCS}$
Complete database	Zion, Surry	0.6 - 1.0	3.0 - 11.0	2.8 - 21.4	0.001 - 0.014
SNL/ANL IET Zion tests $P_{RCS}^0 = 6 \text{ MPa}$	Zion	0.6 - 0.9	4.2	3.9 - 6.0	0.0027
SNL/IET Surry tests $P_{RCS}^0 = 13 \text{ MPa}$	Surry	0.9	3.2	2.9	0.0033
NPP $P_{RCS}^0 = 8 \text{ MPa}$ $D_h^0 = 0.4 \text{ m}$ $T_{RCS}^0 = 1000 \text{ K}$ $M_d^0 = 50 \text{ mt}$	Zion	~1	3.5	6.2	0.002
NPP $P_{RCS}^0 = 16 \text{ MPa}$ $D_h^0 = 0.4 \text{ m}$ $T_{RCS}^0 = 800 \text{ K}$ $M_d^0 = 50 \text{ mt}$	Zion	~1	2.8	3.9	0.002
*Only experiments where dispersal is complete or nearly complete ( $f_{disp} > 0.5$ ) considered.					

**Table 5.4 Validation of melt retention by freezing during cavity dispersal**

Parameter	SNL/IET-1 to 8B Allen et al., 1994	ANL/IET-1R to 8 Binder et al., 1994	SNL/IET-9 to 11 Blanchat et al., 1994
Cavity	Zion	Zion	Surry
Scale	1:10	1:40	1:5.75
Melt simulant	Fe/Al <sub>2</sub> O <sub>3</sub> /Cr	Fe/Al <sub>2</sub> O <sub>3</sub> /Cr	Fe/Al <sub>2</sub> O <sub>3</sub> /Cr
$f_{disp}$ observed	0.62 - 0.89	0.69 - 0.80	0.73 - 0.89
$f_{disp}$ Eq. C.1	0.91	0.85	0.88

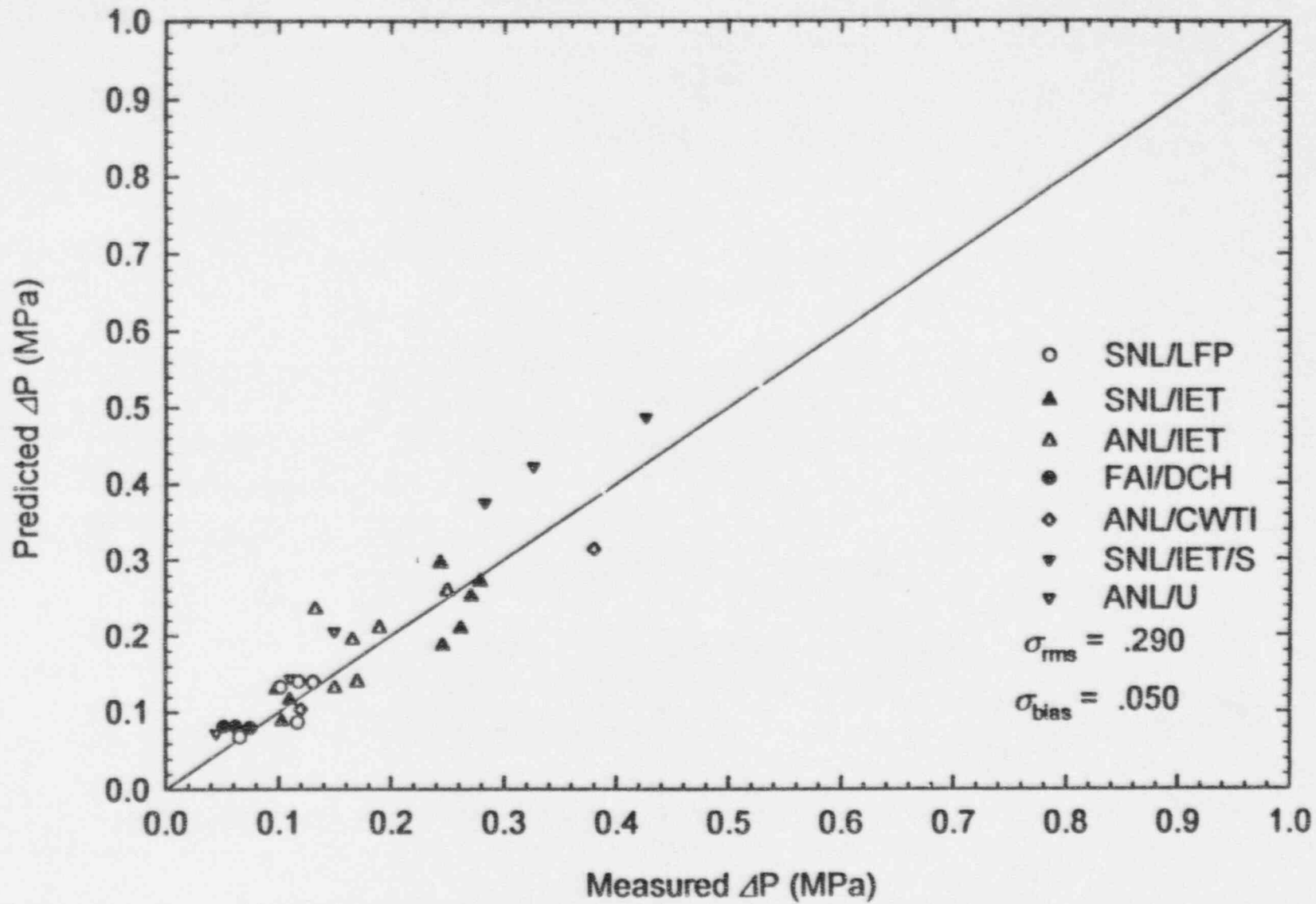


Figure 5.1. Validation of the two-cell equilibrium model against all experiment with compartmentalized geometry.



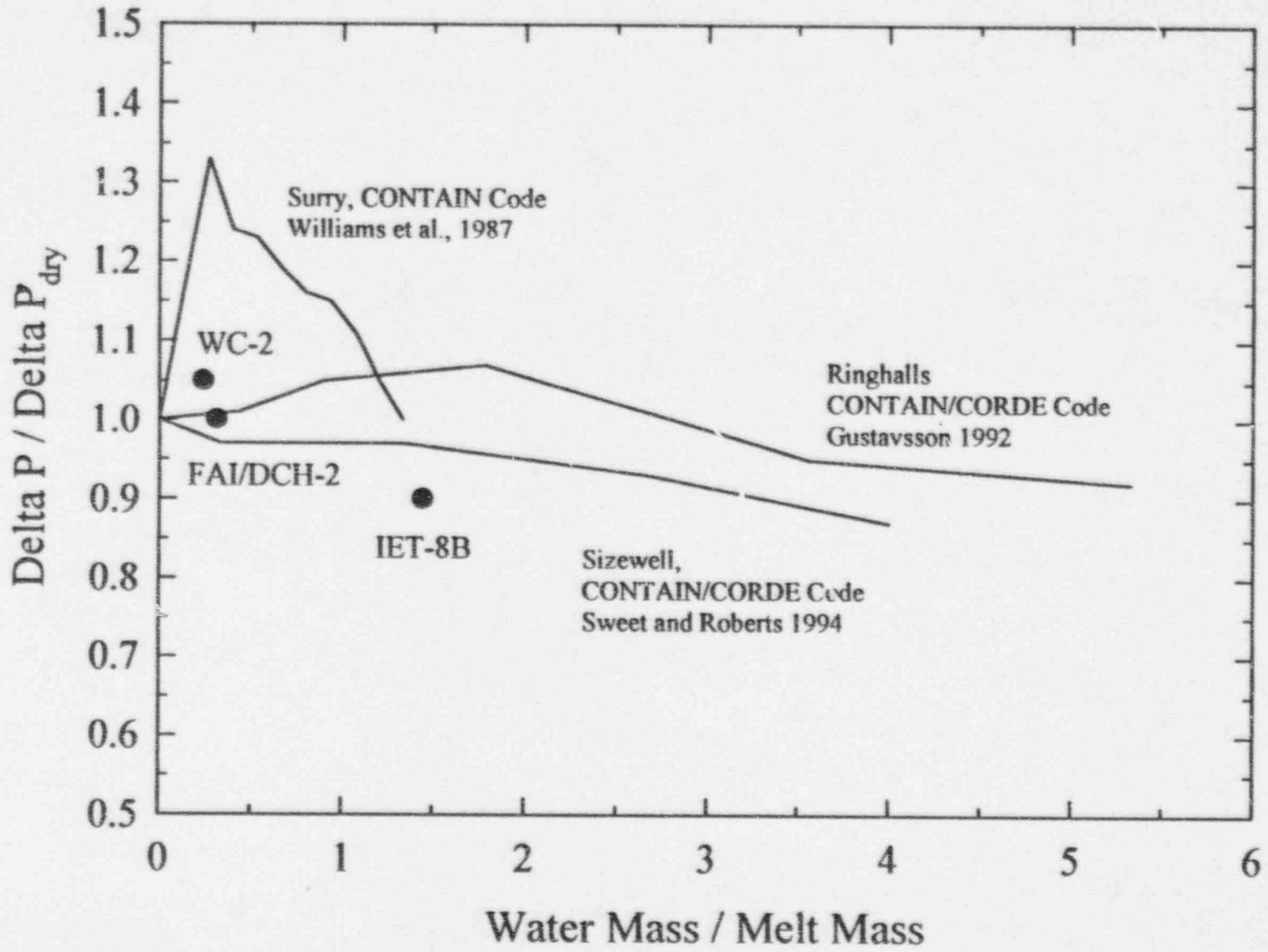


Figure 5.2. Potential impact of codispersed water on DCH loads.

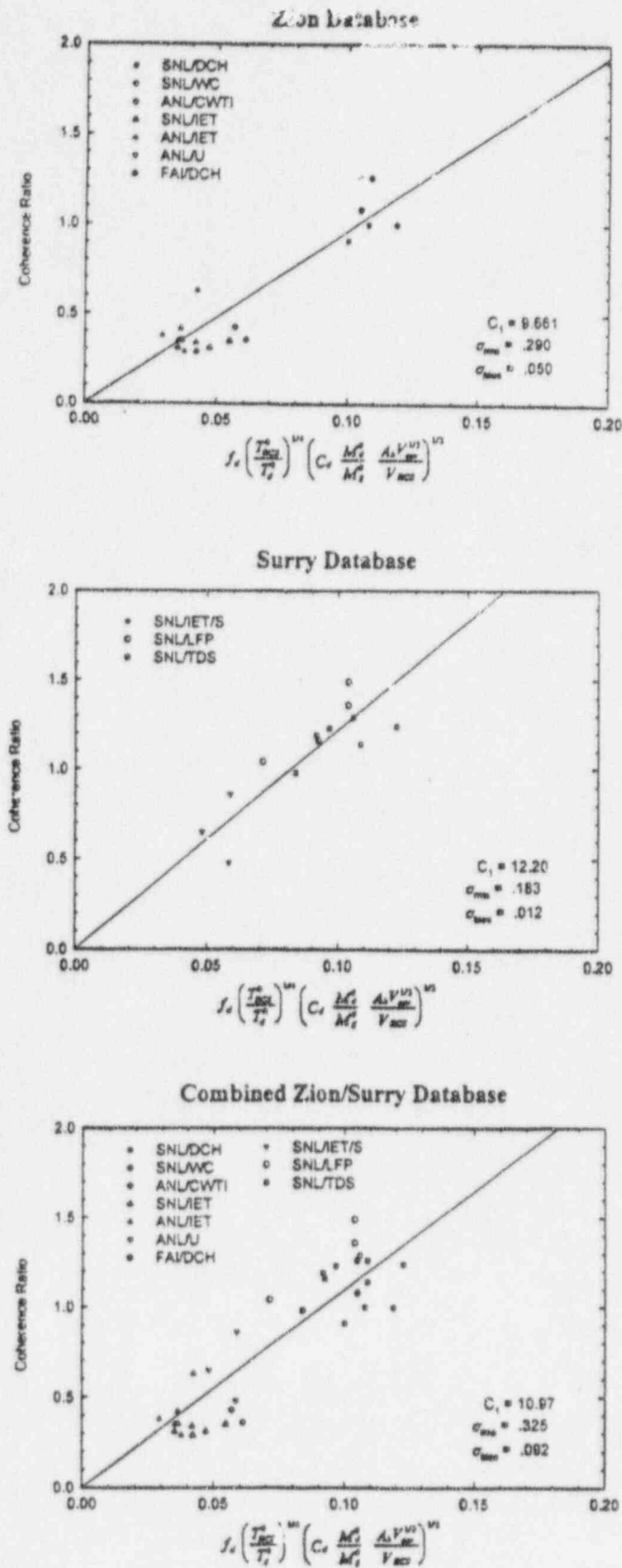


Figure 5.3. Validation of the coherence ratio for scenarios without coejected water.

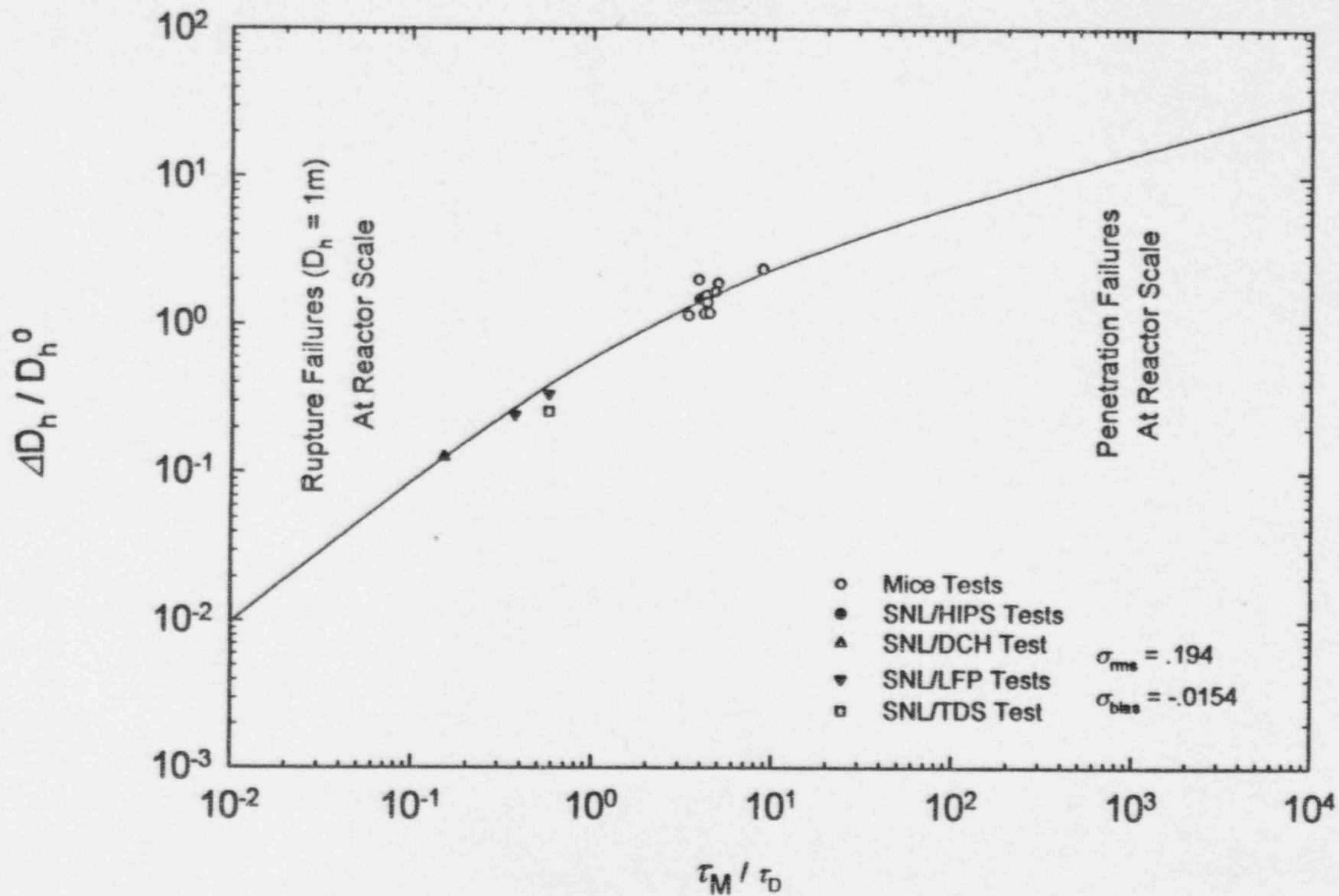


Figure 5.4. Validation of the hole ablation model.

## 6.0 QUANTIFICATION OF CONTAINMENT FRAGILITY

This section characterizes the strength of a reactor containment in probabilistic terms. The pressure capacity of a reactor containment is treated as a random variable because of the variability in material properties, of unknown differences between the as-built and design conditions, and modeling uncertainties. The probability that the containment failure pressure is less than a specified pressure is known as the containment overpressure fragility curve.

Fragility curves represent a probabilistic estimate of the capacity of the containment. In general, the fragility curve could be derived from data and full-scale experiments. However, the containment fragility curves are dependent on site-specific detail and, without detailed model tests, they must be derived from analysis. As a practical matter, the fragility curves are derived from a combination of material property data, tolerances in dimensions from drawings, and judgment of the analyst. Judgment is used in determining what level of analysis is required and what failure mechanisms are considered to govern the containment capacity. Typically, adequate material property data exist to characterize variability in material properties. Finally, analyst judgment is used to assign "modeling" uncertainty to the models to characterize the analyst's confidence in the ability of the selected models to represent the actual failure mechanisms involved. Modeling uncertainty could, in principle, be reduced with further analysis or testing. Funding constraints, however, usually require the analyst to exercise his or her judgment to reflect the uncertainty involved.

The Individual Plant Examinations (IPEs) for all operating Pressurized Water Reactors (PWRs) in the U.S. were assembled and containment fragility curves obtained. The containment capacity results from each of the IPEs were examined and briefly reviewed and the probability of containment failure was taken from them. In many cases, this consisted of fragility curves showing pressure versus cumulative failure probability. In other cases, a mean or median failure pressure was specified along with uncertainty bounds. In some cases, only curves or points for various failure modes were given and a total probability of failure had to be constructed. In all these situations, a single fragility curve resulted that was intended to reflect both modeling uncertainty and stochastic uncertainties due to material property variations. In only two cases, confidence limits were derived and reported. Confidence limits are used to separate modeling uncertainties from stochastic uncertainties. A detailed assessment of the technical basis for the IPE fragility curves is beyond the scope of this study.

For those IPEs presenting only a single curve, the curve was digitized, curve-fit with a spline program and failure probabilities determined at intervals of 1 psig. For IPEs which reported medians and uncertainties, a curve was developed and failure probabilities determined at intervals of 1 psig. The few which reported only median, 5 percent and 95 percent values, were fit to either a log-normal distribution, normal distribution or 3rd order spline function in order to get the best fit and failure probabilities determined at 1 psig intervals. In most situations where this occurred, only a third order spline provided an adequate fit to the three constraints.

Many of the IPE containment capacity analyses did not consider temperature or stated that increased temperatures would have little effect on the capacity. Other IPEs performed the analysis at either single or multiple accident temperatures. For those which determined the capacity at different

## Quantification of Containment Fragility

temperatures, the analysis closest to 400 K (260°F) was selected as best representing the accident temperatures expected in the reactor containment building at the time of vessel breach.

We observed that the licensee's level of effort and our estimate of the reliability of these containment fragility curves varied significantly. In some cases, a detailed analysis was performed for every possible failure mode and an overall cumulative failure curve was determined by combining each mode of failure, while some IPEs simply used containment fragility curves derived from other containments or simply shifted other plant's fragility curves based on what they determined to be the difference in ultimate capacity.

Appendix D briefly discusses (when given enough information) how the fragility curves were determined from each IPE. In addition, the process of digitizing, fitting and tabulating the curves or data given in the IPEs is discussed for every plant, and the detailed results are also tabulated in Appendix D. We interpret our fragility curves as *mean* values, and our compilations, to the extent possible, strive for consistency in this regard.

Functional representations of fragility are subject to possible error when extrapolated to low failure frequencies because excessive extrapolation to low failure frequencies could lose or violate the physical basis on which most of the curve rests. In other cases, some IPEs conservatively tie the low end of the fragility curve to the design pressure. Consequently, the IPE fragility curves might be quite conservative in the tails.

On the other hand, the digitizing process is subject to human error and is dependent on the quality of the working curve. In a few cases, we supplied a curve fit to median, 5 percent, and 95 percent values, and extrapolation to lower failure frequencies may involve error. We will perform a sensitivity study by arbitrarily biasing the fragility curve 0.1 MPa to the left in order to assess the potential impact of these uncertainties.

Table 6.1 provides a concise summary of key plant-specific fragility data for each Westinghouse plant. The plants are grouped into one of four classes depending upon the type and construction of the containment. We see that large variations in containment strengths exist. H.B. Robinson has the least robust containment with a failure pressure of 88 psig at a failure frequency of 10 percent. Seabrook is the strongest containment with a failure pressure of 186 psig at the same failure probability. Thus, we conclude that a containment's fragility is plant-specific. It is to be anticipated that the fragility curves derived for a specific containment are sensitive to local design details, tolerances, and the design philosophy used for that particular containment. While it is likely that various submodels representing different local containment failure modes may be applicable to a variety of containments of a given type, it is also true that the combination of failure mechanisms existing in a given containment is unique. Thus, the reader is cautioned against reading any generic applicability into the fragility curves developed for any specific containment.

A common rule-of-thumb states that the ultimate capacity of a containment is ~ 2 - 3 times its design pressure. Table 6.1 confirms this rule-of-thumb, but the relative standard deviation is large, ~20 percent. Furthermore, the summary statistics for all entries indicates that you do better simply by citing



a failure pressure (at a given frequency) based on the population mean. Consequently, the design pressure is a poor indicator of a containment's ultimate capacity.

We have provided summary statistics for each class of containment thinking that improvement could be realized by examining like kinds. Only Class 2 and Class 3 have sufficient entries for the statistics to be insightful. Unfortunately, no decisive improvement over population statistics is realized. Consequently, the DCH extrapolation study cannot benefit by grouping analyses based on the type of containment. We therefore use the plant-specific IPE fragility curve in our analyses.

Only two plants reported confidence limits (i.e., probability levels) on their fragility curve. Callaway (W) and Palisades (CE) are both large dry containments with post-tensioned concrete cylinder with a steel liner. The high confidence fragility curve for these plants can be obtained (approximately) by shifting the mean curve to the left by  $\sim 0.1$  MPa (15 psig) for Callaway and by  $\sim 0.07$  MPa (10 psig) for Palisades. All other plants combine stochastic and modeling uncertainties into a single curve.

Quantification of Containment Fragility

Table 6.1 Similarity of containment fragility

PLANT	Design Press. psig	Cont. Press (psig) @			Cont. Press/Design Press @		
		Prob.=0.01	Prob.=0.1	Prob.=0.5	Prob.=0.01	Prob.=0.1	Prob.=0.5
Class 1: Large Dry Containment; Steel Cylinder							
Kewaunee	46	113	130	150	2.46	2.83	3.26
Prairie Island 1,2	41	113	130	151	2.76	3.17	3.68
Class 2: Large Dry Containment; Reinforced Concrete Cylinder With Steel Liner							
Comanche Peak 1,2	50	95	104	114	1.90	2.08	2.28
Diablo Canyon 1,2	47	100	117	140	2.13	2.49	2.98
Indian Point 2	47	87	101	126	1.85	2.15	2.68
Indian Point 3	47	102	115	134	2.17	2.45	2.85
Salem 1,2	47	75	92	112	1.60	1.96	2.38
Seabrook	65	164	186	216	2.52	2.86	3.32
Shearon Harris	45	104	121	153	2.31	2.69	3.40
Class 3: Large Dry Containment; Post-Tensioned Concrete Cylinder With Steel Liner							
Braidwood 1	61	81	101	124	1.33	1.66	2.03
Braidwood 2	61	81	90	98	1.33	1.48	1.61
Byron 1	61	81	101	124	1.33	1.66	2.03
Byron 2	65	81	90	98	1.25	1.38	1.51
Callaway	60	104	123	134	1.73	2.05	2.23
Farley 1,2	54	98	105	114	1.81	1.94	2.11
GINNA	60	115	121	129	1.92	2.02	2.15
H.B. Robinson	42	70	88	130	1.67	2.10	3.10
Point Beach 1,2	60	127	146	161	2.12	2.43	2.68
South Texas 1,2	56	71	88	113	1.27	1.57	2.02
Summer	55	105	127	141	1.91	2.31	2.56
Turkey Point	59	118	131	150	2.00	2.22	2.54
Vogtle 1,2	52	100	119	139	1.92	2.29	2.67
Wolf Creek	60	88	108	128	1.47	1.80	2.13
Zion 1,2	47	97	118	133	2.06	2.51	2.83
Class 4: Subatmospheric Containment; Reinforced Concrete Cylinder With Steel Liner							
Beaver Valley 1&2	45	81	101	128	1.80	2.24	2.84
Millstone 3	45	88	103	118	1.96	2.29	2.62
North Anna 1,2	45	81	101	129	1.80	2.24	2.87
Surry 1,2	45	81	101	129	1.80	2.24	2.87
Summary Info							
Mean on Total	52.7	96.8	113.1	133.3	1.9	2.2	2.6
STD on Total	7.4	19.6	20.4	22.1	0.4	0.4	0.5
STD/Mean Total	0.14	0.20	0.18	0.17	0.20	0.19	0.20
Mean on Class 2	49.7	103.9	119.4	142.1	2.1	2.4	2.8
STD on Class 2	5.9	26.3	28.8	33.0	0.3	0.3	0.4
STD/Mean Class 2	0.13	0.25	0.24	0.23	0.14	0.13	0.14
Mean on Class 3	56.9	94.5	110.4	127.7	1.7	2.0	2.3
STD on Class 3	5.9	16.7	17.2	16.7	0.3	0.3	0.4
STD/Mean Class 3	0.10	0.18	0.16	0.13	0.18	0.18	0.19

## 7.0 RESULTS AND SENSITIVITIES

Each scenario identified in Section 4, supplemented by the respective coherence ratio distribution as discussed in Section 5 and the fragility curve of Section 6, was run through the arithmetic defined by the probabilistic framework of Section 3 to produce a probability distribution for the containment pressure. Finally, the containment failure probability was computed. The process was repeated for all Westinghouse plants with large dry or subatmospheric containments. The calculations were carried out using the computer code TCE/LHS as listed in Appendix B of NUREG/CR-6075, Supplement 1 (Pilch et al., 1994b) with 10000 samples.

The figure of merit for DCH resolution is the mean (best estimate) conditional containment failure probability, which is based on the mean containment fragility curve. Table 7.1 summarizes the results for each plant. The mean CCFP is  $\leq 0.01$  for each plant. Based on the merits of the screening study alone, DCH is considered resolved for all Westinghouse plants with large dry or subatmospheric containments, and no additional analyses are required.

Most plants showed no intersections of the loads distributions with the fragility distributions. Only one plant, H.B. Robinson, showed a finite but negligible intersection of the load and fragility distribution for some of the scenarios. Tables 7.2 to 7.5 can be used to identify explanations for DCH sensitivity in H.B. Robinson. H.B. Robinson has containment loads that are about one standard deviation above the mean and has a significant line-of-sight flow path (i.e., a high dome transport fraction), which explains the somewhat higher loads. However, H.B. Robinson has the least robust containment of all the Westinghouse plants considered here. The higher loads for H.B. Robinson come about because of the higher dome transport fraction. The containment is actually somewhat larger than average compared to the fuel loading.

Severe accident issues, such as DCH, are judged based on their contribution to the mean containment failure probability, and this is the approach taken here. However, it is desirable and instructive to explore the margin in our analysis results. We address this need by recomputing the CCFPs for each plant using an estimate of the high confidence fragility curve or an arbitrarily biased fragility curve for each plant.

Only two plants reported confidence limits on their fragility curve, all other plants represent modeling and stochastic uncertainties in a single fragility curve. Callaway (W) and Palisades (CE) are both large dry containments having a post-tensioned concrete cylinder with a steel liner. The high confidence fragility curve for these plants can be obtained (approximately) by shifting the mean curve to the left by  $\sim 0.1$  MPa (15 psig) for Callaway and by  $\sim 0.07$  MPa (10 psig) for Palisades. For our study, we have also shifted the fragility curve of each plant 0.1 MPa to the left. This is equivalent to using high confidence fragility curves for Callaway and Palisades. This bias should be viewed as an arbitrary sensitivity study for all other plants.

Table 7.1 summarizes the CCFP for each plant using biased fragility curves. All plants satisfy NRC's guidance that the CCFP  $\leq 0.1$  for DCH issue resolution. Only H.B. Robinson shows CCFPs  $\geq 0.01$ . Five additional sites show finite but negligible intersections with the fragility curves: Salem 1 &

## Results and Sensitivities

2, Ginna, South Texas 1 & 2, Wolf Creek, and Beaver Valley 1 & 2. These are the more sensitive plants to DCH.

Ranking plants according to the load/strength index for each scenario (Tables 7.2 - 7.5) is another way of identifying plant sensitivity. The load/strength, as in Tables 7.2 - 7.5, is used only as a metric to rank plant sensitivity to DCH; and as such, it emphasizes the high end of the load distribution and the low end of the fragility distribution. A ratio greater than one indicates containment threatening conditions only for the very low probability conditions under which it is computed. The two most sensitive plants using this metric are H.B. Robinson and South Texas 1 and 2, and the primary cause for this sensitivity is that the low end of the fragility distribution extends to lower pressures relative to most other plants.

Another metric for load-to-strength sensitivity is the safety margin, which is defined as

$$SM = \frac{\mu(S) - \mu(L)}{(\sigma^2(S) + \sigma^2(L))^{1/2}} \quad (7.1)$$

The safety margin reflects the relative difference between the mean values for strength and fragility. A small value of the safety margin denotes a more sensitive plant.

The safety margin is computed for each plant in Tables 7.6 - 7.9. The safety margin also identifies H.B. Robinson and South Texas 1 and 2 as the most sensitive plants. The mean containment strength for H.B. Robinson is about average. Sensitivity arises because the loads are above average and because of the exceptionally broad fragility distribution. For South Texas 1 and 2 the mean loads are below average, but so too is the fragility by a somewhat greater ratio. The real sensitivity for South Texas 1 and 2 arises again because of the broad fragility distribution. It is significant that uncertainties in fragility play a more dominant role than uncertainties in DCH loads for the more sensitive plants.

Extrapolation of DCH issue resolution beyond the Zion plant was first envisioned in NUREG/CR-6075 (Pilch et al., 1994a) where it was argued that most plants would have load distributions similar to Zion. Similarity of containment loads coupled with an anticipation that there would not be any significant deviations from the Zion fragility curve for containments of a similar class led to the tentative conclusion that DCH could be resolved for most PWRs that had the basic plant layout features of Zion. This report only qualitatively confirms these initial insights through plant-specific analyses, while providing the basis to examine the underlying assumptions of this simplified extrapolation.

Examination of Tables 7.2 to 7.5 shows that the predicted loads for Zion are lower than the mean of all plants. The variation in predicted loads from plant to plant is also large ( $2\sigma \sim 16 - 46$  percent depending on the scenario). The variations would be even larger if you based the comparison on pressure rise instead of total pressure. As an extreme example, the predicted loads for Point Beach 1, 2 in Scenario VI are twice that for Zion. These variations are due in part to differences in plant geometry. Point Beach 1, 2 have significant line-of-sight flow paths to the dome (large dome transport fraction) while Zion does not. On the other hand, Kewaunee and Prairie Island 1, 2 have dome

transport fractions nearly unity but substantially lower loads because the containment is substantially larger (relative to the melt mass).

Tables 7.2 to 7.5 show that the Zion fragility is close to the mean for all plants. However, the variation in fragility from plant to plant is large ( $2\sigma$  ~35 percent). As an extreme example, the containment at H.B. Robinson is only 75 percent as strong as Zion. Section 6 showed that there is no definite correlation of the containment's ultimate capacity with design pressure or construction class.

Extrapolation of DCH issue resolution as envisioned in NUREG/CR-6075 is insightful, but it lacks sufficient rigor to ensure resolution for all plants based on scaling arguments alone. Amongst the population of all plants, the predicted containment pressure +  $2\sigma$  ~ 0.765 MPa at the 99 percent level can be compared with the containment failure pressure -  $2\sigma$  ~ 0.496 at the 1 percent level for Scenario VI; consequently, significant intersections for some plants cannot be ruled out based solely on scaling arguments alone. Extremely high loads are not correlated with extremely weak containments so resolution for all plants could be achieved; however, it was important to perform plant-specific analyses to reach this conclusion.

Tables 7.2 to 7.5 also reveal two interesting trends. On average, intermediate RCS pressures (8 MPa) produced somewhat higher loads (0.530 MPa in Scenario VI and 0.574 MPa in Scenario VIa) than their higher RCS pressure (16 MPa) counterparts (0.454 MPa in Scenario V and 0.567 MPa in Scenario Va). This is attributed to the substantially larger melt masses (~20 mt) ascribed to Scenarios VI and VIa compared to Scenario V and Va.

We also note that scenarios with active containment cooling prior to vessel breach generally produced somewhat higher loads. Although failure of the RPV did not occur, the fan coolers were operational at TMI-II, which kept the steam concentration in the containment to negligible levels. Although the initial pressure in the containment is lower for those scenarios (Va, VIa) with active containment cooling, the final containment pressures following the DCH event are higher than similar scenarios (V and VI respectively) without active containment cooling. This is because a steam free atmosphere favors a more efficient contribution to DCH loads from combustion of preexisting hydrogen.



**Table 7.1 CCFP results**

PLANT	Number of Loops	Mean CCFPs				Est. CCFPs Using Biased Fragility			
		Scn V	Scn Va	Scn VI	Scn VIa	Scn V	Scn Va	Scn VI	Scn VIa
Class 1: Large Dry Containment, Steel Cylinder									
Kewaunee	2	0	0	0	0	0	0	0	0
Prairie Island 1,2	2	0	0	0	0	0	0	0	0
Class 2: Large Dry Containment, Reinforced Concrete Cylinder With Steel Liner									
Shearon Harris	3	0	0	0	0	0	0	0	0
Comanche Peak 1,2	4	0	0	0	0	0	0	0	0
Diablo Canyon 1,2	4	0	0	0	0	0	0	0	0
Indian Point 2	4	0	0	0	0	0	0	0	0
Indian Point 3	4	0	0	0	0	0	0	0	0
Salem 1,2	4	0	0	0	0	0	0.001	0	0.001
Seabrook	4	0	0	0	0	0	0	0	0
Class 3: Large Dry Containment; Post-Tensioned Concrete Cylinder With Steel Liner									
Ginna	2	0	0	0	0	0	0	0.001	0
Point Beach 1,2	2	0	0	0	0	0	0	0	0
Farley 1,2	3	0	0	0	0	0	0	0	0
H.B. Robinson	3	0	0.001	0.004	0.004	0.002	0.010	0.020	0.028
Summer	3	0	0	0	0	0	0	0	0
Turkey Point 3,4	3	0	0	0	0	0	0	0	0
Braidwood 1	4	0	0	0	0	0	0	0	0
Braidwood 2	4	0	0	0	0	0	0	0	0
Byron 1	4	0	0	0	0	0	0	0	0
Byron 2	4	0	0	0	0	0	0	0	0
Callaway	4	0	0	0	0	0	0	0	0
South Texas 1,2	4	0	0	0	0	0	0.001	0	0.003
Vogtle 1,2	4	0	0	0	0	0	0	0	0
Wolf Creek	4	0	0	0	0	0	0.001	0	0.001
Zion 1,2	4	0	0	0	0	0	0	0	0
Class 4: Subatmospheric Containment; Reinforced Concrete Cylinder With Steel Liner									
Beaver Valley 1&2	3	0	0	0	0	0	0.001	0.001	0.001
North Anna 1,2	3	0	0	0	0	0	0	0	0
Surry 1,2	3	0	0	0	0	0	0	0	0
Millstone 3	4	0	0	0	0	0	0.001	0	0

**Table 7.2 Load-to-strength results for Scenario V**

PLANT	Number of	Mean	Pred. Press (MPa)	Failure Press. (MPa)	Load/Strength	Dome	Max UO <sub>2</sub> /Cont. Vol.
	Loops	CCFP	@Prob=0.99	@Prob=0.01		Trans. Fract.	
Class 1: Large Dry Containment; Steel Cylinder							
Kewaunee	2	0	0.433	0.880	0.49	0.58	0.26
Prairie Island 1,2	2	0	0.437	0.880	0.50	0.58	0.25
Class 2: Large Dry Containment; Reinforced Concrete Cylinder With Steel Liner							
Shearon Harris	3	0	0.381	0.818	0.47	0.08	0.42
Comanche Peak 1,2	4	0	0.446	0.756	0.59	0.22	0.59
Diablo Canyon 1,2	4	0	0.463	0.791	0.59	0.21	0.67
Indian Point 2	4	0	0.450	0.701	0.64	0.18	0.68
Indian Point 3	4	0	0.450	0.805	0.56	0.18	0.68
Salem 1,2	4	0	0.465	0.618	0.75	0.23	0.68
Seabrook	4	0	0.447	1.232	0.36	0.17	0.65
Class 3: Large Dry Containment; Post-Tensioned Concrete Cylinder With Steel Liner							
Ginna	2	0	0.450	0.894	0.50	0.50	0.36
Point Beach 1,2	2	0	0.490	0.977	0.50	0.59	0.36
Farley 1,2	3	0	0.448	0.777	0.58	0.20	0.55
H.B. Robinson	3	0	0.485	0.584	0.83	0.62	0.50
Summer	3	0	0.424	0.825	0.51	0.10	0.56
Turkey Point 3,4	3	0	0.490	0.915	0.54	0.18	0.68
Braidwood 1	4	0	0.434	0.660	0.66	0.18	0.61
Braidwood 2	4	0	0.434	0.660	0.66	0.18	0.61
Byron 1	4	0	0.430	0.660	0.65	0.18	0.61
Byron 2	4	0	0.434	0.660	0.66	0.18	0.61
Callaway	4	0	0.475	0.818	0.58	0.17	0.71
South Texas 1,2	4	0	0.445	0.591	0.75	0.16	0.54
Vogtle 1,2	4	0	0.445	0.791	0.56	0.12	0.65
Wolf Creek	4	0	0.475	0.708	0.67	0.17	0.71
Zion 1,2	4	0	0.424	0.770	0.55	0.13	0.62
Class 4: Subatmospheric Containment; Reinforced Concrete Cylinder With Steel Liner							
Beaver Valley 1,2	3	0	0.496	0.660	0.75	0.24	0.60
North Anna 1,2	3	0	0.423	0.660	0.64	0.16	0.58
Surry 1,2	3	0	0.439	0.660	0.67	0.17	0.59
Milstone 3	4	0	0.593	0.708	0.84	0.09	0.77
Mean			0.454	0.766	0.61	0.24	0.57
STD			0.036	0.135	0.11	0.16	0.13
STD/Mean			0.080	0.177	0.18	0.67	0.23

Table 7.3 Load-to-strength results for Scenario Va

PLANT	Number of Loops	Mean CCFP	Pred. Press (MPa)	Failure Press. (MPa)	Load/Strength	Dome	Max UO <sub>2</sub> /Cont. Vol.
			@Prob=0.99	@Prob=0.01		Trans. Fract.	
Class 1: Large Dry Containment; Steel Cylinder							
Kewaunee	2	0	0.539	0.880	0.61	0.58	0.26
Prairie Island 1,2	2	0	0.543	0.880	0.62	0.58	0.26
Class 2: Large Dry Containment; Reinforced Concrete Cylinder With Steel Liner							
Shearon Harris	3	0	0.425	0.818	0.52	0.08	0.42
Comanche Peak 1,2	4	0	0.516	0.756	0.68	0.22	0.59
Diablo Canyon 1,2	4	0	0.567	0.791	0.72	0.21	0.67
Indian Point 2	4	0	0.526	0.701	0.75	0.18	0.68
Indian Point 3	4	0	0.526	0.805	0.65	0.18	0.68
Salem 1,2	4	0	0.551	0.618	0.89	0.23	0.68
Seabrook	4	0	0.572	1.232	0.46	0.17	0.65
Class 3: Large Dry Containment; Post-Tensioned Concrete Cylinder With Steel Liner							
Genoa	2	0	0.705	0.894	0.79	0.50	0.36
Point Beach 1,2	2	0	0.682	0.977	0.70	0.59	0.36
Farley 1,2	3	0	0.571	0.777	0.73	0.20	0.35
H.B. Robinson	3	0.001	0.597	0.584	1.02	0.62	0.50
Summer	3	0	0.590	0.825	0.72	0.10	0.56
Turkey Point 3,4	3	0	0.675	0.915	0.74	0.18	0.68
Braidwood 1	4	0	0.540	0.660	0.82	0.18	0.61
Braidwood 2	4	0	0.540	0.660	0.82	0.18	0.61
Byron 1	4	0	0.540	0.660	0.82	0.18	0.61
Byron 2	4	0	0.540	0.660	0.82	0.18	0.61
Callaway	4	0	0.620	0.818	0.76	0.17	0.71
South Texas 1,2	4	0	0.535	0.591	0.91	0.16	0.54
Vogtle 1,2	4	0	0.575	0.791	0.73	0.12	0.65
Wolf Creek	4	0	0.615	0.708	0.87	0.17	0.71
Zion 1,2	4	0	0.478	0.770	0.62	0.13	0.62
Class 4: Subatmospheric Containment; Reinforced Concrete Cylinder With Steel Liner							
Beaver Valley 1,2	3	0	0.580	0.660	0.88	0.24	0.60
North Anna 1,2	3	0	0.556	0.660	0.84	0.16	0.58
Surry 1,2	3	0	0.563	0.660	0.85	0.17	0.59
Millstone 3	4	0	0.618	0.708	0.87	0.09	0.77
Mean			0.567	0.766	0.76	0.24	0.57
STD			0.058	0.135	0.12	0.16	0.13
STD/Mean			0.102	0.177	0.16	0.67	0.23

Table 7.4 Loads-to-strength results for Scenario VI

PLANT	Number of	Mean	Pred. Press (MPa)	Failure Press. (MPa)	Load/Strength	Dome	Max UO <sub>2</sub> /Cont. Vol.
	Loops	CCFP	@Prob=0.99	@Prob=0.01		Trans. Fract.	
Class 1: Large Dry Containment; Steel Cylinder							
Kewaunee	2	0	0.701	0.880	0.88	0.58	0.78
Prairie Island 1,2	2	0	0.685	0.880	0.78	0.58	0.78
Class 2: Large Dry Containment; Reinforced Concrete Cylinder With Steel Liner							
Shearon Harris	3	0	0.381	0.818	0.47	0.08	0.76
Comanche Peak 1,2	4	0	0.430	0.756	0.57	0.22	0.83
Diablo Canyon 1,2	4	0	0.463	0.791	0.59	0.21	0.94
Indian Point 2	4	0	0.439	0.701	0.63	0.18	0.95
Indian Point 3	4	0	0.439	0.805	0.55	0.18	0.95
Salem 1,2	4	0	0.462	0.618	0.75	0.23	0.95
Seabrook	4	0	0.461	1.232	0.37	0.17	0.92
Class 3: Large Dry Containment; Post-Tensioned Concrete Cylinder With Steel Liner							
Ginna	2	0	0.767	0.894	0.86	0.50	1.06
Point Beach 1,2	2	0	0.855	0.977	0.88	0.59	1.06
Farley 1,2	3	0	0.562	0.777	0.65	0.20	0.98
H.B. Robinson	3	0.004	0.689	0.584	1.18	0.62	0.91
Summer	3	0	0.503	0.825	0.61	0.10	1.01
Turkey Point 3,4	3	0	0.713	0.915	0.78	0.18	1.23
Braidwood 1	4	0	0.430	0.660	0.65	0.18	0.85
Braidwood 2	4	0	0.430	0.660	0.65	0.18	0.85
Byron 1	4	0	0.430	0.660	0.65	0.18	0.85
Byron 2	4	0	0.430	0.660	0.65	0.18	0.85
Callaway	4	0	0.540	0.818	0.66	0.17	0.99
South Texas 1,2	4	0	0.458	0.591	0.77	0.16	0.75
Vogtle 1,2	4	0	0.444	0.791	0.56	0.12	0.92
Wolf Creek	4	0	0.543	0.708	0.77	0.17	0.99
Zion 1,2	4	0	0.408	0.770	0.53	0.13	0.87
Class 4: Subatmospheric Containment; Reinforced Concrete Cylinder With Steel Liner							
Beaver Valley 1,2	3	0	0.598	0.660	0.91	0.24	1.08
North Anna 1,2	3	0	0.544	0.660	0.82	0.16	1.05
Surry 1,2	3	0	0.551	0.660	0.83	0.17	1.06
Millstone 3	4	0	0.577	0.708	0.81	0.09	0.83
Mean			0.530	0.766	0.70	0.24	0.93
STD			0.122	0.135	0.16	0.16	0.11
STD/Mean			0.231	0.177	0.22	0.67	0.12



Table 7.5 Loads-to-strength results for Scenario VIa

PLANT	Number of	Mean	Pred. Press (MPa)	Failure Press. (MPa)	Load/Strength	Dome	Max UO <sub>2</sub> /Cont. Vol.
	Loops	CCFP	@Prob=0.99	@Prob=0.01		Trans. Fract.	
Class 1: Large Dry Containment; Steel Cylinder							
Kewaunee	2	0	0.645	0.880	0.73	0.58	0.78
Prairie Island 1,2	2	0	0.648	0.880	0.74	0.58	0.78
Class 2: Large Dry Containment; Reinforced Concrete Cylinder With Steel Liner							
Shearon Harris	3	0	0.469	0.818	0.57	0.08	0.76
Comanche Peak 1,2	4	0	0.504	0.756	0.67	0.22	0.83
Diablo Canyon 1,2	4	0	0.547	0.791	0.69	0.21	0.94
Indian Point 2	4	0	0.514	0.701	0.73	0.18	0.95
Indian Point 3	4	0	0.514	0.805	0.64	0.18	0.95
Salem 1,2	4	0	0.542	0.618	0.88	0.23	0.95
Seabrook	4	0	0.553	1.232	0.45	0.17	0.92
Class 3: Large Dry Containment; Post-Tensioned Concrete Cylinder With Steel Liner							
Ginna	2	0	0.744	0.894	0.83	0.50	1.06
Point Beach 1,2	2	0	0.749	0.977	0.77	0.59	1.06
Farley 1,2	3	0	0.583	0.777	0.75	0.20	0.98
H.B. Robinson	3	0.004	0.643	0.584	1.10	0.62	0.91
Summer	3	0	0.586	0.825	0.71	0.10	1.01
Turkey Point 3,4	3	0	0.683	0.915	0.75	0.18	1.23
Braidwood 1	4	0	0.524	0.660	0.79	0.18	0.85
Braidwood 2	4	0	0.524	0.660	0.79	0.18	0.85
Byron 1	4	0	0.524	0.660	0.79	0.18	0.85
Byron 2	4	0	0.524	0.660	0.79	0.18	0.85
Callaway	4	0	0.591	0.818	0.72	0.17	0.99
South Texas 1,2	4	0	0.532	0.591	0.90	0.16	0.75
Vogtle 1,2	4	0	0.548	0.791	0.69	0.12	0.92
Wolf Creek	4	0	0.596	0.708	0.84	0.17	0.99
Zion 1,2	4	0	0.486	0.770	0.63	0.13	0.87
Class 4: Subatmospheric Containment; Reinforced Concrete Cylinder With Steel Liner							
Beaver Valley 1,2	3	0	0.599	0.660	0.91	0.24	1.08
North Anna 1,2	3	0	0.564	0.660	0.85	0.16	1.05
Surry 1,2	3	0	0.569	0.660	0.86	0.17	1.06
Millstone 3	4	0	0.595	0.708	0.84	0.09	0.83
Mean			0.574	0.766	0.76	0.24	0.93
STD			0.070	0.135	0.12	0.16	0.11
STD/Mean			0.121	0.177	0.16	0.67	0.12



Table 7.6 Safety margin results for Scenario V

PLANT	Number of Loops	Mean CCFP	$\mu(S)$ MPa	$\sigma(S)$ MPa	$\mu(L)$ MPa	$\sigma(L)$ MPa	SM MPa
Class 1: Large Dry Containment; Steel Cylinder							
Kewaunee	2	0	1.139	0.110	0.371	0.021	6.86
Prairie Island 1,2	2	0	1.143	0.111	0.376	0.020	6.80
Class 2: Large Dry Containment; Reinforced Concrete Cylinder With Steel Liner							
Shearon Harris	3	0	1.184	0.206	0.339	0.019	4.08
Comanche Peak 1,2	4	0	0.891	0.055	0.377	0.030	8.20
Diablo Canyon 1,2	4	0	1.076	0.126	0.388	0.033	5.28
Indian Point 2	4	0	0.964	0.116	0.382	0.032	4.84
Indian Point 3	4	0	1.034	0.110	0.382	0.032	5.69
Salem 1,2	4	0	0.880	0.108	0.391	0.034	4.32
Seabrook	4	0	1.589	0.154	0.379	0.031	7.70
Class 3: Large Dry Containment; Post-Tensioned Concrete Cylinder With Steel Liner							
GINNA	2	0	0.992	0.042	0.384	0.020	13.07
Point Beach 1,2	2	0	1.209	0.076	0.402	0.024	10.13
Farley 1,2	3	0	0.890	0.045	0.378	0.029	9.56
H.B. Robinson	3	0	1.030	0.243	0.395	0.039	2.58
Summer	3	0	1.069	0.073	0.369	0.026	9.03
Turkey Point 3,4	3	0	1.136	0.096	0.406	0.035	7.14
Braidwood 1	4	0	0.953	0.112	0.371	0.029	5.03
Braidwood 2	4	0	0.774	0.036	0.371	0.029	8.72
Byron 1	4	0	0.953	0.112	0.365	0.028	5.09
Byron 2	4	0	0.774	0.036	0.371	0.029	8.72
Callaway	4	0	1.026	0.060	0.398	0.035	9.04
South Texas 1,2	4	0	0.898	0.160	0.378	0.031	3.19
Vogtle 1,2	4	0	1.050	0.095	0.380	0.030	6.73
Wolf Creek	4	0	0.963	0.075	0.398	0.035	6.83
Zion 1,2	4	0	1.015	0.078	0.367	0.028	7.82
Class 4: Subatmospheric Containment; Reinforced Concrete Cylinder With Steel Liner							
Beaver Valley 1,2	3	0	0.973	0.123	0.309	0.049	5.02
North Anna 1,2	3	0	0.973	0.123	0.288	0.037	5.33
Surry 1,2	3	0	0.973	0.123	0.288	0.039	5.31
Millstone 3	4	0	0.909	0.071	0.324	0.065	6.08
Mean			1.016	0.103	0.369	0.032	6.72
STD			0.153	0.047	0.031	0.009	2.28
STD/Mean			0.151	0.461	0.083	0.285	0.34

Table 7.7 Safety margin results for Scenario Va

PLANT	Number of Loops	Mean CCFP	$\mu(S)$ MPa	$\sigma(S)$ MPa	$\mu(L)$ MPa	$\sigma(L)$ MPa	SM MPa
Class 1: Large Dry Containment; Steel Cylinder							
Kewaunee	2	0	1.139	0.110	0.319	0.073	6.21
Prairie Island 1,2	2	0	1.143	0.111	0.312	0.070	6.33
Class 2: Large Dry Containment; Reinforced Concrete Cylinder With Steel Liner							
Shearon Harris	3	0	1.184	0.206	0.288	0.051	4.22
Comanche Peak 1,2	4	0	0.891	0.055	0.296	0.076	6.34
Diablo Canyon 1,2	4	0	1.076	0.126	0.355	0.092	4.62
Indian Point 2	4	0	0.964	0.116	0.284	0.072	4.98
Indian Point 3	4	0	1.034	0.110	0.284	0.072	5.70
Salem 1,2	4	0	0.880	0.108	0.309	0.081	4.23
Seabrook	4	0	1.589	0.154	0.347	0.093	6.90
Class 3: Large Dry Containment; Post-Tensioned Concrete Cylinder With Steel Liner							
Ginna	2	0	0.992	0.042	0.449	0.109	4.65
Point Beach 1,2	2	0	1.209	0.076	0.451	0.103	5.92
Farley 1,2	3	0	0.890	0.045	0.317	0.084	6.01
H.B. Robinson	3	0.001	1.030	0.243	0.401	0.099	2.40
Summer	3	0	1.069	0.073	0.337	0.091	6.27
Turkey Point 3,4	3	0	1.136	0.096	0.419	0.112	4.86
Braidwood 1	4	0	0.953	0.112	0.312	0.084	4.58
Braidwood 2	4	0	0.774	0.036	0.312	0.084	5.06
Byron 1	4	0	0.953	0.112	0.312	0.084	4.58
Byron 2	4	0	0.774	0.036	0.312	0.084	5.06
Callaway	4	0	1.026	0.060	0.407	0.102	5.23
South Texas 1,2	4	0	0.898	0.160	0.306	0.081	3.30
Vogtle 1,2	4	0	1.050	0.095	0.350	0.092	5.29
Wolf Creek	4	0	0.963	0.075	0.406	0.102	4.40
Zion 1,2	4	0	1.015	0.078	0.256	0.061	7.67
Class 4: Subatmospheric Containment; Reinforced Concrete Cylinder With Steel Liner							
Beaver Valley 1,2	3	0	0.973	0.123	0.427	0.080	3.72
North Anna 1,2	3	0	0.973	0.123	0.387	0.088	3.87
Surry 1,2	3	0	0.973	0.123	0.400	0.086	3.82
Millstone 3	4	0	0.909	0.071	0.465	0.073	4.36
Mean			1.016	0.103	0.351	0.085	5.02
STD			0.153	0.047	0.058	0.014	1.14
STD/Mean			0.151	0.461	0.165	0.162	0.23

Table 7.8 Safety margin results for Scenario VI

PLANT	Number of Loops	Mean CCFP	$\mu(S)$ MPa	$\sigma(S)$ MPa	$\mu(L)$ MPa	$\sigma(L)$ MPa	SM MPa
Class 1: Large Dry Containment; Steel Cylinder							
Kewaunee	2	0	1.139	0.110	0.474	0.080	4.89
Prairie Island 1,2	2	0	1.143	0.111	0.473	0.078	4.94
Class 2: Large Dry Containment; Reinforced Concrete Cylinder With Steel Liner							
Shearon Harris	3	0	1.184	0.206	0.34	0.023	4.07
Cornanche Peak 1,2	4	0	0.891	0.055	0.371	0.027	8.49
Diablo Canyon 1,2	4	0	1.076	0.126	0.383	0.032	5.33
Indian Point 2	4	0	0.964	0.116	0.375	0.029	4.93
Indian Point 3	4	0	1.034	0.110	0.375	0.029	5.79
Salem 1,2	4	0	0.880	0.108	0.387	0.033	4.37
Seabrook	4	0	1.589	0.154	0.373	0.032	7.73
Class 3: Large Dry Containment; Post-Tensioned Concrete Cylinder With Steel Liner							
Ginna	2	0	0.992	0.042	0.479	0.100	4.73
Point Beach 1,2	2	0	1.209	0.076	0.574	0.115	4.61
Farley 1,2	3	0	0.890	0.045	0.396	0.043	7.94
H.B. Robinson	3	0.004	1.030	0.243	0.461	0.074	2.24
Summer	3	0	1.069	0.073	0.378	0.041	8.25
Turkey Point 3,4	3	0	1.136	0.096	0.444	0.076	5.65
Braidwood 1	4	0	0.953	0.112	0.365	0.028	5.09
Braidwood 2	4	0	0.774	0.036	0.365	0.028	8.97
Byron 1	4	0	0.953	0.112	0.365	0.028	5.09
Byron 2	4	0	0.774	0.036	0.365	0.028	8.97
Callaway	4	0	1.026	0.060	0.392	0.042	8.66
South Texas 1,2	4	0	0.898	0.160	0.379	0.030	3.19
Vogtle 1,2	4	0	1.050	0.095	0.369	0.030	6.84
Wolf Creek	4	0	0.963	0.075	0.393	0.042	6.63
Zion 1,2	4	0	1.015	0.078	0.357	0.024	8.06
Class 4: Subatmospheric Containment; Reinforced Concrete Cylinder With Steel Liner							
Beaver Valley 1,2	3	0	0.973	0.123	0.431	0.081	3.68
North Anna 1,2	3	0	0.973	0.123	0.379	0.082	4.02
Surry 1,2	3	0	0.973	0.123	0.389	0.083	3.94
Millstone 3	4	0	0.909	0.071	0.424	0.082	4.47
Mean			1.016	0.103	0.402	0.051	5.77
STD			0.153	0.047	0.050	0.027	1.89
STD/Mean			0.151	0.461	0.125	0.533	0.33

Table 7.9 Safety margin results for Scenario VIa

PLANT	Number of Loops	Mean CCFP	$\mu(S)$ MPa	$\sigma(S)$ MPa	$\mu(L)$ MPa	$\sigma(L)$ MPa	SM MPa
Class 1: Large Dry Containment; Steel Cylinder							
Kewaunee	2	0	1.139	0.110	0.499	0.063	5.05
Prairie Island 1,2	2	0	1.143	0.111	0.499	0.063	5.05
Class 2: Large Dry Containment; Reinforced Concrete Cylinder With Steel Liner							
Shearon Harris	3	0	1.184	0.206	0.342	0.069	3.88
Comanche Peak 1,2	4	0	0.891	0.055	0.390	0.057	6.33
Diablo Canyon 1,2	4	0	1.076	0.126	0.430	0.052	4.74
Indian Point 2	4	0	0.964	0.116	0.396	0.060	4.35
Indian Point 3	4	0	1.034	0.110	0.396	0.060	5.09
Salem 1,2	4	0	0.880	0.108	0.422	0.057	3.75
Seabrook	4	0	1.589	0.154	0.433	0.054	7.08
Class 3: Large Dry Containment; Post-Tensioned Concrete Cylinder With Steel Liner							
Ginna	2	0	0.992	0.042	0.566	0.064	5.56
Point Beach 1,2	2	0	1.209	0.076	0.590	0.068	6.07
Farley 1,2	3	0	0.890	0.045	0.449	0.059	5.94
H.B. Robinson	3	0.004	1.030	0.243	0.506	0.060	2.09
Summer	3	0	1.069	0.073	0.455	0.058	6.59
Turkey Point 3,4	3	0	1.136	0.096	0.530	0.061	5.33
Braidwood 1	4	0	0.953	0.112	0.408	0.056	4.35
Braidwood 2	4	0	0.774	0.036	0.408	0.056	5.50
Byron 1	4	0	0.953	0.112	0.408	0.056	4.35
Byron 2	4	0	0.774	0.036	0.408	0.056	5.50
Callaway	4	0	1.026	0.060	0.467	0.052	7.04
South Texas 1,2	4	0	0.898	0.160	0.412	0.056	2.87
Vogtle 1,2	4	0	1.050	0.095	0.430	0.054	5.67
Wolf Creek	4	0	0.963	0.075	0.468	0.052	5.42
Zion 1,2	4	0	1.015	0.078	0.364	0.065	6.41
Class 4: Subatmospheric Containment; Reinforced Concrete Cylinder With Steel Liner							
Beaver Valley 1,2	3	0	0.973	0.123	0.467	0.054	3.77
North Anna 1,2	3	0	0.973	0.123	0.435	0.051	4.04
Surry 1,2	3	0	0.973	0.123	0.439	0.051	4.01
Millstone 3	4	0	0.909	0.071	0.459	0.051	5.15
Mean			1.016	0.103	0.446	0.058	5.03
STD			0.153	0.047	0.056	0.005	1.18
STD/Mean			0.151	0.461	0.125	0.087	0.23



## 8.0 CONCLUSIONS AND RECOMMENDATIONS

This report describes a process for extrapolating the methodology and scenarios developed in NUREG/CR-6075 and NUREG/CR-6075, Supplement 1, to all other PWRs. The first step in the DCH issue resolution process is a screening phase in which loads versus strength comparisons are performed to evaluate the CCFP for each plant using plant-specific data. The results of the screening calculations show that the CCFP based on the mean fragility curves is less than 0.01 for each Westinghouse plant with either a large dry or subatmospheric containment. In fact, only one plant showed a CCFP greater than 0.001. Thus, DCH is considered resolved for all Westinghouse plants, except those with ice condenser containments, and no additional analyses are required.

The CCFPs for each plant were recalculated using a biased fragility curve that is shifted to the left by 0.1 MPa. For Callaway and Palisades, the biased fragility curves are representative of high confidence fragility curves; and for all other plants, the biased fragility curves should be interpreted as arbitrary sensitivity studies. All plants have a CCFP less than the required success criterion of 0.1 even with biased fragility curves. Only H.B. Robinson has a CCFP greater than 0.01; for Scenario VIa, H.B. Robinson shows a CCFP of 0.028. H.B. Robinson appears to be the most sensitive of the plants analyzed because it has a large line-of-sight debris transport pathway to the containment dome and a containment fragility curve to the left of all other plants. Five other sites show finite but negligible intersections of the loads distributions with biased fragility curves: Ginna, Salem 1 & 2, South Texas 1 & 2, Wolf Creek, and Beaver Valley 1 & 2.

Three recommendations for confirmatory work were suggested in NUREG/CR-6075 and were addressed in this work. The recommendations from NUREG/CR-6075 are quoted below and are followed by a paragraph describing how the recommendation was addressed in this report.

1. *Deeply Flooded Cavities*: "This plant-specific item is needed to identify any cases where geometry allows the build-up of water depths significantly higher than the condensate levels examined so far. Need for any additional evaluations will depend on the extent of such situations and on the particulars of each case."

A plant-specific evaluation of the potential for having water in the cavity at vessel breach was performed and is provided in Table C.4. The plants are grouped as either dry (condensate water), wet, or flooded. If there is no RWST injection, then 26 plants will be dry, 11 plants will be wet, and 4 plants did not provide sufficient information. If the RWST tank empties, then 21 plants will be flooded, 11 plants will be wet, 7 plants will be dry, and 2 plants did not provide sufficient information. For cavities with significant amounts of water, existing analyses and experimental data indicate that HPME-induced containment loads are comparable to or less than the loads with dry cavities for oxidic melts. Table C.4 also classifies cavities as either excavated (29 plants) or free standing (12 plants). For cavities with significant amounts of water at vessel breach, the cavity loads due to fuel-coolant interactions could potentially damage or fail free standing cavities. Failure of a free standing cavity would not result in significantly higher DCH loads. In fact, if debris were dispersed directly into the containment basement, cavity failure might reduce the DCH load. Detailed assessments of potential FCIs and their impact on cavity structures is outside the scope of this report.



## Conclusions and Recommendations

2. *System Pressure Level:* "Even though we show that melt expulsion with maximum primary system pressures do not lead to any significant concerns for Zion, we cannot categorically exclude system pressures above 8 MPa at this time for all plants. It may be worthwhile to determine if system pressures above 8 MPa can be excluded. This issue is explicitly addressed in integrated DCH issue resolution task."

The initial conditions working group (NUREG/CR-6075, Supplement 1) recommended performing some DCH analyses at full system pressure to better envelop operator intervention accidents such as TMI-II. Scenarios V and Va were analyzed at 16 MPa and Scenarios VI and VIa were analyzed at 8 MPa. The splinter scenarios were analyzed at these high pressures even though SCDAP/RELAP5 analyses of Zion, Surry, Calvert Cliffs, and Arkansas Nuclear One indicate that there is a high likelihood of system depressurization due to ex-vessel failures for station blackout scenarios without operator intervention.

3. *Containment Strength:* "It remains to be determined whether there are any significant deviations from the Zion fragility for containments of a similar class. Containment capability is affected by design details and must be examined on a plant-specific basis, possibly through the IPE or ongoing research sponsored by the NRC."

Containment fragility has been compiled from the IPEs on a plant-specific basis and is summarized in Section 6 and compiled in Appendix D. From these assessments, we made several important conclusions. The ultimate capacity of the containment does not correlate well with the design pressure. The average estimated failure pressure of all 41 plants at the 1 percent probability level is 97 psig with a standard deviation of  $\pm 20$  psig, i.e., the variation in plant fragilities is relatively large.

## 9.0 REFERENCES

- Allen, M.D. et al. (1990). *A Demonstration Experiment of Steam-Driven, High-Pressure Melt Ejection: The HIPS-10S Test*, NUREG/CR-5373, SAND89-1135, Sandia National Laboratories, Albuquerque, NM.
- Allen, M.D. et al. (1991). *Experiments to Investigate the Effect of Flight Path on Direct Containment Heating (DCH) in the Surtsey Test Facility: The Limited Flight Path (LFP) Tests*, NUREG/CR-5728, SAND91-1105, Sandia National Laboratories, Albuquerque, NM.
- Allen, M.D. et al. (1992). *Experiments to Investigate the Effect of Water in the Cavity on Direct Containment Heating (DCH) in the Surtsey Test Facility - The WC-1 and WC-2 Tests*, SAND91-1173, Sandia National Laboratories, Albuquerque, NM.
- Allen, M.D. et al. (1993). *Experiments to Investigate the Effects of Fuel/Coolant Interactions on Direct Containment Heating*, The IET-8A and IET-8B Experiments, SAND92-2849, Sandia National Laboratories, Albuquerque, NM.
- Allen, M.D. et al. (1994). *Experiments to Investigate Direct Containment Heating Phenomena with Scaled Models of the Zion Nuclear Power Plant in the Surtsey Test Facility*, NUREG/CR-6044, SAND93-1049, Sandia National Laboratories, Albuquerque, NM.
- Bertodano, M. Lopez de (1993). *Direct Containment Heating DCH Source Term Experiment for Annular Reactor Cavity Geometry*, Ninth Proceedings of Nuclear Thermal Hydraulics, 1993 ANS Winter Mtg., Nov. 14-18, 1993, San Francisco, CA, p. 111-120.
- Binder, J.L. et al. (1994). *Direct Containment Heating Integral Effects Tests at 1/40 Scale in Zion Nuclear Power Plant Geometry*, NUREG/CR-6168, ANL-94/18, Argonne National Laboratory, Argonne, IL.
- Blanchat, T.K. et al. (1994). *Experiments to Investigate Direct Containment Heating Phenomena With Scaled Models of the Surry Nuclear Power Plant*, NUREG/CR-6152, SAND93-2519, Sandia National Laboratories, Albuquerque, NM.
- Boyack, B.E. et al. (1985). *CONTAIN Independent Peer Review*, LA-12866, Los Alamos Scientific Laboratory, Los Alamos, NM.
- Denny, V.E., and B.R. Sehgal (1983). "Analytical Prediction of Core Heatup/Liquefaction/Slumping," *Proceedings International Meeting on Light Water Reactor Severe Accident Evaluation*, Aug. 28-Sept. 1, Cambridge, MA.
- Epstein, M., and H.K. Fauske (1989). "The Three Mile Island Unit 2 Core Relocation -- Heat Transfer Mechanisms," *Nuclear Technology*, Vol. 87, p. 1021.

## References

- Gauntt, R.O., R.D. Gasser, and L.J. Ott (1989). *The DF-4 Fuel Damage Experiment in ACRR With a BWR Control Blade and Channel Box*, NUREG/CR-4671, SAND86-1443, Sandia National Laboratories, Albuquerque, NM.
- Hammersley, R.J. et al. (1993). "Experiments to Address Lower Plenum Response Under Severe Accident Conditions," *Proceedings of the International Topical Meeting on Probabilistic Safety Assessment (PSA93)*, Clearwater Beach, FL.
- Hanson, D.J. et al. (1990). *Depressurization as an Accident Management Strategy to Minimize the Consequence of DCH*, NUREG/CR-5447, U.S. Nuclear Regulatory Commission, Washington, DC.
- Heames, T.J., and R.C. Smith (1987). "Integrated MELPROG/TRAC Analyses of a PWR Station Blackout," *Nuclear Engineering and Design*, Vol. 125, pp. 175-188.
- Henry, R.E. et al. (1991). "Direct Containment Heating Experiments in a Zion-like Geometry," in *26th National Heat Transfer Conference*, Vol. 87.
- IDCOR (1985). *Technical Support for Issue Resolution*, IDCOR, Technical Report 85.2, Fauske and Associates, Inc., Burr Ridge, IL.
- Kelly, J.E., et al. (1987). *MELPROG-PWT/MODI Analysis of a TMLB' Accident Sequence*, NUREG/CR-4742, SAND86-2175, Sandia National Laboratories, Albuquerque, NM.
- Knudson, D.L. (1993). Transmittal of SCDAP/RELAP5/MOD3 Results for the Zion Power Station, Letter Report to NRC.
- Knudson, D.L., and C.A. Dobbe (1993). *Assessment of the Potential for High Pressure Melt Ejection Resulting from a Surry Station Blackout Transient*, NUREG/CR-5949, EGG-2689, EG&G Idaho, Inc., Idaho Falls, ID.
- Marshall, B.W. (1988). *Reactor Safety Research Semi-annual Report July-December 1987*, NUREG/CR-5039, SAND87-2411, Vol. 2, p. 244, Sandia National Laboratories, Albuquerque, NM.
- NRC (1992). *Severe Accident Research Program Plan Update*, NUREG-1365, Rev. 1, U.S. Nuclear Regulatory Commission, Washington, DC.
- Pilch, M., and W.W. Tarbell (1985). *High Pressure Ejection of Melt from a Reactor Pressure Vessel: The Discharge Phase*, NUREG/CR-4383, SAND85-0012, Sandia National Laboratories, Albuquerque, NM.
- Pilch, M., and W.W. Tarbell (1986). *Preliminary Calculations on Direct Heating of a Containment Atmosphere by Airborne Core Debris*, NUREG/CR-4455, SAND85-2439, Sandia National Laboratories, Albuquerque, NM.

- Pilch, M.M. et al. (1992). "Counterpart and Replicate DCH Experiments Conducted at Two Different Physical Scales: The SNL/IET-1, 1R and the ANL/IET-1R, 1RR Experiments," Letter Report to the NRC, Sandia National Laboratories, Albuquerque, NM.
- Pilch, M.M. et al. (1994a). "*The Probability of Containment Failure by Direct Containment Heating in Zion*," NUREG/CR-6075, SAND93-1535, Sandia National Laboratories, Albuquerque, NM.
- Pilch, M.M. et al. (1994b). "*The Probability of Containment Failure by Direct Containment Heating in Zion*," NUREG/CR-6075, Supplement 1, Sandia National Laboratories, Albuquerque, NM.
- Pilch, M.M. et al. (1995). "*The Probability of Containment Failure by Direct Containment Heating in Surry*," SAND93-2078, NUREG/CR-6109, Sandia National Laboratories, Albuquerque, NM.
- Pilch, M.M. (1995). "Hydrogen Combustion During DCH Events," to be presented at National Heat Transfer Conference (NHTC), Portland, OR.
- PRAWG (1994). "A Review of NRC Staff Uses of Probabilistic Risk Assessment," PRA Working Group, U.S. Nuclear Regulatory Commission, Washington, DC.
- Rempe, J.L. et al. (1993). *Light Water Reactor Lower Head Failure Analysis*, NUREG/CR-5642, EGG-2618, Idaho National Engineering Laboratory, Idaho Falls, ID.
- Stickler, L.A. et al. (1993). *Calculations to Estimate the Margin to Failure in the TMI-2 Vessel*, TMI V(93)EG01, Idaho National Engineering Laboratory, EG&G Idaho, Inc., Idaho Falls, ID.
- Theofanous, T.G. (1988). "Some Considerations of Severe Accidents at Loviisa," Report Prepared for Imatron Voima 04, Helsinki, Finland.
- Tutu, N.K. et al. (1988). "Low Pressure Cutoff for Melt Dispersion from Reactor Cavities," in *Fourth Proceedings of Nuclear Thermal Hydraulics*, p. 29-37.
- Tutu, N.K. et al. (1990). "Estimation of Containment Pressure Loading Due to Direct Containment Heating for the Zion plant," BNL-NUREG-52181, NUREG/CR-5282, Brookhaven National Laboratory, Upton, NY.
- Williams, D.C. and D.L.Y. Louie (1988). "CONTAIN Analyses of Direct Containment Heating Events in the Surry Plant," ANS/ENS International Meeting, ANS Thermal Hydraulics Division, Washington, DC.
- Williams, D.C. et al. (1995). *Assessment of the CONTAIN Direct Containment Heating (DCH) Model*, SAND94-1174, Sandia National Laboratories, Albuquerque, NM.
- Zuber, N. et al. (1991). *An Integrated Structure and Scaling Methodology for Severe Accident Technical Issue Resolution*, Draft for Comment, NUREG/CR-5809, EGG-2659, EG&G Idaho, Inc., Idaho Falls, ID.

**APPENDIX A**  
**Peer Review of NUREG/CR-6338**

The external peer review process will be documented here.





*Fauske & Associates, Inc.*

July 28, 1995

M. Wayne Hodges, Director  
Division of Systems Technology  
Nuclear Regulatory Commission  
Washington, D.C. 20555-0001

Dear Mr. Hodges:

As your requested I have reviewed the draft copy of NUREG/CR-6338, "Resolution of the Direct Containment Heating Issue for all Westinghouse Plants with Large Dry Containment or Subatmospheric Containments". I find that this is a major step forward in the resolution of this important severe accident issue. I applaud the NRC for taking this step to resolve issues on a design specific basis such that individual plants have a clear understanding of the evaluation as applied to that design.

While this is a substantial step forward, there are some issues that I believe should be addressed more completely. My comments on these issues are delineated in the attached summary.

Thank you for the opportunity to review this document. Should you have any questions regarding my comments, please feel free to call at any time.

Sincerely yours,

Robert E. Henry  
Senior Vice President

REH:lab  
Attachment

cc: Dr. M. Khtaib-Rahbar

16W070 West 83rd Street • Burr Ridge, Illinois 60521 • (708) 323-8750  
Telefax (708) 986-5481

Comments on Draft NUREG-6338

The NRC and its contractors are to be complemented on formulating an approach that enables this important severe accident issue to be resolved on a design specific basis. The approach of considering the various scaled experiments, analyses of the dominant accident sequences and a review of the design specific features that could influence these phenomena for the spectrum of Westinghouse plants is the appropriate path to resolution. Fundamentally, the major elements determining potential loads from a high pressure melt ejection (HPME) are:

- mass of molten core debris that could be dispersed,
- RCS pressure at the time of reactor vessel failure,
- strength of the containment building,
- the internal containment structures that could prevent large fractions of molten core debris from being dispersed and
- the extent of unreacted metals in the molten debris.

This draft document considers all of these in a credible manner for the various design specific features that need to be addressed:

- size of the reactor core,
- spectrum of accident sequences where the RCS could be at an elevated pressure,
- the plant specific structural capabilities for the containment building,
- the structures within the containment building that could influence debris transport, and
- SCDAP/RELAP5 analyses for the extent of metallic constituents in the melt.

Using a screening approach of  $CCFP < 0.01$  is also appropriate. With this screening criteria one can sort out those plants where a more detailed assessment may be required from those where the issue is sufficiently clearly defined that no further evaluations are necessary. Once the screening criteria has been exercised, those designs where a more careful examination is necessary can be compared to the formulation used by the NRC ( $CCFP < 0.1$ ) and if needed, the approaches taken for the various components, i.e. cavity design, containment fragility, etc. can be more closely examined.

The key insights listed with respect to the SCDAP/RELAP5 calculations are consistent with my experience from MAAP4 calculations on similar plants. In particular:

- Hot leg failure is predicted before substantial melt relocation assuming the operator does not intervene and recovery is not attempted.
- There is only a small amount of metal in the molten debris which drains into the lower plenum. Furthermore, this metal is steel.
- There is approximately 60% of the cladding reacted (as an upper bound) and much of the remaining zirconium is contained in metallic blockages that are low in the core and difficult to oxidize.
- The extent of molten material in the lower plenum at the time of lower head failure is 55-66 metric tonnes for a Zion-like reactor.

Consequently, this report addresses the major issues for assessing direct containment heating in the various Westinghouse designs as advertised by the title. There are secondary issues which should be addressed before the report is issued in final form. These are delineated below.

1. A substantial part of the design specific assessment is the extent of molten core debris that is available to be dispersed at the time that the RPV fails. This is given for the three different kinds of RCS designs in Figures 4.5 and 4.7. These result from a simplified geometric argument which is reasonable. To support this, it would be helpful if SCDAP/RELAP5 calculations could be performed for a 2-loop design, in addition to the 3-loop and 4-loop plant results. This would provide the general analytical support for the extent of molten material that exists in the lower plenum at some time after the debris drains into the lower plenum. As an example I would suggest that a time of 1 hour after debris enters the lower plenum be used as a general guide for the interval before RPV failure to analytically support the differences in molten material distributions between the different plants.
2. In the plant specific evaluations there are two plants that do not fall into the representation provided by Zion and Surry, i.e. HB Robinson and the South Texas plants. There is extensive discussion on the resolution for HB Robinson but little on that with regard to resolution of the issue for the South Texas project. The discussion part of the report should be expanded (see 3 and 4 below) such that it is clear on how the issue was resolved for the South Texas design.
3. The report is confusing in the treatment of the South Texas 1 & 2 design. On page 50 it states: "There is no vertical debris transport pathway from the cavity except through the annular gap between the RPV and biological shield wall, so for South Texas 1 & 2 the fraction of debris that can be transported through the lower compartments is assumed to be 0." This text indicates that all the debris which is dispersed must go upward through the gap. Moreover, on page C-27 it states that "Debris could be ejected from these two openings but it would be ejected horizontally and would not reach the dome region. Thus we assume that the only debris transport path away from the cavity was through the RPV annular gap." Here again it is apparent that the debris leaving the cavity flows through the annular gap. However, when looking at the entries on Table

C.5, the fraction transferred to the annular gap is 0.162 which is derived from the geometric ratio of the gap area and the cavity area. Using this it would appear that the report concludes that a substantial fraction of the debris in the evaluation for South Texas 1 & 2 would be retained in the reactor cavity and not dispersed. On the other hand Table C.1 concludes that 92% of the debris discharged to the cavity would be dispersed. The only other potential scenario is that the debris could be dispersed through the personnel access doors but is discounted as being a contributor to direct containment heating. Whatever the logic, it should be explicit because it appears to be substantially different than that used for the other plants.

4. The discussion on the South Texas design mentions a tortuous path out of the reactor cavity to the floor of the containment. This path is through a personnel door that would take no significant pressure. Hence, this is not something that would typically be considered as tortuous and certainly would have a significant area to remove debris during a high pressure melt ejection. Since this is one of the plants which does not fit into a general category, I think the actual design of the South Texas cavity deserves a more extensive narrative and some consideration with respect to how this is treated in the report.
5. On page 43 it is important to note that the potential influence of water in the analysis may not be significant with respect to the containment pressurization, but it may be quite significant with respect to the resulting containment temperatures.
6. On page 64 it should be recognized that some of the containment fragility curves used in the IPE studies may already be quite conservative. A conservatism used in some IPE studies was to "tie" the containment fragility curve to the design basis pressure on the low end of the curve. This extends the very low probability failure "tail" to pressures that are marginally above the design pressure. It is this low pressure "tail" that is principally used in the evaluation for this report. Hence, these specific differences in the analysis approach for IPEs and their inherent conservatisms should be noted in this discussion.
7. On page 65 the word "distinguished" should be removed with respect to the HB Robinson plant.
8. On page 66 the word "fortunately" should be removed. The results are what they are and they are neither fortunate nor unfortunate.
9. On page 72 the HB Robinson containment is characterized as a "weak containment". While this containment may not be as strong as others which are included in the evaluation, within the uncertainties embedded in such containment fragility curves, it is not substantially different from Salem 1, 2, Braidwood 2, Byron 2 and the South Texas containments. All of these containment buildings are extremely strong considering their size. Hence, these discussions should just focus on the "line-of-site debris transport pathway to the containment dome" combined with the plant specific containment fragility

curve as represented in Table 6.1. It is not appropriate to characterize the Robinson containment as being weak.

10. On page 72 the discussion is related to fuel coolant interactions failing free standing cavities should use the words "are current assumed to be sufficient to" unless some analysis is presented that would enable quantification of the word "could".



M. Wayne Hodges, Director  
Division of Systems Technology  
Office of Nuclear Regulatory Research  
Washington D. C. 20555-0001

August 9, 1995

Dear Dr. Hodges,

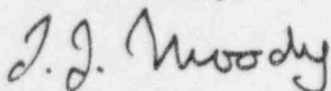
This letter confirms my support of the conclusion that the DCH issue is resolved for all Westinghouse plants with dry containments.

The arguments leading to this conclusion in NUREG/CR-6338 appear to be firmly established. The CCFP (Conditional Containment Failure Probability) calculations performed with the TCE (Two Cell Equilibrium) model for load distributions, combined with the mean fragility curves, are reported to be less than 0.01 for each plant analyzed. The basis for resolution is the NRC recommendation that the DCH issue is resolved for plants with a CCFP less than or equal to 0.1.

The procedure reported begins with a screening process for containment loads and strength. Apparently all the Westinghouse plants with dry containments passed the screening with CCFP's of less than 0.01, a comfortable margin below the NRC recommendation for DCH issue closure.

I have had the privilege of following the history leading to DCH issue resolution for the Zion and Surry plants. The painful attention to detailed initial conditions, probability distributions, experimental and system level computational results demonstrates a degree of thoroughness and competency on the part of the investigators which can be held in confidence by the technical community. All reasonable vulnerabilities in the methodology have been addressed, in my opinion. Beginning with known conservatisms, and refining as necessary to evaluate whether a containment system failure probability is acceptable has led to the development of a mature, efficient approach which is followed in the DCH issue resolution methodology.

Yours truly,



F. J. Moody  
GE Nuclear Energy  
Mail Code 747  
175 Curtner Avenue  
San Jose, CA 95125  
(408) 925-6434

cc: R. Lee (NRC)  
M. Khatib-Rahbar

# LEVY & ASSOCIATES

3880 S. Bascom Ave., Suite 112  
San Jose, CA 95124  
408/369/6500  
FAX 408/369-8720

July 24, 1995

Mr. M. Wayne Hodges, Director  
Division of Systems Technology  
Office of Nuclear Regulatory Research  
Nuclear Regulatory Commission  
Washington, D. C. 20555-0001

Dear Mr. Hodges:

As per your request of June 21, 1995, I have reviewed the draft copy of NUREG/CR-6338, "Resolution of Direct Containment Heating for all Westinghouse Plants with Large Dry Containments or Subatmospheric Containments" and my comments are as follows:

1. The report provides an important perspective about the impact of Direct Containment Heating (DCH) upon the conditional containment failure probability (CCFP) of Westinghouse plants with dry or subatmospheric containments. The impact is found to be small for all such Westinghouse plants. This is a significant result particularly when compared to our state of knowledge at the issuance time of NUREG-1150. The attached Figure ES.11 taken from NUREG-1150 shows that DCH was anticipated to make a big increase to the probability of early containment failure as illustrated for the Surry plant. NUREG/CR-6338 clearly shows that this is not the case for Westinghouse plants with dry or subatmospheric containments. This conclusion was reached because of relentless efforts by the Research Division of NRC and by the Sandia National Laboratories (SNL) and all those involved deserve to be congratulated.

2. In Figure 2.1, NUREG/CR-6338 sets the goal of  $CCFP \leq 0.1$  for DCH from High Pressure Melt Ejections (HPME) into the Zion and Surry containments. It also proposes that the DCH issue should be considered resolved for all other Westinghouse dry and subatmospheric containments if  $CCFP \leq 0.01$  due to DCH. This more stringent requirement was imposed upon all other plants because the models employed in the calculations "are tied to the Zion and Surry data base" and because "other plants have different geometries and flow paths which necessitate some judgment in application of the models". If any plant cannot pass the criterion of  $CCFP \leq 0.01$ , several options are described at the bottom of page 6 of NUREG/CR-6338 to refine the calculations and possibly to resolve the DCH issue. This strategy, needs clarifications and additional support for the following reasons:

a) It is not clear how the value of  $CCFP \leq 0.1$  for DCH was arrived at. There are other NRC publications which propose  $CCFP \leq 0.1$  for all early modes of containment failure.

b) There are several other core damage scenarios which can lead to early containment failure. The attached Figure E.S. 11 from NUREG-1150 shows that the probability of early containment failure for the Surry plant for scenarios not involving DCH ranges from 0.02 to 0.4. The corresponding probability for the Zion plant is lower and goes from about close to zero to 0.16. There is merit to recognizing the early failure containment performance of a plant to all core damage scenarios when assigning a goal to those produced by DCH. Also, this would provide a stronger tie-up of the DCH assessments to the PRA's or IPE's generated for the plants.

c) The Zion and Surry plants CCFP's for DCH were based upon an extensive data base and models validated for those specific geometries. They were also found to be quite small, i.e.  $CCFP's \leq 0.01$ . Those small values helped relieve many of the concerns this reviewer had about the uncertainties associated with that methodology and data base and the need to quantify them. Those uncertainties will certainly grow when the Zion/Surry data base and models are applied to plants of "different geometries and flow paths" and NUREG/CR-6338 does not attempt to quantify that degree of extrapolation and the associated increase in uncertainties. In other words, no quantitative justification is provided that a  $CCFP \leq 0.01$  is adequate for the "screening" calculations carried out in NUREG/CR-6338.

d) Similarly, no quantitative information is provided to justify the adequacy of options provided at the bottom of page 6 of NUREG/CR-6338. For example, how does one reach the conclusion that a  $CCFP \leq 0.1$  is adequate for the screening of plants if combined with a high confidence fragility curve?

In summary, NUREG/CR-6338 shows that Westinghouse plants with dry or subatmospheric containments yield "screening"  $CCFP's \leq 0.01$  for DCH but it does not provide enough basis to show that the result is adequate to account for the uncertainties introduced by the screening methodology. The report should try to quantitatively address that issue and to take into account that the Zion/Surry plants achieved  $CCFP's \leq 0.01$  without the same screening uncertainties.

3. NUREG/CR-6338 utilizes a considerable amount of plant information to carry out its screening calculations. It is not clear that the information has been validated or verified by the plant owners. If this has not been done, the NRC should encourage it to happen (e.g., as part of PRA's or IPE's review). In fact, there is a significant advantage to reverting to the usual process of having the licensees perform their own DCH assessments using NUREG/CR-6338 as a guide and incorporating those results in their own PRA's or IPE's. This would assure not only the use of correct plant information but also provide the licensees with a better understanding of DCH phenomena and ways to formulate an improved PRA or IPE.

4. With respect to initial conditions:

a) Insufficient insight was derived from the code results of SCDAP-RELAP5. For example, one suspects that the fuel specific power influences the initial conditions

because the higher the fuel specific power and core power density the greater will be the amount of molten material to be ejected and the earlier the reactor vessel failure will occur. The results obtained for Calvert Cliffs and ANO-2 from SCDAP-RELAP5 support this premise (see last statement on page B-5 of NUREG/CR-6338) and could help quantify that parameter so that plants operating with reduced or increased specific power fuel can recognize its benefit or penalty.

b) The grouping of Westinghouse plants into two, three, and four loops is reasonable because it is generally indicative of plant power and reactor fuel mass. However, there are exceptions which deserve attention. For instance, the South Texas plant is an outlier of the four loop plants because of its increased output and its fuel and zirconium contents being about 20 to 25 percent above the other four loop plants. I believe South Texas employs fuel 14 ft instead of 12 ft length and this needs to be recognized in NUREG/CR-6338 and possibly its impact assessed through a SCDAP-RELAP5 run. Similarly, the melt mass assigned to two-loop plants may be too low because it relies upon an approximate prescription given in NUREG/CR-6075, Supplement 1 which takes advantage of the assumption that the last row of fuel assemblies does not melt. SCDAP-RELAP5 does not support that judgment. Here again, a SCDAP-RELAP5 run could have been helpful to assess the behavior differences of two-loop plants.

c) The dry scenarios VII and VIII are not considered in NUREG/CR-6338 because they are associated with complete depressurization of the reactor vessel and, therefore, they are not pertinent to DCH. However, they involve significant metallic contents which could be released to the cavity and become oxidized if the cavity contains water. These scenarios pose different risks beyond DCH to the containment integrity and they need to be considered in overall containment risk assessments.

To summarize, the impact of fuel specific power, of variations in core size and, particularly, of their fuel contents, and of small reactor cores need to be strengthened.

5. In NUREG/CR-6338, the Zion/Surry DCH data base and models are force-fitted to all other Westinghouse plants with dry or subatmospheric containments. This approach raises several issues which are not addressed adequately in the report:

a) NUREG/CR-6338 categorizes all cavities into three groups: Zion-like, Surry-like, and other. Only the South Texas 1 & 2 plants fall into the other category. This allows NUREG/CR-6338 to apply the Zion or Surry coherence ratio correlations to 95 percent of the considered Westinghouse plants. In the case of South Texas 1 & 2, the Zion/Surry data base was also employed after it was combined and biased by one standard deviation. The authors state that the "process is one of interpolation rather than extrapolation" and justify it by claiming that the "coherence correlation is a weak function of the cavity type". This perception is reinforced by the statement on page 44 of NUREG/CR-6338 which requires "a model for coherence ratio as a function of hole size" without any mention of cavity geometry. In fact, we have data on two cavity geometries and it is difficult to justify interpolation or extrapolation with only two sets of data points. Furthermore, the available data show a dependence upon geometry, i.e. about a 25 percent difference in the correlation constant. Furthermore, the cavity sketches developed by IDCOR show considerable variations in geometry and necessitated their classification into a total of 14 different types by IDCOR. It is also worthwhile to note that the IDCOR



study of cavities had suggested that the Surry-like cavity would be more retentive than the Zion cavity and the SNL DCH tests have shown an opposite trend. Based upon such considerations of limited cavity geometric testing, the large variations among geometries, and the difficulty to pass judgment on cavity performance, it is surprising that the Zion/Surry data base was utilized in NUREG/CR-6338 with no bias added for 95 percent of the considered Westinghouse plants and with only one standard deviation being applied to the South Texas 1 & 2 plants. Without further justification by the authors, it could make much more sense to apply the Zion/Surry data base only to plants with identical geometries to the data base, to add one standard deviation to plants which are similar, and two standards to plants with significant differences; and a three standard deviation may be in order for other plants.

b) On page 49 of NUREG/CR-6338, a 5 percent dome transport fraction is suggested for 32 out of 41 plants even though the Zion and Surry experiments showed about a 9 percent dome transport. Several reasons are given for the use of 5 percent, but it is not clear whether that reduction is supported by tests or that it is applicable to the 32 plants. Again, it might make more sense to use a 9 percent transport to the dome to cover this lack of test data and potential variations in geometries.

c) The models used for transport of debris through the gap, i.e. Eq. (5.9), and for the debris transport through line-of-sight flow paths, i.e. Eq. (5.10) are oversimplified expressions which rely exclusively upon area ratios. They are not supported by extensive tests and they do not cover geometric variations. For that reason, they may not apply literally to all plant conditions. For example, in the case of South Texas 1 & 2, "there is no vertical debris transport pathway except through the annular gap." However, Eq. (5.9) is applied to a cavity "access labyrinth which has two openings to the lower compartment: a ventilation duct and a personnel access hatch". In fact, the labyrinth path may be subject to a different pressure drop than an opening in the cavity. Also, it is expected that the access hatch would be closed during operations so that its structural strength and failure mode could reduce the values used in Eq. (5.9). (Note that such pressure drop arguments are made by the authors on page C-26 for the Salem 1 & 2 plants when they help reduce the flow along the vessel). Here again, there may be a need to modify Eqs. (5.9) and (5.10) or to provide a factor to account for such differences.

6. Several judgments are made without providing sufficient justification. Typical examples are:

a) After a study and evaluation of degree of cavity flooding with water, the statement is made (see page 43) that "consistent with the limited data, we ignore the potential impact of cavity water in our analyses".

b) 12 plants are reported to have free standing cavities which are "potentially vulnerable to damage from high cavity pressure resulting from explosive or non-explosive FCIs in the cavity" (See page 43). Any impact such damage may have on the coherence ratio or the line of sight flow paths is not considered.

c) About 10mt of the debris being ejected is assumed to be solid and to be able to participate in DCH. Because such debris would have to be fragmented to particles about 1mm in size to participate in DCH, "the impact of solid debris on DCH loads is judged to



be insignificant and is neglected in these evaluations". There is no data for supporting that position.

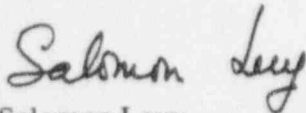
d) On page 44, it is stated that "the calculations and results presented here are performed by ignoring any impact of coejected water". The reason given for ignoring such impact is that "the margins are significant to DCH threat for Westinghouse plants".

Such judgments need additional support or some estimate of their potential impact should be provided. This is necessary because the available data on these issues are rather limited and in some cases non-existent.

7. The report identifies several items which will be dealt with hopefully before the issuance of the final report. For example, on page 47, it is recognized that some of the plants have significant, higher dome transport fractions than the existing data base. It is proposed to address this potential impact in upcoming tests to be conducted in Combustion Engineering geometry. Similarly, the authors indicate in a few places that they lack plant information and they should get it to avoid later changes.

My overall summary is that NUREG/CR-6338 shows that the DCH impact is small for Westinghouse plants with dry and subatmospheric containments as long as the Zion/Surry data based and models are applicable to the plants. It fails to account to a sufficient degree for the variations in geometries, structural designs, and conditions at time of DCH. An effort to estimate or bound the various issues raised in this letter and a calculation of loads under such estimated or bounding conditions could strengthen the report conclusions. It would show quantitatively that the probability of early containment failure by DCH is still small with conservative assumptions. Also, involvement of plant licensees is urged in validating plant characteristics and in applying DCH methodology.

Sincerely yours,



Salomon Levy

cc: Dr. M. Khatib-Rahbar, ERI

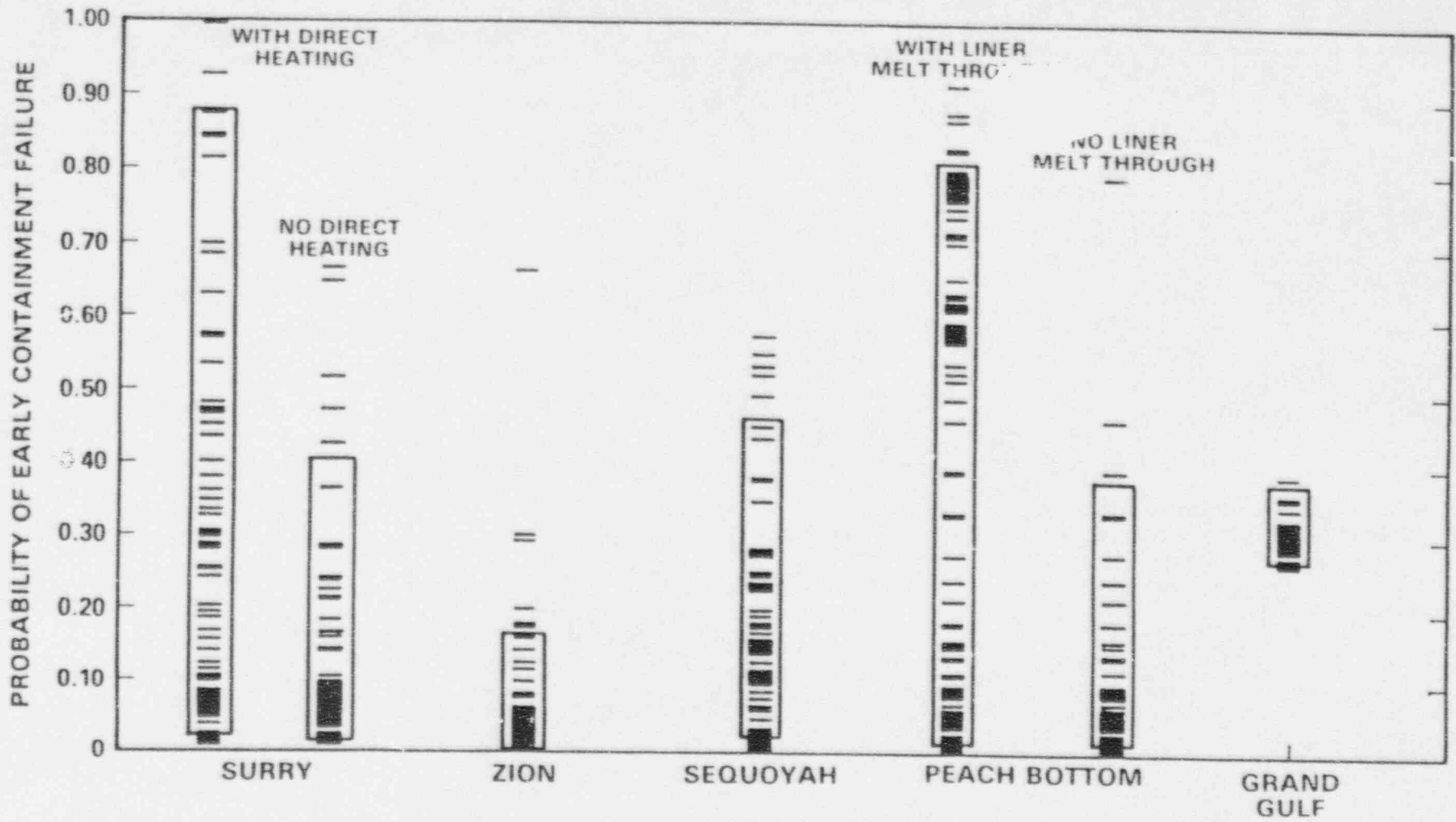


Figure ES.11 Comparison of early containment failure probabilities

GRADUATE AERONAUTICAL LABORATORIES  
CALIFORNIA INSTITUTE OF TECHNOLOGY  
PASADENA, CALIFORNIA 91125

GUGGENHEIM AERONAUTICAL  
LABORATORY

Mail Stop: 1G3-50  
Telephone: 818 395 3283  
Fax: 818 449 2677  
E-mail: jeshep@galcit.caltech.edu

22 August, 1995

H. Esmaili  
Energy Research Inc.  
P. O. Box 2034  
Rockville, MD 20847

FAX 301 881 0867

RE: NUREG/CR-6338 review and ERI-NRC-046 Task 6, Workorder 9.

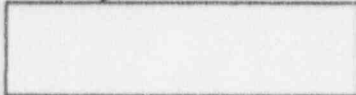
Dear Dr. Esmaili:

I regret that I am unable to review the supplied document. I had been very busy this summer with organizing an international conference and now trying catch up with my primary work responsibilities. In glancing through the document, I also realized that much of this material is concerned with plant-specific problems that are outside my area of expertise. Unlike the previous reports, I do not feel that I am able to other substantive comments on these specific issues.

Since I am unable to render the services called for the work agreement, I relinquish any claim on compensation.

I apologize for taking so long to respond to you writing.

Sincerely,



Joseph E. Shepherd  
Associate Professor of Aeronautics



## UNIVERSITY OF MARYLAND AT COLLEGE PARK

GLENN L. MARTIN INSTITUTE OF TECHNOLOGY • A. JAMES CLARK SCHOOL OF ENGINEERING

DEPARTMENT OF MATERIALS AND NUCLEAR ENGINEERING • NUCLEAR ENGINEERING PROGRAM

Dr. Mohsen Khatib-Rahbar  
Energy Research, Inc.  
P.O. Box 2034  
Rockville, MD 20847

July 25, 1995

### RE: Review of Draft NUREG/CR-6338

Dear Dr. Khatib-Rahbar:

I have completed my review of NUREG/CR-6338: "Resolution of the Direct Containment Heating Issue for All Westinghouse Plants With Large Dry Containment or Subatmospheric Containments." As before, my review mainly focuses on the probabilistic treatments in the report. The report is consistent with Zion and Surry approach described in NUREG/CR-6075 (and its Supplement 1), and NUREG/CR-6109. The screening results reported in NUREG/CR-6338 are generally reasonable. However, to make the results more credible, there are some areas that need improvement or corrections. I have discussed these areas in the following comments.

### General Comments

#### 1.0 Resolution Methodology

The "figure of merit" is too high. I believe that a figure of merit representing conditional containment failure probability (CCFP) of about 0.01 is more defensible. Also, a figure of merit for unconditional failure frequency of radioactive release from containment due to DCH around  $1.0 \times 10^{-6}$  / year is more reasonable. I would also recommend that for plants that their CCFP exceeds 0.01, a rough estimate of the frequency of HPME be multiplied by the "screened" CCFP estimate. If the result is

smaller than  $1.0 \times 10^{-6}$  / year, then no DCH susceptibility should be assumed, otherwise a refined containment analysis, an HPME frequency evaluation, or a combination of the two would be necessary. I believe that this two-stage screening approach reduces the need for detailed evaluation of other plants (especially the ice condenser plants).

Also, in Figure 2.1 the value of  $CCFP \leq 0.01$  pointing out of the box entitled "Containment Loads/Strength Screening on Remaining PWRs" should be 0.1 (unless if the authors agree with my recommendation of 0.01). Additionally, the acceptance criterion (figure of merit) pointing out of the box entitled "HPME Probability Evaluation on Remaining PWRs" should reflect a figure of merit based on the frequency of occurrence of HPME and not CCFP. This is because a more accurate estimate of HPME frequency does not affect the conditional containment failure probability. Similarly, the criteria for the box entitled "Integrated Load/Strength and HPME Probabilities on Remaining PWRs" should reflect the figure of merit for unconditional containment failure frequency (e.g.,  $1.0 \times 10^{-6}$  / year).

## 2.0 Quantification of CCFP

The idea that was originally proposed for calculating CCFP (for example in NUREG/CR-6075) was to convolute the containment fragility distribution with the containment pressure distribution. In Zion and Surry, the two distributions did not have any overlap, as such, CCFPs were considered negligible. In this exercise, however, some plants have small overlaps. It is not clear from the discussions in this report whether these two distributions were actually convoluted or not. NUREG/CR-6338 reports some sensitivity calculations reported in Tables 7.2 - 7.5. Here, from the containment pressure distribution, the study reports a "Pred. Press. (MPa)" value such that the likelihood that a DCH yields a containment pressure less than this value is 0.99 (conversely, the likelihood of exceeding this value is 0.01). Accordingly, from the fragility distribution a "Failure Press. (MPa)" value is obtained, below which the likelihood of containment failure is 0.01. Finally, the fraction of "Pred. Press (MPa)" and "Failure Press. (MPa)" is calculated and defined as the load/strength ratio. Since this fraction is not the fraction of the means of the load and strength, I am not sure about the meaning of this fraction. Later I will suggest a better method to deal with this problem.

For sensitivity analysis, it is more appropriate to change (by several factors) poorly known parameters or assumptions that affect fragility and containment pressure. The fraction of new mean containment pressure and new mean containment failure pressure is the sensitivity of Load/Strength to these changes.

In general, I suggest that by using a convolution approach the probability that load exceeds strength should be obtained. That is,  $CCFP = Pr(L > S)$ . Of course this



requires some form of a Monte Carlo simulation. Accordingly, for finding a probabilistic measure of the degree to which strength exceeds load, one can use the concept of a safety margin defined as

$$SM = \frac{\mu(S) - \mu(L)}{[\sigma^2(S) + \sigma^2(L)]^{1/2}}$$

Where,  $\mu$  (.) and  $\sigma^2$  (.) are mean and variance of either strength (S) or load (L). This formula is a more objective way of measuring the differences between the load and strength and incorporates the uncertainties inherent in their distributions. Also, the load vs. strength fraction should be obtained from

$$\mu(L/S) = \frac{\mu(L)}{\mu(S)}$$

$$\sigma^2(L/S) = \mu(L/S)^2 \left[ \frac{\sigma^2(S)}{\mu^2(S)} + \frac{\sigma^2(L)}{\mu^2(L)} \right]$$

Above formulas apply to cases where S and L are independent, which is the case here.

In order to account for uncertainties the study cites the recommendations of the PRA working group. This is done by reducing the mean containment failure pressure for each plant by 0.1 MPa (based on Callaway's IPE upper probability limit for the families of fragility curves). No discussion about the reason that such a change would be applicable to other plants has been offered. Nor it has been explained why the spread (e.g., the variance) of the fragility distributions would be the same for other plants. I believe that the study has not met the intent of the PRAWG and ACRS recommendations. Also, the results of the uncertainty calculation should show the uncertainty bounds for the final answers. For example, the study should show the distribution of the CCFP for those plants that show any appreciable overlapping probability densities (e.g., for H.B. Robinson, Ginna, Salem 1&2, South Texas 1&2, Wolf Creek, Beaver Valley 1&2, North Anna 1&2, Surry 1&2, and Millstone 3). The spread of CCFP should also be compared to the figure of merit for CCFP. If an appreciable portion of the CCFP distribution falls below the figure of merit, then one can confidently conclude that DCH is not an issue for that plant.

## Specific Comments

Page 6; 3rd line: The discussion about using  $CCFP \leq 0.01$  instead of  $CCFP \leq 0.1$  gives the impression that the authors are not sure about the validity of 0.1 value. This is consistent with my belief and further supports my recommendation of using a 0.01 figure of merit in the first place.

Page 61; 3rd paragraph: In the NUREG/CR-6075 Supplement 1, I was concerned about the so-called "eyeball" error, which occurs because of digitizing fragility curves. Errors of several factors in the tails of the distributions are possible when using this approach. Since the authors have no access to the digital fragility data, I think that for some sensitive plants (e.g., for H.B. Robinson, Ginna, Salem 1&2, South Texas 1&2, Wolf Creek, Beaver Valley 1&2, North Anna 1&2, Surry 1&2, and Millstone 3), a sensitivity calculation should be performed to account for possible digitizing errors (for example up to a factor of 5 variations may be applied to the tails of the distributions.)

Page 61; 4th paragraph: Please describe the criteria used to select lognormal, normal, or 3rd order Spline function for the fragility distributions.

Page 62; 2nd paragraph: The mean of CCFP may be obtained from the fragility curve. Furthermore, if families of fragility curves are used, each curve may be associated with a confidence (or probability) level.

Page 62; 3rd paragraph: We calculate the "probability" of containment failure from the fragility curves not the "frequency." This also applies to Table 6.1.

Page 64; 4th paragraph: I am concerned about this exercise of repeating the simulation with different "seed numbers." The results of a reasonably unbiased simulation with enough iterations should not change by modifying the seed number. If the authors get noticeably different CCFP distribution by changing the seed number, then the accuracy of their simulation process may be in question. For example, they may need to increase the number of iterations to greater than 1000, or their simulation routine may be yielding biased results. One can, however, account for the maximum anticipated error from a Monte Carlo simulation using the Central Limit Theorem approximation. If this is the concern of the authors, they should refer to the widely available literature.

Page 64; 5th paragraph, last sentence: I don't think Tables 7.2 - 7.5 provide any idea about the "cause" of DCH sensitivity.

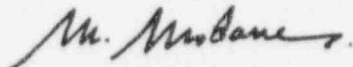
Page 65; 4th paragraph: Change CCFF to CCFP.

Page 73; Last sentence: I suggest changing ". . . 1 percent confidence level . . ." to ". . . 1 percent probability level . . ."

Page D-15; Section D.4.2: Some fragility curves reported and compared in this section are not about the plants within the scope of this study. For example, fragility curves of some ice condenser, CE and B&W plants are presented. Also, I fail to see the main purpose and significance of this comparison effort in the CCFP calculations. For example, Figures D.1 through D.17 seem to have no or small relevance to this analysis.

Please don't hesitate to call me at (301)405-5226, if there are any questions.

Sincerely yours,



Mohammad Modarres  
Professor of Nuclear  
Engineering

# PURDUE UNIVERSITY



SCHOOL OF NUCLEAR ENGINEERING

August 7, 1995

Dr. M. Wayne Hodges, Director  
Division of Systems Research  
U.S. Nuclear Regulatory Commission  
Washington, D.C. 20555-0001

Dear Dr. Hodges:

In response to your request to review a draft copy of NUREG/CR-6338, "Resolution of the Direct Containment Heating Issue for All Westinghouse Plants with Large Dry Containments or Subatmospheric Containments," I have completed the review of the technical content of the above report. The following are my specific comments.

#### Comment 1. Issue Resolution Method.

The DCH issue resolution for the Zion and Surry plants has been addressed in previous NUREG/CR-6075 and NUREG/CR-6109. The issue resolution method for these plants has been peer reviewed in detail and the method can be considered well established. However, for all other Westinghouse plants, NUREG/CR-6338 proposed and applied somewhat different approach. The major reasons for the difference in the approaches are the lack of the scaled integral test data for these plants and the limited time and man-power available to carry out a similar analysis such as performed for the Zion and Surry. In Section 2.0, it is explained that two-step method is used in NUREG/CR-6338. The initial attempt is to extrapolate the models for the Zion and Surry. This step is described as screening, and the success criterion is set at  $CCFP \leq 0.01$ . If this fails, a more detailed analysis is carried out to demonstrate that  $CCFP \leq 0.1$ . These two steps are *not clearly demonstrated* in the report. Furthermore, it is difficult to see how CCFP can be reduced by a factor of 10 by simply introducing more detailed information for a plant.

I recommend that the authors show detailed analyses of two demonstration cases, namely the one which satisfies  $CCFP < 0.01$  and the other which requires  $CCFP < 0.1$  with more detailed handling of splinter cases. It should be clear what is meant by the extrapolation of the Zion and Surry analyses.

#### Comment 2. Reduction of CCFP Value.

It is stated on page 7 that demonstrating that the probability of HPME events is sufficiently low offers an independent path to resolving the DCH issue. This is particularly true and useful for a plant for which it is difficult to evaluate the impact of the different cavity and subcompartment geometries. It is not clear to me whether this approach has been incorporated into the overall DCH resolution in NUREG/CR-6338 or not. If this approach was necessary for a certain plant, it should be stated in the report.

Comment 3. Refined Load/Strength Analyses.

It is indicated that the CONTAIN can be used to assess the applicability of the TCE model for situations far from the existing data base. However, both the TCE model and CONTAIN model are not mechanistic. Both models have empirical factors which were adjusted to fit the integral test data. I am not sure what can be accomplished by studying the sensitivity of the predictions to the initial input conditions beyond the applicable ranges for either model.

Comment 4. Effect of Co-dispersed Cavity Water.

It is stated that co-dispersed cavity water can augment DCH loads, rather than mitigating loads under some circumstances. It is also easy to develop a phenomenological model which can do either of these depending on the degree of thermal and momentum interactions between the debris and water. Furthermore, the experimental data are not very reliable, because it is not clear how the water in the actual cavity can be scaled by a small amount of water in the integral tests. However, the authors concluded that they could ignore the potential impact of cavity water in their analyses consistent with the limited data. A relatively deep water in the cavity may lead to a significant FCI approaching a vapor explosion. The potential for this type of interaction should be evaluated.

Comment 5. Coherency Factor.

The analysis in NUREG/CR-6338 is based on the assumption that the coherency factor is only a function of the cavity geometry and not of the subcompartment geometry. However, this is a false assumption. The subcompartment geometry is not important, only if the droplet flight path before entrapment in the subcompartment is very short as in the Zion or Surry. This is a different issue from the flight path for small droplets escaping capture in the subcompartment. This latter effect is correctly modeled in the report. It may be that all these Westinghouse plants have a flow obstruction at the exit of the cavity. However, this should be demonstrated. If not, the magnitude of the coherency factor should be significantly increased by a factor based on the ratio of the subcompartment direct flight path and the cavity length.

Sincerely,



M. Ishii  
Professor of Nuclear Engineering

MI/ks



## APPENDIX B

### Melt Mass/Composition Distributions

Martin M. Pilch  
Sandia National Laboratories

#### B.1 Introduction

The prescription for quantifying melt mass and composition had its origins in NUREG/CR-6075 (Pilch et al., 1994a), which was peer reviewed by 13 experts representing national laboratories, universities, and industry. The peer reviewers generally characterized the initial conditions as optimistic. Specifically, they expressed concerns that the melt mass distributions were too narrow and that the melt composition did not contain sufficient metallics (Zr and steel). The reviewers also stressed that SCDAP/RELAP5 analyses should be performed and used in a consistent manner in establishing initial conditions.

The NRC convened a working group to make recommendations on how to address residual concerns for Zion. Their recommendations are documented in Appendix A of Pilch et al. (1994b) for Zion. Some modification of the splinter scenarios resulted, and the melt mass distributions were generally broadened and additional zirconium was considered. The prescription was then applied to Surry in NUREG/CR-6109 (Pilch et al., 1995) using Surry-specific input.

The prescription represents a synthesis of insights about accident sequences, TMI-II insights, phenomenological insights, insights from experiments, and insights from SCDAP/RELAP5. These system code calculations are used to justify or validate the melt mass and composition selections. SCDAP/RELAP5 calculations have been performed for Zion (W 4-loop plants with downcomer bypass), Surry (W 3-loop plants with downcomer bypass), Calvert Cliffs (CE lowest power density), and ANO-2 (CE highest power density). The credible range of pump seal leaks have been examined for each plant and sensitivity studies have been performed. SCDAP/RELAP5 will also analyze B&W plants in a similar fashion as part of the DCH resolution effort for those plants. When complete, SCDAP/RELAP5 will have analyzed each of the major reactor types from each supplier of PWR nuclear steam supply systems in the U.S.

Sections B.2 and B.3 focus on quantifying the distribution of molten  $UO_2$  for all PWRs during core relocation and at the time of vessel breach using the approved prescription. We expect that the quantity of molten  $UO_2$  will be a function of core size, which can vary from vendor to vendor and even within a given vendor. Fortunately, the core size of all PWRs can be grouped into eight core size groups, which are correlated by vendor. Section B.4 compares the full melt mass and composition quantifications with available results from system-level codes.

## B.2 Scenarios V and Va - SBLOCA with Repressurization of the RCS by Operator Intervention

Scenarios V and Va represent a core melt accident that progresses with water still present in the lower portions of the core. Such conditions lead to formation of a crust within the core followed by a massive release of melt when the crust fails. Accumulation of core material on the lower head of the RPV causes the lower head to heat up. Eventually, its structural strength is so degraded it can no longer withstand the stresses induced in the lower head by elevated RCS pressures. Thus, creep rupture of the lower head is the expected failure mechanism. The distinguishing feature of Scenarios V and Va is that operator actions are assumed to refill the RPV with water and to fully repressurize the RCS. Analysis of DCH for a repressurized RCS is deemed conservative because we expect operators to depressurize the RCS in a core damage accident.

Consistent with TMI-II, the potential release of molten material to the lower head is controlled by the formation of a hemispherical crucible that excludes only the outer assemblies of the core (Figure B.1). The outer assemblies are generally not expected to be in a severely degraded state because the RPV is flooded. Asymmetries in crucible growth ensure that localized penetration of the outer assembly and the core barrel would most likely occur when the crucible has grown (on average) to the outer assembly. This is consistent with the observed end state at TMI-II. We ascribe, however, no rigorous meaning to the assembly dimensions; instead, we use the assembly dimensions as representative of a thin outer region of the core where cooling is adequate to prevent significant degradation and melting.

Table B.1 lists the eight core size groups and a summary of key inputs leading to calculation of the distribution for molten  $\text{UO}_2$ . A hemispherical crucible that excludes the outer assemblies would be filled with a predominantly oxidic melt with a density of  $\sim 10,000 \text{ kg/m}^3$ . The maximum mass of  $\text{UO}_2$  and  $\text{ZrO}_2$  that the crucible can contain is listed in Table B.1. The amount of melt released from the crucible is a function of where the crucible fails, with downward and sideward representing the two extremes. Recent studies by Schmidt and Humphries (1994), which consider only conduction processes, suggest that bottom failure of a crucible is very unlikely. Natural convection patterns in the molten pool, should they develop, would only reinforce the prediction of side failure of the crucible. Natural convective patterns produce edge-peaked heat flux distributions. The MP-2 experiment (Gasser et al., 1994) tends to confirm that downward failure of an oxidic crust is unlikely, even in the absence of active cooling. To establish an upper bound ( $p \sim 0.01$ ) on the  $\text{UO}_2$  mass that relocates to the lower plenum, it was assumed that the crucible could fail at the bottom, releasing the entire volume of the crucible to the lower plenum head.

To fix the composition a little more closely, we note that  $\sim 80 - 90$  percent of the relocated melt is  $\text{UO}_2$  and the remainder is  $\text{ZrO}_2$ . As a best estimate, and consistent with TMI-II observations and working group recommendations, side failure of the crucible is expected to release about half of the material contained in the crucible to the lower head. Likewise, the best estimate on the amount of relocated  $\text{UO}_2$  is listed in Table B.1. On this basis, the distribution for the amount of  $\text{UO}_2$  released from the crucible can be constructed as in Figure B.2.

It should be noted that the amount of  $UO_2$  released from the crucible exceeds the amount of *molten* material available to participate in DCH at the time of vessel failure. First, not all material released from the TMI-II crucible reached the lower head. Some froze between the core former plate and the core barrel and some additional material froze on other structures as it drained into the lower plenum. Second, some molten material will quench and freeze as it flows through the water in the lower plenum. Calculations using the THIRMAL code (Rempe et al., 1993) suggest that as much as ~50 percent might freeze during this process if the water is subcooled. Experiments (Spencer et al., 1994) tend to confirm this number if the water is subcooled, but suggest that only ~10 percent will quench if the water is saturated. Third, some of the molten material accumulated on the lower head will form an upper crust resulting from heat transfer to the overlying water. Finally, some of the molten material will freeze as it transfers heat to the lower head and drives it to failure.

The extent to which these solidified materials persist to vessel rupture is coupled to generation of decay heat within the debris and the time required to heat the vessel to rupture. SCDAP/RELAP5 calculations for Zion (Appendix C in Pilch et al., 1994b) indicate that ~20-25 mt of material are frozen on the lower head at the time of vessel breach. The SCDAP/RELAP5 calculations are themselves a lower bound since they do not account for water intruding into the melt through cracks in the overlying crust or gaps along the vessel wall. These additional cooling mechanisms were identified as part of the TMI-II vessel investigation program (Stickler et al., 1993).

As a bound, we consider only melt freezing in the process of heating the lower head to rupture. Boucheron (referenced in Zuber et al., 1991) shows that ~10 - 15 mt of oxide will freeze (with decay heat coupling) in order to heat the lower head to a point where it loses its strength and ruptures. With this in mind, we shift the  $UO_2$  distributions in Figure B.2 an additional 10 mt to the left. The distribution of *molten*  $UO_2$  at the time of vessel breach is then given by Figure B.3 for each core size group. We emphasize the conservative nature of these distributions given the additional quenching mechanisms that have been ignored. The data presented in Figures B.2 and B.3 are tabulated in Tables B.2 and B.3.

We acknowledge that some of the ~10 mt of solid material may be ejected with the melt into the reactor cavity and that this solid material may participate in DCH. The solids, however, are oxidic, and sensitivity studies (Pilch et al., 1994b, Appendix A, Response H19) indicate that DCH loads are not sensitive to the total quantity of oxides in the melt. Furthermore, Griffith (Appendix H in Zuber et al., 1991) indicates that complete ejection of the solid material is not expected even if it exists as loose debris particles. The extent to which ejected solids can participate in DCH may be further limited by the particle size, since fragmentation to ~1mm is necessary for efficient debris gas heat transfer, and debris oxidation is severely limited for solidified materials. Consequently, the impact of solid debris on DCH loads is judged to be insignificant and is neglected in these evaluations.

### **B.3 Scenario VI - SBLOCA Under Wet Core Conditions**

The potential release of molten material to the lower head is again controlled by the formation and failure of a crucible in the core region. Water occupies only the lowest regions of the core, so radial cooling of a growing crucible is reduced in this situation. Consistent with SCDAP/RELAP5 predictions, the crucible could take on the bounding shape of an upright cylinder as depicted in Figure

B.4. We note that SCDAP/RELAP5 conservatively assumes that the melt pool must grow to the core boundary as a condition for core relocation. Thus, SCDAP/RELAP5 shows some localized involvement of the outer assemblies. We expect, however, that asymmetries in crucible growth ensure that localized penetration of the outer assembly and core barrel would likely occur when the crucible has grown (on average) to the outer assembly. Consequently, the outer assemblies are excluded from our assessments.

In the extreme of this geometry, ~70 - 80 percent of the core can be contained in the crucible with the specific values listed in Table B.4. The upper bound to the  $\text{UO}_2$  distribution is obtained again by noting that ~80 - 90 percent of the relocated melt is  $\text{UO}_2$ . Again, the calculations of Schmidt and Humphries (1994) favor side failure before the crucible obtains these extreme proportions. As a best estimate we assume that half of the  $\text{UO}_2$  can be released from the crucible. With this in mind, the distribution of  $\text{UO}_2$  released from the crucible can be constructed as indicated in Figure B.5 for each core size grouping. Again allowing (~10 mt) only for melt freezing in order to heat the lower head to rupture, the distribution of molten  $\text{UO}_2$  at the time of vessel failure is given by Figure B.6 for each group. The data presented in Figures B.5 and B.6 are tabulated in Tables B.5 and B.6.

South Texas is an exception amongst the Westinghouse four-loop plants in that its core is 15% taller than the others. We recommend increasing the  $\text{UO}_2$  masses for South Texas relative to the other Westinghouse four-loop plants. This applies only to Scenario VI. For the other vendors, the core height is always the same for cores of the same diameter.

### **B.4 Comparison of Melt Masses and Composition with Prior Work**

Because many of the melt constituents are correlated, it is useful to tabulate the lower bound, best-estimate, and upper bound masses for a more direct comparison of quantifications for the current assessments with prior work. This is done in Tables B.7 through B.10 for four different plants: Zion, Surry, ANO-2, and Calvert Cliffs. The lower and upper bounds are taken at the ~1 percent probability level.

Consider first the comparison of Scenarios V and VI by composition using the prescription. The  $\text{ZrO}_2$  values are a function of both the  $\text{UO}_2$  mass and the fraction of Zr oxidized. For this comparison, the three  $\text{UO}_2$  masses are used in conjunction with the best estimate for the fraction of Zr oxidized. This ensures that lower and upper bounds to the  $\text{ZrO}_2$  values are also at the ~1 percent probability level; however, this prescription is not unique. For instance, it is possible to use the best estimate for the  $\text{UO}_2$  mass in conjunction with the lower, best-estimate, and upper bound values for the fraction of Zr oxidized. This procedure, however, gives somewhat less  $\text{ZrO}_2$  mass for the best-estimate and upper bound value.

At the outset, we should state that no potential comparisons are fully consistent with the plant and scenarios discussed in this report, so some compromise is necessary to make suitable comparisons. Prior summary efforts (i.e., NUREG-1150 and SASM) are therefore the most useful for comparison since these activities employed panels of knowledgeable experts who were able to synthesize the experimental and analytical information available at the time. Since the time of these summary efforts,



new information in the form of best estimate SCDAP/RELAP5 calculations have become available and these new data are reflected in our current quantifications.

NUREG-1150 was the first summary assessment of core melt progression parameters and this study only addressed the core fraction that is molten and the fraction of cladding oxidized. NUREG-1150 assessments were largely based on MARCH, early MAAP, and preliminary MELPROG calculations. The distribution of the molten core fraction in Scenario VI is in good agreement with the expert elicitation results in NUREG-1150.

SASM (Zuber et al., 1991) is the most recent of the summary assessments, and it was focused specifically on the DCH issue. The SASM assessments were based on input and calculations specific to Surry, so we only compare our quantifications for Surry with the SASM recommendations. The SASM recommendations for molten oxides are enveloped by the current quantifications; however, the metals are outside the current assessments. Assessment of steel mass in the SASM effort was largely based on a MELPROG calculation (Kelly et al., 1987) of a station blackout accident in which significant upper plenum melting was predicted. Melting of upper plenum steel is strongly correlated with surge line or hot leg failure, which in fact was predicted in the MELPROG calculation. Specifically, gases hot enough to melt upper plenum steel are also hot enough to rupture the surge line or hot leg. This is also consistent with the current SCDAP/RELAP5 assessments. The large quantities of Zr and CRM in the SASM assessment are traceable to a MELPROG modeling assumption that crucible failure occurs as a massive event carrying most of the metallic blockage into the lower plenum. Thus, the SASM assessment of metals in the melt is not consistent with our current understanding of core melt progression, especially under wet core conditions.

Tables B.7 through B.10 also summarize the melt mass predicted by SCDAP/RELAP5 at the time of vessel failure for the spectrum of credible pump seal leaks. Current quantifications (Scenario VI) for oxide mass are in general agreement with the system code predictions. These code predictions are interpreted as upper bounds because SCDAP/RELAP5 assumes complete drainage of the in-core molten pool, because the molten pool must grow to the core boundary before SCDAP/RELAP5 relocates material, and because SCDAP/RELAP5 always predicted complete depressurization of the RCS. Complete depressurization delays bottom head failure and increases the time available for frozen material to remelt on the lower head. Here, we compare only to Scenario VI because Scenario V progresses with water in the core (operator action), which was not modeled in the SCDAP/RELAP5 calculations. SCDAP/RELAP5 predicts essentially no Zr in the melt while our quantifications chose to bound the amount. The amount of lower plenum steel predicted by SCDAP/RELAP5 is somewhat greater than the current assessments for the Westinghouse plants (Zion and Surry). The CE plants (ANO-2 and Calvert Cliffs) have integral lower heads, so there is essentially no thin steel in the lower plenum. Calvert Cliffs has a low power density relative to ANO-2; consequently, Calvert Cliffs shows a substantially smaller fraction of the core molten at vessel breach.

## B.5 References

Gasser, R.D. et al. (1994 draft). *Late Phase Melt Progression Experiment-MP-2, Results and Analysis*, NUREG/CR-6167, SAND93-3931, Sandia National Laboratories, Albuquerque, NM.



## Melt Mass/Composition Distributions

- Kelly, J.E., et al. (1987). *MELPROG-PWT/MODI Analysis of a TMLB' Accident Sequence*, NUREG/CR-4742, SAND86-2175, Sandia National Laboratories, Albuquerque, NM.
- Pilch, M.M., et al. (1994a). *"The Probability of Containment Failure by Direct Containment Heating in Zion,"* NUREG/CR-6075, SAND93-1535, Sandia National Laboratories, Albuquerque, NM.
- Pilch, M.M. et al. (1994b). *"The Probability of Containment Failure by Direct Containment Heating in Zion,"* NUREG/CR-6075, Supplement 1, Sandia National Laboratories, Albuquerque, NM.
- Pilch, M.M. et al. (1995). *"The Probability of Containment Failure by Direct Containment Heating in Surry,"* SAND93-2078, NUREG/CR-6109, Sandia National Laboratories, Albuquerque, NM.
- Rempe, J.L. et al. (1993). *Light Water Reactor Lower Head Failure Analysis*, NUREG/CR-5642, EGG-2618, Idaho National Engineering Laboratory, Idaho Falls, ID.
- Schmidt, R.L., and L.L. Humphries (1994). *Late Phase Melt Progression Scoping and Sensitivity Studies*, Draft, SAND92-2831, Sandia National Laboratories, Albuquerque, NM.
- Spencer, B.W. et al. (1994). *Fragmentation and Quench Behavior of Corium Melt Streams in Water*, NUREG/CR-6133, ANL-93/32, Argonne National Laboratory, Argonne, IL.
- Stickler, L.A. et al. (1993). *Calculations to Estimate the Margin to Failure in the TMI-2 Vessel*, TMI V(93)EG01, Idaho National Engineering Laboratory, EG&G Idaho, Inc., Idaho Falls, ID.
- Zuber, N. et al. (1991). *An Integrated Structure and Scoping Methodology for Severe Accident Technical Issue Resolution*, Draft for Comment, NUREG/CR-5809, EGG-2659, EG&G Idaho, Inc., Idaho Falls, ID.

**Table B.1 Calculation of UO<sub>2</sub> melt relocation for Scenarios V and Va**

Group	Core Dia. (m)	Assembly Dim. (m)	Hemisphere Vol. (m <sup>3</sup> )	Total Mass Relocated (mt)	Max UO <sub>2</sub> (mt)	Best Est. UO <sub>2</sub> (mt)
W 4-loop	3.37	0.214	7.0	70	60	30
W 3-loop	3.04	0.214	4.6	46	40	20
W 2-loop	2.45	0.197	2.3	23	20	10
B&W	3.27	0.217	6.0	60	50	25
CE-1	2.70	~0.2	3.2	32	30	15
CE-2	3.13	0.202	5.3	53	46	23
CE-3	3.45	0.202	7.4	75	64	32
CE-4	3.65	0.202	9.0	90	77	38.5

Table B.2 Distribution for molten UO<sub>2</sub> mass at the time of melt relocation to the lower plenum for Scenarios V and Va

UO <sub>2</sub> Mass (mt) Range	Discrete Probability	UO <sub>2</sub> Mass (mt)	Cumulative Probability	UO <sub>2</sub> Mass (mt) Range	Discrete Probability	UO <sub>2</sub> Mass (mt)	Cumulative Probability
<b>W 2-Loop Plants (2.45m Core Dia.)</b>				<b>CE Plants (2.70m Core Dia.)</b>			
0 - 3.0	0.01	0	0	0 - 5.0	0.01	0	0
3.0 - 6.5	0.10	3.0	0.01	5.0 - 10.0	0.10	5.0	0.01
6.5 - 13.5	0.78	6.5	0.11	10.0 - 20.0	0.78	10.0	0.11
13.5 - 16.5	0.10	13.5	0.89	20.0 - 25.0	0.10	20.0	0.89
16.5 - 20.0	0.01	16.5	0.99	25.0 - 30.0	0.01	25.0	0.99
		20.0	1.00			30.0	1.00
<b>W 3-Loop Plants (3.04m Core Dia.)</b>				<b>CE Plants (3.13m Core Dia.)</b>			
0 - 6.7	0.01	0	0	0 - 7.6	0.01	0	0
6.7 - 13.3	0.10	6.7	0.01	7.6 - 15.3	0.10	7.6	0.01
13.3 - 26.7	0.78	13.3	0.11	15.3 - 30.7	0.78	15.3	0.11
25.7 - 33.3	0.10	25.7	0.89	30.7 - 38.4	0.10	30.7	0.89
33.3 - 40.0	0.01	33.3	0.99	38.4 - 46.0	0.01	38.4	0.99
		40.0	1.00			46.0	1.00
<b>W 4-Loop Plants (3.37m Core Dia.)</b>				<b>CE Plants (3.45m Core Dia.)</b>			
0 - 10.0	0.01	0	0	0 - 11.0	0.01	0	0
10.0 - 20.0	0.10	10.0	0.01	11.0 - 21.5	0.10	11.0	0.01
20.0 - 40.0	0.78	20.0	0.11	21.5 - 42.5	0.78	21.5	0.11
40.0 - 50.0	0.10	40.0	0.89	42.5 - 53.0	0.10	42.5	0.89
50.0 - 60.0	0.01	50.0	0.99	53.0 - 64.0	0.01	53.0	0.99
		60.0	1.00			64.0	1.00
<b>B&amp;W Plants (3.27m Core Dia.)</b>				<b>CE Plants (3.65m Core Dia.)</b>			
0 - 8.0	0.01	0	0	0 - 12.5	0.01	0	0
8.0 - 16.5	0.10	8.0	0.01	12.5 - 25.5	0.10	12.5	0.01
16.5 - 33.5	0.78	16.5	0.11	25.5 - 51.5	0.78	25.5	0.11
33.5 - 42.0	0.10	33.5	0.89	51.5 - 64.5	0.10	51.5	0.89
42.0 - 50.0	0.01	42.0	0.99	64.5 - 77.0	0.01	64.5	0.99
		50.0	1.00			77.0	1.00

Table B.3 Distribution for molten UO<sub>2</sub> mass at the time of vessel breach for Scenarios V and Va

UO <sub>2</sub> Mass (mt) Range	Discrete Probability	UO <sub>2</sub> Mass (mt)	Cumulative Probability	UO <sub>2</sub> Mass (mt) Range	Discrete Probability	UO <sub>2</sub> Mass (mt)	Cumulative Probability
<u>W 2-Loop Plants (2.45m Core Dia.)</u>				<u>CE Plants (2.70m Core Dia.)</u>			
0 - 3.5	0.89	0	0	0 - 10.0	0.89	0	0
3.5 - 6.5	0.10	3.5	0.89	10.0 - 15.0	0.10	10.0	0.89
6.5 - 10.0	0.01	6.5	0.99	15.0 - 20.0	0.01	15.0	0.99
		10.0	1.00			20.0	1.00
<u>W 3-Loop Plants (3.04m Core Dia.)</u>				<u>CE Plants (3.13m Core Dia.)</u>			
0 - 3.3	0.10	0	0	0 - 5.3	0.10	0	0
3.3 - 16.7	0.79	3.3	0.10	5.3 - 20.7	0.79	5.3	0.10
16.7 - 23.3	0.10	16.7	0.89	20.7 - 28.4	0.10	20.7	0.89
23.3 - 30.0	0.01	23.3	0.99	28.4 - 36.0	0.01	28.4	0.99
		30.0	1.00			36.0	1.00
<u>W 4-Loop Plants (3.37m Core Dia.)</u>				<u>CE Plants (3.45m Core Dia.)</u>			
0 - 10.0	0.10	0	0	0 - 1.0	0.61	0	0
10.0 - 30.0	0.79	10.0	0.10	1.0 - 11.5	0.10	1.0	0.01
30.0 - 40.0	0.10	30.0	0.89	11.5 - 32.5	0.78	11.5	0.11
40.0 - 50.0	0.01	40.0	0.99	32.5 - 43.0	0.10	32.5	0.89
		50.0	1.00	43.0 - 54.0	0.01	43.0	0.99
						54.0	1.00
<u>B&amp;W Plants (3.27m Core Dia.)</u>				<u>CE Plants (3.65m Core Dia.)</u>			
0 - 6.5	0.10	0	0	0 - 2.5	0.01	0	0
6.5 - 23.5	0.79	6.5	0.10	2.5 - 15.5	0.10	2.5	0.01
23.5 - 32.0	0.10	23.5	0.89	15.5 - 41.5	0.78	15.5	0.11
32.0 - 40.0	0.01	32.0	0.99	41.5 - 54.5	0.10	41.5	0.89
		40.0	1.00	54.5 - 67.0	0.01	54.5	0.99
						67.0	1.00

Table B.4 Calculation of UO<sub>2</sub> melt relocation for Scenario VI

Group	Representative UO <sub>2</sub> (mt) Inventory	Core Dia. (m)	Assembly Dim. (m)	Core Fraction	Max UO <sub>2</sub> (mt)	Best Est. UO <sub>2</sub> (mt)
W 4-loop	100	3.37	0.214	0.80	80	40
W 3-loop	79.8	3.04	0.214	0.80	64	32
W 2-loop	55	2.45	0.197	0.70	40	20
B&W	94	3.27	0.217	0.75	74	37
CE-1	54	2.70	~0.2	0.75	44	22
CE-2	84	3.13	0.202	0.75	66	33
CE-3	94	3.45	0.202	0.80	80	40
CE-4	118	3.65	0.202	0.80	94	47

Melt Mass/Composition Distributions



Table B.5 Distribution for molten UO<sub>2</sub> mass at the time of melt relocation to the lower plenum for Scenario VI and VIa

UO <sub>2</sub> Mass (mt) Range	Discrete Probability	UO <sub>2</sub> Mass (mt)	Cumulative Probability	UO <sub>2</sub> Mass (mt) Range	Discrete Probability	UO <sub>2</sub> Mass (mt)	Cumulative Probability
<b>W 2-Loop Plants (2.45m Core Dia.)</b>				<b>CE Plants (2.70m Core Dia.)</b>			
0 - 6.6	0.01	0	0	0 - 7.0	0.01	0	0
6.6 - 13.3	0.10	6.6	0.01	7.0 - 14.5	0.10	7.0	0.01
13.3 - 26.7	0.78	13.3	0.11	14.5 - 29.5	0.78	14.5	0.11
26.7 - 33.4	0.10	26.7	0.89	29.5 - 37.0	0.10	29.5	0.89
33.4 - 40.0	0.01	33.4	0.99	37.0 - 44.0	0.01	37.0	0.99
		40.0	1.00			44.0	1.00
<b>W 3-Loop Plants (3.04m Core Dia.)</b>				<b>CE Plants (3.13m Core Dia.)</b>			
0 - 10.6	0.01	0	0	0 - 11.0	0.01	0	0
10.6 - 21.3	0.10	10.6	0.01	11.0 - 22.0	0.10	11.0	0.01
21.3 - 42.7	0.78	21.3	0.11	22.0 - 44.0	0.78	22.0	0.11
42.7 - 53.4	0.10	42.7	0.89	44.0 - 55.0	0.10	44.0	0.89
53.4 - 64.0	0.01	53.4	0.99	55.0 - 66.0	0.01	55.0	0.99
		64.0	1.00			66.0	1.00
<b>W 4-Loop Plants (3.37m Core Dia.)</b>				<b>CE Plants (3.45m Core Dia.)</b>			
0 - 15.0	0.01	0	0	0 - 13.2	0.01	0	0
15.0 - 30.0	0.10	15.0	0.01	13.2 - 26.6	0.10	13.2	0.01
30.0 - 50.0	0.78	30.0	0.11	26.6 - 53.4	0.78	26.6	0.11
50.0 - 65.0	0.10	50.0	0.89	53.4 - 66.8	0.10	53.4	0.89
65.0 - 80.0	0.01	65.0	0.99	66.8 - 80.0	0.01	66.8	0.99
		80.0	1.00			80.0	1.00
<b>B&amp;W Plants (3.27m Core Dia.)</b>				<b>CE Plants (3.65m Core Dia.)</b>			
0 - 12.0	0.01	0	0	0 - 15.0	0.01	0	0
12.0 - 24.5	0.10	12.0	0.01	15.0 - 31.0	0.10	15.0	0.01
24.5 - 49.5	0.78	24.5	0.11	31.0 - 63.0	0.78	31.0	0.11
49.5 - 62.0	0.10	49.5	0.89	63.0 - 79.0	0.10	63.0	0.89
62.0 - 74.0	0.01	62.0	0.99	79.0 - 94.0	0.01	79.0	0.99
		74.0	1.00			94.0	1.00

Table B.6 Distribution of molten UO<sub>2</sub> mass at the time of vessel breach for Scenario VI and VIa

UO <sub>2</sub> Mass (mt) Range	Discrete Probability	UO <sub>2</sub> Mass (mt)	Cumulative Probability	UO <sub>2</sub> Mass (mt) Range	Discrete Probability	UO <sub>2</sub> Mass (mt)	Cumulative Probability
<b>W 2-Loop Plants (2.45m Core Dia.)</b>				<b>CE Plants (2.70m Core Dia.)</b>			
0 - 3.3	0.10	0	0	0 - 4.5	0.10	0	0
3.3 - 16.7	0.79	3.3	0.10	4.5 - 19.5	0.79	4.5	0.10
16.7 - 23.4	0.10	16.7	0.89	19.5 - 27.0	0.10	19.5	0.89
23.4 - 30.0	0.01	23.4	0.99	27.0 - 34.0	0.01	27.0	0.99
		30.0	1.00			34.0	1.00
<b>W 3-Loop Plants (3.04m Core Dia.)</b>				<b>CE Plants (3.13m Core Dia.)</b>			
0 - 1.0	0.01	0	0	0 - 1.0	0.01	0	0
1.0 - 12.0	0.10	1.0	0.01	1.0 - 12.0	0.10	1.0	0.01
12.0 - 34.0	0.78	12.0	0.11	12.0 - 34.0	0.78	12.0	0.11
34.0 - 45.0	0.10	34.0	0.89	34.0 - 45.0	0.10	34.0	0.89
45.0 - 54.0	0.01	45.0	0.99	45.0 - 56.0	0.01	45.0	0.99
		54.0	1.00			56.0	1.00
<b>W 4-Loop Plants (3.37m Core Dia.)</b>				<b>CE Plants (3.45m Core Dia.)</b>			
0 - 5.0	0.01	0	0	0 - 3.2	0.01	0	0
5.0 - 20.0	0.10	5.0	0.01	3.2 - 16.6	0.10	3.2	0.01
20.0 - 40.0	0.78	20.0	0.11	16.6 - 43.4	0.78	16.6	0.11
40.0 - 55.0	0.10	40.0	0.89	43.4 - 56.8	0.10	43.4	0.89
55.0 - 70.0	0.01	55.0	0.99	56.8 - 70.0	0.01	56.8	0.99
		70.0	1.00			70.0	1.00
<b>B&amp;W Plants (3.27m Core Dia.)</b>				<b>CE Plants (3.65m Core Dia.)</b>			
0 - 2.0	0.01	0	0	0 - 5.0	0.01	0	0
2.0 - 14.5	0.10	2.0	0.01	5.0 - 21.0	0.10	5.0	0.01
14.5 - 39.5	0.78	14.5	0.11	21.0 - 53.0	0.78	21.0	0.11
39.5 - 52.0	0.10	39.5	0.89	53.0 - 69.0	0.10	53.0	0.89
52.0 - 64.0	0.01	52.0	0.99	69.0 - 84.0	0.01	69.0	0.99
		64.0	1.00			84.0	1.00

**Table B.7 Comparison with prior work for Zion**

Parameter	Scenario V	Scenario VI	NUREG-1150	SCDAP/RELAP5 NUREG/CR-6075, Sup. 1 Case 1-2-3
UO <sub>2</sub> mass (mt)	0/20/50	0/30/70		43.3-52.8-44.4
ZrO <sub>2</sub> mass (mt)	0/2.2/5.5	0/3.3/7.7		11.2-13.4-12.3
Zr mass (mt)	0/0.6/1.5	0/0.9/2.0		0-0.5-0
Steel mass (mt)	0.3/1.1/2.3	0.3/1.8/4.4		4.8-8.2-5.0
CRM mass (mt)	0	0		0-3.3-2.2
Total melt mass (mt)	0.3/23.9/59.3	0.3/36.0/84.1		59.3-78.2-63.9
Core fraction molten	0.002/0.19/0.47	0.002/0.29/0.67	0/0.28/0.60	0.47-0.63-0.51
Fraction Zr oxidized	0.15/0.40/0.65	0.15/0.40/0.65	0.08/0.32/0.76	0.53-0.59-0.48
Case 1 = 0 gpm/pump (minimum); Case 2 = 250 gpm/pump (best estimate); Case 3 = 480 gpm/pump (maximum).				

**Table B.8 Comparison with prior work for Surry**

Parameter	Scenario V	Scenario VI	NUREG-1150	SASM NUREG/CR-5809	SCDAP/RELAP5 NUREG/CR-6109 Case-3
UO <sub>2</sub> mass (mt)	0/10/30	0/23/55		15.7	38.1
ZrO <sub>2</sub> mass (mt)	0/1.1/3.3	0/2.5/5.9		4.45	9.7
Zr mass (mt)	0/0.3/0.9	0/0.7/1.6		6.35	0.0
Steel mass (mt)	0.3/0.6/1.3	0.3/1.1/2.3		13.8	5.4
CRM mass (mt)	0	2		2.7	1.9
Total melt mass (mt)	0.3/12.0/35.5	2.3/29.3/66.8		43	55.1
Core fraction molten	0.003/0.1/0.33	0.02/0.29/0.65	0/0.28/0.60	0.42	0.54
Fraction Zr oxidized	0.15/0.40/0.65	0.15/0.40/0.65	0.08/0.32/0.76	0.40-0.50	0.53
Case 3 = 480 gpm/pump (maximum)					

Table B.9 Comparison with prior work for ANO-2

Parameter	Scenario V	Scenario VI	NUREG-1150	SCDAP/RELAP5 Case 1-2
UO <sub>2</sub> mass (mt)	0/13/36	0/23/56		42.1-50.6
ZrO <sub>2</sub> mass (mt)	0/2.0/5.5	0/3.5/8.6		12.4-14.5
Zr mass (mt)	0/0.4/1.0	0/0.7/1.6		0-0.04
Steel mass (mt)	0	0		0-3.9
CRM mass (mt)	0	5		4.8-4.9
Total melt mass (mt)	0/15.4/42.5	0/32.2/71.2		59.3-73.9
Core fraction molten	0/0.14/0.38	0/0.29/0.63	0/0.28/0.60	0.53-0.66
Fraction Zr oxidized	0.15/0.40/0.65	0.15/0.40/0.65	0.08/0.32/0.76	0.47-0.45
Case 1 = 1.5 gpm/pump (best estimate); Case 2 = 220 gpm/pump (maximum).				

Table B.10 Comparison with prior work for Calvert Cliffs

Parameter	Scenario V	Scenario VI	NUREG-1150	SCDAP/RELAP5 Case 1-2
UO <sub>2</sub> mass (mt)	0/22/54	0/30/70		36.3-34.8
ZrO <sub>2</sub> mass (mt)	0/3.3/8.1	0/4.5/10.5		9.4-9.0
Zr mass (mt)	0/0.66/1.6	0/0.69/2		0-0
Steel mass (mt)	0	0		0-0.4
CRM mass (mt)	0	5		1.7-1.6
Total melt mass (mt)	0/25.9/63.7	0/40.4/87.5		47.4-45.8
Core fraction molten	0/0.21/0.51	0/0.33/0.70	0/0.28/0.60	0.38-0.37
Fraction Zr oxidized	0.15/0.40/0.65	0.15/0.40/0.65	0.08/0.32/0.76	0.41-0.37
Case 1 = 1.5 gpm/pump (best estimate); Case 2 = 220 gpm/pump (maximum).				

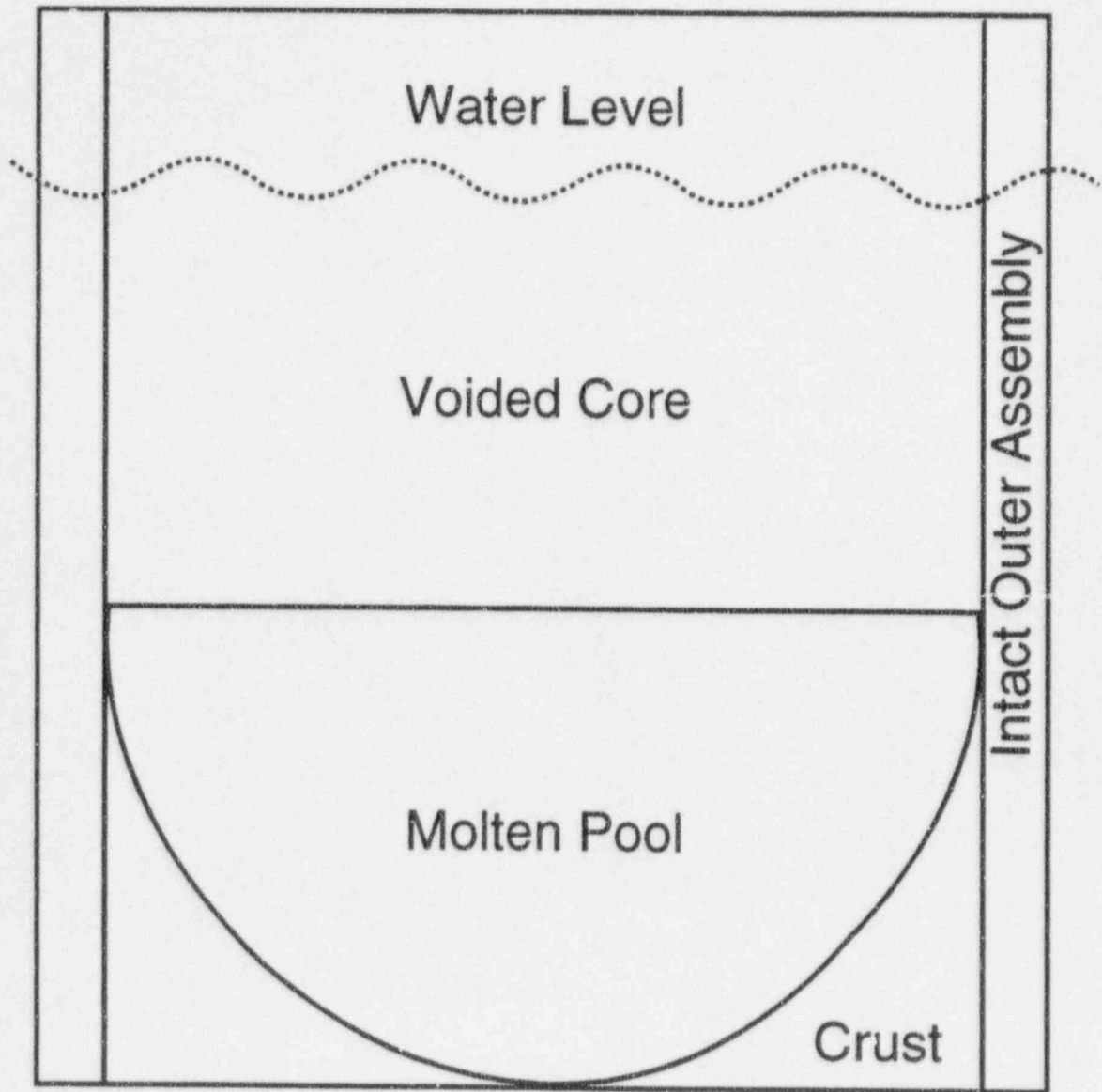


Figure B.1 Crucible formation in a flooded RPV for Scenarios V and Va.



# Melt Mass/Composition Distributions

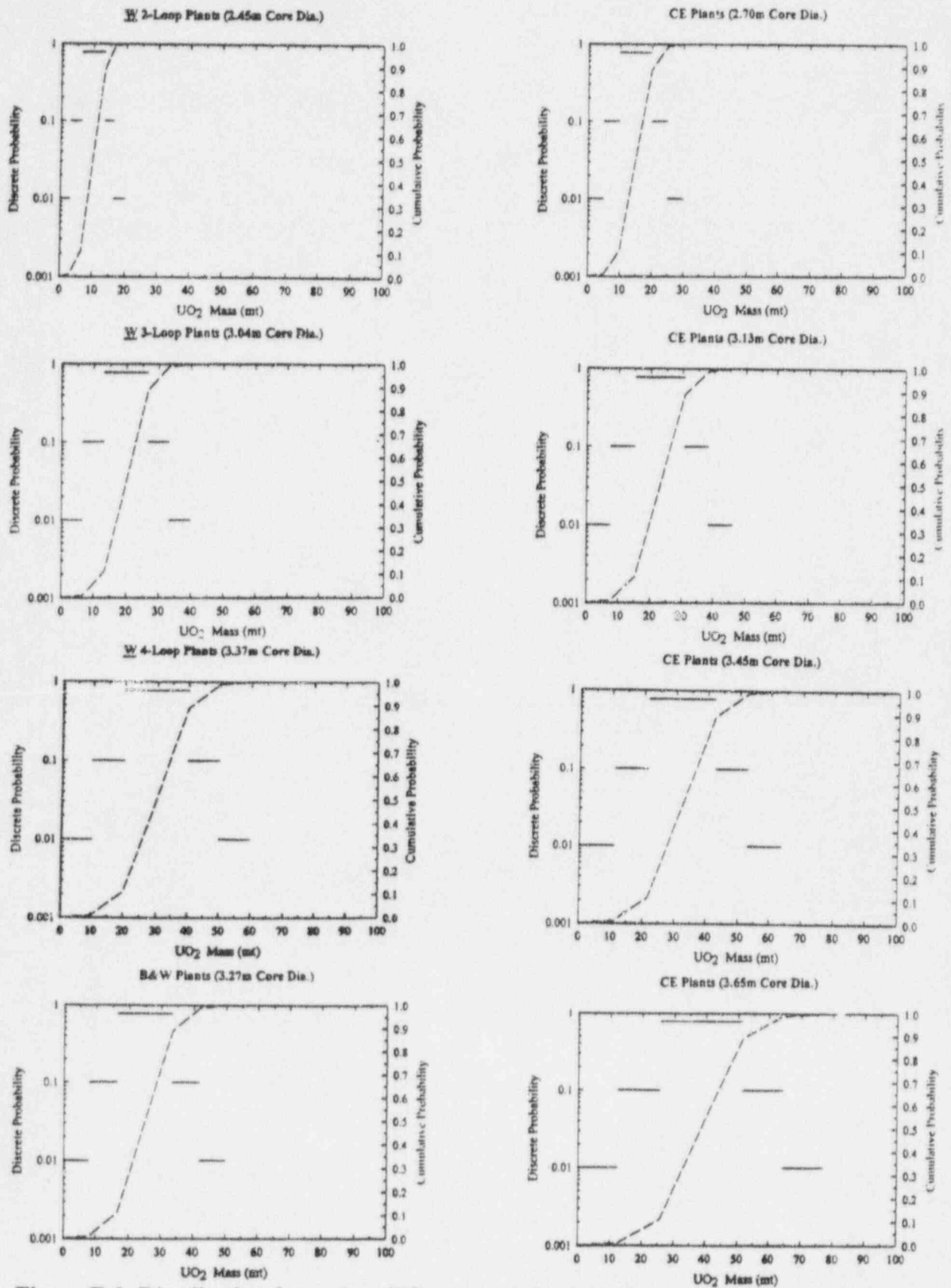


Figure B.2 Distribution for molten  $UO_2$  mass at the time of melt relocation to the lower plenum for Scenarios V and Va.

# Melt Mass/Composition Distributions

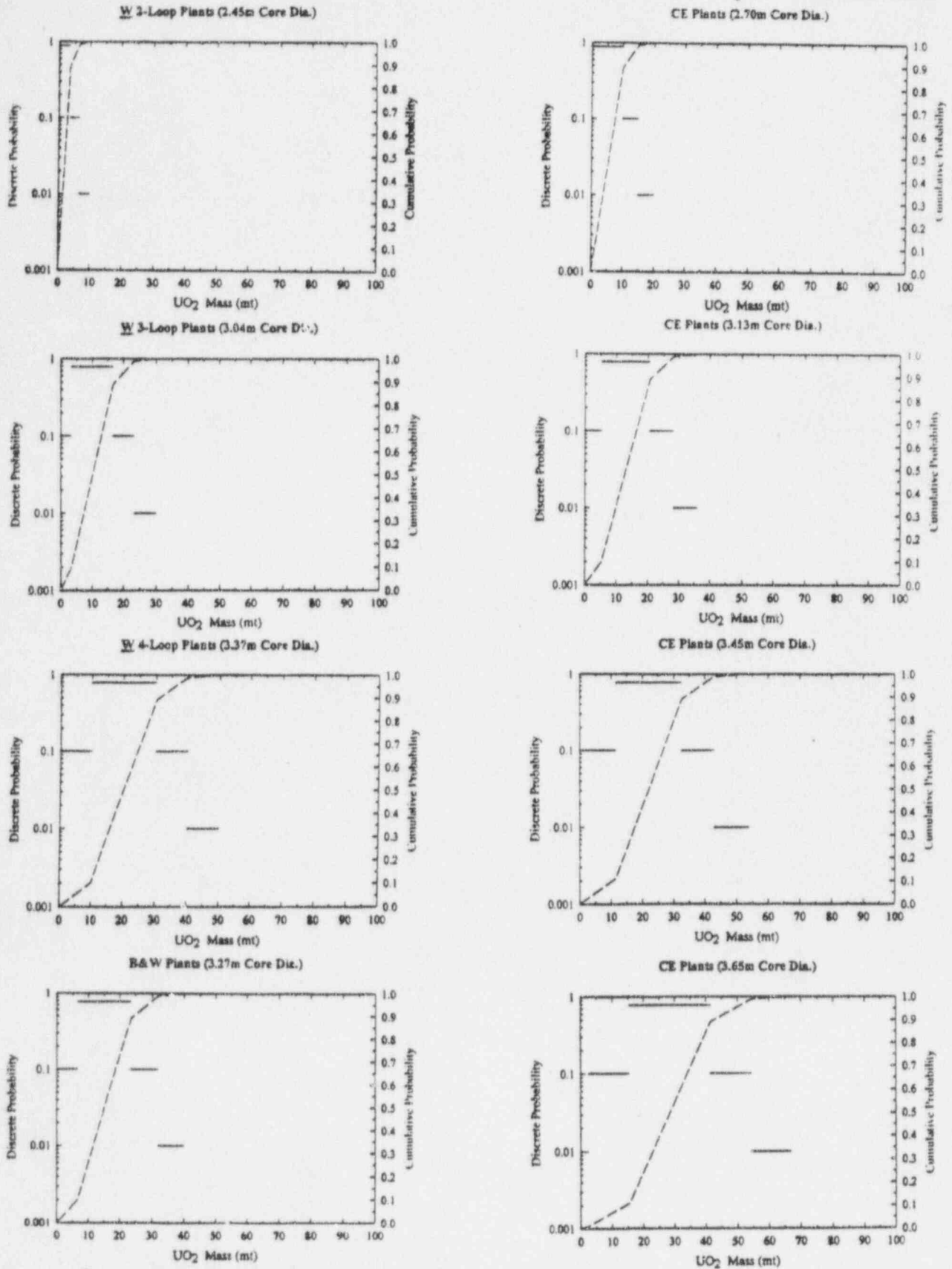


Figure B.3 Distribution for molten  $UO_2$  mass at the time of vessel breach for Scenarios V and Va.

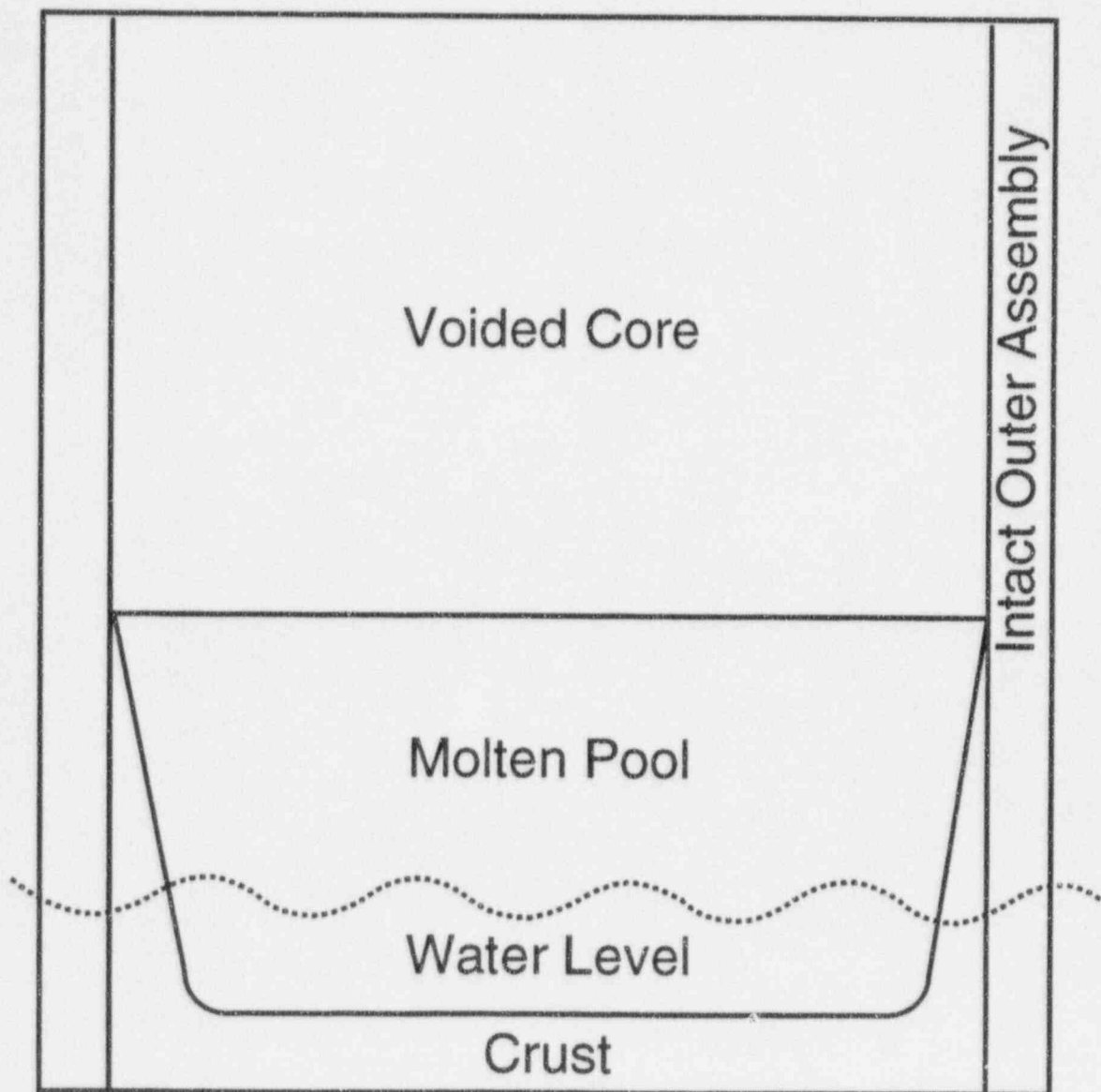


Figure B.4 Crucible formation in wet core scenario with partial operator intervention - Scenario VI.

# Melt Mass/Composition Distributions

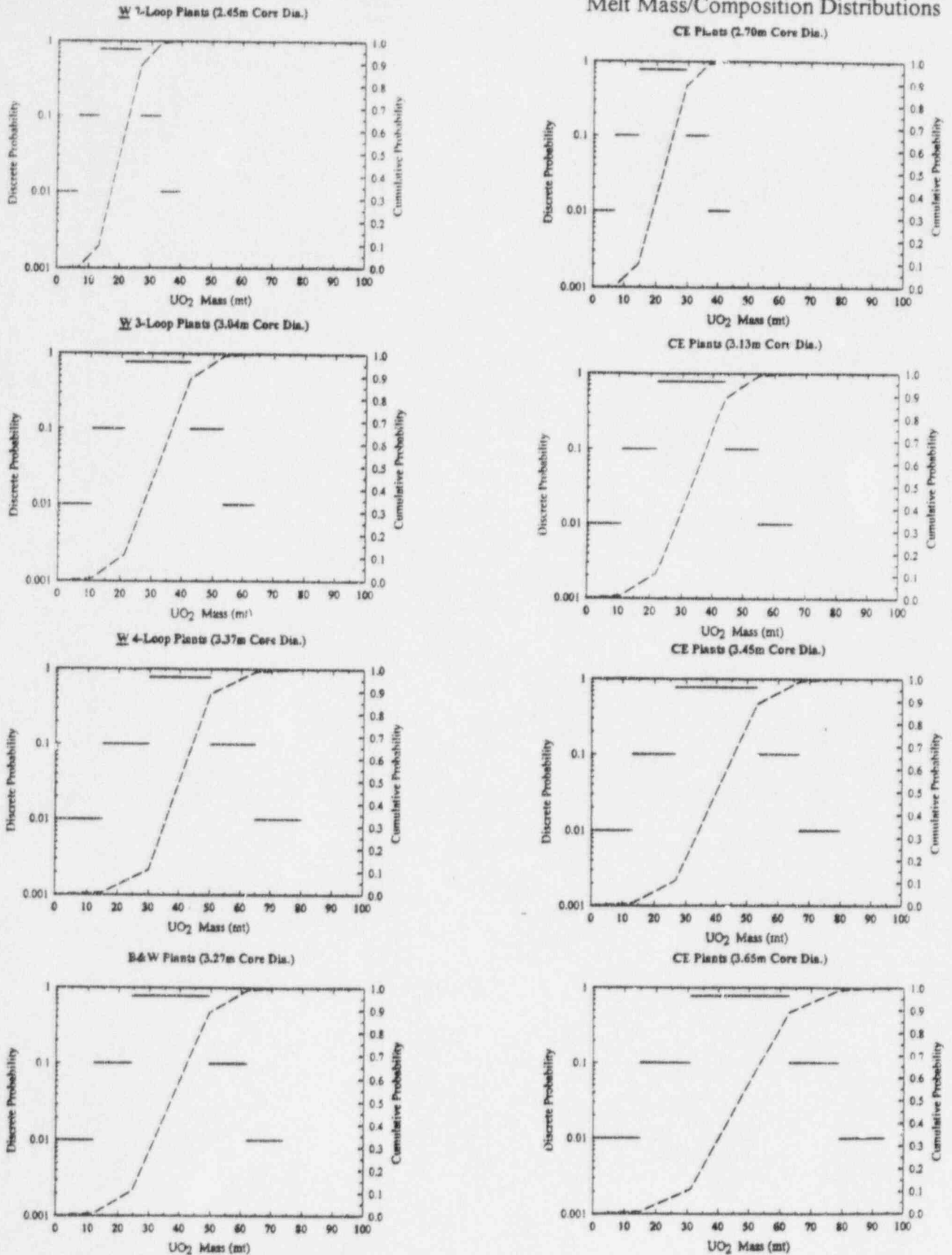


Figure B.5 Distribution for molten UO<sub>2</sub> mass at the time of melt relocation to the lower plenum for Scenario VI.

# Melt Mass/Composition Distributions

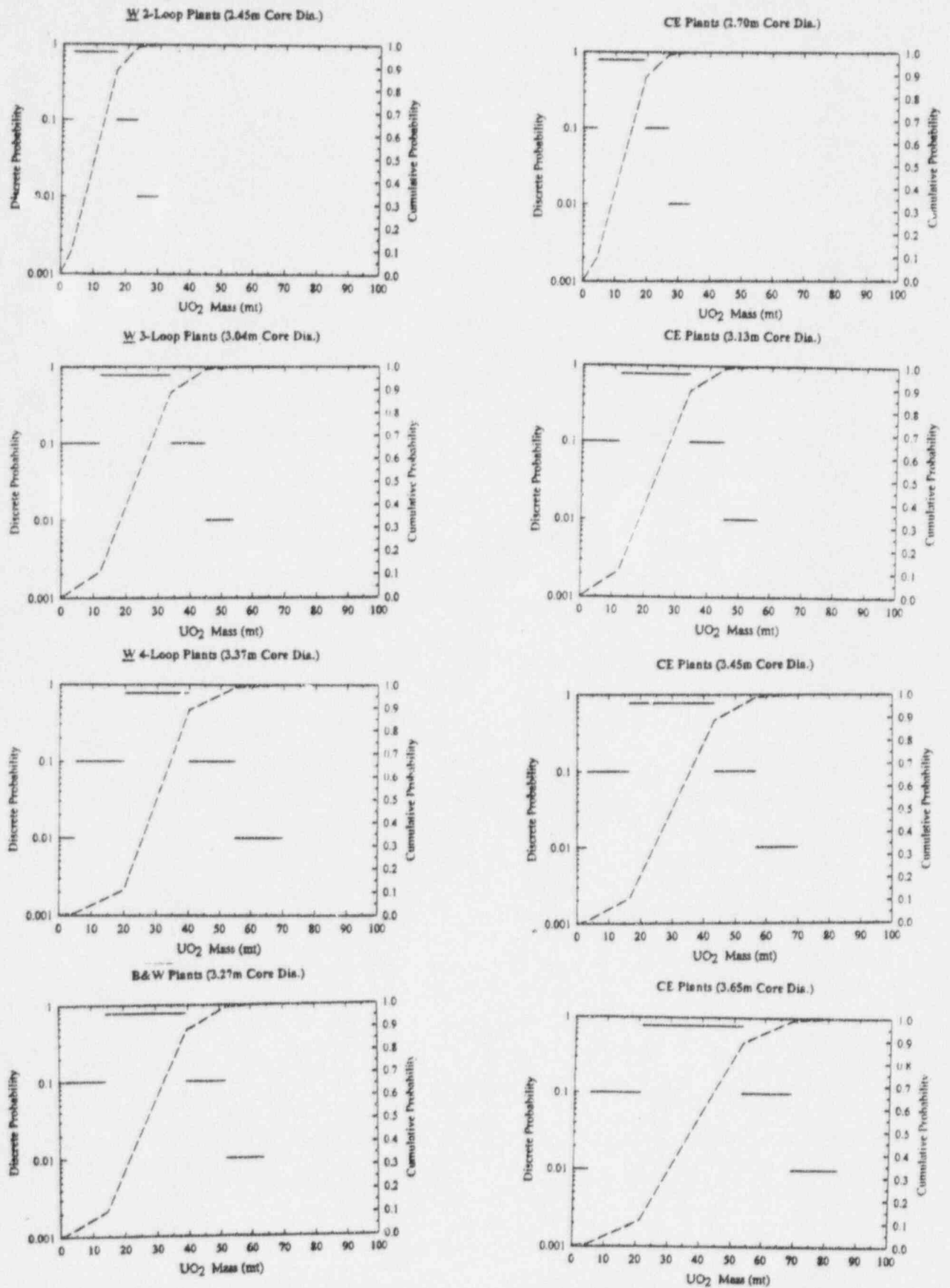


Figure B.6 Distribution of molten  $UO_2$  mass at the time of vessel breach for Scenario VI.



## APPENDIX C Plant Geometry

Michael D. Allen and Martin M. Pilch  
Sandia National Laboratories

### C.1 Introduction

This appendix summarizes plant-specific information on the reactor cavity and subcompartment region for each operating Westinghouse plant with a large dry containment or subatmospheric containment. This information serves four needs:

1. To quantify debris dispersal fractions and to provide assessments of dispersal pathways,
2. To quantify the coherence ratio,
3. To quantify transport of debris to the dome, and
4. To catalog the potential for the reactor cavity to be deeply flooded.

These quantifications are discussed below in greater detail.

### C.2 Reactor Cavity Geometry

IDCOR (1985) categorized cavity geometries in 14 classes and provided a subjective assessment of the dispersive qualities of each cavity. For completeness, the IDCOR descriptions for all cavity types are listed below. The IDCOR descriptions refer to some plants that are no longer operational, but we have made no attempt to update the discussion. Figure C.1 provides a schematic of each of the IDCOR cavities. We have consulted the IPEs, FSARs, PSARs, and sometimes the utilities to obtain a schematic of the cavity for all Westinghouse plants (excluding ice condenser plants). This catalog of cavity schematics is shown in Figure C.2.

Table C.1 associates an IDCOR cavity type with each Westinghouse plant. IDCOR did not provide an assessment for Kewaunee or Salem 1 & 2, so we have provided our own subjective assessment (noted by parenthesis). In two cases, Dia'blo Canyon 1 & 2 and Vogtle 1 & 2, we did not agree with the IDCOR assessment. For these plants we have supplemented the IDCOR assessment with our own. The cavity geometry potentially impacts debris dispersal, coherence ratio, and the possible impact of cavity water. Specific quantifications for these issues are addressed in Sections C.2.1, C.2.2, and C.2.3, respectively.

The following is the IDCOR discussion of reactor cavity groups:

#### IDCOR Type A

This configuration is representative of Braidwood 1 & 2, Byron 1 & 2, and Zion 1 & 2, all of which are Westinghouse/Sargent & Lundy plants. This configuration would allow debris dispersal during a high pressure blowdown of the primary system as predicted in the Zion

## Plant Geometry

Probabilistic Safety Study and confirmed by the ANL and SNL experiments. The containment structures that could possibly entrap debris after it was ejected from the reactor cavity and instrument tunnel would be the lower side of the seal table room and two of the nearby walls.

### IDCOR Type B

This configuration is representative of Seabrook, Indian Point 2 & 3, and Trojan which are Westinghouse/United Engineers and Constructors and Bechtel plants. This geometry would also not retain much debris after high-pressure melt ejection. It also has an additional manway which would serve as a vent during such an event. The debris that would be ejected and propelled upward from this type cavity would impact upon the bottom of the floor of the seal table room. There is somewhat more surface area for the debris to impact upon than for a type A configuration and thus more potential for aerosol generation.

### IDCOR Type C

This configuration is representative of Sequoyah 1 & 2, Catawba 1 & 2, McGuire 1 & 2, Diablo Canyon 1 & 2, Vogtle 1 & 2, and Watts Bar 1 & 2. These plants all have a Westinghouse NSSS but a variety of containment A/E's (TVA, Duke, Pacific Gas & Electric, Southern Services, and Bechtel). This type has a reduced potential for direct entrainment and an increased potential for retaining a considerable amount of debris at steps and standoff regions away from the main gas flow. The manway into this reactor cavity would serve as a vent during such an event. The impingement locations for any ejected debris from the reactor cavity from which an aerosol could perhaps be produced would be under the floor containing the seal table and on the edges of some of the adjacent walls.

### IDCOR Type D

This configuration is representative of Millstone 3, Beaver Valley 1 & 2, Ginna, Harris 1, North Anna 1 & 2, Robinson 2, and Surry 1 & 2. All these plants have a Westinghouse NSSS, and the containment A/E's were Stone & Webster, Gilbert & Associates, and Ebasco. This configuration is expected to retain essentially all of the debris. Most of the debris would be anticipated to initially accumulate at the sump end of this reactor cavity type. Authors Note: Since the time of the IDCOR study, many experiments using low-temperature and high-temperature simulant fluids have demonstrated that Surry-like cavities are not retentive as the IDCOR study suggested.

### IDCOR Type E

This is the configuration of South Texas 1 & 2, which are Westinghouse/Bechtel plants. Little debris will escape this reactor cavity because the instrument tubes are individually sealed through the concrete wall in the reactor cavity and the manway represents a tortuous path to the upper compartments in the containment. The manway continues around in a circular pattern for about 45° from the door location after which it starts up a flight of stairs. It is the horizontal surface area of the roof in this stairwell compartment that provides nearly all the

impaction area for the hypothetical generation of an aerosol that could then possibly be carried up further into the containment.

#### IDCOR Type F

This configuration is representative of Calvert Cliffs 1 & 2, Arkansas 2, Millstone 2, and Palisades which are all Combustion Engineering/Bechtel plants. Most all of the debris would escape through the annulus between the reactor vessel and the biological shield. Most of the ejected debris would then impact on the missile shield over the control rod drive mechanisms and be accumulated in the refueling pool.

#### IDCOR Type G

This is the configuration of Oconee 1, 2, and 3 which are Babcock & Wilcox/Duke-Bechtel plants. Not much core debris is expected to escape from this reactor cavity since the instrument tunnel is dead ended. The instrument tubes are individually sealed as they pass through separate penetrations in the floor before they enter the seal tank. Hence, significant fractions of the debris inventory could not migrate up into the containment via this path. The ~0.76 m diameter access passage to the reactor cavity is brick filled but without any mortar. If this is opened by the blowdown, debris would be distributed onto the containment floor and would not provide for significant direct heating.

#### IDCOR Type H

This configuration is representative of Summer 1, Maine Yankee, Palo Verde 1, 2, 3, WNP 3, Farley 1 & 2, Prairie Island 1 & 2, and Turkey Point 3 & 4. These plants have Combustion Engineering & Westinghouse NSSS, and the containment A/Es were Stone & Webster, Bechtel, Ebasco, Southern Services, Gilbert & Associates, and Pioneer. Little debris is expected to escape from this configuration partially because of the trapping of such material at the sump end of the lower cavity. The upper wall adjacent to where debris would accumulate at the sump is also chambered thus providing additional flow area for the gas/vapor flow to negotiate the turns without entraining the heavier debris.

#### IDCOR Type I

This configuration is representative of St. Lucie 1 & 2, Point Beach 1 & 2, and Waterford 3. These plants have Westinghouse and Combustion Engineering NSSS, and the containment A/Es were Bechtel and Ebasco. Not much core debris is expected to migrate to the upper regions of the containment primarily because of the tortuous path involved in this configuration. Furthermore, the flow area enlarges as the upper floor is approached, reducing the velocity of the debris.

IDCOR Type J

This is the configuration of San Onofre 2 & 3 which are Combustion Engineering/Bechtel plants with top-mounted in-core instrumentation. A considerable amount of core material is expected to escape from this reactor cavity through the cooling ducts and up around the RPV. Most of the debris would probably pass up around the RPV since the total cooling duct flow area is only about 40 percent of that around the RPV. Consequently, most of the debris impaction area for possible aerosol generation would be on the main coolant lines just outside of the RPV before they penetrate the concrete biological shield and also on the missile shield over the control rod drive mechanisms.

IDCOR Type K

This configuration is representative of Arkansas Nuclear One and WNP 1 which have Babcock & Wilcox NSSS and containments designed by Bechtel and United Engineers & Constructors, respectively. Not much core material is expected to escape from this type even with the large volume of the instrument tunnel because it is dead ended where the instrument tubes pass through individually sealed penetrations in the floor supporting the seal tank. The most likely debris migration path in such an event would be up around the RPV where the impaction area would be that imposed by the main coolant lines between the RPV outer wall and concrete biological shield as well as on the missile shield.

IDCOR Type L

This is the configuration of Bellefonte 1 & 2, which are Babcock & Wilcox/Tennessee Valley Authority plants. Even though the instrument tunnel and the ventilating ducts are shown in the same plant for simplicity, they are actually rotated about 120° from each other. Some core material would be anticipated to escape from this configuration. Most is expected to traverse up around the RPV and also out through the outboard cooling duct. Not much is anticipated to migrate through the smaller flow area, inboard cooling duct, or through the large volume instrument tunnel because it is sealed where the instrument tubes pass through the floor supporting the seal tank. The impaction of core debris would most likely occur on the structure above the outboard cooling duct exit and on the main coolant line in the annulus surrounding the RPV.

IDCOR Type M

This configuration is representative of Callaway 1, Comanche Peak 1 & 2, Wolf Creek, and Davis Besse 1. These plants have Westinghouse and Babcock & Wilcox NSSS and containments designed by Bechtel, Gibbs & Hill, and Sargent & Lundy. This particular reactor cavity arrangement is expected to retain a good fraction of the core material ejected from the RPV. Most of this debris is anticipated to accumulate in the corner opposite the RPV which contains the sump. The debris retention capabilities are enhanced by the manway which could serve as a vent and the chamfered wall adjacent to the sump which would create more flow area to relieve the gas/vapor flow during the blowdown.



### IDCOR Type N

This is the configuration of Yankee Rowe which is a Westinghouse/Stone & Webster plant. It is expected that a reasonable fraction of the core material ejected from the RPV would exit this cavity. The debris would most likely traverse up around the RPV because there are apparently no penetrations nor vents in the lower region of the reactor vessel cavity. One of the few structures that would most likely impede the debris migration out of the LRC would be the borated water tank surrounding the RPV. Impaction of core debris on the main coolant lines would occur as the debris exited the cavity. Authors' Note: No operational reactors have this cavity type.

#### C.2.1 Debris Dispersal

Debris dispersal from the reactor cavity has been the focus of many programs since the Zion Probabilistic Safety Study (ZPSS, 1981). Spencer et al. (1982; 1983) showed that the threshold for dispersal from the Zion reactor cavity is reasonably predicted by the Kutateladze criterion proposed in the Zion Probabilistic Safety Study. IDCOR (1985) categorized existing cavity geometries into 14 classes and provided a subjective assessment of the dispersive or nondispersive qualities of each class. The IDCOR notion that cavity geometry influences debris dispersal has been confirmed only partially by more recent experiments. Separate effects experiments using low-temperature simulant fluids in the Zion, Surry, and Watts Bar geometries (Tutu et al., 1988a; b; Tutu, 1990; Tutu and Ginsberg, 1990), in the Sizewell B geometry (MacBeth and Trenberth, 1987; Rose, 1987; MacBeth et al., 1988), and in Korean designs (Kim et al., 1992; Chun et al., 1991) all show that cavity geometry is important only at low RCS pressures where dispersal is incomplete. However, correlations proposed by these authors and independent correlations (Levy, 1991) based on some of the same data all suggest that debris dispersal is nearly complete at reactor scale for RCS pressures in excess of about 4 MPa, regardless of the cavity geometry.

Typical dispersal fractions of 62 - 89 percent have been observed in recent large-scale integral-effects DCH experiments (Allen et al., 1994a; Blanchat et al., 1994) and some smaller-scale counterparts at ANL (Binder et al., 1994). The retained material predominantly appears as a thin frozen crust on all cavity surfaces. This retention by freezing did not occur in dispersal experiments using low temperature simulant fluids.

Henry (1989) and Ishii et al. (1993) analyzed the dispersal process as a competition between film sweepout and surface entrainment. Ishii's predictions have been confirmed qualitatively by recent separate effects tests conducted at Purdue University (Ishii et al., 1993) using water as a simulant for molten core material. These models, although differing in their details, both predict that surface entrainment dominates the dispersal process for representative conditions of interest if heating of the blowdown gas is significant. These predictions and conclusions are consistent with the Ishii and Mishima (1989) correlation for the entrained liquid flux in annular two-phase flow.

The experiments of MacBeth et al. (1988) suggest that the fraction of melt swept from the cavity is independent of physical scale. Correlations by Tutu and Ginsberg (1990) for the Zion and Surry cavities (based on 1/42 scale experiments conducted at BNL and unpublished 1/10



scale experiments conducted at SNL) suggest that the extent of dispersal is nearly independent of physical scale. The correlations of Levy (1991), which are based on the same data suggest that dispersal increases with physical scale. Other experiments (Kim et al., 1992; Chun et al., 1991) also show that the extent of dispersal is nearly independent of physical scale. More recently, the large-scale (1:10) integral effects DCH experiments (high temperature melts) conducted at SNL (Allen et al., 1992c-h, Allen et al., 1993) and their smaller-scale counterparts (1:40) at ANL (Binder et al., 1992a-f) show that the extent of melt dispersal is independent of physical scale.

Reactor cavities normally exist so in-core instrument guide tubes can have access to the lower head of the RPV. Most dispersal experiments have been conducted without these structures in the cavity. Rose (1987) found that modeling the guide tubes and their supports dramatically reduced dispersal of low temperature simulant fluids from a model of the Sizewell B cavity. The support structures are much more massive in the Sizewell reactor than typical U.S. reactors. Allen et al. (1990), however, found that the guide tubes and their supports were forcibly ejected from a model of the Surry cavity during the dispersal process. The distinguishing feature here is that a high temperature melt cut (by ablation) the supports free from the anchors in the floor of the cavity.

Surface entrainment results in fine fragmentation of the melt. Particle sizes have been measured in some high temperature DCH experiments using either a Fe/Al<sub>2</sub>O<sub>3</sub> thermite (Tarbell et al., 1987; Allen et al., 1991, 1992a,b, 1994a,b) or a uranium thermite (Blomquist et al., 1985, 1986). Particle sizes are distributed lognormally with a mass mean diameter of ~0.5 - 1.5 mm and a geometric standard deviation of ~4. Sienicki and Spencer (1986) showed that the mass mean sizes in these experiments are qualitatively consistent with the correlation of Kataoka and Ishii (1982). Ishii et al. (1993) and Zhang et al. (1994) have performed separate effects tests with water and woods metal and found that the Kataoka correlation can underpredict the particle size by as much as a factor of two. Zhang and Ishii (1995) attribute this to entrance region effects.

The Kataoka correlation sometimes predicts particle sizes from entrainment that are sufficiently large that secondary fragmentation ( $We \geq 12$ ) can occur in the gas core (Sienicki and Spencer, 1986; Ishii et al., 1993). Using mean gas velocities and ignoring heating of the blowdown gas, Ishii et al. (1993) predict a mass mean particle size of ~0.6 mm for a representative set of DCH conditions. Larger particles are expected if secondary fragmentation does not go to completion or if entrained debris slows the gas. On the other hand, smaller particles are expected if localized gas velocities near the entrainment surface significantly exceed the mean gas velocity or if heating of the blowdown gas is significant.

In summary, we expect that debris dispersal will be complete for RCS conditions of most interest to DCH, except for some retention by freezing on cavity surfaces, for all cavity designs representative of Westinghouse plants. We also expect that dispersal will be dominated by surface entrainment and that the melt will be fragmented to sizes of ~1 mm.

We now seek a first order accounting of the quantity of melt that can freeze on cavity structures. The fraction of melt that can disperse where freezing on cavity structures is the sole mechanism for retention is given by

$$f_{disp} = 1 - \frac{\delta A_s \rho_d}{M_d^o} \sim 1 - \frac{2\lambda_c (\alpha_c R_\tau \tau_b)^{1/2} 6V_c^{2/3} \rho_d}{M_d^o} \quad (C.1)$$

The definition of each of these terms is given in the nomenclature section, C.5. The crust growth constant ranges from  $\lambda \sim 0.14$  for thermite on concrete to  $\lambda_c \sim 0.48$  for corium on concrete. We assume that freezing occurs on cavity surfaces during the debris dispersal interval  $t = R_\tau \tau_b$  where  $R_\tau$  is the coherence ratio as discussed later in Section C.2.2 and  $\tau_b$  is the characteristic blowdown time given by

$$\tau_b = \frac{1}{C_{d,h}} \left( \frac{\gamma + 1}{2} \right)^{\frac{\gamma + 1}{2(\gamma - 1)}} \frac{V_{RCS}}{A_h} \left( \frac{MW_{g,RCS}}{R_u T_{RCS}^o} \right)^{1/2} \quad (C.2)$$

Table C.2 validates the model predictions against the major DCH integral tests. Reactor applications are both plant-specific and scenario-specific. The former is true because of geometric differences and the latter is true because of the scenario dependent melt masses and RCS pressures. Table C.1 lists the fraction dispersed for each plant and for each scenario, with the evaluation being performed for the upper end of the mass distributions as quantified in Appendix B. It is seen that freezing on cavity surfaces retains only ~10 percent of the melt for each plant and scenario.

### C.2.2 Coherence Ratio

The TCE model assumes that debris/gas interactions are limited to that portion of the blowdown gas that is coherent with the dispersal process. The ratio of the characteristic dispersal time to the characteristic time constant for blowdown is termed the coherence ratio. Smaller values of the coherence ratio means that the primary heat sink for debris/gas thermal interactions is smaller and that metal/steam reactions are more likely to be steam limited.

The notion that noncoherence (between debris dispersal and RCS blowdown) can limit DCH interactions is not unique to the TCE model. Ginsberg and Tutu (1987) were the first to suggest this limitation. Early CONTAIN calculations (Williams and Louie, 1988) also exhibited some sensitivity to coherence, though the effect found was not large. The CLCH model (Yan and Theofanous, 1993) also considers noncoherence as a basic modeling process. These analytic reflections all have a solid basis in experiment observations. Unpublished real-time flash x-rays taken at SNL show that dispersal is complete well before blowdown. In addition, many experiments have been conducted (e.g., Allen et al., 1991; Allen et al., 1992a,b) with pyrometers focused on the cavity exit. Pyrometer signals also confirm the notion of noncoherence, and they suggest that cavity pressurization records can also be used to define the coherent interval. Despite this physical evidence, no systematic experiments have ever been performed for the purpose of directly validating the impact of noncoherence on DCH loads.

The database for the coherence ratio largely overlaps the range of individual parameters that are of interest to reactor applications. However, the database does not include all possible combinations of parameters for each of the potential applications; consequently, a correlation for

## Plant Geometry

the coherence ratio is required in order to fill gaps in the database. It is significant that any such process is more closely analogous to interpolation rather than order of magnitude extrapolation.

Pilch (Appendix E in Pilch et al., 1994a) developed a correlation for the coherence ratio based on momentum considerations. The Pilch correlation can be expressed as

$$R_r = \frac{\tau_e}{\tau_b} = C_{Rr} f_{disp} \left( \frac{T_{RCS}^o}{T_d^o} \right)^{1/4} \left( C_{d,h} \frac{M_d^o}{M_g^o} \frac{A_h V_c^{1/3}}{V_{RCS}} \right)^{1/2}, \quad (C.3)$$

where  $C_1$  is a cavity-specific (weakly) multiple that is determined from experiment data. For an isentropic blowdown of the RCS, the fraction of blowdown gas that is coherent with debris dispersal is given by

$$f_{coh} = 1 - \frac{M_g^o}{M_{g,e}^o} = 1 - \left( \frac{P_{e,RCS}}{P_{RCS}^o} \right)^{\frac{1}{\gamma}} = 1 - \left( 1 + \frac{\gamma - 1}{2} R_r \right)^{\frac{-2}{\gamma - 1}}. \quad (C.4)$$

for  $R_r \leq 0.5$ ,  $f_{coh} \sim R_r$ , so that  $R_r$  is directly proportional to the amount of blowdown gas that can react with the debris.

Table C.1 summarizes information needed to quantify the coherence ratio for each plant. Specifically, the coherence ratio correlation contains a lead multiplier that is a weak function of plant geometry. Our goal is to quantify the multiplier and other geometric information needed to compute the coherence ratio for each plant. In addition, we must specify a relative standard deviation in our quantification of the coherence ratio.

The database on which the coherence ratio correlation is based contains Zion-like geometries and Surry-like geometries, and the lead constant on the correlation is a weak function of the cavity type. Our intent here is to further reduce the IDCOR categorization into 3 groups: Zion-like, Surry-like, and other. We define Zion-like cavities as having a U-tube layout with a slanted riser section, and we define Surry-like cavities as having a U-tube layout with a vertical riser section. Only two plants, South Texas 1 & 2, cannot be characterized as Zion-like or Surry-like. Our assessments are summarized in Table C.1. Westinghouse cavities (41 total) are 27 percent Zion-like, 68 percent Surry-like, and 5 percent neither. We expect no significant impact of subcompartment geometry on coherence because all Westinghouse plants evaluated in this study have a significant impaction structure near the cavity exit (i.e., flight paths similar to Surry and Zion).

Having further grouped the cavity designs, we assign the lead constant and relative standard deviation appropriate to Zion to all Zion-like cavities. A similar procedure is followed for Surry. Only South Texas 1 & 2 cannot be characterized as Zion-like or Surry-like. We biased (in the conservative direction) the lead constant for South Texas 1 & 2 for the combined Zion/Surry database by one standard deviation and then assigned the relative standard deviation appropriate to the combined database to the biased correlation. Uncertainties resulting from a geometry

significantly outside the current database are bounded in this fashion while still maintaining a generous uncertainty distribution. The coherence constant and the relative standard deviation are tabulated in Table C.3.

### C.2.3 Cavity Water

NUREG/CR-6075 (Pilch et al., 1994a) identified the need to catalog the extent of cavity flooding prior to vessel breach. The need is born from two questions:

1. What impact does cavity water have on DCH loads?
2. Can explosive or non-explosive FCIs in the cavity cause structural damage to the cavity?

This section catalogs the necessary information (to the extent available) to address these issues.

All reactor cavities will always contain some water due to condensation on cavity surfaces. This water will typically collect in the cavity sump, so we refer to this situation as "dry." The issue then becomes whether the cavity can act as a collection point for condensate from the entire containment or act as a collection point for RWST water should it be injected into the containment during spray operation, ECCS operation, or operator action.

The IPEs generally assessed the likelihood that water will be present in the reactor cavity. We consider three categories:

1. *Dry* cavities which contain only condensate levels of water,
2. *Wet* cavities which are only partially full, and
3. *Flooded* cavities which will overflow onto the basement floor.

We note, however, that a flooded cavity does not always mean that the lower head of the RPV is submerged. A catalog of the IPE assessments of cavity water is provided at the end of this section. These assessments are summarized in Table C.4. The IPE descriptions are sometimes supplemented with our own subjective interpretations of the IPE descriptions in order to categorize each cavity.

Reactor cavities are more likely to be dry if the RWST water is not injected into the containment. Most cavities are either free standing or have a curb around the cavity entrance that prevents containment condensate from draining into the cavity. The reactor cavity is a sump for containment condensate in only four plants: Comanche Peak 1 & 2 and Indian Point 2 & 3. These cavities will not be deeply flooded, however, because cavity and RCS volumes are comparable and some RCS boiloff will exist as steam in the atmosphere and drainage of condensate from structures to the cavity will not be complete.

Many reactor cavities will be deeply flooded if the RWST water is injected into the containment through spray operation, ECCS operation, or operator action. Only 7 plants will have dry cavities under these conditions: Farley 1 & 2, Kewaunee, South Texas 1 & 2, and Vogtle 1 & 2.



## Plant Geometry

Operation of the containment sprays is a dominant mode for injecting the RWST into the containment (a LOCA with ECCS injection is the other). Table C.4 lists the spray activation setpoint for each plant. The sprays can be activated in those SBO sequences where power is recovered but core melt progression and lower head failure are not terminated. The spray setpoints can be compared to maximum containment pressure rise any time prior to vessel breach, assuming hot leg failure does not occur. For a large dry containment such as Zion (Tadios and Stamps, Appendix D in Pilch et al., 1994b) the maximum pressure rise was  $\Delta P \sim 0.15$  MPa (22 psig); and for a subatmospheric containment such as Surry (Tadios and Stamps, Appendix D in Pilch et al., 1995), the maximum pressure rise was  $\Delta P \sim 0.17$  MPa (17 psig). Thus, spray activation seems likely for some containments.

Table C.4 further categorizes the cavities as excavated or free standing. Free standing cavities are potentially vulnerable to damage in the event of high cavity pressures resulting from explosive or non-explosive FCIs in the cavity. The failure pressure for each free standing cavity is not known; but should cavity failure occur, the debris will be dispersed on the containment floor thus minimizing DCH interactions. Excavated cavities are not vulnerable to damage from high cavity pressures.

The following catalog of cavity water assessments was compiled from IPE and other PSA reports.

### Beaver Valley 1 & 2

Access to the keyway is through a steel hatch, which is hinged on one end of the hatch and positively latched to the steel decking on the opposite end of the hatch with a screw. The platform is located at Elevation 707'6", whereas the floor of the keyway is at Elevation 690'11". Thus, water in the containment proper would have to rise to a level of 14'7" above the floor before it would overflow into the keyway. The exception is the case of a LOCA involving leaking instrument tubes that would directly wet the cavity. Conversely, water that enters the reactor cavity from the refueling tank would be unavailable for recirculation until the reactor cavity and instrumentation tunnel filled to a level 16'7" above the cavity floor before it reached the decking above the keyway. Approximately 64,800 gallons are estimated to be required to fill the reactor cavity and instrumentation tunnel up to the RHR platform elevation.

Approximately 1,092,000 gallons of water are required to reach the 707'6" level in the containment (excluding the volume in the keyway). The RWST has a minimum capacity of 441,000 gallons. Another 78,500 gallons are available from the accumulators, chemical addition tank, and reactor coolant system.

As is the case for the Surry Unit 1 containment, the Beaver Valley Unit 2 reactor cavity does not communicate directly with the containment sump. A small sump pump (rated at 10 gpm) is located at the bottom of the instrument tunnel near where the instrumentation tubes rise vertically toward the seal table.



Since it is not possible (unless an outside source of makeup is provided) to flood the reactor cavity via "overflow" from the containment, the only significant source of water in the reactor cavity prior to vessel failure results from operation of the quench spray (QS) system. If both QS pumps operate, it is estimated that approximately 140 gpm of the spray will fall into the reactor cavity. At this rate, water level in the reactor cavity and instrumentation tunnel would rise approximately 0.03 feet/minute.

#### Braidwood 1 & 2

The lower compartment and reactor cavity regions communicate via the cavity instrument tunnel and the reactor vessel nozzle openings in the biological shield wall. A removable hatch cover is located at the top of the instrument tunnel at the 377' elevation, and is essentially leak-tight. With containment spray operation, some water will accumulate in the refueling cavity until it overflows the 400'-1½" elevation and spills through the refueling seal area and the RPV annulus into the reactor cavity. This means that most sequences will result in accumulation of some water in the reactor cavity and, depending on timing and operation of containment spray, some sequences may have enough time to immerse the lower head of the vessel. This ability to flood the reactor cavity (even if only part way) is an important feature of the Braidwood containment since the presence of water in the cavity plays a strong mitigative role in many severe accident sequences.

#### Byron 1 & 2

A removable hatch cover is located at the top of the instrument tunnel at the 377' elevation. The hatch cover is not leak-tight. Also, there is an opening in the Unit 1 deck plate to permit routing of the cavity sump pump discharge line, while in the Unit 2 deck plate there is an opening to permit installation of a temporary sump pump during refueling outages. The cross-sectional areas of the opening are estimated at 0.036 ft.<sup>2</sup> and 0.222 ft.<sup>2</sup>, respectively. This permits some water to flow from the containment basement into the reactor cavity. In addition, containment spray operation will cause water to accumulate in the refueling cavity until it overflows the 400'-1½" elevation and spills through the refueling seal area and the RPV annulus into the reactor cavity. This means that most sequences will result in accumulation of some water in the reactor cavity and, depending on timing and operation of containment spray, some sequences may have enough time to immerse the lower head of the vessel. This ability to flood the reactor cavity (even if only part way) is a very important feature of the Byron containment since the presence of water in the cavity plays a strong mitigative role in many severe accident sequences.

#### Callaway

The plant-specific details of the cavity configuration were evaluated to determine whether water can accumulate during core damage. The volume of the cavity is 16,837.8 ft.<sup>3</sup>, with a projected floor area of 645.72 ft.<sup>2</sup>. The volume of RWST inventory that would be injected into the containment is approximately 245,000 gal. or 32,700 ft.<sup>3</sup>, based on the assured Technical Specification volume plus instrument error. Thus, if a vessel breach were to occur and all of the RWST water were injected into the containment, the cavity would be flooded approximately 31

## Plant Geometry

feet above the floor of the cavity. The bottom of the reactor vessel is 16.2 ft. above the floor of the cavity.

Another advantage of the Callaway cavity design is that the second opening to the lower compartment has a small (6 inch) curb around it. This curb is low enough such that, as water is boiled away from the cavity by molten debris and condensed by containment coolers and/or sprays onto the floor of the lower compartment, the resulting height of water on the lower compartment floor is sufficient to ensure backflow into the cavity.

### Comanche Peak 1 & 2

The absence of a curb between the cavity and the lower compartment allows nearly all the water in the containment to drain into the cavity.

### Diablo Canyon 1 & 2

An important consideration in Level 2 analysis is the accessibility of water to the reactor cavity where it potentially would cool any core debris that may collect in the reactor cavity floor. Water that can collect on the containment floor does not have direct access to the reactor cavity except for leakage through the RCDT room fire door and damper gaps and the possible gaps in the access covers. Air and water leakage through the RCDT room fire door and damper is extremely limited. The seal table and ventilation duct are too high to provide injected RWST water access. However, if the containment spray system is operating, a portion of the flow will fall into the refueling cavity and drain into the reactor cavity via the clearance between the reactor vessel thermal insulation and the biological shield. Additionally, after vessel breach, water in the reactor coolant system will flow into the reactor cavity through the breach in the vessel. Water that collects in the reactor cavity cannot drain out of the reactor cavity.

### Farley 1 & 2

The FNP containment design does not facilitate flooding of the reactor cavity. Although water can easily drain from the upper compartment to the annular and lower compartment floors, the water on the lower compartment floor would have to reach a depth of 16 ft. before it could spill into the reactor cavity. This is unlikely to occur at FNP, even during a severe accident in which the entire usable refueling water storage tank (RWST) volume (450,000 gal) is injected into the containment.

### Ginna

The floor of the reactor cavity is located 25.7 ft. below the floor of the main containment region. A six inch curbing exists above the floor of the main containment compartment at the top of the instrument tunnel (where the instrument tubes exit the roof of the cavity). Hence, whenever the contents of the RWST are injected into the containment, the cavity will be completely filled and will remain filled (unless water inventory leaks from containment due to a containment breach).

H.B. Robinson

The cavity geometry creates the potential for reactor vessel submergence at vessel breach. A submerged vessel affects vessel bottom head coolability and has the potential to mitigate ex-vessel steam explosions and pressure loads associated with direct containment heating (DCH) during HPME. During scenarios in which the RWST is completely injected, the water level would be approximately 20 ft. above the bottom of the reactor vessel. The volume of the cavity region is 8548 ft.<sup>3</sup>, with a floor area of 453 ft.<sup>2</sup>. The height of the vessel bottom head relative to the cavity floor is 15.16 ft. The base of the HBR2 cavity is at an elevation approximately 27 ft. below that of the containment floor external to the cavity. Unlike other plants, the HBR2 cavity is not surrounded by a concrete curb on the containment floor. Therefore, only a small fraction of the RWST must be injected or approximately 50 percent of the RCS inventory lost to containment in order to have water present in the cavity.

Indian Point 2 & 3

The Indian Point 2 design is such that water fills the reactor cavity when the primary system contents are released. Also, the design of the sump is such that the containment floor is also covered with water even when the RWST contents are not injected into containment. However, if the debris is not in a coolable configuration then basemat melt-through may occur at Indian Point 2. Basemat melt-through was considered in the Indian Point 2 IPE containment analysis.

Kewaunee

The Kewaunee containment does not facilitate flooding of the reactor cavity. Although water can readily flow from the upper compartment to the lower and annular compartment floors, water cannot access the cavity due to the instrument tunnel wall in the annular compartment. A potential flow path does exist in the form of two access hatches located on the instrument tunnel wall, approximately 2 feet off the floor of the annular compartment. These hatches are closed during normal operations, but if they were left open the cavity could be easily flooded if the RWST were injected into the containment.

Millstone 3

No assessment of cavity water was found.

North Anna 1 & 2

Water can enter the cavity in one of two ways. Following vessel failure any water being injected into the vessel will enter the cavity. If quench or recirculation sprays are operating then that portion of the spray flow which falls into the refueling pool (estimated to be 16 percent of total spray flow) will flow into the cavity (after the refueling transfer canal is filled). All other spray water will flow to the containment sump. With full operation of all spray systems, the cavity will fill with water in approximately 20 minutes.

## Plant Geometry

The maximum water elevation on the containment floor (outside the cavity) considering the entire contents of the refueling water storage tank and the contents of the primary system is approximately 6.0 ft. This is far short of the required depth of 16.5 ft. for overflow from the lower containment/sump into the reactor cavity.

### Point Beach 1 & 2

The PBNP containment facilitates flooding of the reactor cavity. Water can readily flow from the upper compartment to the lower and annular compartment floors and access the cavity. Access is in the form of two floor drains in the annular compartment. If there is water present on the containment floor, the cavity will be wet. During most severe accident sequences, there will be a water pool in the cavity. This feature of the PBNP containment has important implications for core-concrete interactions, ex-vessel steam explosions, etc. Also, this feature allows for the possibility of cooling the reactor vessel lower head externally, thereby averting vessel failure altogether. No credit was taken for this latter possibility, however, in the PBNP PSA.

### Prairie Island 1 & 2

The Prairie Island containment facilitates flooding of the reactor cavity. Water can readily flow from the upper compartment to the annular containment floors and access the cavity. Access is in the form of two personnel entry hatches located on the instrument tunnel, approximately 18" off the floor of the containment. These two hatches are left slightly ajar during normal plant operation. The base case assumption is that if the RWST is injected into containment, either by continuous containment spray operation, or by injection flow out of a break in the primary system, water will accumulate on the floor of the containment. Once the containment water level exceeds 18", water will begin to overflow into the cavity through the two access hatches. Since the flow velocity going into the instrument tunnel may be sufficient enough to pull the doors closed, the issue of RPV lower coolability will be treated as a sensitivity. This feature of the Prairie Island containment has important implications for core-concrete interactions, ex-vessel steam explosions, hydrogen combustion, etc. Also, this feature allows for the possibility of cooling the reactor vessel lower head externally, thereby averting vessel failure altogether.

### Salem 1 & 2

The reactor cavities of each plant (Zion and Salem) allow cavity flooding if the refueling water storage tank (RWST) is injected.

### Seabrook

In the Seabrook design, the reactor cavity forms a well 27 feet below the level of the containment floor. It has a volume of about 14,700 ft.<sup>3</sup> and thus will accommodate about 30 percent of the water volume which is injected from the RWST. Water can reach the reactor cavity prior to vessel melt-through if the refueling water storage tank is discharged into the containment building. In this case, water can reach the reactor cavity either by: (1) spray water draining from the elevated portion of the refueling canal floor into the annulus region between the



reactor vessel and the vessel support concrete structure, or (2) by spilling over the reactor cavity curb after approximately 60 percent of the RWST is discharged on the containment floor. It is concluded that with the RWST injected into the containment, the reactor cavity will always be filled with water and the water level in the containment will be above the elevation of the reactor cavity curb.

In the Seabrook plant, accident sequences in which the RWST is not discharged via the safety injection or residual heat removal (RHR) pumps (no injection) and in which the sprays do not operate would have no water in the reactor cavity prior to vessel melt-through. This is because even spilling the entire primary coolant system inventory, including the accumulators, would result in a water depth on the containment floor of less than half the curb height. Therefore, such sequences would exhibit a dry cavity for Seabrook, whereas in the Indian Point design, the curb was sufficiently low to have water present in the reactor cavity even without RWST discharge. In the Seabrook containment response analysis, dry reactor cavity cases will therefore be given greater emphasis, and these sequences will be referred to as dry sequences. Accident sequences with the RWST injected will be referred to as wet sequences.

The Seabrook cavity design includes a 30" high curb around the reactor cavity. This means that in the Seabrook design, most of the RWST contents must be injected before water will spill over into the cavity. For Seabrook, the reactor cavity is full of water with RWST injection and is dry without RWST injection.

Another difference is related to the height of the curb on the containment floor surrounding the reactor cavity. The Seabrook design includes a 30" high curb, while in the comparison plants, the curb height is only 6" high. This means that in the Seabrook design, most of the RWST contents must be injected before water will spill over into the cavity. In the comparison plant designs, only a small fraction of the RWST must be injected before flooding of the cavity occurs. However, for both Seabrook and the comparison plants, the reactor cavity is full of water (wet) with RWST injection and is dry without RWST injection.

#### Shearon Harris

During scenarios in which the RWST is injected, the water level would be approximately 13.5 ft. above the bottom of the cavity. The height of the vessel bottom head relative to the cavity floor is 15 ft. 5 in. Thus, the bottom head would not be submerged as a result of discharging the normal RWST inventory into containment, and ex-vessel cooling is not likely to happen at SHNPP. The SHNPP cavity is surrounded by a 1.5 ft. concrete curb on the containment floor. Thus, only in cases with the RWST injected would there be water present in the cavity prior to RPV failure.

#### South Texas 1 & 2

Water access to the reactor cavities could be via the ventilation access tunnel at the reactor cavity floor level (or) backup drainage through the single 4" diameter floor drain. There is no possibility of water draining into the cavity around the penetrations for the instrument tubes where



## Plant Geometry

they penetrate through the biological shield wall. There is no clearance around these pipes in the concrete wall. The area where the instrument tubes penetrate through the biological shield wall is a recessed hatch area about 3 ft. high going into concrete about 3 to 4 ft. In this area it might be difficult to get water access for debris cooling, even if water covers the debris in the main cavity area. The in-core instrumentation room is level with the containment floor. The in-core instrumentation tubes come out of the biological shield wall through a steel seal plate. The instrument tubes in the instrument tube room are much thinner than on the reactor cavity side. The view from the instrument tube room side also confirms that there is no water access from the instrument room to the reactor cavity. Access to the instrument room is by a 4x4 ft. hollow steel door at the floor level.

The refueling pit (refueling cavity) was inspected for any possibility of spray water draining from the refueling pit around the reactor vessel into the reactor cavity. There is an approximately 8" high lip around the reactor vessel that will divert any water on the refueling pit floor to flow around the reactor vessel and drain into the lower portion of the refueling pit where the fuel transfer tube is located. The reactor vessel was filled up to the top of this 8" diversion lip and there was no appearance of any water draining around the reactor vessel.

### Summer

No assessment of cavity water was found.

### Surry 1 & 2

Water can enter the cavity in one of two ways. Following vessel failure any water being injected into the vessel will enter the cavity. If containment sprays are operating then that portion of the spray flow which falls into the refueling pool (estimated to be 16 percent of total spray flow) will flow into the cavity (after the refueling transfer canal is filled). All other spray water will flow to the containment sump. With full operation of all spray systems, the cavity will fill with water in approximately 20 minutes.

The maximum water elevation on the containment floor (outside the cavity), considering the entire contents of the refueling water storage tank and the contents of the primary system, is approximately 4.5 ft. This is far short of the required depth of 14.5 ft. for overflow from the lower containment/sump into the reactor cavity.

### Turkey Point 3 & 4

The Turkey Point containment internal design is such that all the floor drains are directed into the reactor cavity sump via drain pipes. This feature makes the reactor cavity 'wet' for essentially all the important sequences analyzed in the Turkey Point IPE.

### Vogtle 1 & 2

The VEGP containment does not facilitate flooding of the reactor cavity. Although water can easily drain from the upper compartment to the annular and lower compartment floors, the water on the lower compartment floor would have to reach a depth of 9 ft. 2 in. before it could spill into the reactor cavity through the cavity sump pump discharge pipe penetration. This is unlikely to occur at VEGP, even during a severe accident in which the entire usable RWST volume (628,000 gal) is injected into the containment.

### Wolf Creek

The WCGS containment does not facilitate flooding of the reactor cavity. Although water can easily drain from the upper compartment to the annular and lower compartment floors, the water on the lower compartment floor would preferentially drain into the annular compartment since a 6" curb exists around the cavity manway and the annular compartment floor is 16" below that of the lower compartment. Thus, the annular compartment would have to be flooded to a depth of 22" and the lower compartment to a depth of 6", which would require a total liquid volume of ~114,500 gallons, prior to water entry into the cavity via the cavity manway opening. This implies that only limited flooding of the cavity region is possible for sequences in which injection of the RWST inventory occurs and that the cavity would be essentially dry otherwise.

### Zion 1 & 2

The Zion containment facilitates submerging the bottom portion of the reactor vessel with only minimal water injection to the containment. Water can easily drain from the upper compartment to the annular and lower compartment floors. Once the water on the lower compartment floor reaches a depth of 6", it will spill into the cavity through the opening at the top of the instrument tunnel. Injection of the RWST inventory above its low-level alarm setpoint would completely flood the reactor cavity, fully submerging the RPV lower head and part of the vessel cylinder. This ability to flood the reactor cavity (even if only part way) is a very important feature of the Zion containment since the presence of water in the cavity plays a strong mitigative role in many severe accident sequences.

## **C.3 Debris Transport to the Containment Dome**

There are two primary debris transport pathways from the cavity to the containment dome in Westinghouse plants: (1) through the annular gap between the RPV and the biological shield wall, and (2) from the in-core instrument tunnel through the lower compartments. In the calculations performed to assess the CCFP for W PWRs, all of the debris dispersed from the cavity is assumed to enter these two debris transport pathways. The fraction of the debris that is dispersed through each of these pathways is calculated by dividing the minimum flow area of that pathway by the total flow area out of the cavity. Most of the debris (90 percent) that flows through the annular gap reaches the containment dome. On the other hand, much of the debris that is ejected into the lower compartments from the cavity exit is trapped in the lower compartments. This debris trapping is a major mitigation mechanism for DCH loads in W plants.

## C.3.1 Debris Transport Through the RPV Annular Gap

The annular gap around the RPV is a debris transport pathway to the upper dome. The SNL IET-11 experiment showed that the melt-laden gas will melt the insulation and sweep it from the gap. The SNL HIPS-8C experiment also simulated the gap without insulation. Analysis of these two experiments indicates that the fraction of dispersed debris that goes through the gap is equivalent to the minimum flow area (without insulation) through the gap divided by the sum of the minimum gap and tunnel flow areas (see Appendix I in Pilch et al., 1994a for more development of the phenomena involved and validation against a database for Zion and Surry designs). The HIPS-10S experiment (Allen et al., 1990) showed that the in-core instrument tubes and their supports are forcibly ejected from the cavity; consequently, the minimum tunnel flow area is evaluated without the presence of these structures. This assessment of gap transport may be conservative because the experiments did not model the neutron shields or other structures in the gap, because water is expected to be coejected from the RPV with the melt, and because approximately 10 percent of the melt could be intercepted by the missile shield (Bertodano, 1993). Nonetheless, containment loads are not sensitive to reasonable variations in debris transport to the dome because hydrogen combustion is the dominant contributor to loads.

The fraction of the debris transported through the annular gap between the RPV and the biological shield wall ( $f_{gap}$ ) is calculated in a manner consistent with what has been done previously for Zion and Surry. Specifically, the gap transport fraction is calculated with the equation below:

$$f_{gap} = \frac{A_{gap}}{A_{gap} + A_{cavity}} \quad (C.5)$$

where  $A_{gap}$  = the minimum flow area through the RPV annular gap between the RPV and biological shield wall; this flow area was taken at the nozzles and was reduced by the projected area of the nozzles, but the insulation, neutron shields, and refueling seal rings were not considered, and  $A_{cavity}$  = the minimum flow area out of the cavity through the instrument tunnel.

$A_{gap}$ ,  $A_{cavity}$ , and  $f_{gap}$  for all 41 W PWRs are listed in Table C.5. We have taken nominal credit for flow through the nozzle cutouts in the biological shield wall and nominal credit for knockdown by the missile shield. Specifically, 10 percent of what goes up the gap is assumed to be knocked down by the missile shield or flows out the nozzle cutouts into the steam generator compartments. We base this estimate on woods metal experiments performed at Purdue University (Bertodano, 1993) where nozzle cutouts and the missile shield were simulated. In these experiments, ~17 - 20 percent of the melt going up the gap went through the nozzle cutouts and another ~10 percent was knocked down by the missile shield. However, these tests were performed at 1000 psi and other data indicate a decreasing trend with increasing pressure. Lacking a model, or even a scaling rationale, we take only nominal credit for these processes.

## C.3.2 Debris Transport Through the Lower Compartments

To perform TCE loads calculations for each W plant, we had to assess the fraction of the debris ejected from the instrument tunnel exit that transported through the lower compartments

into the containment dome. Plant drawings from all of the Westinghouse PWRs (41 plants at 25 sites) were reviewed. These drawings were reviewed with several key questions in mind: (1) Are there at least two floors between the cavity exit and the containment upper dome that cause significant trapping in the lower compartment region, as there were in both Zion and Surry? (2) Are there significant direct line-of-sight debris transport pathways from the cavity exit to the containment upper dome? (3) Do the plants look enough like Zion or Surry so that the dome transport fractions used in NUREG/CR-6075 for Zion (Pilch et al., 1994a) or in NUREG/CR-6109 for Surry (Pilch et al., 1995) can be used in the extrapolation calculations? (4) Is there additional information needed about individual plants that will allow us to make an estimate of the dome transport fraction? and (5) Do the utilities make judgments about debris transport to the upper dome in their IPE submittals that are relevant?

After reviewing the IPE drawings of all 41 Westinghouse plants, we were able to categorize the lower compartment geometries into four distinct types: (1) Zion-like (17 plants); (2) Surry-like (15 plants); (3) two-loop plants (6 plants); and (4) others (3 plants). These classifications are shown in Table C.5. The IPEs often provided a short description of dispersal pathways through lower compartment structures. Some of the typical descriptions are included in Section C.3.3.

In Zion geometry, numerous experiments have shown that a small amount of debris dispersed from the cavity through the instrument tunnel (not the annular gap) will enter the upper dome, some through the seal table room and some through vents above the reactor coolant pumps. For the evaluations in this report, we assume 5 percent transport through the seal table room to the upper dome. This subcompartment debris transport fraction is believed to be conservative because the Zion experiments did not model the seal table that blocks access into the seal table room, the "penthouse" over the cavity exit (a steel enclosure with blowout panels intended to deny unauthorized personnel access to the cavity), or the vast array of in-core instrument guide tubes that will be dispersed from the cavity with the debris. These additional structures are expected to significantly reduce debris transport to the dome. Minimal transport to the dome is supported by additional scoping experiments using water (FAI, 1991; Ginsberg and Tutu, 1988). A concrete plug must be displaced from the roof of the seal table room before debris can pass to the upper dome. The concrete plug was simulated in the IET-1,3 experiments (Allen et al., 1994a). The concrete plug was displaced in IET-1 but not in IET-3.

Debris transport through the seal table room to the dome is also expected in Surry geometry, but the database is limited to only three experiments: SNL IET-9, 10, and 11 (Blanchat et al., 1994). The seal table (which was simulated in two of the experiments) failed in IET-10, allowing transport through the seal table room to the dome. The seal table, however, remained intact in IET-11, partially blocking transport through the seal table room. An important difference in the tests is that the annular gap around the RPV (which exists in the plant) was modeled in IET-11 but not in IET-10. For the evaluations in this report, we assume 5 percent transport through the seal table room to the upper dome. Such treatment, however, is deemed conservative because the Surry experiments did not model the steel hatch (which restricts personnel access to the cavity), because the seal table may not fail, because the experiments did not model the vast array of in-core instrument guide tubes that will be dispersed from the cavity with the debris, and because concrete plugs in the roof of the seal table room were not modeled.



## Plant Geometry

For all of the plants that are Zion or Surry-like, a transport fraction from the cavity exit to the upper dome ( $f_{sub}$ ) of 0.05 will be used in the extrapolation calculations, which is consistent with NUREG/CR-6075 for Zion and NUREG/CR-6109 for Surry. In all of these plants, there are at least two floors between the cavity exit and the upper dome (usually the seal table room floor and ceiling, which is the operating deck level) and there are no significant direct line-of-sight debris transport pathways to the upper dome.

The two-loop plants (Ginna, Kewaunee, Point Beach 1 & 2, and Prairie Island 1 & 2) have two floors between the cavity exit and the upper dome: the seal table room floor and the operating deck floor. However, these plants do have direct line-of-sight debris transport pathways from the instrument tunnel exit to the containment dome. For this reason, the subcompartment debris transport fraction ( $f_{sub}$ ), which were determined from experiments and used for all Zion-like and Surry-like plants, cannot be used for two-loop plants.

There are three plants (H.B. Robinson and South Texas 1&2) that are marked as "other" in Table C.5. These plants do not look either like Zion or Surry and do not appear to meet the criteria for using the debris transport fractions used for Zion in NUREG/CR-6075 and for Surry in NUREG/CR-6109. The H.B. Robinson plant has two floors but has significant direct line-of-sight debris transport pathways to the upper dome and will be treated using the same approach as used for two-loop plants. South Texas 1&2 also are sufficiently different from both Zion and Surry that a separate evaluation must be performed. In South Texas 1&2, the instrument guide tubes are sealed by 2 feet of concrete and the only debris transport pathway out of the cavity besides the RPV annular gap is through a tortuous manway into the lower compartments. There is no vertical debris transport pathway from the cavity except through the annular gap between the RPV and biological shield wall, so for South Texas 1&2 the fraction of debris that can be transported through the lower compartments is assumed to be zero.

For plants with direct line-of-sight debris transport pathways from the instrument tunnel exit to the containment dome, the subcompartment debris transport fraction ( $f_{sub}$ ) will be calculated with a simple area ratio model that is tied to the Surry database, specifically SNL IET-10. In Surry, the area of the seal table room opening ( $A_{str}$ ) over the area of the instrument tunnel exit ( $A_{cav\ exit}$ ) is 0.28, and in IET-10, the fraction of the debris that was ejected from the cavity exit that entered the seal table room was about 0.28. Thus, debris ejected at an opening will go through that opening, and transport through openings can be calculated with simple area ratios. The exception to this rule is if the cavity exit is much larger than the seal table room opening and the seal table room opening is directly above the half of the cavity furthest from the RPV. DCH experiments show that almost all of the debris is entrained out of the instrument tunnel along the wall furthest away from the reactor pressure vessel. In some plants with very large cavity exit areas, virtually all of the debris would be ejected from the half of the opening furthest away from the RPV. Furthermore, if area ratios are greater than 1, the fraction is set to 1 since more than 100 percent of the debris cannot be ejected through an opening. The simple model for the subcompartment debris transport fraction ( $f_{sub}$ ) is



$$f_{sub} = \min \left\{ \frac{A_{str}}{\frac{1}{2} A_{cav\ exit}} ; 1 \right\} \min \left\{ \frac{A_{op\ deck}}{A_{str}} ; 1 \right\} - 0.05 \quad (C.6)$$

where

- $A_{str}$  = the area of the seal table room opening,  
 $A_{cav\ exit}$  = the area of the instrument tunnel (cavity) exit, and  
 $A_{op\ deck}$  = the area of the opening in the operating deck that is directly above the seal table.

In Equation C.6, nominal credit (0.05) is taken for the last array of equipment and structures that could impede flow into or out of the seal table room. These include: steel hatches or "penthouses" which restrict personnel access to the cavity, partial failure or nonfailure of the seal table, the array of in-core instrument guide tubes and their support structures that will be dispersed from the cavity with the debris, and equipment in the seal table room.

Two-loop plants and H.B. Robinson 2 have an opening in the seal table room and in the operating deck directly above the cavity exit. The subcompartment debris transport fraction ( $f_{sub}$ ) is calculated with Equation C.6 for these plants and is listed in Table C.5. We were unable to obtain opening dimensions for Ginna, Kewaunee, and Prairie Island 1 & 2, and thus we are using  $f_{sub} = 0.40$  until we get the dimensions from the utilities.

Dome transport is the sum of contributions through the annular gap and through the lower compartment structures, which is given by the equation below.

$$f_{dome} = f_{gap} (1 - f_{noz/shld}) + f_{sub} (1 - f_{gap}) \quad (C.7)$$

The values of these fractions are listed in Table C.5 for all of the W PWRs. The dome transport fraction ( $f_{dome}$ ) is used directly in the TCE model to calculate the DCH load for all W plants.

### C.3.3 IPE Descriptions of Debris Transport Through the Lower Compartments

After reviewing the IPEs from all 25 sites having Westinghouse plants, we characterized debris transport through the lower compartments as belonging to one of the four following groups: (1) Zion-like, (2) Surry-like, (3) two-loop plants, and (4) other. Our justification for assigning each plant to one of these groups is given below. In addition, the IPEs submitted by the utilities often contain brief descriptions of their assessments of debris transport through the lower compartments. Their descriptions are included here for each of the plants.

## Plant Geometry

### Beaver Valley 1 & 2

The lower compartment region of Beaver Valley 1 & 2 is essentially identical to Surry and, therefore, the subcompartment transport fraction ( $f_{sub}$ ) used for Surry in NUREG/CR-6109 (Pilch et al., 1995) will also be used for Beaver Valley. We did not have a copy of the Beaver Valley IPE.

### Braidwood 1 & 2

The lower compartment region of Braidwood 1 & 2 is essentially identical to Zion and, therefore, the subcompartment transport fraction ( $f_{sub}$ ) used for Zion in NUREG/CR-6075, Supplement 1 (Pilch et al., 1994b), will also be used for Braidwood. The IPE states that a removable, leak-tight hatch cover is located at the exit of the instrument tunnel; however, the instrument tunnel exit cover is not expected to significantly affect gas and core debris flow from the cavity if the reactor vessel fails at high pressure. The seal table configuration is an important feature of the Braidwood containment. The seal table configuration is expected to effectively remove core debris entrained by gas flowing from the cavity following a high pressure vessel blowdown.

### Byron 1 & 2

The lower compartment region of Byron 1 & 2 is essentially identical to Zion and, therefore, the subcompartment transport fraction ( $f_{sub}$ ) used for Zion in NUREG/CR-6075, Supplement 1, will also be used for Byron. The Byron IPE states that the exit of the instrument tunnel is closed by a removable cover. Although the instrument tunnel exit cover is not expected to significantly affect gas and core debris flow from the cavity if the reactor vessel fails at high pressure, the seal table configuration is an important feature of the Byron containment. The seal table configuration is expected to effectively remove core debris entrained by gas flowing from the cavity following a high pressure vessel blowdown.

### Callaway

The Callaway NPP is similar to Surry with multiple floors and no direct line-of-sight debris transport pathway to the containment dome. The subcompartment transport fraction ( $f_{sub}$ ) used for Surry will also be used for Callaway. The Callaway IPE states that the transport of core debris through the reactor vessel annulus is hindered by the presence of a permanent, welded neutron shield/reactor cavity seal ring. There is only a 2 inch annular gap between the reactor vessel flange and the seal ring. Even if the seal ring were to be removed by the dynamic forces following vessel failure, a larger flow area would be available through the instrument tunnel than through the annulus around the vessel.

### Comanche Peak 1 & 2

Comanche Peak 1 & 2 are Zion-like with multiple floor levels and no direct line-of-sight to the containment dome. The subcompartment transport fraction ( $f_{sub}$ ) used for Zion will also be used

for Comanche Peak. The IPE states that there is an always open but tortuous path through the containment lower compartment, which makes direct containment heating (DCH) difficult because the obstacles would cause most of the debris to be de-entrained from the blowdown gases.

#### Diablo Canyon 1 & 2

Diablo Canyon 1 & 2 are similar to Zion except for a vertical access hatch between the cavity and the containment basement floor. The subcompartment transport fraction ( $f_{sub}$ ) used for Zion will also be used for Diablo Canyon. The IPE states that the clearance around the reactor vessel is the only significant flow path between the reactor cavity and the main containment volume, which is normally unobstructed. Less significant flow paths exist under and around the reactor coolant drain tank (RCDT) room door, through the dampers and around the concrete covers. All other potentially significant pathways would require the forceful removal of a barrier, such as a damper, ventilation ducting, a door, or an access hatch cover.

#### Farley 1 & 2

The lower compartment design in Farley 1 & 2 is similar to the configuration in Surry. The subcompartment transport fraction ( $f_{sub}$ ) used for Surry will also be used for Farley. A large opening (approximately 63 ft<sup>2</sup>) at the top of the instrument tunnel provides communication between the instrument tunnel and the lower compartments. The IPE states that the seal table configuration is an important feature of the Farley NPP containment because it provides an effective structural barrier to debris entrainment from the cavity following a high-pressure vessel blowdown.

#### Ginna

Ginna is a two-loop plant that appears to have no line-of-sight debris transport pathways to the containment dome, and thus, we have assumed that the subcompartment debris transport fraction ( $f_{sub}$ ) is zero. The Ginna IPE states that at the outer end of the instrument tunnel the instrument tubes are directed vertically upward and exit through the ceiling of the cavity. The ceiling of the cavity tunnel includes an opening above the cavity sump (covered by a removable metal plate) and an opening for air ducting. The combined area of these two openings is 21.3 ft<sup>2</sup>. This is a likely pathway for debris (and water and gases) to be expelled from the cavity under high reactor vessel pressure failure conditions. Two other possible pathways for debris to be dispersed from the cavity involve transport through the annulus between the reactor vessel and biological shield to enter the refueling pool or to the main coolant piping penetrations through the biological shield wall.

#### H.B. Robinson

H.B. Robinson is classified as an "other" in Table C.5 because there are significant direct line-of-sight debris transport pathways from the cavity to the containment dome. The IPE states that for sequences in which debris is dispersed from the cavity tunnel and into the area of reactor

## Plant Geometry

coolant pump "B" bay, there is the possibility that debris can flow (or be expelled) through the 6 drain holes at the bottom of the crane wall, enter the annular compartment, and then directly contact the liner. The drain holes are each 2 ft. square.

### Indian Point 2 & 3

The lower compartment configuration in Indian Point 2 & 3 looks similar to Zion. There are two floors, the seal table room floor and the operating deck, and there are no direct line-of-sight debris transport pathways from the reactor cavity to the containment dome. Therefore, the subcompartment debris transport fraction ( $f_{sub}$ ) for Zion will also be used for Indian Point.

### Kewaunee

Kewaunee is a two-loop design that has major direct line-of-sight debris transport pathways to the containment dome. The instrument tunnel exit is a 5'6" diameter pipe leading to the seal table, which is not enclosed in a room but is open to the entire containment. The IPE states that the geometry of the cavity and structures at the exit of the seal table are important features of the Kewaunee containment because they act to limit the extent of debris dispersed from the cavity following a high-pressure melt ejection (HPME); however, based on their plant drawings, we could only take marginal credit for the seal table and other structures because they would be removed by high pressures or ablation by molten debris. The subcompartment debris transport fraction ( $f_{sub}$ ) for Kewaunee is assumed to be 0.95.

### Millstone 3

The lower compartment configuration in Millstone 3 is similar to Surry. There are two floors between the instrument tunnel exit and the containment dome region: the seal table room floor and the operating deck. There are no direct line-of-sight debris transport pathways in Millstone 3. Furthermore, there do not appear to be large access openings between the seal table room and the operating deck. As a result, we conservatively chose the subcompartment debris transport fraction ( $f_{sub}$ ) to be the same as used for Surry.

### North Anna 1 & 2

The lower compartment configuration in North Anna 1 & 2 is very similar to Surry. We use the same subcompartment debris transport fraction ( $f_{sub}$ ) to the dome as was used for Surry, which was based on 1/6<sup>th</sup> and 1/10<sup>th</sup> scale experiments performed with Surry structures. The North Anna IPE explains that the outer end of the instrument tunnel away from the reactor vessel is not sloped as in some designs (e.g., Zion). This should result in a geometry somewhat less favorable for debris dispersion out of the cavity following vessel failure. At the outer end of the instrument tunnel the instrument tubes are directed vertically upward through a "cofferdam" raised above the adjacent tunnel ceiling penetrating the seal table into the residual heat pump and heat exchanger region. This is a likely pathway for debris (and water and gases) to be expelled from the cavity under high reactor vessel pressure failure conditions. Other pathways for debris to be expelled from the cavity include an approximate 9 ft<sup>2</sup> vertical ventilation duct on the roof of the instrument



tunnel and an approximate 2 ft<sup>2</sup> horizontal ventilation duct at the 231 ft elevation through the cylindrical portion of the reactor cavity wall. Two other possible pathways for debris to be dispersed from the cavity involve transport through the annulus between the reactor vessel and biological shield to either the refueling pool or to the main coolant pipe penetrations through the biological shield wall.

The North Anna IPE states that transport of material through the reactor vessel annulus is hindered by the presence of the massive neutron shield tanks which occupy most of the volume within the region between the reactor vessel and shield wall. In the remaining 6.5 in. gap between the reactor vessel and neutron shield tank is 3.0 in. of insulation. There is approximately 20 ft<sup>2</sup> of flow area around the reactor coolant piping penetrations in the shield wall. Stone and Webster and Argonne National Laboratory have reviewed the Surry cavity design and judge that the Benelux shield cans above the vessel nozzles would very likely be crushed and impacted against the water seal ring at the top of the vessel-shield wall annulus (by the high pressure expulsion of gases, from the reactor vessel accelerating debris/water up the annulus) closing off the flow pathway for debris to the refueling pool region in the upper containment. Similar phenomena would occur at North Anna since the configuration is similar at both plants.

#### Point Beach 1 & 2

Point Beach 1 & 2 are two-loop plants that are sufficiently different from Zion and Surry that an independent assessment of the dome transport fraction had to be performed. Fortunately, there were good drawings of the cavity and lower compartments in the Point Beach IPE. In addition, we contacted representatives of the Point Beach NPP directly to obtain additional information. There are two floors between the cavity and the containment dome region that will trap debris in the lower compartments: the seal table room floor (with a 10' x 10' opening) and the operating deck above the seal table room (with a 6'5<sup>1</sup>/<sub>4</sub>" x 6'5<sup>1</sup>/<sub>4</sub>" opening). These openings are both directly above the exit of the instrument tunnel and therefore represent a direct line-of-sight debris transport pathway to the containment upper dome. For this reason, Point Beach cannot be treated like Zion or Surry. We have performed an independent assessment of debris transport to the dome region based on our understanding of the Point Beach geometry and the relevant experimental data. For the Point Beach configuration, the subcompartment debris transport fraction was determined using the methodology described in Section C.3.2 to be 0.41. The Point Beach IPE states that the geometry of the cavity and structures at the exit of the seal table are important features of the Point Beach NPP containment because they act to limit the extent of debris dispersed from the cavity following a High Pressure Melt Ejection (HPME).

#### Prairie Island 1 & 2

Prairie Island 1 & 2 are two-loop plants that appear to be similar to Kewaunee. The instrument tunnel exit is a 6'6" diameter pipe that leads to the seal table, which is not enclosed in a room but is open to the containment atmosphere. The Prairie Island IPE states that the geometry of the cavity and instrument tunnel, structures at the exit of the seal table, and openings in the instrument tunnel are important features of the Prairie Island containment because they act to limit the extent of debris dispersed from the cavity following a high pressure melt ejection (HPME).



## Plant Geometry

Since the seal table and other steel structures would be removed rapidly by high pressure or ablation by molten debris, we only took marginal credit for these structures. The subcompartment debris transport fraction for Prairie Island 1 & 2 is assumed to be 0.95.

### Salem 1 & 2

The lower compartment configuration of Salem 1 & 2 is similar to Zion. We have chosen to use the same subcompartment debris transport fraction ( $f_{sub}$ ) for Salem 1 & 2 that was used for Zion. The IPE provided the following two paragraphs on debris transport out of the cavity to the containment dome region.

One possible flow path from the reactor cavity is up around the 4.6-inch radial gap between the reactor vessel insulation and the cylindrical concrete shield wall surrounding the vessel. Flow going in this direction would split, part going out the openings around the hot and cold leg insulation (a 3.25-inch radial gap), which flows into the lower compartment, and the remaining continuing upward around the vessel flange into the upper compartment.

The minimum flow area going up the instrument tunnel and out the instrument room is about 21 ft<sup>2</sup>. The flow area around the lower part of the reactor vessel is about 20 ft<sup>2</sup>. Since these flow areas are nearly equal, if there were no other considerations, we would expect the core debris to split almost equally between these two paths (with the flow around the vessel then splitting again as mentioned above). However, we assume that all of the molten debris leaving the cavity in a high pressure melt ejection would exit via the instrument tunnel path and out into the containment annulus. If molten debris were to exit the bottom of the reactor vessel at a high velocity, to leave the cavity via around the reactor vessel, the debris would have to make a complete 180° turn after impacting the cavity floor. For the debris to exit the cavity up the instrument tunnel, the debris must make a 90° turn after impacting the cavity floor, and then a 45° turn as it reaches the tunnel. We believe that this geometric configuration of the cavity strongly favors the instrument tunnel path. To further argue against the flow path around the reactor vessel, we believe that there is a high likelihood that the vessel insulation could be stripped off the vessel, perhaps restricting this flow path.

### Seabrook

The lower compartment configuration for the Seabrook NPP is similar to Zion. After reviewing the IPE drawings, our assessment is that the subcompartment debris transport fractions ( $f_{sub}$ ) used for Zion in NUREG/CR-6075 (Pilch et al., 1994a), which were based on an extensive database, also apply to the Seabrook plant. The Seabrook IPE has some discussion of DCH and rules out DCH as a threat at Seabrook. It states that the impact of a DCH event at Seabrook is mitigated by the cavity opening arrangement which does not easily permit the debris to be dispersed above the lower compartment level. The PORV study evaluated the pressure increase resulting from a DCH event and found the peak pressure to be within the capacity of the containment. This event is precluded if the RPV pressure at vessel failure is low, the operator depressurizes using the PORV (DP=S), or the hot leg fails (HL=S).

### Shearon Harris

The Shearon Harris NPP has a lower compartment configuration similar to Surry. It has two floors over the instrument tunnel exit: the seal table room floor and the operating deck floor. There do not appear to be any direct line-of-sight debris transport pathways to the containment dome. In addition, Shearon Harris appears to have a substantial missile shield that would probably trap significant amounts of debris, dispersed through the annular gap, in the refueling canal. Our assessment is that the subcompartment debris transport fraction ( $f_{sub}$ ) for the Shearon Harris NPP would be the same as for Surry. The IPE has a brief description about debris transport in the lower compartments. It states that for sequences in which debris is dispersed from the cavity tunnel and into the area surrounding the mouth of the cavity, there is the possibility that debris can flow (or be expelled) through the drain holes at the bottom of the secondary shield wall, enter the annular compartment, and then directly contact the containment liner. The drain holes are each 2.25 ft square.

### South Texas 1 & 2

The lower compartment structures in South Texas 1 & 2 do not look like those in Zion, Surry, or any other plant that we have reviewed. A plan view of the reactor cavity and lower compartments is shown in Figure C.3. The instrument guide tubes are sealed in 2 feet of concrete in the instrument tunnel; this obstruction would block debris transport through the instrument tunnel. There is an access labyrinth that has two openings to the lower compartments: a ventilation duct and a personnel access hatch. In a HPME accident, debris could be ejected from these two openings ( $A_{cav} = 2.97\text{m}^2$ ) but it would be ejected horizontally and would not reach the containment dome region. Debris dispersed from the cavity through this pathway would not be actively involved in heating the containment atmosphere, and thus, we assumed  $f_{sub} = 0$  for South Texas 1 & 2. We also concluded that the only debris transport pathway from the cavity directly to the containment dome was through the RPV annular gap ( $A_{gap} = 0.65\text{m}^2$ ), and therefore, the fraction of debris transported through the gap ( $f_{gap}$ ) was calculated from equation C.5 to be 0.18. Of the 92% of the molten debris that is assumed to be dispersed from the cavity, area ratios indicate that most would be dispersed into the lower compartments and only 18% would be transported to the dome where it would participate in the DCH event.

The IPE compares the South Texas Plant (STP) to Zion. It states that one notable difference between the STP and Zion containments is the layout of the reactor cavity and containment floor. Like Zion, STP has a cavity ventilation flowpath up around the reactor vessel and primary coolant pipes to the steam generator compartment. However, the flowpaths to the lower part of the cavity are different. Zion has a sunken cavity connected to the lower compartment by an instrument tunnel, which provides a rather direct pathway to the lower and upper compartments. On the other hand, in STP the bottom of the cavity is on the same level as the remainder of the containment building floor. STP does not have an instrument "tunnel"; rather the instrument tubes go through individual penetrations in a 2 ft thick concrete wall to the in-core instrument room, which is adjacent to the cavity and on the same level. In place of a tunnel, STP does have pathways between the cavity and lower compartment. There are connecting floor drains and there

## Plant Geometry

is an access labyrinth leading to an opening or keyway in the primary shield wall, containing both a ventilation duct and a personnel door.

### Summer

The lower compartment configuration of the Summer NPP is similar to Surry. There appear to be three floors that will obstruct vertical debris transport to the containment dome region: a floor at the instrument tunnel exit, the seal table room floor, and the operating deck floor. Furthermore, there are no direct line-of-sight debris transport pathways through the lower compartments. Our assessment is that debris transport from the cavity to the dome would be less in Summer than in Surry, but we will conservatively use the Surry value for  $f_{sub}$  in the containment loads evaluations performed with the TCE model.

### Surry 1 & 2

We have extensively reviewed drawings of the Surry lower compartments and have walked through the plant. Surry has two floors over the exit of the instrument tunnel that trap debris in the lower compartments: the seal table room floor and the operating deck floor. Debris trapping in the lower compartments is a major mitigation feature in all W plants. The SNL IET experiments performed in the Surry geometry (IET-9, 10, 11, and 12) showed that significant amounts of debris was knocked down by the bottom of the seal table room floor into the residual heat removal heat exchanger platform area and the containment basement. Much of the debris that entered the seal table room was trapped there. A small amount of debris (5 percent) flowed through the subcompartments and reached the containment dome region. Plants that appear to have Surry-like lower compartment features will be assigned the same subcompartment transport fraction ( $f_{sub}$ ) as Surry for the TCE loads evaluations.

### Turkey Point 3 & 4

The lower compartment configuration of Turkey Point 3 & 4 is similar to Surry. Turkey Point has two floors over the instrument tunnel exit that would obstruct debris transport to the containment dome region: the seal table room floor and the operating deck floor. There is a small direct line-of-sight penetration in the operating deck floor directly above the seal table. There is a 24-inch polyethylene port for pulling the in-core instrument tubes. Our assessment is that Turkey Point is sufficiently like Surry such that the same subcompartment debris transport fraction ( $f_{sub}$ ) through the lower compartments can be used in the TCE loads evaluations.

### Vogtle 1 & 2

The lower compartment configuration of Vogtle 1 & 2 is similar to Zion. Vogtle has two floors between the instrument tunnel exit and the containment dome region that obstruct debris transport to the dome: the seal table room floor and the operating deck floor. There do not appear to be any direct line-of-sight debris transport pathways to the dome. Our assessment is that the lower compartments are sufficiently like Zion so that the same subcompartment debris transport fraction ( $f_{sub}$ ) can be used. The IPE has some description about debris transport through

the lower compartments. It states that the instrument tunnel extends upward from the cavity floor to the ceiling of the seal table enclosure. Near the top of the instrument tunnel, a concrete platform extends nearly halfway across the seal table enclosure. The area above this platform is open to the annular compartment. The seal table configuration is an important feature of the Vogtle containment because it provides an effective structural barrier to debris entrainment from the cavity following a high-pressure vessel blowdown.

### Wolf Creek

Wolf Creek Generating Station (WCGS) has a similar lower compartment configuration to Surry. It has at least two floors between the instrument tunnel exit and the containment dome region. These floors, the seal table room floor and the operating deck floor, are a major obstruction to debris transport to the dome. Furthermore, there are no direct line-of-sight debris transport pathways to the dome and there are substantial other structures in the potential debris flight path that will obstruct debris transport to the dome. Our assessment is that Wolf Creek is enough like Surry that the subcompartment debris transport fraction ( $f_{sub}$ ) can be used. The Wolf Creek IPE states that the seal table configuration is an important feature of the WCGS containment because it provides an effective structural barrier to debris entrainment from the cavity following a high-pressure vessel blowdown.

### Zion 1 & 2

We have extensively reviewed drawings of the Zion lower compartments and have walked through the plant. Zion has two floors over the exit of the instrument tunnel that trap debris in the lower compartments: the seal table room floor and the operating deck floor. Debris trapping in the lower compartments is a major mitigation feature in all W plants. The SNL IET experiments performed in the Zion geometry (Allen et al., 1994a) showed that significant amounts of debris was knocked down by the bottom of the seal table room floor into the containment basement. Much of the debris that entered the seal table room was trapped there. A small amount of debris (5 percent) flowed through the subcompartments and reached the containment dome region. Plants that appear to have Zion-like lower compartment features will be assigned the same subcompartment debris transport fraction ( $f_{sub}$ ) as Zion for the TCE loads evaluations.

## **C.4 References**

Allen, M.D. et al. (1990). *A Demonstration Experiment of Steam-Driven, High-Pressure Melt Ejection: The HIPS-10S Test*, NUREG/CR-5373, SAND89-1135, Sandia National Laboratories, Albuquerque, NM.

Allen, M.D. et al. (1991). *Experiments to Investigate the Effect of Flight Path on Direct Containment Heating (DCH) in the Surtsey Test Facility: The Limited Flight Path (LFP) Tests*, NUREG/CR-5728, SAND91-1105, Sandia National Laboratories, Albuquerque, NM.



## Plant Geometry

Allen, M.D. et al. (1992a). *Experiments to Investigate the Effect of Water in the Cavity on Direct Containment Heating (DCH) in the Surtsey Test Facility - The WC-1 and WC-2 Tests*, SAND91-1173, Sandia National Laboratories, Albuquerque, NM.

Allen, M.D. et al. (1992b). *Experimental Results of Tests to Investigate the Effects of Hole Diameter Resulting from Bottom Head Failure on Direct Containment Heating (DCH) in the Surtsey Test Facility - The WC-1 and WC-3 Tests*, SAND91-2153, Sandia National Laboratories, Albuquerque, NM.

Allen, M.D. et al. (1992c). *Experiments to Investigate the Effects of 1:10 Scale Zion Structures on Direct Containment Heating (DCH) in the Surtsey Test Facility: The IET-1 and IET-1R Tests*, SAND92-0255, Sandia National Laboratories, Albuquerque, NM.

Allen, M.D. et al. (1992d). *The Third Integral Effects Test (IET-3) in the Surtsey Test Facility*, SAND92-0166, Sandia National Laboratories, Albuquerque, NM.

Allen, M.D. et al. (1992e). *The Effects of Condensate Levels of Water on Direct Containment Heating (DCH) in Zion-Like Geometry: The Fourth Integral Effects Test (IET-4) Conducted in the Surtsey Test Facility*, SAND92-1241, Sandia National Laboratories, Albuquerque, NM.

Allen, M.D. et al. (1992f). *Experimental Results of an Integral Effects Test in a Zion-Like Geometry to Investigate the Effects of a Classically Inert Atmosphere on Direct Containment Heating: The IET-5 Experiment*, SAND92-1623, Sandia National Laboratories, Albuquerque, NM.

Allen, M.D. et al. (1992g). *An Integral Effects Test in a Zion-Like Geometry to Investigate the Effects of Preexisting Hydrogen on Direct Containment Heating in the Surtsey Test Facility - The IET-6 Experiment*, SAND92-1802, Sandia National Laboratories, Albuquerque, NM.

Allen, M.D. et al. (1992h). *An Integral Effects Test to Investigate the Effects of Condensate Levels of Water and Preexisting Hydrogen on Direct Containment Heating in the Surtsey Test Facility - The IET-7 Experiment*, SAND92-2021, Sandia National Laboratories, Albuquerque, NM.

Allen, M.D. et al. (1993). *Experiments to Investigate the Effects of Fuel/Coolant Interactions on Direct Containment Heating: The IET-8A and IET-8B Experiments*, SAND92-2849, Sandia National Laboratories, Albuquerque, NM.

Allen, M.D. et al. (1994a). *Experimental Results of Integral Effects Tests with Zion-Like Structures to Investigate Direct Containment Heating*, NUREG/CR-6044, SAND93-1049, Sandia National Laboratories, Albuquerque, NM.

Allen, M.D. et al. (1994b). *Test Results on Direct Containment Heating by High-Pressure Melt Ejection into the Surtsey Vessel: The TDS Test Series*, SAND91-1208, Sandia National Laboratories, Albuquerque, NM.



- Bertodano, M. Lopez de (1993). *Direct Containment Heating DCH Source Term Experiment for Annular Reactor Cavity Geometry*, Ninth Proceedings of Nuclear Thermal Hydraulics, 1993 ANS Winter Mtg., Nov. 14-18, 1993, San Francisco, CA, p. 111-120.
- Binder, J.L. et al. (1992a). *Quick Look Data Report on the Integral Effects Test IR in the Corexit Facility at Argonne National Laboratory*, draft for review, Argonne National Laboratory, Argonne, IL.
- Binder, J.L. et al. (1992b). *Quick Look Data Report on the Integral Effects Test IRR in the Corexit Facility at Argonne National Laboratory*, draft for review, Argonne National Laboratory, Argonne, IL.
- Binder, J.L. et al. (1992c). *Quick Look Data Report on the Integral Effects Test-3 in the Corexit Facility at Argonne National Laboratory*, draft for review, Argonne National Laboratory, Argonne, IL.
- Binder, J.L. et al. (1992d). *Quick Look Data Report on the Integral Effects Test-6 in the Corexit Facility at Argonne National Laboratory*, draft for review, Argonne National Laboratory, Argonne, IL.
- Binder, J.L. et al. (1992e). *Quick Look Data Report on the Integral Effects Test-7 in the Corexit Facility at Argonne National Laboratory*, draft for review, Argonne National Laboratory, Argonne, IL.
- Binder, J.L. et al. (1992f). *Quick Look Data Report on the Integral Effects Test-8 in the Corexit Facility at Argonne National Laboratory*, draft for review, Argonne National Laboratory, Argonne, IL.
- Binder, J.L. et al. (1994). *Direct Containment Heating Integral Effects Tests at 1/40 Scale in Zion Nuclear Power Plant Geometry*, NUREG/CR-6168, ANL-94/18, Argonne National Laboratory, Argonne, IL.
- Blanchat, T.K. et al. (1994). *Experiments to Investigate Direct Containment Heating Phenomena with Scaled Models of the Surry Nuclear Power Plant*, NUREG/CR-6152, SAND93-2519, Sandia National Laboratories, Albuquerque, NM.
- Blomquist, C.A. et al. (1985). "Data Report for Corium/Water Thermal Interaction Test CWTI-13," Argonne National Laboratory, Argonne, IL.
- Blomquist, C.A. et al. (1986). "Data Report for Corium/Water Thermal Interaction Test CWTI-14," Argonne National Laboratory, Argonne, IL.
- Chun, M.H. et al. (1991). "A Parametric Study of the High Pressure Melt Ejection from Two Different Scale Reactor Cavity Models," *Int. Con. Heat Mass Trans.*, Vol. 18, pp. 619-628.

FAI (1991). *Zion IPE Position Paper on Direct Containment Heating*, FAI/91-18, submitted to Commonwealth Edison Co., Chicago, IL.

Ginsberg, T. and N.K. Tutu (1987). *Safety Research Programs Sponsored by Office of Nuclear Regulatory Commission*, Quarterly Progress Report, NUREG/CR-2331, Vol. 7, No. 2.

Ginsberg, T. and N.K. Tutu (1988). "Progress in Understanding Direct Containment Heating Phenomena in Pressurized Light Water Reactors," *Third International Topical Meeting on Nuclear Power Plant Thermal Hydraulics and Operations*, Seoul, Korea.

Henry, R.E. (1989). "Evaluation of Fission Product Release Rates During Debris Dispersal," PSA 1989, *Proc. of the ANS/ENS International Topical Meeting: Probability Reliability and Safety Assessment*, p. 375-383.

Henry, R.E. et al. (1991). "Direct Containment Heating Experiments in a Zion-like Geometry," in *26th National Heat Transfer Conference*, Vol. 87.

IDCOR (1985). *Technical Support for Issue Resolution*, IDCOR, Technical Report 85.2, Fauske and Associates, Inc., Burr Ridge, IL.

Ishii, M. and K. Mishima (1989). "Droplet Entrainment Correlation in Annular Two-Phase Flow," *Int. J. Heat Mass Transfer*, Vol. 32, No. 10, pp. 1835-1846.

Ishii, M. et al. (1993). *Separate Effects Experiments on Phenomena of Direct Containment Heating - Air-Water Simulation Experiments in Zion Geometry*, PU NE-93/1, Purdue University, West Lafayette, IN.

Kataoka, I. and M. Ishii (1982). *Mechanism and Correlation of Droplet Entrainment and Deposition in Annular Two-Phase Flow*, NUREG/CR-2885, ANL-82-44, Argonne National Laboratories, Argonne, IL.

Kim, M. et al. (1992). "Experimental Study on Direct Containment Heating Phenomena," in *ANS Winter Meeting*, Chicago, IL.

Levy, S. (1991). "Debris Dispersal From Reactor Cavity During Low Temperature Simulant Tests of Direct Containment Heating. Part I: Tests with Constant Gas Flow Rates; Part II: Tests with Blowdown Gas Conditions," *Proceedings of National Heat Transfer Conference*, Minneapolis, MN.

MacBeth, R.W., and R. Trenberth (1987). *Experimental Modeling of Core Debris Dispersion from the Vault Under a PWR Pressure Vessel - Part 1. "Preliminary Experimental Results,"* AEEW-R1888, UK Atomic Energy Authority, AEE Winfrith, UK.

- MacBeth, R.W. et al. (1988). *Experimental Modeling of Core Debris Dispersion from the Vault Under PWR Pressure Vessel - Part 3*. "Results of Varying the Size Scaling Factor of the Model Use," AEEW-R2426, UK Atomic Energy Authority, AEE Winfrith, UK.
- Pilch, M.M. et al. (1994a). *The Probability of Containment Failure by Direct Containment Heating in Zion*, NUREG/CR-6075, SAND93-1535, Sandia National Laboratories, Albuquerque, NM.
- Pilch, M.M. et al. (1994b). *The Probability of Containment Failure by Direct Containment Heating in Zion*, NUREG/CR-6075, Supplement 1, Sandia National Laboratories, Albuquerque, NM.
- Pilch, M.M. et al. (1995). *The Probability of Containment Failure by Direct Containment Heating in Surry*, SAND93-2078, NUREG/CR-6109, Sandia National Laboratories, Albuquerque, NM.
- Rose, P.W. (1987). *Experimental Modeling of Core Debris Dispersion from the Vault Under a PWR Pressure Vessel - Part 2*. Results of Including the Instrument Tubes Support Structure in the Experiment, AEEW-R2143, UK Atomic Energy Authority, AEE Winfrith, UK.
- Sienicki, J.J. and B.W. Spencer (1986). Corium Droplet Size in Direct Containment Heating," *Transactions of the ANS*, TANSO 53, pp. 557-558.
- Spencer, B.W. et al. (1982). *Sweepout Thresholds in Reactor Cavity Interactions*, ANL/LWR/SAF 82-1, Argonne National Laboratory, Argonne, IL.
- Spencer, B.W. et al. (1983). *Hydrodynamics Aspects of Ex-Vessel Debris Dispersal in Zion-Type Containment Design*, ANL/LWR/SAF 83-1, Argonne National Laboratory, Argonne, IL.
- Tarbell, W.W. et al. (1987). *Results from the DCH-1 Experiment*, NUREG/CR-4871, SAND86-2483, Sandia National Laboratories, Albuquerque, NM.
- Tutu, N.K. et al. (1988a). *Debris Dispersal from Reactor Cavities During High Pressure Melt Ejection Accident Scenarios*, NUREG/CR-5146, BNL-NUREG-52147, Brookhaven National Laboratory, Upton, NY.
- Tutu, N.K. et al. (1988b). "Low Pressure Cutoff for Melt Dispersal from Reactor Cavities," *Fourth Proc. of Nuclear Thermal Hydraulics*, 29-37.
- Tutu, N.K. (1990). *Melt Dispersal Characteristics of the Watts Bar Cavity*, Technical Report A-3024, Brookhaven National Laboratory, Upton, NY.
- Tutu, N.K., and T. Ginsberg (1990). "The Results of Melt Dispersal Experiments with Surry and Zion Cavity Models," Letter Report, Brookhaven National Laboratory, NY.

Williams, D.C. and D.L.Y. Louie (1988). "CONTAIN Analyses of Direct Containment Heating Events in the Surry Plant," *Proceedings of the ANS/ENS Winter Meeting*, Thermal Hydraulics Division, Washington, DC.

Yan, H. and T.G. Theofanous (1993). "The Prediction of Direct Containment Heating," *ANS Proceedings*, 1993 National Heat Transfer Conference, Atlanta, GA, p. 294-309.

Zhang, G.J. et al. (1994). "Simulation Experiment on Corium Dispersion in Direct Containment Heating Using Air-Water and Air-Woods Metal," *Tenth Proceedings of Nuclear Thermal Hydraulics*, 1994 ANS Winter Meeting. Washington, DC.

Zhang, G.J. and M. Ishii (1995). "Entrance Effect on Droplet Entrainment in DCH," *ANS Proceedings*, 1995 National Heat Transfer Conference, Portland, OR.

ZPSS (1981). *Zion Probabilistic Safety Study*, Commonwealth Edison Co., Chicago, IL.

### C.5 Nomenclature

$A_{cav\ exit}$	=	area of instrument tunnel exit
$A_{cavity}$	=	minimum flow area through the reactor cavity
$A_{gap}$	=	minimum flow area through the annular gap around the RPV
$A_h$	=	area of hole in the RPV lower head
$A_{op\ deck}$	=	area of the opening in the operating deck that is directly above the seal table
$A_s$	=	surface area of the reactor cavity
$A_{str}$	=	area of the seal table room opening
$C_{Rr}$	=	constant in coherence ratio correlation
$C_{d,h}$	=	discharge coefficient
$f_{coh}$	=	fraction of blowdown steam coherent with debris dispersal
$f_{disp}$	=	fraction of debris dispersed from cavity
$f_{dome}$	=	fraction of dispersed debris that enters dome
$f_{gap}$	=	fraction of dispersed debris that enters the annular gap around the RPV
$f_{noz/shld}$	=	fraction of dispersed debris that enters the RPV gap that flows back into the subcompartments through nozzle cutouts in the biological shield wall or that gets knocked down by the missile shield
$f_{sub}$	=	fraction of dispersed debris that enters the subcompartment and subsequently passes through to the dome
$M_d^0$	=	initial melt mass
$M_g^0$	=	initial mass of RCS gas
$M_{g,e}$	=	gas remaining in the RCS at the end of debris dispersal
$MW_{g,RCS}$	=	molecular weight of RCS gas
$P_{e,RCS}$	=	RCS pressure at the end of debris dispersal
$P_{RCS}^0$	=	initial pressure in the RCS
$R_u$	=	universal gas constant
$R_r$	=	coherence ratio
$T_d^0$	=	initial temperature of molten debris

$T_{RCS}^0$	=	initial temperature of RCS gases
$V_c$	=	cavity volume
$V_{RCS}$	=	RCS volume

## Greek

$\alpha_c$	=	thermal diffusivity of frozen core material
$\delta$	=	thickness of frozen core debris on cavity walls
$\rho_d$	=	density of molten core debris
$\lambda_c$	=	growth rate constant for conduction limited freezing of a superheated liquid on an infinite substrate
$\tau_b$	=	characteristic blowdown time
$\gamma$	=	ratio of molar specific heats, $C_p/C_v$
$\tau_e$	=	characteristic debris dispersal interval



Table C.1 Cavity dispersal summary for Westinghouse plants

PLANT	ARCHITECT/ENGINEER	IDCOR	F disp	F disp	COHERENCE	CAV. VOL.	COHMUL	COH. REL.
		TYPE	Scn V, Va	Scn VI	CATEGORY	m**3		STD. DEV.
Beaver Valley 1,2	Stone & Webster	D	0.91	0.92	Surry-Like	251	12.2	0.18
Braidwood 1,2	Sargent & Lundy	A	0.93	0.93	Zion-Like	339	9.661	0.29
Byron 1,2	Sargent & Lundy	A	0.93	0.93	Zion-Like	339	9.661	0.29
Callaway	Bechtel	M	0.90	0.90	Surry-Like	488	12.2	0.18
Comanche Peak 1,2	Gibbs & Hill	M	0.91	0.91	Zion-Like	385	9.661	0.29
Diablo Canyon 1,2	Utility	C (B)	0.91	0.91	Zion-Like	377	9.661	0.29
Farley 1,2	Southern Services/Bechtel	H	0.89	0.91	Surry-Like	300	12.2	0.18
Ginna	Gilbert	D	0.77	0.87	Surry-Like	278	12.2	0.18
H.B. Robinson	Ebasco	D	0.91	0.92	Surry-Like	248	12.2	0.18
Indian Point 2,3	United Engin. and Const.	B	0.94	0.94	Zion-Like	286	9.661	0.29
Kewaunee	Pioneer	(H)	0.87	0.93	Surry-Like	136	12.2	0.18
Millstone 3	Stone & Webster	D	0.94	0.94	Surry-Like	232	12.2	0.18
North Anna 1,2	Stone & Webster	D	0.91	0.92	Surry-Like	252	12.2	0.18
Point Beach 1,2	Bechtel	I (H)	0.85	0.92	Surry-Like	157	12.2	0.18
Prairie Island 1,2	Pioneer	H	0.86	0.92	Surry-Like	143	12.2	0.18
Salem 1,2	Utility	(A)	0.94	0.94	Zion-Like	251	9.661	0.29
Seabrook	United Engin. and Const.	B	0.91	0.91	Zion-Like	491	9.661	0.29
Shearon Harris	Ebasco	D	0.91	0.92	Surry-Like	256	12.2	0.18
South Texas 1,2	Bechtel	E	0.92	0.92	Other	304	14.6	0.33
Summer	Gilbert	H	0.90	0.92	Surry-Like	284	12.2	0.18
Surry 1,2	Stone & Webster	D	0.88	0.90	Surry	360	12.2	0.18
Turkey Point 3,4	Bechtel	H	0.89	0.91	Surry-Like	303	12.2	0.18
Vogtle 1,2	Southern Services/Bechtel	C (M)	0.93	0.93	Zion-Like	275	9.661	0.29
Wolf Creek	Bechtel/Sargent & Lundy	M	0.93	0.93	Surry-Like	275	12.2	0.18
Zion 1,2	Sargent & Lundy	A	0.95	0.95	Zion	230	9.661	0.29
Averages			0.90	0.92		290		
Standard Deviations			0.037	0.016		86		
Summary								
41 Plants		8 A			17 Zion-Like			
		5 B			22 Surry-Like			
		10 D			2 Other			
		2 E						
		10 H						
		6 M						

NUREG/CR-6338

C-36

Plant Geometry

Table C.2 Validation of melt retention by freezing during cavity dispersal

Parameter	SNL/IET-1 to 8B Allen et al. 1994b	ANL/IET-1R to 8 Binder et al. 1994	SNL/IET-9 to 11 Blanchat et al. 1994
Cavity	Zion	Zion	Surry
Scale	1:10	1:40	1:5.75
Melt Simulant	Fe/Al <sub>2</sub> O <sub>3</sub> /Cr	Fe/Al <sub>2</sub> O <sub>3</sub> /Cr	Fe/Al <sub>2</sub> O <sub>3</sub> /Cr
f <sub>disp</sub> observed	0.62 - 0.89	0.69 - 0.80	0.73 - 0.89
f <sub>disp</sub> Eq. C.1	0.91	0.85	0.88

Table C.3 Input for coherence ratio correlation

Cavity Type	Coherence Constant	Relative Standard Deviation
Zion-like	9.661	0.29
Surry-like	12.2	0.18
Other	14.6	0.33

Table C.4 Cavity water summary for Westinghouse plants

PLANT	ARCHITECT/ENGINEER	CONTAINMENT	CAVITY WATER		CONT. SPRAY SETFNT (PSIG)	FOUNDATION SUPPORT
		TYPE	NO RWST INJ	WITH RWST INJ		
Beaver Valley 1,2	Stone & Webster	Sub. Atm.	Dry	Wet	1.5	Free Standing
Braidwood 1,2	Sargent & Lundy	Large Dry	Dry	Wet		Excavated
Byron 1,2	Sargent & Lundy	Large Dry	Wet	Flooded		Excavated
Callaway	Bechtel	Large Dry	Dry	Flooded	27	Excavated
Comanche Peak 1,2	Gibbs & Hill	Large Dry	Wet	Flooded		Excavated
Diablo Canyon 1,2	Utility	Large Dry	Dry	Wet	22	Excavated
Farley 1,2	Southern Services/Bechtel	Large Dry	Dry	Dry		Excavated
GINNA	Gilbert	Large Dry	Dry	Flooded	28	Excavated
H.B. Robinson	Ebasco	Large Dry	Wet	Flooded	20.3	Excavated
Indian Point 2,3	United Engin. and Const.	Large Dry	Wet	Flooded	28	Excavated
Kewaunee	Pioneer	Large Dry	Dry	Dry		Free Standing
Millstone 3	Stone & Webster	Sub. Atm.				Free Standing
North Anna 1,2	Stone & Webster	Sub. Atm.	Dry	Wet		Free Standing
Point Beach 1,2	Bechtel	Large Dry	Wet	Flooded		Excavated
Prairie Island 1,2	Pioneer	Large Dry	Dry	Flooded		Free Standing
Salem 1,2	Utility	Large Dry		Flooded	25.3	Excavated
Seabrook	United Engin. and Const.	Large Dry	Dry	Flooded		Excavated
Shearon Harris	Ebasco	Large Dry	Dry	Flooded	10.3	Excavated
South Texas 1,2	Bechtel	Large Dry	Dry	Dry	9.5	Free Standing
Summer	Gilbert	Large Dry				Excavated
Surry 1,2	Stone & Webster	Sub. Atm.	Dry	Wet	5	Free Standing
Turkey Point 3,4	Bechtel	Large Dry	Wet	Flooded		Excavated
Vogtle 1,2	Southern Services/Bechtel	Large Dry	Dry	Dry		Excavated
Wolf Creek	Bechtel/Sargent & Lundy	Large Dry	Dry	Wet		Excavated
Zion 1,2	Sargent & Lundy	Large Dry	Dry	Flooded	23	Excavated
Averages					18.2	
Standard Deviations					9.3	
Summary		7 Sub Atm	0 Flooded	21 Flooded		29 Excavated
41 Plants		34 Large Dry	11 Wet	11 Wet		12 Free Standing
			26 Dry	7 Dry		
			4 Unknown	2 Unknown		

Table C.5 Dome transport comparison table

PLANT	ARCHITECT/ENGINEER	SUBCOMP.	MIN. GAP	MIN. CAV.	GAP TRANS	SUB. TRANS.	NOZ./SHLD	DOMES TRANS.
		CATEGORY	AREA m2	AREA m2	FRACT.	FRACT.	FRACT.	FRACT.
Beaver Valley 1,2	Stone & Webster	Surry-Like	1.00	3.51	0.222	0.05	0.1	0.238
Braidwood 1,2	Sargent & Lundy	Zion-Like	1.50	8.38	0.152	0.05	0.1	0.179
Byron 1,2	Sargent & Lundy	Zion-Like	1.50	8.38	0.152	0.05	0.1	0.179
Callaway	Bechtel	Surry-Like	2.20	12.9	0.146	0.05	0.1	0.174
Comanche Peak 1,2	Gibbs & Hill	Zion-Like	2.75	11.2	0.197	0.05	0.1	0.218
Diablo Canyon 1,2	Utility	Zion-Like	1.20	5.35	0.183	0.05	0.1	0.206
Farley 1,2	Southern Services/Bechtel	Surry-Like	1.21	5.67	0.176	0.05	0.1	0.199
Ginna	Gilbert	Two-Loop	1.03	3.97	0.206	0.00	0.1	0.185
H.B. Robinson	Ebasco	Other	0.61	3.33	0.155	0.57	0.1	0.621
Indian Point 2,3	United Engin. and Const.	Zion-Like	1.20	6.95	0.147	0.05	0.1	0.175
Kewaunee	Pioneer	Two-Loop	1.08	1.89	0.364	0.95	0.1	0.932
Millstone 3	Stone & Webster	Surry-Like	0.39	9.03	0.041	0.05	0.1	0.085
North Anna 1,2	Stone & Webster	Surry-Like	1.00	7.01	0.125	0.05	0.1	0.156
Point Beach 1,2	Bechtel	Two-Loop	1.60	2.18	0.423	0.36	0.1	0.589
Prairie Island 1,2	Pioneer	Two-Loop	1.08	1.89	0.364	0.95	0.1	0.932
Salem 1,2	Utility	Zion-Like	1.88	7.02	0.211	0.05	0.1	0.230
Seabrook	United Engin. and Const.	Zion-Like	1.20	7.11	0.144	0.05	0.1	0.173
Shearon Harris	Ebasco	Surry-Like	0.68	16.7	0.039	0.05	0.1	0.083
South Texas 1,2	Bechtel	Other	0.65	2.97	0.180	0.00	0.1	0.162
Summer	Gilbert	Surry-Like	0.44	7.30	0.057	0.05	0.1	0.098
Surry 1,2	Stone & Webster	Surry	1.00	6.4	0.135	0.05	0.1	0.165
Turkey Point 3,4	Bechtel	Surry-Like	0.59	3.24	0.154	0.05	0.1	0.181
Vogtle 1,2	Southern Services/Bechtel	Zion-Like	0.87	9.89	0.081	0.05	0.1	0.119
Wolf Creek	Bechtel/Sargent & Lundy	Surry-Like	1.20	7.39	0.140	0.05	0.1	0.169
Zion 1,2	Sargent & Lundy	Zion	0.54	5.6	0.088	0.05	0.1	0.125

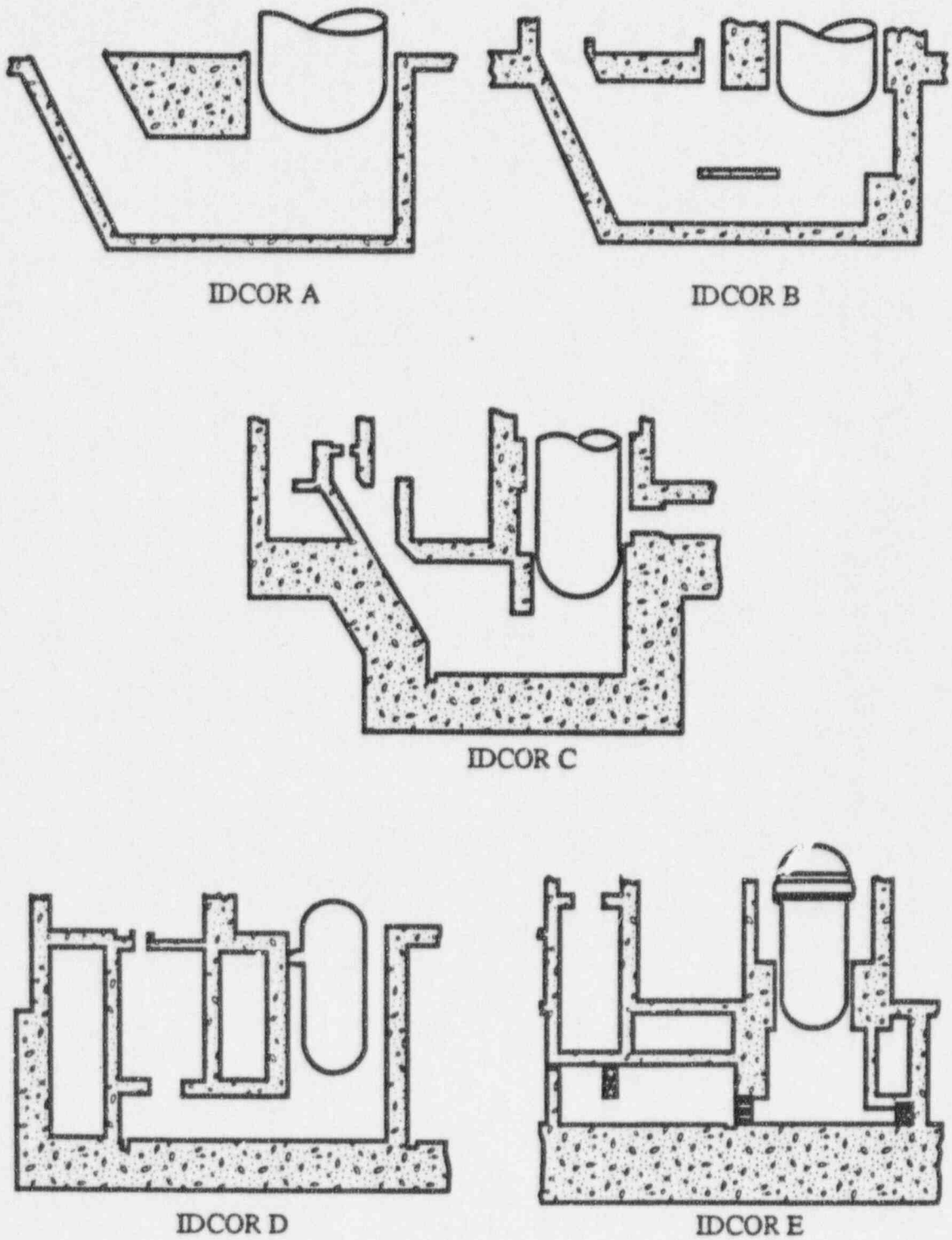
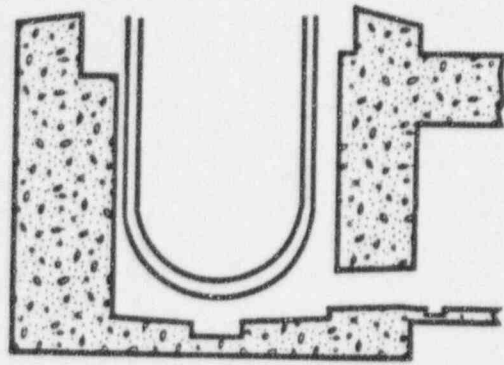
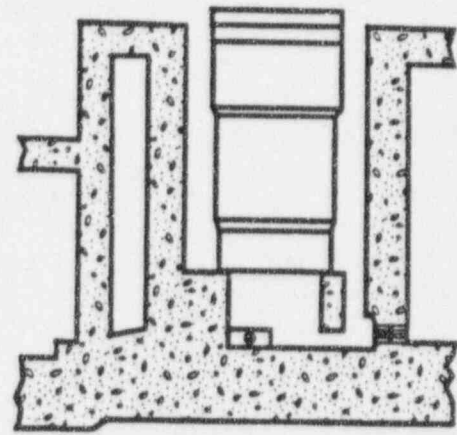


Figure C.1. Schematic drawings of the IDCOR cavity groups.

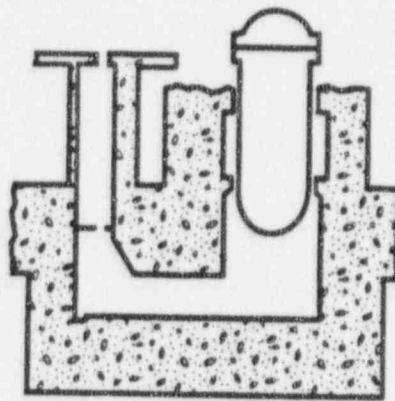




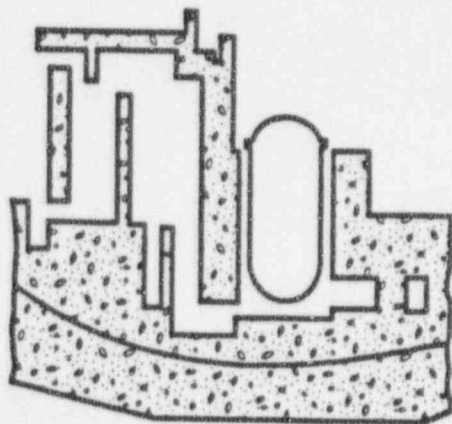
IDCOR F



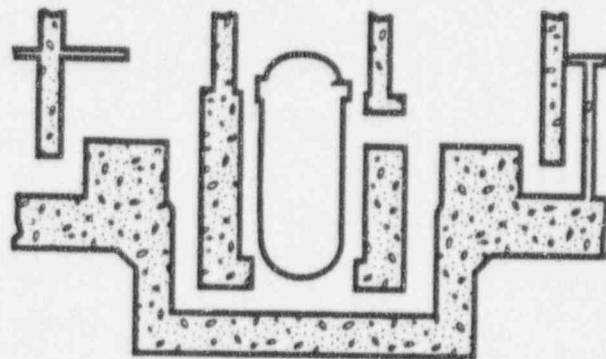
IDCOR G



IDCOR H

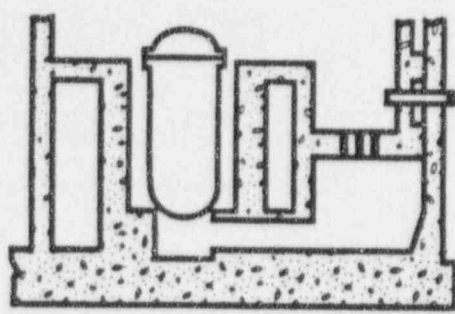


IDCOR I

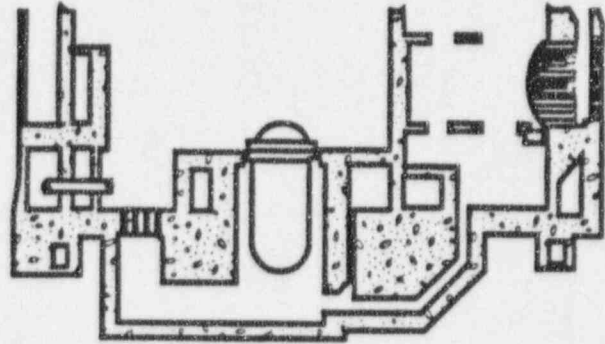


IDCOR J

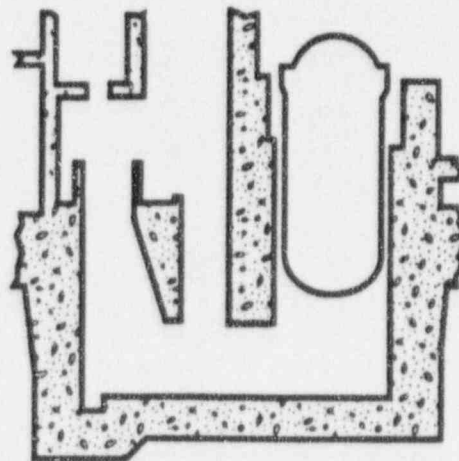
Figure C.1. Schematic drawings of the IDCOR cavity groups (continued).



IDCOR K



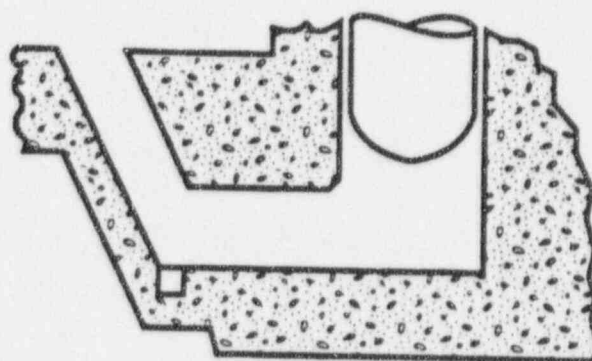
IDCOR L



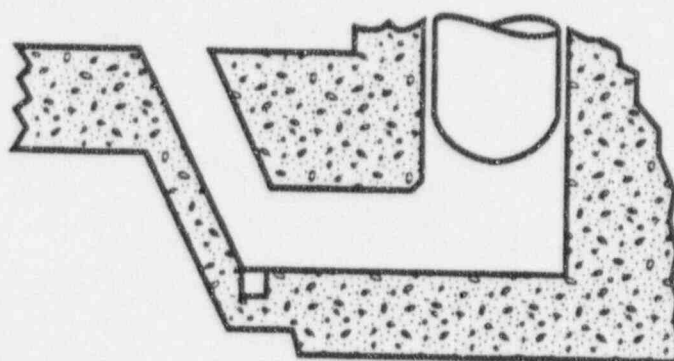
IDCOR M

Figure C.1. Schematic drawings of the IDCOR cavity groups (concluded).

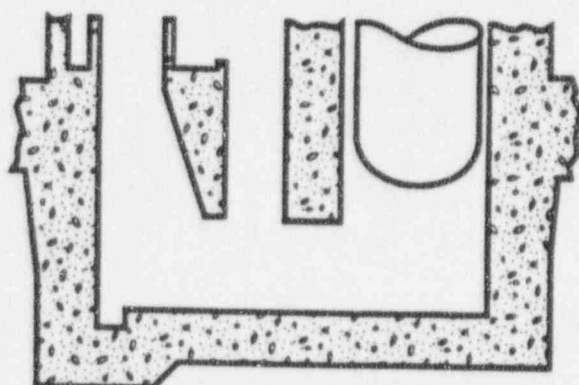
No Cavity Drawing Available  
Beaver Valley 1 & 2



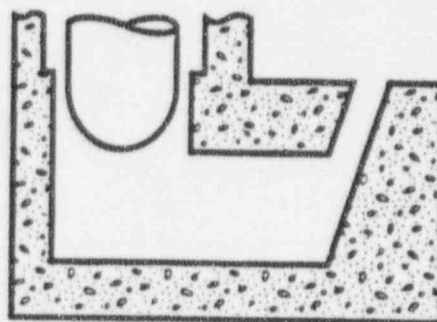
Braidwood 1 & 2



Byron 1 & 2

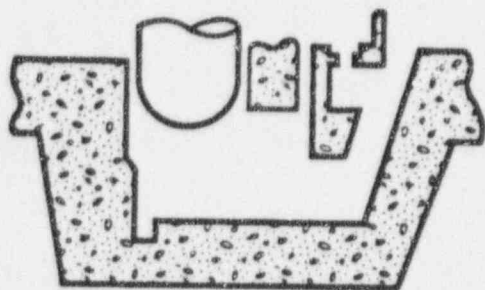


Callaway

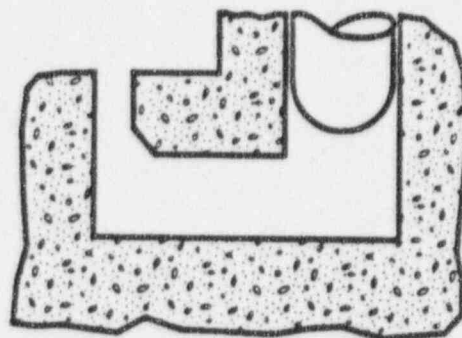


Comanche Peak 1 & 2

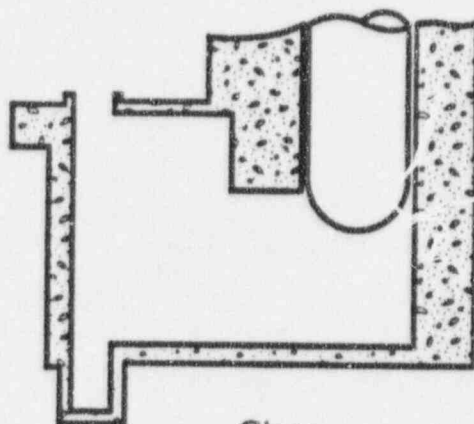
Figure C.2. Schematic drawings of all Westinghouse cavities (excluding plants with ice condenser containments).



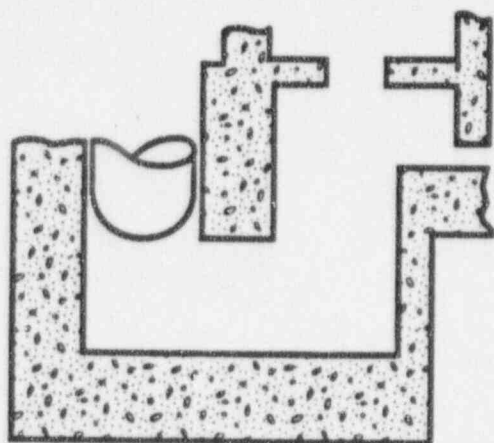
Diablo Canyon 1 & 2



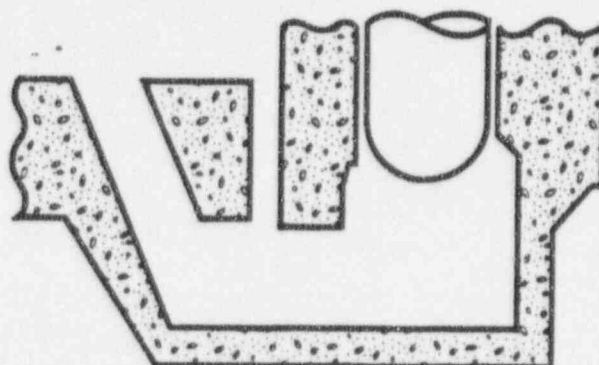
Farley 1 & 2



Ginna

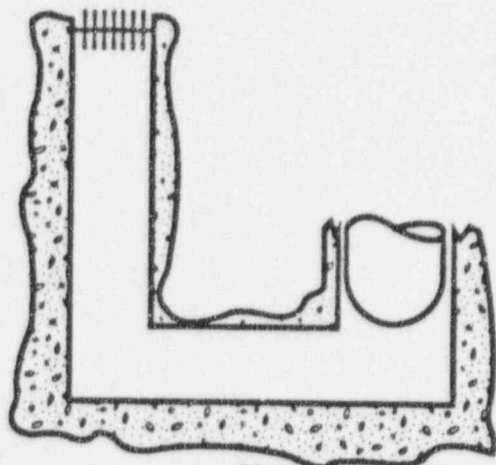


H.B. Robinson

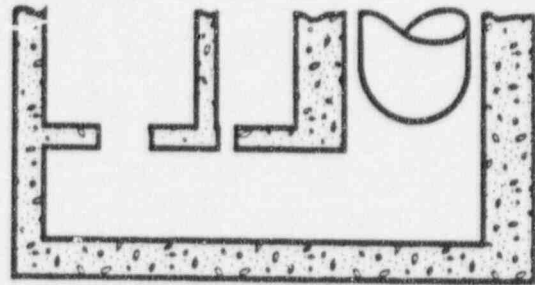


Indian Point 2 & 3

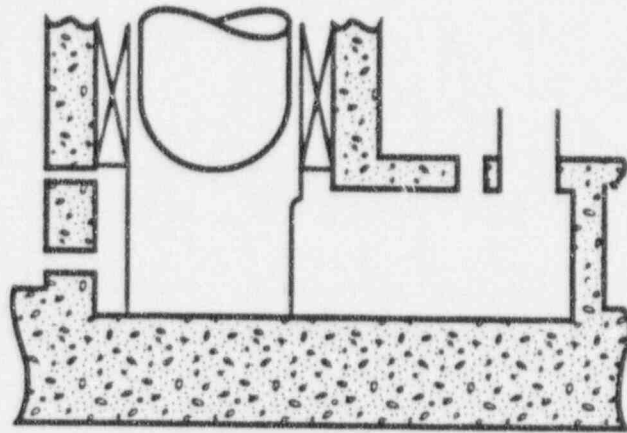
Figure C.2. Schematic drawings of all Westinghouse cavities (excluding plants with ice condenser containments) (continued).



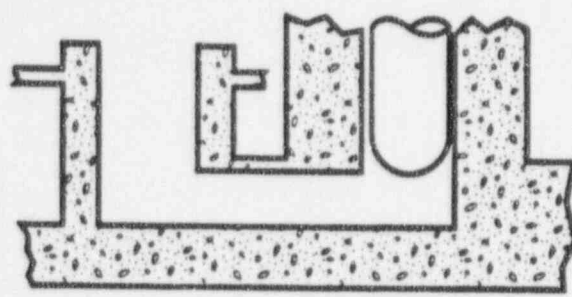
Kewaunee



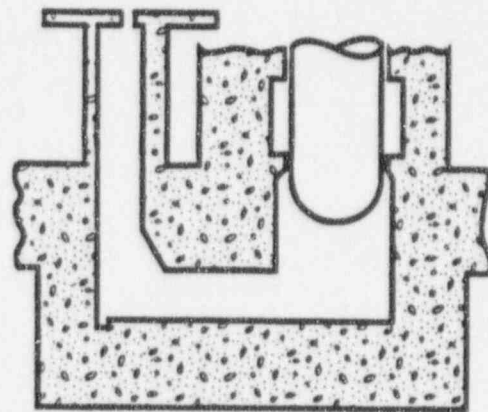
Millstone 3



North Anna 1 & 2



Point Beach 1 & 2

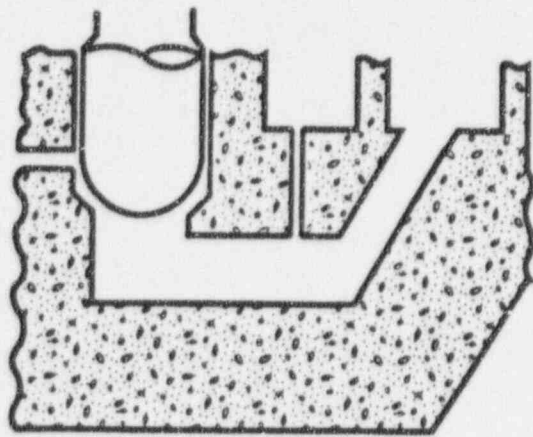


Prairie Island 1 & 2

Figure C.2. Schematic drawing of all Westinghouse cavities (excluding plants with ice condenser containments) (continued).



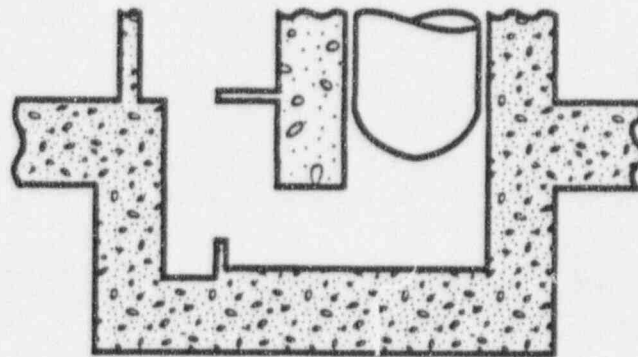
Plant Geometry



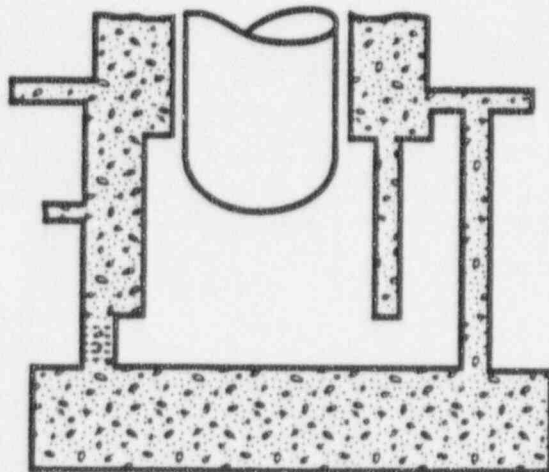
Salem 1 & 2



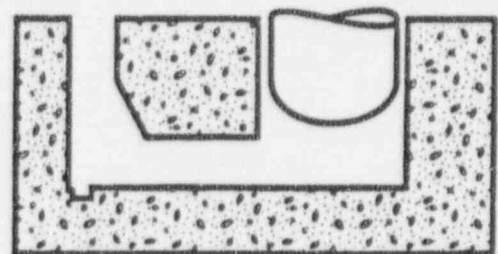
Seabrook



Shearon Harris

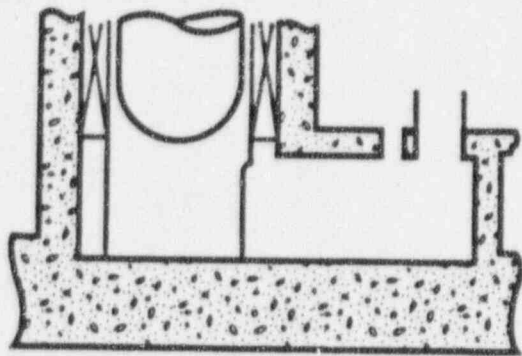


South Texas 1 & 2

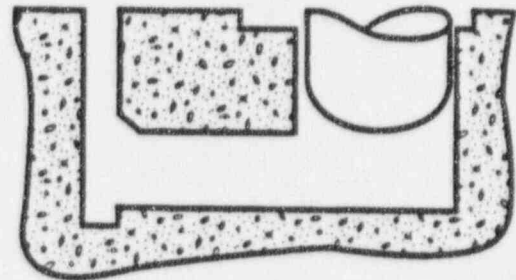


Summer

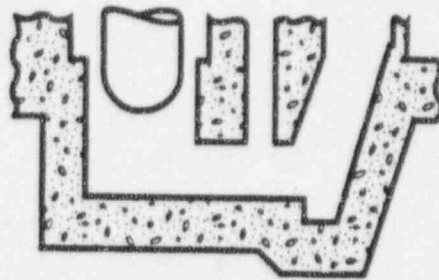
Figure C.2. Schematic drawing of all Westinghouse cavities (excluding plants with ice condenser containments) (continued).



Surry 1 & 2



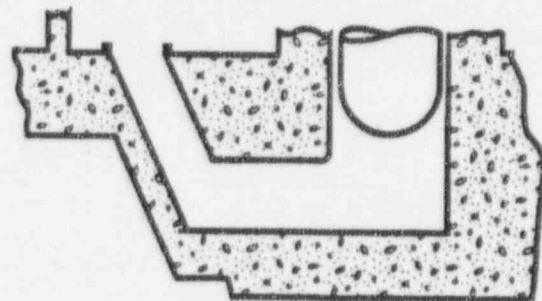
Turkey Point 3 & 4



Vogtle 1 & 2



Wolf Creek



Zion 1 & 2

Figure C.2. Schematic drawing of all Westinghouse cavities (excluding plants with ice condenser containments) (concluded).

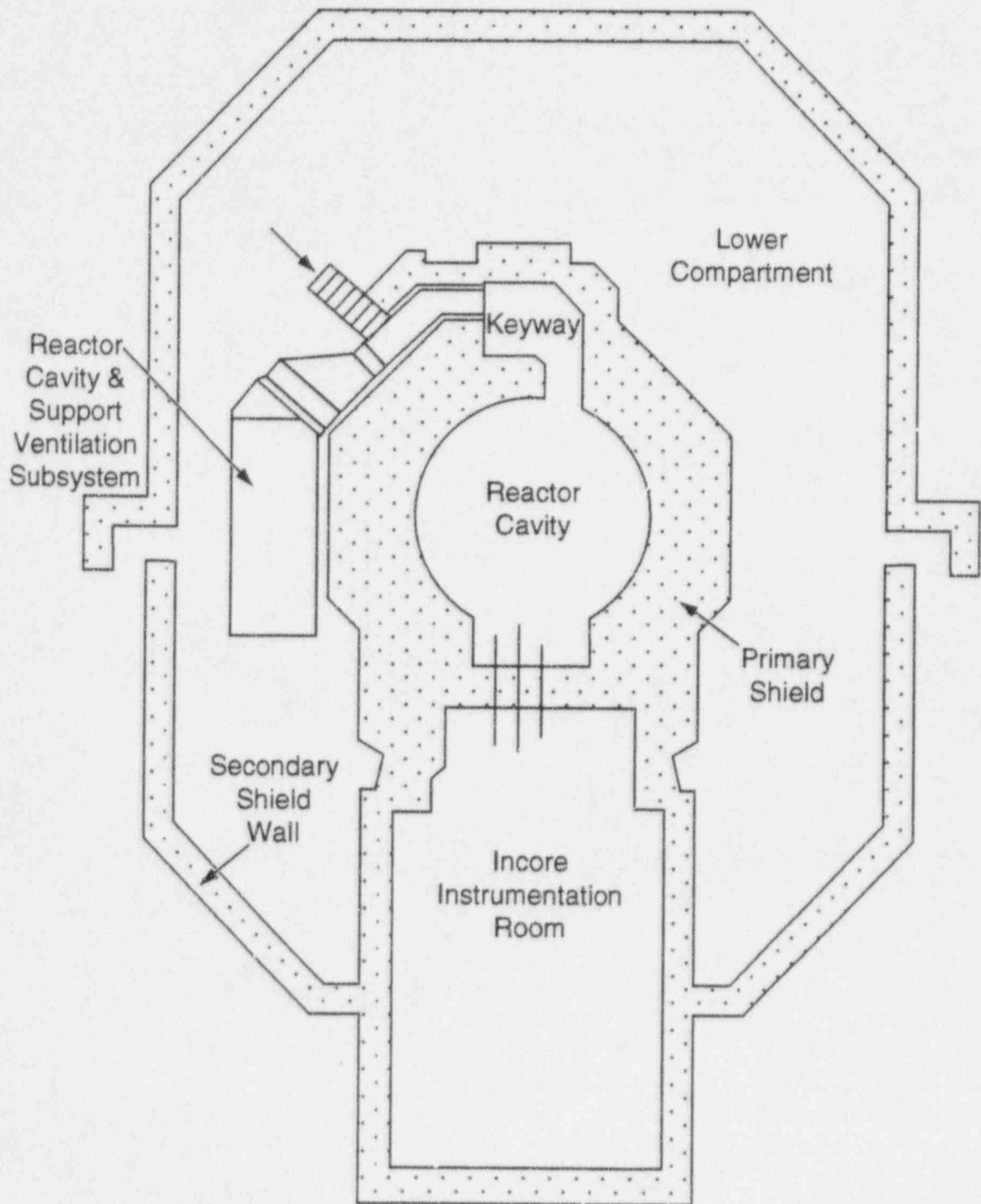


Figure C.3. Reactor cavity and lower compartments of South Texas 1 and 2.

**APPENDIX D**  
**Catalog of the IPE Containment Fragility Curves for Operating**  
**Pressurized Water Reactors (PWRs)**

Eric W. Klamerus  
Sandia National Laboratories

**D.1 Introduction**

At the request of the U.S. NRC, the Individual Plant Examinations (IPEs) for all operating Pressurized Water Reactors (PWRs) in the U.S. were assembled and containment fragility curves obtained. Although this report focuses only on Westinghouse plants with large dry or subatmospheric containments, we catalogue the fragility curves for all PWRs because this information will be used in future DCH resolution efforts for the remaining plants. A list of the all PWRs in the U.S. is shown in Table D.1 as taken from Lobner et al. (1990). The current status of these plants is shown in the last column of this table. The containment fragility curves were taken from the IPEs of all the plants listed as operating. The only exception is for Trojan, which submitted the IPE before it shut down and this is included in this database.

The containment capacity results from each of the IPEs were examined and briefly reviewed and the probability of containment failure was taken from them. In many cases this consisted of fragility curves showing pressure versus cumulative failure probability. In other cases a mean or median failure pressure was specified along with uncertainty bounds. In some cases, only curves or points for various failure modes were given and a total probability of failure had to be constructed.

For those IPEs presenting only a single curve, the curve was digitized, curve-fit with a spline program and failure probabilities determined at intervals of 1 psig. For IPEs which reported medians and uncertainties, a curve was developed and failure probabilities determined at intervals of 1 psig. The few which reported only median, 5 percent and 95 percent values were fit to either a log-normal distribution, normal distribution, or 3rd order spline function in order to get the best fit and failure probabilities determined at 1 psig intervals. In most situations where this occurred, only the third order spline provided an adequate fit to the three constraints.

Many of the IPE containment capacity analyses did not consider temperature or stated that increased temperatures would have little effect on the capacity. Other IPEs performed the analysis at either a single or multiple accident temperatures. For those which determined the capacity at different temperatures, the analysis closest to 260°F (400 K) was selected as best representing the accident temperatures expected in the DCH study.

It was observed that the licensee's level of effort and our estimate of the reliability of these containment fragility curves varied significantly. In some cases a detailed analysis was performed for every possible failure mode and an overall cumulative failure curve was determined by combining each mode of failure. Other IPEs simply used containment fragility curves derived from other containments or simply shifted other plant's fragility curves based on what they determined to be the difference in ultimate capacity.

## IPE Fragility Curves

This report briefly discusses (when given enough information) how the fragility curves were determined from each IPE. In addition, the process of digitizing, fitting and tabulating the curves or data given in the IPEs is discussed for every plant.

### D.2 Steel Containments

#### D.2.1 Individual Containment Failure Curve Development

##### Catawba 1 & 2

The "Containment Capacity Assessment" for Catawba was performed as part of a PRA submitted along with the Catawba IPE and is documented in Appendix G of the Catawba PRA. Catawba is an ice condenser containment with a design pressure of 30 psig. The overall shell capacity analysis was performed as part of the original FSAR. Leakage or failure of penetrations and other modes of failure were analyzed. A mean failure pressure of 84.5 psig was computed and uncertainty assumed. A single curve was developed and is shown in the PRA. This IPE curve was then digitized, fitted using a spline program and failure probabilities determined at intervals of 1 psig. Temperature effects were not considered in the analysis.

##### Davis Besse

The "Containment Failure Characterization" for Davis Besse is presented in Section 4 of the Davis Besse IPE. Davis Besse is a large dry containment with a design pressure of 40 psig. The failure determination was based on a capacity assessment performed for St. Lucie. The limiting vessel strength was determined by hand calculations based on minimum required yield strengths at ambient and elevated temperatures. Other failure modes were reviewed and screened. The resulting mean failure pressure at 264°F was determined to be 85.2 psig with a COV of 0.16. Two plots were developed for Davis Besse representing failure at ambient and 264°F temperatures. The IPE curve representing T = 264°F was digitized, fitted using a spline program and failure probabilities determined at intervals of 1 psig.

##### Kewaunee

The "Containment Failure Characterization" for Kewaunee is presented in Section 4.2 of the Kewaunee IPE. Kewaunee is a large dry containment with a design pressure of 46 psig. A plant-specific structural analysis of the containment was conducted and results presented. Four failure modes were considered and a mean failure pressure of 166 psia (151 psig) was determined along with a 95 percent upper bound pressure and 5 percent lower bound pressure. The resulting plot as shown in the IPE was digitized, fitted using a spline program and failure probabilities determined at intervals of 1 psig. Temperature effects were not considered in the analysis.



### Prairie Island 1 & 2

The "Containment Failure Characterization" for Prairie Island is presented in Section 4.4 of the Prairie Island IPE. Prairie Island is a large dry containment with a design pressure of 41 psig. A plant-specific structural analysis of the containment was conducted and results presented. Four failure modes were considered and a mean failure pressure of 165 psia (150 psig) was given along with a 95 percent upper bound pressure and 5 percent lower bound pressure. The resulting plot as shown in the IPE was digitized, fitted using a spline program and failure probabilities determined at intervals of 1 psig. Temperature effects were not considered in the analysis.

### Sequoyah 1 & 2

The "Containment Structural Evaluation and Failure Characterization" for Sequoyah is presented in Section 4.4 of the Sequoyah IPE for unit 1. Sequoyah is an ice condenser containment with a design pressure of 10.8 psig. A plant-specific analysis was performed by EQE Engineering. A total of seven failure modes were considered. For each failure mode a median failure pressure and log-normal composite uncertainty ( $\beta_c$ ) were listed for various temperatures ranging from room temperature to 800°F. For this study, a log-normal curve was developed from the medians and  $\beta_c$  for each failure mode corresponding to a temperature of 200°F. These curves were then combined assuming total independence and failure probabilities computed at intervals of 1 psig. This resulted in a median failure pressure of about 68 psig.

### St. Lucie 1 & 2

The "Containment Performance Analysis" for St. Lucie is presented in Section 4 and Appendix G of the St. Lucie IPE. St. Lucie is a large dry containment with a design pressure of 44 psig. The limiting vessel strength was determined by hand calculations and minimum required yield strengths at ambient temperatures. The resulting mean failure pressure was given as 95.4 psig. For uncertainty, a lower bound 0 percent failure probability was assumed at 80 psig and an upper bound 100 percent was assumed at 120 psig. A curved line was then fit through these three points as presented in the IPE. The IPE curve was digitized, fitted using a spline program and failure probabilities determined at intervals of 1 psig. Temperature effects were not considered in the analysis.

### Waterford 3

The "Containment Failure Characterization" for Waterford is presented in Section 4.4 of the Waterford IPE. Waterford is a large dry containment with a design pressure of 44 psig. A median capacity of 135 psig was assumed based on comparisons with other containments. The uncertainty was assumed to represent a log-normal distribution with a COV = 0.15. For this study, a log-normal curve was developed from this information and failure probabilities computed at intervals of 1 psig. Temperature effects were not considered in the analysis.

## IPE Fragility Curves

### Watts Bar 1 & 2

The "Containment Structural Evaluation and Failure Characterization" for Watts Bar is presented in Section 4.4 of the Watts Bar IPE for Unit 1. Watts Bar is an ice condenser containment with a design pressure of 15 psig. A plant-specific analysis was performed by EQE Engineering. A total of seven failure modes were considered. For each failure mode a median failure pressure and log-normal composite uncertainty ( $\beta_c$ ) were listed for various temperatures ranging from room temperature to 800°F. For this study, a log-normal curve was developed from the medians and  $\beta_c$  for each failure mode corresponding to a temperature of 200°F. These curves were then combined assuming total independence and failure probabilities computed at intervals of 1 psig. This resulted in a median failure pressure of about 90 psig.

#### D.2.2 Comparison of Steel Containments

All the data above were combined into a single spreadsheet for plotting and comparison purposes. Figure D.1 compares all the large dry steel containment fragility curves. Similarly, Figure D.2 compares all ice condenser type steel containment fragility curves. Both graphs were plotted over the same range of pressures (40-200 psig) for comparison purposes. The ice condenser containments were plotted separately because of their lower design pressures (10.8-30 psig), which probably lead to a lower fragility curve. However, the fragility curves for the dry containments, with higher design pressures (40-46 psig), were not always much greater and have very different median capacities (85-151 psig).

These variations in the fragilities might result from the different accident pressures used in the original containment design. Therefore, each of the containment fragility curves was normalized to the design accident pressure for that containment. These normalized fragility curves are shown for all the steel containments in Figure D.3. Here, most of the curves are quite comparable with median failure ratios in the range of 2-4 times the design pressure. The only exception to this is for two of the ice condenser containments with the lowest design pressures, Sequoyah (10.8 psig) and Watts Bar (15 psig). These two containments had higher median failures of 6.3 (Sequoyah) and 6.0 (Watts Bar) times the design pressure.

### D.3 Reinforced Concrete Containments

#### D.3.1 Individual Containment Failure Curve Development

##### Beaver Valley 1 & 2

The "Containment Failure Characterization" for Beaver Valley is presented in Section 4.4 of the Beaver Valley IPE. Beaver Valley is a subatmospheric containment with a design pressure of 45 psig. The failure capacity analysis was based on the Surry NUREG-1150 containment capacity results. This was defended by comparing the two containments, which were very similar in design. The same mean failure pressure for Surry of about 128 psig was used in the Beaver Valley IPE. Therefore the same fragility curve developed for Surry was digitized, fitted using a spline program and failure probabilities determined at intervals of 1 psig. Temperature effects were not considered in the analysis.

### Comanche Peak 1 & 2

The "Containment Failure Characterization" for Comanche Peak is presented in Section 4.4 of the Comanche Peak IPE. Comanche Peak is a large dry containment with a design pressure of 50 psig. The capacity of various failure modes were evaluated separately. Failure of the liner was predicted to have a mean failure pressure of 114 psig and was given as the governing failure mode. The uncertainty was assumed to represent a normal distribution with a COV = 0.07. For this study, a normally distributed curve was developed from this information and failure probabilities computed at intervals of 1 psig. Temperature effects were not considered in the analysis.

### D. C. Cook 1 & 2

The "Containment Failure Characterization" for D. C. Cook is presented in Section 4.3 of the D. C. Cook IPE. D. C. Cook is an ice condenser containment with a design pressure of 12 psig. A plant-specific structural analysis of the containment was conducted and results presented. The dominant failure mode was identified as bending shear failure of the basemat. The median pressure capacity at this location was given as 57.8 psig with a  $\beta_U = 0.14$  and  $\beta_R = 0.14$  ( $\beta_C = 0.2$ ). For this study, a log-normal curve was developed from this information and failure probabilities computed at intervals of 1 psig. Temperature effects were not considered in the analysis.

### Diablo Canyon 1 & 2

The "Containment Failure Characterization" for Diablo Canyon is presented in Section 4.4 of the Diablo Canyon IPE. Diablo Canyon is a large dry containment with a design pressure of 47 psig. A plant-specific analysis was performed, which examined ten separate failure modes. Temperature effects were considered up to 350°F. For each failure mode a median failure pressure and log-normal composite uncertainty ( $\beta_c$ ) were listed. For this study, a log-normal curve was developed from the medians and  $\beta_c$  for each failure mode. These curves were then combined assuming total independence and failure probabilities computed at intervals of 1 psig. This resulted in a median failure pressure of about 140 psig.

### Haddam Neck

The "Containment Failure Characterization" for Haddam Neck is presented in Section 4.4 of the Haddam Neck IPE. Haddam Neck is a large dry containment with a design pressure of 40 psig. Much of the containment capacity analysis was based using the NUREG-1150 results for the Surry containment. A median probability of failure was given as 90 psig. A 95 percent upper bound pressure was given as 105 psig and 5 percent lower bound pressure was given as 66.7 psig. For this study, a spline was fitted through these three points and failure probabilities determined at intervals of 1 psig. Temperature effects were considered by applying correction factors to the pressure but remained about 1.0 up to temperatures of 340°F.

## IPE Fragility Curves

### Indian Point 2

The "Containment Building Failure Characterization" for Indian Point 2 is presented in Section 4.4 of the Indian Point 2 IPE. Indian Point 2 is a large dry containment with a design pressure of 47 psig. Much of the containment capacity analysis was based using the NUREG-1150 results for the Surry containment. Several possible failure modes were examined and a median probability of failure was given as 126 psig. A 95 percent upper bound pressure was given as 150 psig and 5 percent lower bound pressure was given as 95 psig. For this study, a spline was fitted through these three points and failure probabilities determined at intervals of 1 psig. Temperature effects were not considered in the analysis.

### Indian Point 3

The "Containment Failure Characterization" for Indian Point 3 is presented in Section 4.5 of the Indian Point 3 IPE. Indian Point 3 is a large dry containment with a design pressure of 47 psig. Failure of the containment was predicted to be liner tears near penetrations. The median failure pressure was given as 134 psig along with a 95 percent upper bound pressure and 5 percent lower bound pressure, at a temperature of 400°F. A curve was fit through these points and presented in the IPE. This IPE curve was then digitized, fitted using a spline program and failure probabilities determined at intervals of 1 psig.

### Maine Yankee

The "Containment Ultimate Strength Evaluation" for Maine Yankee is presented in Section 4.4 of the Maine Yankee IPE. Maine Yankee is a large dry containment with a design pressure of 55 psig. A plant-specific structural analysis of the containment was conducted and results presented. Twelve failure modes were considered at temperatures ranging from 300°F to 900°F. Medians and uncertainties were quantitatively assessed for each failure mode. The composite containment failure probability distribution was developed at several temperatures. The composite curve at a temperature of 376°F as shown in the IPE was digitized, fitted using a spline program and failure probabilities determined at intervals of 1 psig.

### McGuire 1 & 2

The "Containment Capacity Assessment" for McGuire was performed as part of a PRA submitted along with the McGuire IPE and is documented in Appendix G of the McGuire PRA. McGuire is an ice condenser containment with a design pressure of 28 psig. Three modes of failure were considered to dominate the containment capacity: overall shell, anchorage, and airlock. For each of these modes, a mean failure pressure was given along with a standard deviation. These failures were combined (by the analyst) to form a single curve representing the overall containment failure probability distribution, with a mean failure pressure of 77 psig, as shown in the IPE. This IPE curve was then digitized, fitted using a spline program and failure probabilities determined at intervals of 1 psig. Temperature effects were not considered in the analysis.



### Millstone 3

The "Containment Failure Characterization" for Millstone 3 is presented in Section 4.4 of the Millstone 3 IPE. Millstone 3 is a large dry containment with a design pressure of 45 psig. A full structural analysis was performed to identify containment failure modes and failure pressures. The various containment failure modes and corresponding failure pressure and variances were then combined to give a containment failure distribution curve with a median failure pressure of 117.7 psig. This curve was given in the IPE both graphically and in tabular form. The table of failure probabilities at increments of 5 psig was fitted using a spline program and failure probabilities determined at intervals of 1 psig. Temperature effects were not considered in the analysis.

### North Anna 1 & 2

The "Containment Building Failure Characterization" for North Anna is presented in Section 4.4 of the North Anna IPE. North Anna is a subatmospheric containment with a design pressure of 45 psig. The failure capacity analysis was based on the Surry NUREG-1150 containment capacity results. This was defended by comparing the two containments, which were very similar in design. The same mean failure pressure for Surry of about 128 psig was used in the North Anna IPE. Therefore the same fragility curve developed for Surry was digitized, fitted using a spline program and failure probabilities determined at intervals of 1 psig. Temperature effects were not considered in the analysis.

### Salem 1 & 2

The "Containment Structural Evaluation and Failure Characterization" for Salem is presented in Section 4.4 of the Salem IPE. Salem is a large dry containment with a design pressure of 47 psig. A plant-specific analysis was performed by EQE Engineering. A total of ten failure modes were considered. For each failure mode a median failure pressure and log-normal composite uncertainty ( $\beta_c$ ) were listed for various temperatures ranging from 300°F to 800°F. These failure modes were combined and plotted in the IPE. The IPE curve corresponding to a containment temperature of 300°F was then digitized, fitted using a spline program and failure probabilities determined at intervals of 1 psig. The median failure pressure at 300°F was about 112 psig.

### Seabrook 1

The "Containment Failure Characterization" for Seabrook is presented in Section 4.4 of the Seabrook IPE. Seabrook is a large dry containment with an unusually high design pressure of 65 psig. A full structural analysis was performed to identify containment failure modes and failure pressures. Small leaks were determined to occur at a median pressure of 181 psia (166 psig). The lowest major structural failure was expected in the cylindrical wall of the containment resulting in hoop failure at a median pressure of 216 psig. The resulting containment fragility curve as shown in the IPE is based on this major structural failure mode. This IPE curve (representing a major structural failure) was then digitized, fitted using a spline program and failure probabilities determined at intervals of 1 psig. Temperature effects were not considered in the analysis.



## IPE Fragility Curves

### Shearon Harris 1

The "Containment Failure Characterization" for Shearon Harris is presented in Section 4.4 of the Shearon Harris IPE. Shearon Harris is a large dry containment with a design pressure of 45 psig. A failure assessment of the containment was conducted and results presented. Four major failure modes were considered for temperatures ranging from 300°F to 800°F. Median capacities and log-normal uncertainties were listed for each failure mode. The lowest median capacity was due to failure of the basemat in shear, for which a median failure pressure of 153 psig was given, and adopted as the characteristic failure response of the containment. The basemat shear failure curve was developed at 300°F but also applies at higher temperatures. This IPE curve was then digitized, fitted using a spline program and failure probabilities determined at intervals of 1 psig.

### Surry 1 & 2

The "Containment Failure Characterization" for Surry is presented in the Surry IPE. Surry is a subatmospheric containment with a design pressure of 45 psig. The failure capacity analysis was based on the NUREG-1150 containment capacity results for the Surry containment. The identical containment fragility curve was presented in the IPE. This best estimate curve, based on expert elicitation, was then digitized, fitted using a spline program and failure probabilities determined at intervals of 1 psig. Temperature effects were not considered in the analysis.

### D.3.2 Comparison of Reinforced Concrete Containments

All the data above was combined into a single spreadsheet for plotting and comparison purposes. Figures D.4 through D.8 compare all the reinforced concrete containment fragility curves. All graphs were plotted over the same range of pressures (40-200 psig) for comparison purposes, except Figure D.5, the fragility curve for Seabrook (140-300 psig). The ice condenser containments were also plotted separately because of their lower design pressures (12-28 psig), which probably lead to lower fragility curves as shown in Figure D.8. The fragility curves for the other containments with higher design pressures (40-65 psig) were usually higher but have very different median capacities (90-216 psig). This group of non-ice condenser type containments was also split up into three groups based on their design pressure; those with higher design pressures (50-65 psig) in Figure D.4, those with a medium design pressure (47 psig) in Figure D.6, and those with lower design pressures (40-45 psig) in Figure D.7.

These variations in the fragilities might result from the different accident pressures used in the original containment design. Therefore, each of the containment fragility curves was normalized to the design accident pressure for that containment. These normalized fragility curves are shown for all the reinforced concrete containments in Figures D.9 and D.10. Figure D.9 shows the larger containments (diameter = 135-140 ft) and Figure D.10 shows the smaller containments (diameter = 115-130 ft). The larger containments shown in Figure D.9 (all non-ice condenser types), show very comparable median failure ratios in the range of 2-3.5 times the design pressure. The smaller containments in Figure D.10 are very comparable except for D.C. Cook, which is a low pressure (12 psig) ice condenser type containment with a median failure of about 4.8 times the design pressure.

## D.4 Prestressed Concrete Containments

### D.4.1 Individual Containment Failure Curve Development

#### ANO-1

The "Containment Failure Characterization" for ANO-1 is presented in Section 4.4 of the ANO-1 IPE. ANO-1 is a large dry containment with a design pressure of 59 psig. Both global and local reactor building failure analysis were performed. The most likely failure was judged to be liner tearing and subsequent leakage due to reactor building overpressurization. The estimated mean failure pressure was given as 154.3 psig. ANO-1 then utilized the NUREG-1150 fragility curves developed for Surry and simply shifted them so the resulting mean would be 154.3 psig. For this study, the Surry fragility curve already digitized was shifted to give a mean of 154.3 psig. Temperature effects were not considered in the analysis.

#### ANO-2

The "Containment Failure Characterization" for ANO-2 is presented in Section 4.4 of the ANO-2 IPE. ANO-2 is a large dry containment with a design pressure of 54 psig. Both global and local reactor building failure analysis were performed. The most likely failure was judged to be liner tearing and subsequent leakage due to reactor building overpressurization. The estimated mean failure pressure was given as 141.3 psig. ANO-2 then utilized the NUREG-1150 fragility curves developed for Surry and simply shifted them so the resulting mean would be 141.3 psig. For this study, the Surry fragility curve already digitized was shifted to give a mean of 141.3 psig.

#### Braidwood 1 & 2

The "Containment Failure Characterization" for Braidwood is presented in Section 4.3 of the Braidwood IPE. Braidwood is a large dry containment with a design pressure of 61 psig. The containment capacity was taken directly from the analysis for Byron, which is apparently identical in design. Various failure modes were considered and mean failure pressures and uncertainties were listed for each mode. The most likely failure location in Unit 2 was determined to occur in the Bunker Ramo electrical penetrations at 108 psig. Unit 1 did not contain these type of penetrations and therefore resulted in a much higher median failure pressure of 125 psig. Unit 2, due to several Bunker Ramo electrical penetrations, had a median failure pressure of about 98 psig. Therefore, two separate fragilities were developed and plotted in the IPE. Both these IPE curves (Unit 1 & 2) were then digitized, fitted using a spline program and failure probabilities determined at intervals of 1 psig. Temperature effects were not considered in the analysis.

#### Byron 1 & 2

The "Containment Failure Characterization" for Byron is presented in Section 4.3 of the Byron IPE. Byron is a large dry containment with a design pressure of 61 psig. A plant-specific structural analysis of the containment was conducted and results presented. Various failure modes were considered and mean failure pressures and uncertainties were listed for each mode. The most likely failure location in

## IPE Fragility Curves

Unit 2 was determined to occur in the Bunker Ramo electrical penetrations at 108 psig. Unit 1 did not contain these type of penetrations and therefore resulted in a much higher median failure pressure of 125 psig. Unit 2, due to several Bunker Ramo electrical penetrations, had a median failure pressure of about 98 psig. Therefore, two separate fragilities were developed and plotted in the IPE. Both these IPE curves (Unit 1 & 2) were then digitized, fitted using a spline program and failure probabilities determined at intervals of 1 psig. Temperature effects were not considered in the analysis.

### Callaway

The "Containment Failure Characterization" for Callaway is presented in Section 4.4 of the Callaway IPE. Callaway is a large dry containment with a design pressure of 60 psig. A plant-specific structural analysis of the containment was conducted and results presented. The containment strength analysis identified the median ultimate pressure capacity to be 134.9 psig. The analysis was performed for a containment temperature of 400°F. Composite containment failure curves were developed for different confidence levels (5, 50, and 95 percent) and plotted in the IPE. For this study, a single mean curve was developed. This was accomplished by first digitizing the three IPE confidence curves at ten equally spaced probability intervals, then fitting a curve through these three points resulting in a confidence curve at each probability interval. These curves were then averaged at each pressure increment in order to get a single cumulative mean failure probability curve at intervals of 1 psig.

### Calvert Cliffs 1 & 2

The "Containment Ultimate Strength Evaluation" for Calvert Cliffs is presented in Section 4.4 of the Calvert Cliffs IPE. Calvert Cliffs is a large dry containment with a design pressure of 50 psig. A plant-specific analysis was performed by EQE Engineering. A total of seven failure modes were considered. For each failure mode a median failure pressure and log-normal composite uncertainty ( $\beta_c$ ) were listed for various temperatures ranging from 400°F to 800°F. These failure modes were combined and plotted in the IPE. The IPE curve corresponding to a containment temperature of 400°F was then digitized, fitted using a spline program and failure probabilities determined at intervals of 1 psig. The median failure pressure at 400°F was about 116 psig.

### Crystal River 3

The "Containment Ultimate Strength Evaluation" for Crystal River is presented in Section 4.4 of the Crystal River IPE. Crystal River is a large dry containment with a design pressure of 55 psig. A plant-specific analysis was performed by ABB Impell Corporation. A total of seven failure modes were considered. For each failure mode a median failure pressure and log-normal composite uncertainty ( $\beta_c$ ) were listed for various temperatures ranging from 300°F to 800°F. These failure modes were combined and plotted in the IPE. The IPE curve corresponding to a containment temperature of 300°F was then digitized, fitted using a spline program and failure probabilities determined at intervals of 1 psig. The median failure pressure at 300°F was about 122 psig.

### Farley 1 & 2

The "Containment Failure Characterization" for Farley is presented in Section 4.4 of the Farley IPE. Farley is a large dry containment with a design pressure of 54 psig. A plant-specific analysis of the containment was performed and results presented. Various failure modes were considered and mean failure pressures and log-normal uncertainties given for each mode. The most likely failure location was determined to occur in the cylinder wall due to excessive vertical stress. The total containment failure probability curve was computed by combining the fragility curves for each failure mode using Monte Carlo analysis. The combined containment fragility curve is shown in the IPE. This IPE curve was then digitized, fitted using a spline program, and failure probabilities determined at intervals of 1 psig. Temperature effects were not considered in the analysis.

### Fort Calhoun 1

The "Containment Capacity Under Internal Overpressurization" for Fort Calhoun is presented in Section 4.4 of the Fort Calhoun IPE. Fort Calhoun is a large dry containment with a design pressure of 60 psig. A total of eleven failure modes were considered. Mean capacities along with log-normal random and systematic uncertainties were developed for only the seven most probable failure modes. For this study, a log-normal curve was developed from the medians and combined uncertainties ( $\beta_c$ ) for each failure mode. These curves were then combined assuming total independence and failure probabilities computed at intervals of 1 psig. This resulted in a mean failure pressure of about 197 psig. Temperature effects were not considered in the analysis.

### Ginna

The "Containment Failure Characterization" for Ginna is presented in Section 4.4 of the Ginna IPE. Ginna is a large dry containment with a design pressure of 60 psig. A plant-specific analysis was performed by Ebasco Services. Global structural failure was found to be initiated in the hoop reinforcement at a pressure of 155 psia. Liner tearing was estimated to occur at a pressure of 145 psia. These two failure modes with uncertainties of 5 percent were combined to give a median failure pressure of 144 psia (129 psig). This combined containment fragility curve was plotted in the IPE. This IPE curve was then digitized, fitted using a spline program and failure probabilities determined at intervals of 1 psig. Temperature effects were not considered in the analysis.

### Millstone 2

The "Containment Failure Characterization" for Millstone 2 is presented in Section 4.4 of the Millstone 2 IPE. Millstone 2 is a large dry containment with a design pressure of 54 psig. Three modes of failure were subjected to a detailed plant-specific analysis. For each failure mode a median failure pressure and log-normal uncertainties ( $\beta$ ) were listed for various temperatures ranging from 400°F to 800°F. For this study, a log-normal curve was developed from the medians and  $\beta$ s for each failure mode corresponding to a temperature of 400°F. These curves were then combined assuming total independence and failure probabilities computed at intervals of 1 psig. This resulted in a median failure pressure of about 136 psig.



## IPE Fragility Curves

### Oconee 1, 2, & 3

The "Containment Capacity Assessment" for Oconee was performed as part of a PRA submitted along with the Oconee IPE and is documented in Appendix G of the Oconee PRA. Oconee is a large dry containment with a design pressure of 59 psig. The overall shell capacity was determined using finite element analysis and resulted in a mean ultimate capacity of 144 psig. A coefficient of variation was assumed and a curve developed. This IPE curve was then digitized, fitted using a spline program and failure probabilities determined at intervals of 1 psig. Temperature effects were not considered in the analysis.

### Palisades

The "Containment Structural Response and Failure Characterization" for Palisades is presented in Section 3.4 of the Palisades IPE. Palisades is a large dry containment with a design pressure of 55 psig. A plant-specific structural analysis of the containment was conducted and results presented. The compound containment fragility curve was presented in the form of two confidence curves, each curve representing only the random uncertainty. The median failure pressure at 50 percent confidence was about 141 psig. For this study, a single mean curve was developed. This was accomplished by first digitizing the two IPE confidence curves at ten equally spaced probability intervals, then fitting a curve through these two points with a log-normal uncertainty resulting in a confidence curve at each probability interval. These curves were then averaged at each pressure increment in order to get a single cumulative mean failure probability curve at intervals of 1 psig. Temperature effects were not considered in the analysis.

### Palo Verde 1, 2, & 3

The "Containment Failure Characterization" for Palo Verde is presented in Section 11.4 of the Palo Verde IPE. Palo Verde is a large dry containment with a design pressure of 60 psig. A total of seven failure modes were considered. For each failure mode a median failure pressure was given. After combining these failure modes and applying uncertainties a mean containment failure pressure was given as 169 psig. The probability of containment failure was presented in tabular form at increments of 2 psig. Therefore, the IPE data was input, fitted using a spline program and failure probabilities determined at intervals of 1 psig. Temperature effects were not considered in the analysis.

### Point Beach 1 & 2

The "Containment Failure Characterization" for Point Beach is presented in Section 4.4 of the Point Beach IPE. Point Beach is a large dry containment with a design pressure of 60 psig. A plant-specific evaluation of the containment ultimate strength was performed. Two failure modes were determined to determine the containment capacity, hoop tendons and basemat/shell junction. Combining these two modes of failure resulted in a mean failure pressure of 177 psia (162 psig). A plot was developed showing the total failure probability curve and the contribution of each of the two failure modes and is shown in the IPE. This IPE total failure probability curve was then digitized, fitted using a spline program and failure probabilities determined at intervals of 1 psig. Temperature effects were not considered in the analysis.



### Robinson 2

The "Containment Failure Characterization" for Robinson is presented in Section 4.4 of the Robinson IPE. Robinson is a large dry containment with a design pressure of 42 psig. A containment failure assessment was performed and identified five possible failure modes. The median capacity and a plot of failure probability for all five failure modes are shown in the IPE at a temperature of 300°F. However, when the plots were all shown on one graph they changed significantly and appear to be incorrect. Also, a bounding curve was shown to simply envelop the highest failure modes. This is unrealistic since it assumes total dependence between each failure mode. For this study, two containment fragility curves were re-computed for Robinson using the specified medians and determining uncertainties. The first was developed using only the failure mode (wall-basemat shear failure) which yields the highest early failure and has a median failure pressure of 130 psig. The other curve, which is more realistic, was generated by re-combining all the failure modes assuming total independence and resulted in a median failure pressure of 112 psig. Both curves were developed at increments of 1 psig.

### San Onofre 2 & 3

The "Containment Failure Characterization" for San Onofre 2&3 is presented in Section 4.4 of the San Onofre 2&3 IPE. San Onofre is a large dry containment with a design pressure of 60 psig. A plant-specific analysis was performed by EQE Engineering. A total of eight failure modes were considered. For each failure mode a median failure pressure and log-normal composite uncertainty ( $\beta_c$ ) were listed for an initial temperature of 420°F. For this study, a log-normal curve was developed from the medians and  $\beta_c$  for each failure mode corresponding to a temperature of 420°F. These curves were then combined assuming total independence and failure probabilities computed at intervals of 1 psig. This resulted in a median failure pressure of about 135 psig.

### South Texas 1 & 2

The "Containment Structure Evaluation and Failure Characterization" for South Texas is presented in Section 4.4 of the South Texas IPE. South Texas is a large dry containment with a design pressure of 56 psig. Based on a review of the results of a number of plant-specific studies of containment strength and the South Texas design report, median capacities at a temperature of 300°F were assumed. Hoop failure in the cylinder wall was determined in the IPE to govern gross structural failure at a median failure pressure of 136 psig. However, liner tearing is expected to occur much earlier, at a median failure pressure of 112.8 psig. For this study, liner tearing was assumed to govern the containment failure and a fragility curve was developed with the specified log-normal uncertainty of 0.2, and failure probabilities computed at intervals of 1 psig.

### Summer

The "Containment Failure Characterization" for Summer is presented in Section 4.3.2 of the Summer IPE. Summer is a large dry containment with a design pressure of 55 psig. A plant-specific evaluation of the containment ultimate strength was performed. Three failure modes were determined

## IPE Fragility Curves

to dominate the containment capacity. Combining these three modes of failure resulted in a mean failure pressure of 142 psig. A plot was developed showing the total failure probability curve and the contribution of each of the three failure modes and is shown in the IPE. This IPE total failure probability curve was then digitized, fitted using a spline program and failure probabilities determined at intervals of 1 psig. Temperature effects were not considered in the analysis.

### Three Mile Island 1

The "TMI-1 Containment Capacity" for Three Mile Island 1 (TMI-1) was performed as part of a PRA submitted along with the TMI-1 IPE and is documented in Appendix I of the TMI-1 PRA. TMI-1 is a large dry containment with a design pressure of 55 psig. Comparisons were made in the PRA with the containment at Oconee and it was determined that the containment fragility curves for Oconee could be used directly for TMI-1. The same mean failure pressure for Oconee of 144 psig was not modified in the TMI-1 PRA. Therefore the same fragility curve developed for Oconee was digitized, fitted using a spline program and failure probabilities determined at intervals of 1 psig. Temperature effects were not considered in the analysis.

### Trojan

The "Containment Failure Characterization" for Trojan is presented in Section 4.4 of the Trojan IPE. Although the Trojan Nuclear Plant is now closed, the IPE was already submitted and easily accessible, so the containment fragility curves were cataloged for this study. Trojan is a large dry containment with a design pressure of 60 psig. Several failure modes were considered and their individual ultimate pressure capacities given. Failure in the cylinder tendons due to excessive hoop stresses was the limiting failure pressure with a capacity of 151 psig. This value was then taken as a median and using the uncertainty developed for the NUREG-1150 Zion containment, a probability of containment failure was developed and shown in the IPE. This IPE curve was then digitized, fitted using a spline program and failure probabilities determined at intervals of 1 psig. Temperature effects were not considered in the analysis.

### Turkey Point 3 & 4

The "Turkey Point Containment Failure Pressure Characterization" is presented in Section 4.4 of the Turkey Point IPE. Turkey Point is a large dry containment with a design pressure of 59 psig. The containment response to potential pressure loads was evaluated for two failure modes, structural failure and liner tearing. The overall containment failure pressure was estimated to be 150 psig. To obtain uncertainty, an adjustment of the pressure loads calculated for Surry in the NUREG-1150 study were used to characterize the pressure distribution for Turkey Point. The resulting containment fragility curve is shown in the IPE in Section 4.6. This IPE curve was then digitized, fitted using a spline program and failure probabilities determined at intervals of 1 psig. Temperature effects were not considered in the analysis.

### Vogle 1 & 2

The "Containment Failure Characterization" for Vogle is presented in Section 4.4 of the Vogle IPE. Vogle is a large dry containment with a design pressure of 52 psig. A plant-specific evaluation of the containment ultimate strength was performed. Three failure modes were determined to dominate the containment capacity. Combining these three modes of failure resulted in a mean failure pressure of about 139 psig. A plot was developed showing the total failure probability curve and the contribution of each of the three failure modes and is shown in the IPE. This IPE total failure probability curve was then digitized, fitted using a spline program and failure probabilities determined at intervals of 1 psig. Temperature effects were not considered in the analysis.

### Wolf Creek

The "Containment Failure Characterization" for Wolf Creek is presented in Section 4.2.5 of the Wolf Creek IPE. Wolf Creek is a large dry containment with a design pressure of 60 psig. A plant-specific evaluation of the containment ultimate strength was performed. A median probability of failure was given as 127.6 psig. A 95 percent upper bound pressure was given as 136 psig and 5 percent lower bound pressure was given as 99 psig. For this study, a spline was fitted through these three points and failure probabilities determined at intervals of 1 psig. Temperature effects were not considered in the analysis.

### Zion 1 & 2

The "Containment Analysis" for Zion is presented in Section 4.3 of the Zion IPE. Zion is a large dry containment with a design pressure of 47 psig. A plant-specific evaluation of the containment ultimate strength was performed. Two failure modes were determined to dominate the containment capacity, hoop tendons and basemat/cylinder junction. Combining these two modes of failure resulted in a mean failure pressure of about 134 psig. A plot was developed showing the total failure probability curve and the contribution of each of the two failure modes and is shown in the IPE. This IPE total failure probability curve was then digitized, fitted using a spline program and failure probabilities determined at intervals of 1 psig. Temperature effects were not considered in the analysis.

## D.4.2 Comparison of Prestressed Concrete Containments

All the data above was combined into a single spreadsheet for plotting and comparison purposes. Figures D.11 through D.14 compare all the prestressed concrete containment fragility curves. All graphs were plotted over the same range of pressures (40-200 psig) for comparison purposes. There are no ice condenser type prestressed concrete containments. It is interesting to note that for containments with the highest design pressures (59-61 psig), the larger containments (diameter = 135-150 ft) typically failed at lower pressure than did the smaller containments (diameter = 105-124 ft), as shown in Figures D.11 and D.12. The containments with a medium design pressure (55-56 psig) and lower design pressures (42-54 psig) were both very similar, with median failure pressures all in the range of 110-150 psig, as shown in Figures D.13 and D.14.

## IPE Fragility Curves

These variations in the fragilities might result from the different accident pressures used in the original containment design. Therefore, each of the containment fragility curves was normalized to the design accident pressure for that containment. These normalized fragility curves are shown for all the prestressed concrete containments in Figures D.15 through D.17. The larger containments (diameter = 135-150 ft) are shown in Figure D.15, the medium sized containments (diameter = 124-130 ft) in Figure D.16, and the smaller containments (diameter = 105-116 ft) in Figure D.17. All these plots show very good agreement among all prestressed concrete containments. The size of the containment does not appear to greatly influence the capacity. Out of the 25 prestressed concrete containments shown, only two have median failures outside 2-3 times the design pressure range.

### D.5 Spreadsheet of Containment Failure Probabilities

The failure probabilities developed above in Sections D.2 through D.4 for all the PWR steel, reinforced and prestressed concrete containments were combined into a single spreadsheet. This spreadsheet lists each of the PWR containment by name across the top and pressure along the first column in increments of 1 psig, ranging from 20 psig up to 300 psig. The MPa-abs conversion is in the second column and ranges from 0.239 to 2.170. Each of the containment failure probabilities were then entered to match the appropriate internally applied pressure for all 51 containment fragility curves. This spreadsheet was then used to compare failure probabilities and plot the containment fragility curves shown in this report. This spreadsheet is shown in Table D.2 for every containment and pressure ranging from 20 to 260 psig (0.239 to 1.894 MPa-abs).

A separate spreadsheet was also developed for all the containment fragility curves normalized to the design pressure of each containment. This spreadsheet is in the same format as the spreadsheet described above except that the first column is the ratio of applied pressure to design pressure ranging from 0.20 to 8.00 in increments of 0.02. The primary use of this spreadsheet was to plot the normalized containment fragility curves for comparison purposes, as shown in Sections D.2 through D.4.

### D.6 References

Lobner, P., et al. (1990). *Overview and Comparison of U.S. Commercial Nuclear Power Plants*, NUREG/CR-5640, SAIC-89/1541, Science Applications International Corporation.



Table D.1 Comparison of PWR Containments

Plant Name	Construction Material	Design Pressure (psig)	Internal Diameter (ft)	Primary Containment Type	Status
ANO-1	Prestressed Concr.	59	116	Dry	Oper.
ANO-2	Prestressed Concr.	54	116	Dry	Oper.
Beaver Valley 1 & 2	Reinforced Concr.	45	126	Subatmosp.	Oper.
Bellefonte 1 & 2	Prestressed Concr.	50	135	Dry	Cancel.
Braidwood 1 & 2	Prestressed Concr.	61	140	Dry	Oper.
Byron 1 & 2	Prestressed Concr.	61	140	Dry	Oper.
Callaway	Prestressed Concr.	60	140	Dry	Oper.
Calvert Cliffs 1 & 2	Prestressed Concr.	50	130	Dry	Oper.
Catawba 1 & 2	Steel	30	115	Ice Condens.	Oper.
Comanche Peak 1 & 2	Reinforced Concr.	50	135	Dry	Oper.
Crystal River 3	Prestressed Concr.	55	130	Dry	Oper.
D. C. Cook 1 & 2	Reinforced Concr.	12	115	Ice Condens.	Oper.
Davis Besse	Steel	40	130	Dry	Oper.
Diablo Canyon 1 & 2	Reinforced Concr.	47	140	Dry	Oper.
Farley 1 & 2	Prestressed Concr.	54	130	Dry	Oper.
Fort Calhoun 1	Prestressed Concr.	60	110	Dry	Oper.
Ginna	Prestressed Concr.	60	105	Dry	Oper.
Haddam Neck	Reinforced Concr.	40	136	Dry	Oper.
Indian Point 2	Reinforced Concr.	47	135	Dry	Oper.
Indian Point 3	Reinforced Concr.	47	135	Dry	Oper.
Kewaunee	Steel	46	108	Dry	Oper.
Maine Yankee	Reinforced Concr.	55	135	Dry	Oper.
McGuire 1 & 2	Reinforced Concr.	28	115	Ice Condens.	Oper.
Millstone 2	Prestressed Concr.	54	130	Dry	Oper.
Millstone 3	Reinforced Concr.	45	140	Subatmosp.	Oper.
North Anna 1 & 2	Reinforced Concr.	45	126	Subatmosp.	Oper.



Table D.1 Comparison of PWR Containments (continued)

Plant Name	Construction Material	Design Pressure (psig)	Internal Diameter (ft)	Primary Containment Type	Status
Oconee 1, 2, & 3	Prestressed Concr.	59	116	Dry	Oper.
Palisades	Prestressed Concr.	55	116	Dry	Oper.
Palo Verde 1, 2, & 3	Prestressed Concr.	60	146	Dry	Oper.
Point Beach 1 & 2	Prestressed Concr.	60	105	Dry	Oper.
Prairie Island 1 & 2	Steel	41	105	Dry	Oper.
Rancho Seco	Prestressed Concr.	59	130	Dry	Closed
Robinson 2	Prestressed Concr.	42	130	Dry	Oper.
Salem 1 & 2	Reinforced Concr.	47	140	Dry	Oper.
San Onofre 1	Steel	47	140	Dry	Closed
San Onofre 2 & 3	Prestressed Concr.	60	150	Dry	Oper.
Seabrook 1	Reinforced Concr.	65	140	Dry	Oper.
Sequoyah 1 & 2	Steel	10.8	106	Ice Condens.	Oper.
Shearon Harris 1	Reinforced Concr.	45	130	Dry	Oper.
South Texas 1 & 2	Prestressed Concr.	56	150	Dry	Oper.
St. Lucie 1 & 2	Steel	44	140	Dry	Oper.
Summer	Prestressed Concr.	55	126	Dry	Oper.
Surry 1 & 2	Reinforced Concr.	45	126	Subatmosph.	Oper.
Three Mile Island 1	Prestressed Concr.	55	130	Dry	Oper.
Trojan	Prestressed Concr.	60	124	Dry	Closed
Turkey Point 3 & 4	Prestressed Concr.	59	116	Dry	Oper.
Vogtle 1 & 2	Prestressed Concr.	52	140	Dry	Oper.
Waterford 3	Steel	44	140	Dry	Oper.
Watts Bar 1 & 2	Steel	15	115	Ice Condens.	Constr.
Wolf Creek	Prestressed Concr.	60	135	Dry	Oper.
Yankee Rowe	Steel	34	125	Dry	Closed
Zion 1 & 2	Prestressed Concr.	47	141	Dry	Oper.

Table D.2 Cumulative containment failure probabilities

Name	ANQ-1	ANQ-2	Beaver V.	Braidw 1	Braidw 2	Byron 1	Byron 2	Celewey	Celvert	Celewob	Comanche	Crystal	Cook	
Material	Pre Conc.	Pre Conc.	Re Conc.	Pre Conc.	Pre Conc.	Pre Conc.	Pre Conc.	Pre Conc.	Pre Conc.	Steel	Re Conc.	Pre Conc.	Re Conc.	
Cont. Type	Dry	Dry	Bub.	Dry	Dry	Dry	Dry	Dry	Dry	Ice	Dry	Dry	Ice	
Design Pressure (psig)	56	54	45	61	61	61	61	60	60	30	60	65	12	
Analysis Temp.	No Temp	No Temp	No Temp	No Temp	No Temp	No Temp	No Temp	400 F	400 F	30	No Temp	300 F	12	
FR Type	adj Surry	adj Surry	Surry	Byron 1	Byron 2	Best Est.	Best Est.	Est FR	Best Est.	Best Est.	Normal	Best Est.	LnM&B	
PSIG	MPa abs													
20	0.239	0	0	0	0	0	0	0	0	0	0	0	0	
21	0.246	0	0	0	0	0	0	0	0	0	0	0	0	
22	0.253	0	0	0	0	0	0	0	0	0	0	0	0	
23	0.260	0	0	0	0	0	0	0	0	0	0	0	0	
24	0.267	0	0	0	0	0	0	0	0	0	0	0	0	
25	0.274	0	0	0	0	0	0	0	0	0	0	0	0	
26	0.281	0	0	0	0	0	0	0	0	0	0	0	0	
27	0.287	0	0	0	0	0	0	0	0	0	0	0	0	
28	0.294	0	0	0	0	0	0	0	0	0	0	0	0.0001	
29	0.301	0	0	0	0	0	0	0	0	0	0	0	0.0001	
30	0.308	0	0	0	0	0	0	0	0	0	0	0	0.0002	
31	0.315	0	0	0	0	0	0	0	0	0	0	0	0.0005	
32	0.322	0	0	0	0	0	0	0	0	0	0	0	0.0008	
33	0.329	0	0	0	0	0	0	0	0	0	0	0	0.0014	
34	0.336	0	0	0	0	0	0	0	0	0	0	0	0.0023	
35	0.343	0	0	0	0	0	0	0	0	0	0	0	0.0037	
36	0.350	0	0	0	0	0	0	0	0	0	0	0	0.0057	
37	0.356	0	0	0	0	0	0	0	0	0	0	0	0.0084	
38	0.363	0	0	0	0	0	0	0	0	0	0	0	0.0121	
39	0.370	0	0	0	0	0	0	0	0	0	0	0	0.0171	
40	0.377	0	0	0	0	0	0	0	0	0	0	0	0.0235	
41	0.384	0	0	0	0	0	0	0	0	0	0	0	0.0315	
42	0.391	0	0	0	0	0	0	0	0	0	0	0	0.0414	
43	0.398	0	0	0	0	0	0	0	0	0	0	0	0.0534	
44	0.405	0	0	0	0	0	0	0	0	0	0	0	0.0676	
45	0.412	0	0	0	0	0	0	0	0	0	0	0	0.0841	
46	0.418	0	0	0	0	0	0	0	0	0	0	0	0.103	
47	0.425	0	0	0	0	0	0	0	0	0	0	0	0.1244	
48	0.432	0	0	0	0	0	0	0	0	0	0	0	0.1481	
49	0.439	0	0	0	0	0	0	0	0	0	0	0	0.174	
50	0.446	0	0	0	0	0	0	0	0	0	0	0	0.2021	
51	0.453	0	0	0	0	0	0	0	0	0	0	0	0.232	
52	0.460	0	0	0	0	0	0	0	0	0	0	0	0.2636	
53	0.467	0	0	0	0	0	0	0	0	0	0	0	0.2966	
54	0.474	0	0	0	0	0	0	0	0	0	0	0	0.3307	
55	0.481	0	0	0	0	0	0	0	0	0	0	0	0.3656	
56	0.487	0	0	0	0	0	0	0	0	0	0	0	0.401	
57	0.494	0	0	0	0	0	0	0	0	0.0033	0	0	0.4365	
58	0.501	0	0	0	0	0	0	0	0	0.0058	0	0	0.4719	
59	0.508	0	0	0	0	0	0	0	0	0.0089	0	0	0.507	
60	0.515	0	0	0	0	0	0	0	0	0.0075	0	0	0.5413	
61	0.522	0	0	0	0	0	0	0	0	0.0089	0	0	0.5748	
62	0.529	0	0	0	0	0	0	0	0	0.0115	0	0	0.607	
63	0.536	0	0	0	0	0	0	0	0	0.0151	0	0	0.6384	
64	0.543	0	0	0	0	0	0	0	0	0.0196	0	0.0001	0.6682	
65	0.549	0	0	0	0	0	0	0	0	0.0251	0	0.0003	0.6966	
66	0.556	0	0	0	0	0	0	0	0.0002	0.0319	0	0.0009	0.7234	
67	0.563	0	0	0	0	0	0	0	0.001	0.0403	0	0.0017	0.7486	
68	0.570	0	0	0	0	0	0	0	0.0023	0.0504	0	0.0027	0.7722	
69	0.577	0	0	0	0	0	0	0	0.0039	0.0621	0	0.0039	0.7941	
70	0.584	0	0	0	0	0	0	0	0.0055	0.0753	0	0.0052	0.8145	
71	0.591	0	0	0	0	0	0	0	0.007	0.0901	0	0.0069	0.8333	
72	0.598	0	0	0	0	0	0	0	0.0086	0.1067	0	0.0087	0.8506	
73	0.605	0	0	0	0	0	0	0	0.0104	0.1257	0	0.0106	0.8664	
74	0.612	0	0	0.0003	0.0001	0.0003	0.0001	0	0.0127	0.1482	0	0.0124	0.8808	
75	0.618	0	0	0.0005	0.0006	0.0005	0.0006	0.0005	0	0.0154	0.1739	0	0.0142	0.894
76	0.625	0	0	0.0012	0.0016	0.001	0.0016	0.001	0	0.0183	0.1991	0	0.0163	0.9059
77	0.632	0	0	0.0024	0.0038	0.0029	0.0038	0.0029	0	0.0213	0.2242	0	0.0188	0.9166
78	0.639	0	0	0.0039	0.0052	0.0043	0.0052	0.0043	0	0.0247	0.2531	0	0.0217	0.9263
79	0.646	0	0	0.0056	0.0066	0.006	0.0066	0.006	0	0.0287	0.2863	0	0.0248	0.935
80	0.653	0	0	0.0076	0.008	0.008	0.008	0.008	0	0.0335	0.3193	0	0.0282	0.9427
81	0.660	0	0	0.0096	0.0095	0.0104	0.0095	0.0104	0	0.0394	0.3501	0	0.0317	0.9497
82	0.667	0	0	0.0117	0.011	0.0132	0.011	0.0132	0	0.0457	0.3812	0	0.0352	0.9558
83	0.674	0	0	0.0138	0.0125	0.0164	0.0125	0.0164	0	0.0534	0.4165	0	0.0389	0.9613
84	0.680	0	0	0.0156	0.0142	0.02	0.0142	0.02	0	0.0614	0.4512	0.0001	0.0427	0.9662
85	0.687	0	0	0.0173	0.016	0.0242	0.016	0.0242	0	0.0698	0.4819	0.0001	0.0466	0.9705
86	0.694	0	0	0.0188	0.018	0.0299	0.018	0.0299	0	0.073	0.513	0.0002	0.0513	0.9743
87	0.701	0	0.0001	0.0204	0.0202	0.0382	0.0202	0.0382	0	0.0807	0.5452	0.0004	0.0565	0.9776
88	0.708	0	0.0004	0.0222	0.0226	0.0504	0.0226	0.0504	0	0.09	0.5789	0.0006	0.0623	0.9805
89	0.715	0	0.001	0.0246	0.0253	0.0675	0.0253	0.0675	0	0.1002	0.6152	0.0009	0.0687	0.9831
90	0.722	0	0.002	0.0278	0.0283	0.0882	0.0283	0.0882	0	0.1101	0.738	0.0013	0.0735	0.9854
91	0.729	0	0.0034	0.032	0.0317	0.1115	0.0317	0.1115	0	0.1188	0.7747	0.002	0.0802	0.9873
92	0.736	0	0.0051	0.0371	0.0355	0.1436	0.0355	0.1436	0.0002	0.1273	0.8062	0.0029	0.0848	0.989
93	0.743	0	0.007	0.0429	0.0399	0.1902	0.0399	0.1902	0.0006	0.1373	0.8337	0.0043	0.0918	0.9905
94	0.749	0	0.009	0.0492	0.0449	0.2463	0.0449	0.2463	0.0011	0.1504	0.8583	0.0061	0.1	0.9918
95	0.756	0	0.0111	0.0557	0.0506	0.3068	0.0506	0.3068	0.0018	0.1652	0.8807	0.0086	0.111	0.993
96	0.763	0	0.0131	0.0623	0.057	0.3772	0.057	0.3772	0.0025	0.179	0.9006	0.0121	0.1256	0.9939
97	0.770	0	0.015	0.0689	0.0641	0.4615	0.0641	0.4615	0.0034	0.1898	0.9174	0.0166	0.14	0.9948
98	0.777	0	0.0168	0.0757	0.0718	0.5478	0.0718	0.5478	0.0043	0.1988	0.9314	0.0225	0.1502	0.9955
99	0.784	0	0.0183	0.0829	0.0801	0.629	0.0801	0.629	0.0052	0.2082	0.9429	0.0301	0.1605	0.9962
100	0.791	0.0001	0.0199	0.0906	0.089	0.7048	0.089	0.7048	0.0061	0.2199	0.9523	0.0397	0.1712	0.9967

Table D.2 Cumulative containment failure probabilities (continued)

Name	ANO-1	ANO-2	Beaver V.	Straded 1	Straded 2	Byron 1	Byron 2	Cadwney	Cadwney	Cadwney	Comanche	Crystal	Cook	
Material	Pre Conc	Pre Conc	Re Conc.	Pre Conc	Pre Conc	Pre Conc	Pre Conc	Pre Conc	Pre Conc	Pre Conc	Re Conc.	Pre Conc	Re Conc.	
Cont. Type	Dry	Dry	Sub.	Dry	Dry	Dry	Dry	Dry	Dry	Dry	Dry	Dry	Ice	
Design Pressure (psig)	50	64	45	61	61	61	61	60	50	30	60	65	12	
Analysis Temp.	No Temp	No Temp	No Temp	No Temp	No Temp	No Temp	No Temp	400 F	400 F	No temp	No Temp	300 F	No Temp	
Fit Type	adj Surry	adj Surry	Surry	Byron 1	Byron 2	Best Est	Best Est	Est Fit	Best Est	Best Est	HorM&V	Best Est	LnM&B	
PSIG	MPa abs													
101	0.798	0.0004	0.0216	0.0099	0.0985	0.7748	0.0985	0.7748	0.007	0.2339	0.9507	0.0516	0.1825	0.9976
102	0.805	0.001	0.0239	0.1079	0.1067	0.8365	0.1067	0.8365	0.0078	0.2457	0.9585	0.0663	0.1845	0.9979
103	0.811	0.002	0.0289	0.1171	0.1196	0.8576	0.1196	0.8576	0.0087	0.2656	0.9752	0.084	0.2071	0.9982
104	0.818	0.0034	0.0306	0.1296	0.1311	0.9276	0.1311	0.9276	0.0096	0.2838	0.9802	0.1051	0.2203	0.9985
105	0.825	0.0051	0.0356	0.136	0.1432	0.9509	0.1432	0.9509	0.0106	0.301	0.9836	0.1297	0.2337	0.9987
106	0.832	0.007	0.0412	0.1456	0.156	0.9766	0.156	0.9766	0.0116	0.3179	0.986	0.158	0.2472	0.9989
107	0.839	0.009	0.0473	0.156	0.1694	0.9885	0.1694	0.9885	0.0127	0.3341	0.988	0.1902	0.2602	0.9991
108	0.846	0.0111	0.0538	0.1678	0.1836	0.9952	0.1836	0.9952	0.0139	0.3502	0.99	0.2261	0.2733	0.9992
109	0.853	0.0131	0.0602	0.1818	0.1987	0.9987	0.1987	0.9987	0.0152	0.3667	0.9916	0.2655	0.2868	0.9993
110	0.860	0.015	0.0667	0.1985	0.2148	1	0.2148	1	0.0167	0.3841	0.9928	0.3061	0.3012	0.9994
111	0.867	0.0168	0.0734	0.2194	0.2318	1	0.2318	1	0.0185	0.4026	0.9936	0.3535	0.3164	0.9995
112	0.874	0.0183	0.0804	0.2425	0.2497	1	0.2497	1	0.0205	0.4206	0.9945	0.401	0.332	0.9996
113	0.880	0.0199	0.0879	0.2664	0.2682	1	0.2682	1	0.023	0.4377	0.9959	0.4501	0.3474	0.9996
114	0.887	0.0216	0.0961	0.2892	0.2871	1	0.2871	1	0.0259	0.4544	0.9975	0.5	0.3624	0.9997
115	0.894	0.0239	0.1049	0.309	0.3064	1	0.3064	1	0.0294	0.4725	1	0.5499	0.3772	0.9997
116	0.901	0.0269	0.1141	0.3242	0.3261	1	0.3261	1	0.0336	0.4917	1	0.599	0.3918	0.9998
117	0.908	0.0308	0.1236	0.3355	0.3462	1	0.3462	1	0.0386	0.5114	1	0.6465	0.4063	0.9998
118	0.915	0.0356	0.1332	0.3444	0.3665	1	0.3665	1	0.0447	0.5307	1	0.6919	0.4212	0.9998
119	0.922	0.0412	0.1428	0.3526	0.387	1	0.387	1	0.052	0.5488	1	0.7345	0.4369	0.9999
120	0.929	0.0473	0.1528	0.3616	0.4076	1	0.4076	1	0.0608	0.5654	1	0.7739	0.453	0.9999
121	0.936	0.0538	0.1641	0.3728	0.4283	1	0.4283	1	0.0712	0.5821	1	0.8098	0.4692	0.9999
122	0.942	0.0602	0.1774	0.3863	0.4496	1	0.4496	1	0.0837	0.6002	1	0.842	0.485	0.9999
123	0.949	0.0667	0.1934	0.4018	0.4719	1	0.4719	1	0.0985	0.6193	1	0.8703	0.5013	0.9999
124	0.956	0.0734	0.2128	0.4187	0.4958	1	0.4958	1	0.1159	0.6379	1	0.8949	0.519	0.9999
125	0.963	0.0804	0.2354	0.4365	0.52	1	0.52	1	0.1362	0.6549	1	0.916	0.5367	1
126	0.970	0.0879	0.2592	0.4548	0.5438	1	0.5438	1	0.1597	0.6698	1	0.9337	0.5525	1
127	0.977	0.0961	0.2826	0.4731	0.567	1	0.567	1	0.1868	0.6843	1	0.9484	0.5669	1
128	0.984	0.1049	0.3034	0.491	0.5899	1	0.5899	1	0.2176	0.6998	1	0.9603	0.5812	1
129	0.991	0.1141	0.3201	0.506	0.6126	1	0.6126	1	0.2521	0.716	1	0.9699	0.5965	1
130	0.998	0.1236	0.3324	0.5242	0.6352	1	0.6352	1	0.2904	0.7321	1	0.9775	0.6126	1
131	1.005	0.1332	0.3419	0.5402	0.6579	1	0.6579	1	0.3322	0.7475	1	0.9834	0.6285	1
132	1.011	0.1428	0.3501	0.5562	0.6808	1	0.6808	1	0.3774	0.7618	1	0.9879	0.6435	1
133	1.018	0.1528	0.3587	0.5728	0.704	1	0.704	1	0.4254	0.7748	1	0.9914	0.6577	1
134	1.025	0.1641	0.3691	0.5903	0.7273	1	0.7273	1	0.4756	0.7873	1	0.9938	0.6716	1
135	1.032	0.1774	0.3821	0.6093	0.7501	1	0.7501	1	0.5271	0.7998	1	0.9957	0.6853	1
136	1.039	0.1934	0.397	0.63	0.7719	1	0.7719	1	0.5789	0.8129	1	0.9971	0.699	1
137	1.046	0.2128	0.4135	0.6524	0.7923	1	0.7923	1	0.6301	0.8262	1	0.998	0.7126	1
138	1.053	0.2354	0.4311	0.6762	0.8112	1	0.8112	1	0.6796	0.8393	1	0.9987	0.726	1
139	1.060	0.2592	0.4493	0.7012	0.8293	1	0.8293	1	0.7266	0.8518	1	0.9991	0.7392	1
140	1.067	0.2826	0.4677	0.7272	0.8469	1	0.8469	1	0.7704	0.8634	1	0.9994	0.7522	1
141	1.073	0.3034	0.4857	0.7538	0.8645	1	0.8645	1	0.8103	0.8743	1	0.9995	0.765	1
142	1.080	0.3201	0.503	0.7809	0.8813	1	0.8813	1	0.8461	0.8844	1	0.9996	0.7775	1
143	1.087	0.3324	0.5194	0.8082	0.8968	1	0.8968	1	0.8775	0.8937	1	0.9999	0.7894	1
144	1.094	0.3419	0.5354	0.8354	0.9103	1	0.9103	1	0.9046	0.9023	1	0.9999	0.8004	1
145	1.101	0.3501	0.5514	0.862	0.9216	1	0.9216	1	0.9275	0.9101	1	0.9999	0.8109	1
146	1.108	0.3587	0.5677	0.8873	0.9322	1	0.9322	1	0.9462	0.9172	1	1	0.821	1
147	1.115	0.3691	0.585	0.9107	0.9422	1	0.9422	1	0.9614	0.9236	1	1	0.8309	1
148	1.122	0.3821	0.6034	0.9317	0.9519	1	0.9519	1	0.9733	0.9294	1	1	0.8409	1
149	1.129	0.397	0.6236	0.9495	0.9611	1	0.9611	1	0.9823	0.9349	1	1	0.851	1
150	1.136	0.4135	0.6455	0.9635	0.9691	1	0.9691	1	0.9889	0.9402	1	1	0.8606	1
151	1.142	0.4311	0.669	0.9734	0.9761	1	0.9761	1	0.9934	0.9457	1	1	0.8702	1
152	1.149	0.4493	0.6936	0.9798	0.9819	1	0.9819	1	0.9965	0.9513	1	1	0.879	1
153	1.156	0.4677	0.7193	0.9835	0.9867	1	0.9867	1	0.9983	0.9569	1	1	0.8872	1
154	1.163	0.4857	0.7458	0.9855	0.9907	1	0.9907	1	0.9993	0.9622	1	1	0.8949	1
155	1.170	0.503	0.7727	0.9866	0.9938	1	0.9938	1	0.9998	0.9671	1	1	0.9021	1
156	1.177	0.5194	0.8	0.9876	0.9962	1	0.9962	1	1	0.9714	1	1	0.909	1
157	1.184	0.5354	0.8273	0.9888	0.9979	1	0.9979	1	1	0.975	1	1	0.9155	1
158	1.191	0.5514	0.8541	0.99	0.9991	1	0.9991	1	1	0.9778	1	1	0.9215	1
159	1.198	0.5677	0.8799	0.9913	0.9997	1	0.9997	1	1	0.9795	1	1	0.9271	1
160	1.204	0.585	0.9039	0.9926	1	1	1	1	1	0.9807	1	1	0.9323	1
161	1.211	0.6034	0.9257	0.994	1	1	1	1	1	0.9819	1	1	0.9372	1
162	1.218	0.6236	0.9445	0.9955	1	1	1	1	1	0.9833	1	1	0.9419	1
163	1.225	0.6455	0.9567	0.997	1	1	1	1	1	0.9849	1	1	0.9466	1
164	1.232	0.669	0.9708	0.9985	1	1	1	1	1	0.9867	1	1	0.9512	1
165	1.239	0.6936	0.9781	1	1	1	1	1	1	0.9877	1	1	0.9558	1
166	1.246	0.7193	0.9826	1	1	1	1	1	1	0.988	1	1	0.96	1
167	1.253	0.7458	0.985	1	1	1	1	1	1	0.993	1	1	0.9637	1
168	1.260	0.7727	0.9863	1	1	1	1	1	1	0.9953	1	1	0.9667	1
169	1.267	0.8	0.9873	1	1	1	1	1	1	0.9976	1	1	0.9693	1
170	1.273	0.8273	0.9885	1	1	1	1	1	1	1	1	1	0.9717	1
171	1.280	0.8541	0.9897	1	1	1	1	1	1	1	1	1	0.9745	1
172	1.287	0.8799	0.991	1	1	1	1	1	1	1	1	1	0.9778	1
173	1.294	0.9039	0.9924	1	1	1	1	1	1	1	1	1	0.9814	1
174	1.301	0.9257	0.9938	1	1	1	1	1	1	1	1	1	0.9845	1
175	1.308	0.9445	0.9953	1	1	1	1	1	1	1	1	1	0.9865	1
176	1.315	0.9567	0.9969	1	1	1	1	1	1	1	1	1	0.9874	1
177	1.322	0.9708	0.9984	1	1	1	1	1	1	1	1	1	0.9879	1
178	1.329	0.9781	1	1	1	1	1	1	1	1	1	1	0.9884	1
179	1.335	0.9826	1	1	1	1	1	1	1	1	1	1	0.989	1
180	1.342	0.985	1	1	1	1	1	1	1	1	1	1	0.99	1

Table D.2 Cumulative containment failure probabilities (continued)

Name	AND-1	AND-2	Beaver V.	Braided 1	Braided 2	Byron 1	Byron 2	Calhoun	Calvert	Catawba	Comanche	Crystal	Cook
Material	Pre Conc	Pre Conc	Re Conc.	Pre Conc	Pre Conc	Pre Conc	Pre Conc	Pre Conc	Pre Conc	Steel	Re Conc.	Pre Conc	Re Conc.
Cont. Type	Dry	Dry	Sub.	Dry	Dry	Dry	Dry	Dry	Dry	Ice	Dry	Dry	Ice
Design Pressure (psig)	89	84	45	61	61	61	61	60	50	30	60	65	12
Analysis Temp.	No Temp	No Temp	No Temp	No Temp	No Temp	No Temp	No Temp	400 F	400 F	No temp	No Temp	300 F	No Temp
Fit Type	adj Surry	adj Surry	Surry	Byron 1	Byron 2	Best Est.	Best Est.	Est Fit	Best Est.	Best Est.	NonW&V	Best Est.	LW&B
PSIG	MPa abs												
181	1.349	0.9863	1	1	1	1	1	1	1	1	1	0.9914	1
182	1.356	0.9873	1	1	1	1	1	1	1	1	1	0.9934	1
183	1.363	0.9885	1	1	1	1	1	1	1	1	1	0.996	1
184	1.370	0.9897	1	1	1	1	1	1	1	1	1	0.9985	1
185	1.377	0.991	1	1	1	1	1	1	1	1	1	1	1
186	1.384	0.9924	1	1	1	1	1	1	1	1	1	1	1
187	1.391	0.9938	1	1	1	1	1	1	1	1	1	1	1
188	1.396	0.9953	1	1	1	1	1	1	1	1	1	1	1
189	1.404	0.9969	1	1	1	1	1	1	1	1	1	1	1
190	1.411	0.9984	1	1	1	1	1	1	1	1	1	1	1
191	1.418	1	1	1	1	1	1	1	1	1	1	1	1
192	1.425	1	1	1	1	1	1	1	1	1	1	1	1
193	1.432	1	1	1	1	1	1	1	1	1	1	1	1
194	1.439	1	1	1	1	1	1	1	1	1	1	1	1
195	1.446	1	1	1	1	1	1	1	1	1	1	1	1
196	1.453	1	1	1	1	1	1	1	1	1	1	1	1
197	1.460	1	1	1	1	1	1	1	1	1	1	1	1
198	1.466	1	1	1	1	1	1	1	1	1	1	1	1
199	1.473	1	1	1	1	1	1	1	1	1	1	1	1
200	1.480	1	1	1	1	1	1	1	1	1	1	1	1
201	1.487	1	1	1	1	1	1	1	1	1	1	1	1
202	1.494	1	1	1	1	1	1	1	1	1	1	1	1
203	1.501	1	1	1	1	1	1	1	1	1	1	1	1
204	1.506	1	1	1	1	1	1	1	1	1	1	1	1
205	1.515	1	1	1	1	1	1	1	1	1	1	1	1
206	1.522	1	1	1	1	1	1	1	1	1	1	1	1
207	1.529	1	1	1	1	1	1	1	1	1	1	1	1
208	1.536	1	1	1	1	1	1	1	1	1	1	1	1
209	1.542	1	1	1	1	1	1	1	1	1	1	1	1
210	1.549	1	1	1	1	1	1	1	1	1	1	1	1
211	1.556	1	1	1	1	1	1	1	1	1	1	1	1
212	1.563	1	1	1	1	1	1	1	1	1	1	1	1
213	1.570	1	1	1	1	1	1	1	1	1	1	1	1
214	1.577	1	1	1	1	1	1	1	1	1	1	1	1
215	1.584	1	1	1	1	1	1	1	1	1	1	1	1
216	1.591	1	1	1	1	1	1	1	1	1	1	1	1
217	1.597	1	1	1	1	1	1	1	1	1	1	1	1
218	1.604	1	1	1	1	1	1	1	1	1	1	1	1
219	1.611	1	1	1	1	1	1	1	1	1	1	1	1
220	1.618	1	1	1	1	1	1	1	1	1	1	1	1
221	1.625	1	1	1	1	1	1	1	1	1	1	1	1
222	1.632	1	1	1	1	1	1	1	1	1	1	1	1
223	1.639	1	1	1	1	1	1	1	1	1	1	1	1
224	1.646	1	1	1	1	1	1	1	1	1	1	1	1
225	1.653	1	1	1	1	1	1	1	1	1	1	1	1
226	1.660	1	1	1	1	1	1	1	1	1	1	1	1
227	1.666	1	1	1	1	1	1	1	1	1	1	1	1
228	1.673	1	1	1	1	1	1	1	1	1	1	1	1
229	1.680	1	1	1	1	1	1	1	1	1	1	1	1
230	1.687	1	1	1	1	1	1	1	1	1	1	1	1
231	1.694	1	1	1	1	1	1	1	1	1	1	1	1
232	1.701	1	1	1	1	1	1	1	1	1	1	1	1
233	1.708	1	1	1	1	1	1	1	1	1	1	1	1
234	1.715	1	1	1	1	1	1	1	1	1	1	1	1
235	1.722	1	1	1	1	1	1	1	1	1	1	1	1
236	1.728	1	1	1	1	1	1	1	1	1	1	1	1
237	1.735	1	1	1	1	1	1	1	1	1	1	1	1
238	1.742	1	1	1	1	1	1	1	1	1	1	1	1
239	1.749	1	1	1	1	1	1	1	1	1	1	1	1
240	1.756	1	1	1	1	1	1	1	1	1	1	1	1
241	1.763	1	1	1	1	1	1	1	1	1	1	1	1
242	1.770	1	1	1	1	1	1	1	1	1	1	1	1
243	1.777	1	1	1	1	1	1	1	1	1	1	1	1
244	1.784	1	1	1	1	1	1	1	1	1	1	1	1
245	1.791	1	1	1	1	1	1	1	1	1	1	1	1
246	1.797	1	1	1	1	1	1	1	1	1	1	1	1
247	1.804	1	1	1	1	1	1	1	1	1	1	1	1
248	1.811	1	1	1	1	1	1	1	1	1	1	1	1
249	1.818	1	1	1	1	1	1	1	1	1	1	1	1
250	1.825	1	1	1	1	1	1	1	1	1	1	1	1
251	1.832	1	1	1	1	1	1	1	1	1	1	1	1
252	1.839	1	1	1	1	1	1	1	1	1	1	1	1
253	1.846	1	1	1	1	1	1	1	1	1	1	1	1
254	1.853	1	1	1	1	1	1	1	1	1	1	1	1
255	1.859	1	1	1	1	1	1	1	1	1	1	1	1
256	1.866	1	1	1	1	1	1	1	1	1	1	1	1
257	1.873	1	1	1	1	1	1	1	1	1	1	1	1
258	1.880	1	1	1	1	1	1	1	1	1	1	1	1
259	1.887	1	1	1	1	1	1	1	1	1	1	1	1
260	1.894	1	1	1	1	1	1	1	1	1	1	1	1

IPE Fragility Curves

Table D.2 Cumulative containment failure probabilities (continued)

Name	Devils-Bass	Dietrich	Ferley	Fort Calhoun	Ginna	Haddam	Indian 2	Indian 3	Kewaunee	Maine Y.	McGuire	Missiles 2	Missiles 3
Material	Steel	Re Conc.	Pre Conc.	Pre Conc.	Pre Conc.	Re Conc.	Re Conc.	Re Conc.	Steel	Re Conc.	Re Conc.	Pre Conc.	Re Conc.
Cont. Type	Dry	Dry	Dry	Dry	Dry	Dry	Dry	Dry	Dry	Dry	Ice	Dry	Sub.
Design Pressure (psig)	40	47	64	60	60	40	47	47	46	56	28	64	45
Analysis Temp.	264 F	350 F	No Temp	No Temp	No Temp	200 F	No Temp	400 F	No temp	376 F	No Temp	400 F	No Temp
Rk Type	Best Est.	LNM&B	Best Est.	LNM&B	Best Est.	3-Pr Bt	3-Pr Bt	Best Est.	Best Est.	Best Est.	Best Est.	LNM&B	Best Est.
PSIG	MPa abs												
20	0.239	0	0	0	0	0	0	0	0	0	0	0	0
21	0.246	0	0	0	0	0	0	0	0	0	0	0	0
22	0.253	0	0	0	0	0	0	0	0	0	0	0	0
23	0.260	0	0	0	0	0	0	0	0	0	0	0	0
24	0.267	0	0	0	0	0	0	0	0	0	0	0	0
25	0.274	0	0	0	0	0	0	0	0	0	0	0	0
26	0.281	0	0	0	0	0	0	0	0	0	0	0	0
27	0.287	0	0	0	0	0	0	0	0	0	0	0	0
28	0.294	0	0	0	0	0	0	0	0	0	0	0	0
29	0.301	0	0	0	0	0	0	0	0	0	0	0	0
30	0.308	0	0	0	0	0	0	0	0	0	0	0	0
31	0.315	0	0	0	0	0	0	0	0	0	0	0	0
32	0.322	0	0	0	0	0	0	0	0	0	0	0	0
33	0.329	0	0	0	0	0	0	0	0	0	0	0	0
34	0.336	0	0	0	0	0	0	0	0	0	0	0	0
35	0.343	0	0	0	0	0	0	0	0	0	0	0	0
36	0.350	0	0	0	0	0	0	0	0	0	0	0	0
37	0.356	0	0	0	0	0	0	0	0	0	0	0	0
38	0.363	0	0	0	0	0	0	0	0	0	0	0	0
39	0.370	0	0	0	0	0	0	0	0	0	0	0	0
40	0.377	0	0	0	0	0	0	0	0	0	0	0	0
41	0.384	0	0	0	0	0	0	0	0	0	0	0	0
42	0.391	0	0	0	0	0	0	0	0	0	0	0	0
43	0.398	0	0	0	0	0	0	0	0	0	0	0	0
44	0.405	0	0	0	0	0	0	0	0	0	0	0	0
45	0.412	0	0	0	0	0	0	0	0	0	0	0	0
46	0.418	0	0	0	0	0	0	0	0	0	0	0	0
47	0.425	0	0	0	0	0	0	0	0	0	0	0	0
48	0.432	0	0	0	0	0	0	0	0	0	0	0	0
49	0.439	0	0	0	0	0	0	0	0	0	0	0	0
50	0.446	0	0	0	0	0	0	0	0	0	0	0	0
51	0.453	0.0011	0	0	0	0	0	0	0	0	0	0	0
52	0.460	0.0022	0	0	0	0.0004	0	0	0	0	0.0002	0	0
53	0.467	0.0031	0	0	0	0.0008	0	0	0	0	0.0009	0	0
54	0.474	0.004	0	0	0	0.0015	0	0	0	0	0.0024	0	0
55	0.481	0.0049	0	0	0	0.0025	0	0	0	0	0.0049	0	0
56	0.487	0.0061	0	0	0	0.0038	0	0	0	0	0.0084	0	0
57	0.494	0.008	0	0	0	0.0055	0	0	0	0	0.0131	0	0
58	0.501	0.0105	0	0	0	0.0076	0	0	0	0	0.0191	0	0
59	0.508	0.0137	0	0	0	0.0102	0	0	0	0	0.0266	0	0
60	0.515	0.0175	0	0	0	0.0132	0	0	0	0	0.0359	0	0
61	0.522	0.022	0	0	0	0.0189	0	0	0	0.0001	0.047	0	0
62	0.529	0.0275	0	0	0	0.0211	0	0	0	0.0005	0.0603	0.0001	0
63	0.536	0.0342	0	0	0	0.0259	0	0	0	0.0013	0.0757	0.0001	0
64	0.543	0.0425	0	0	0	0.0314	0	0	0	0.0026	0.0936	0.0001	0
65	0.549	0.0525	0	0	0	0.0376	0	0	0	0.0046	0.1141	0.0001	0
66	0.556	0.0641	0	0	0	0.0446	0	0	0	0.0071	0.1372	0.0002	0
67	0.563	0.0772	0	0	0	0.0524	0	0	0	0.01	0.1622	0.0002	0
68	0.570	0.0919	0	0	0	0.0611	0	0	0	0.0132	0.1887	0.0003	0.0001
69	0.577	0.1079	0	0	0	0.0706	0	0	0	0.0186	0.2171	0.0004	0.0001
70	0.584	0.1256	0	0	0	0.0809	0	0	0	0.02	0.2482	0.0005	0.0001
71	0.591	0.1458	0	0	0	0.0922	0	0	0	0.0233	0.2814	0.0006	0.0002
72	0.598	0.169	0	0	0	0.1044	0	0	0	0.0266	0.3162	0.0007	0.0002
73	0.605	0.1931	0	0	0	0.1175	0	0	0	0.0299	0.3524	0.0009	0.0003
74	0.612	0.216	0	0	0	0.1316	0	0	0	0.0334	0.3893	0.0011	0.0005
75	0.618	0.2398	0	0	0	0.1466	0	0	0	0.0371	0.4244	0.0013	0.0006
76	0.625	0.2676	0	0	0	0.1626	0	0	0	0.0411	0.4561	0.0016	0.0008
77	0.632	0.2978	0	0	0	0.1796	0	0	0	0.0456	0.4882	0.0019	0.001
78	0.639	0.3266	0.0001	0	0	0.1976	0	0	0	0.0505	0.5207	0.0022	0.0013
79	0.646	0.359	0.0001	0	0	0.2167	0	0	0	0.0558	0.557	0.0027	0.0017
80	0.653	0.3859	0.0001	0	0	0.2366	0	0	0	0.0615	0.5953	0.0031	0.0021
81	0.660	0.4184	0.0001	0	0	0.258	0.0003	0	0	0.0676	0.6355	0.0037	0.0026
82	0.667	0.4502	0.0002	0	0	0.2803	0.001	0	0	0.0741	0.6777	0.0043	0.0033
83	0.674	0.479	0.0002	0	0	0.3037	0.002	0	0	0.081	0.7268	0.006	0.004
84	0.680	0.5073	0.0003	0	0	0.3282	0.0035	0	0	0.088	0.7808	0.0069	0.005
85	0.687	0.5392	0.0004	0	0	0.3539	0.0054	0	0	0.0949	0.84	0.0068	0.0061
86	0.694	0.5711	0.0005	0	0	0.3807	0.0077	0	0	0.1017	0.8964	0.0078	0.0073
87	0.701	0.5995	0.0007	0	0	0.4087	0.0105	0	0	0.1081	0.9501	0.0089	0.0088
88	0.708	0.6251	0.0009	0	0	0.4379	0.0137	0	0	0.1142	0.9105	0.0102	0.0106
89	0.715	0.6516	0.0011	0	0	0.4683	0.0174	0	0	0.1205	0.9275	0.0116	0.0127
90	0.722	0.6792	0.0014	0	0	0.5	0.0215	0	0	0.1278	0.9414	0.0132	0.0151
91	0.729	0.7057	0.0017	0	0	0.5329	0.0262	0	0	0.136	0.9527	0.0149	0.0179
92	0.736	0.7296	0.0021	0	0	0.5666	0.0314	0	0	0.1459	0.9617	0.0168	0.0211
93	0.743	0.7516	0.0026	0.0001	0	0.6011	0.037	0	0	0.1566	0.9668	0.0189	0.0249
94	0.749	0.7715	0.0032	0.0006	0	0.6356	0.0432	0	0	0.1673	0.9747	0.0211	0.0291
95	0.756	0.7907	0.0039	0.002	0	0.6705	0.05	0	0	0.1776	0.9796	0.0236	0.034
96	0.763	0.8097	0.0046	0.0045	0	0.705	0.0573	0	0	0.1874	0.9838	0.0262	0.0395
97	0.770	0.8279	0.0058	0.008	0.0001	0.7388	0.0652	0	0	0.1971	0.9871	0.0291	0.0456
98	0.777	0.8446	0.0069	0.0119	0.0001	0.7717	0.0736	0.0008	0	0.207	0.9896	0.0322	0.053
99	0.784	0.8596	0.0082	0.0164	0.0001	0.8034	0.0825	0.0025	0	0.2174	0.9912	0.0355	0.0611
100	0.791	0.8734	0.0096	0.0231	0.0001	0.8335	0.0919	0.0048	0	0.2284	0.9921	0.0391	0.0702





IPE Fragility Curves

Table D.2 Cumulative containment failure probabilities (continued)

Name	Devis-Bes	Diablo	Ferley	Fort Calh	Glenn	Haddam	Indian 2	Indian 3	Kewaunee	Maine Y.	McGuire	Mission 2	Mission 3	
Material	Steel	Re Conc.	Pre Conc.	Pre Conc.	Pre Conc.	Re Conc.	Re Conc.	Re Conc.	Steel	Re Conc.	Re Conc.	Pre Conc.	Re Conc.	
Cont. Type	Dry	Dry	Dry	Dry	Dry	Dry	Dry	Dry	Dry	Dry	Ice	Dry	Sub.	
Design Pressure (psig)	40	47	54	60	60	40	47	47	46	55	28	64	45	
Analysis Temp	264 F	350 F	No Temp	No Temp	No Temp	200 F	No Temp	400 F	No temp	376 F	No Temp	400 F	No Temp	
Fit Type	Best Est.	LWAB	Best Est.	LWAB	Best Est.	3-Pt Fit	3-Pt Fit	Best Est.	Best Est.	Best Est.	Best Est.	LWAB	Best Est.	
PSIG	MPa abs													
181	1.349	1	0.9835	1	0.2626	1	1	1	0.9962	0.9754	0.9624	1	0.9986	1
182	1.356	1	0.9855	1	0.2948	1	1	1	0.9971	0.9796	0.9645	1	0.9989	1
183	1.363	1	0.9873	1	0.3072	1	1	1	0.9978	0.9831	0.9666	1	0.9991	1
184	1.370	1	0.9888	1	0.3199	1	1	1	0.9984	0.9862	0.9686	1	0.9993	1
185	1.377	1	0.9902	1	0.3327	1	1	1	0.9989	0.9886	0.9705	1	0.9994	1
186	1.384	1	0.9915	1	0.3456	1	1	1	0.9993	0.9905	0.9724	1	0.9995	1
187	1.391	1	0.9926	1	0.3591	1	1	1	0.9996	0.9921	0.9742	1	0.9996	1
188	1.398	1	0.9935	1	0.3725	1	1	1	0.9998	0.9939	0.9759	1	0.9997	1
189	1.404	1	0.9944	1	0.3861	1	1	1	0.9999	0.9959	0.9776	1	0.9998	1
190	1.411	1	0.9951	1	0.3998	1	1	1	1	0.9979	0.9792	1	0.9998	1
191	1.418	1	0.9956	1	0.4136	1	1	1	0.9994	0.9807	1	1	0.9999	1
192	1.425	1	0.9964	1	0.4276	1	1	1	1	0.9821	1	1	0.9999	1
193	1.432	1	0.9969	1	0.4416	1	1	1	1	0.9834	1	1	0.9999	1
194	1.438	1	0.9973	1	0.4556	1	1	1	1	0.9847	1	1	0.9999	1
195	1.446	1	0.9977	1	0.47	1	1	1	1	0.9858	1	1	0.9999	1
196	1.453	1	0.998	1	0.4842	1	1	1	1	0.9867	1	1	1	1
197	1.460	1	0.9983	1	0.4984	1	1	1	1	0.9876	1	1	1	1
198	1.466	1	0.9985	1	0.5127	1	1	1	1	0.9883	1	1	1	1
199	1.473	1	0.9988	1	0.5269	1	1	1	1	0.9889	1	1	1	1
200	1.480	1	0.9989	1	0.5411	1	1	1	1	0.9894	1	1	1	1
201	1.487	1	0.9991	1	0.5553	1	1	1	1	0.9899	1	1	1	1
202	1.494	1	0.9992	1	0.5694	1	1	1	1	0.9904	1	1	1	1
203	1.501	1	0.9994	1	0.5834	1	1	1	1	0.9908	1	1	1	1
204	1.508	1	0.9995	1	0.5973	1	1	1	1	0.9913	1	1	1	1
205	1.515	1	0.9995	1	0.6111	1	1	1	1	0.9919	1	1	1	1
206	1.522	1	0.9996	1	0.6247	1	1	1	1	0.9925	1	1	1	1
207	1.529	1	0.9997	1	0.6382	1	1	1	1	0.9931	1	1	1	1
208	1.535	1	0.9997	1	0.6516	1	1	1	1	0.9937	1	1	1	1
209	1.542	1	0.9998	1	0.6647	1	1	1	1	0.9943	1	1	1	1
210	1.549	1	0.9998	1	0.6777	1	1	1	1	0.9948	1	1	1	1
211	1.556	1	0.9998	1	0.6904	1	1	1	1	0.9953	1	1	1	1
212	1.563	1	0.9999	1	0.703	1	1	1	1	0.9958	1	1	1	1
213	1.570	1	0.9999	1	0.7152	1	1	1	1	0.9961	1	1	1	1
214	1.577	1	0.9999	1	0.7273	1	1	1	1	0.9963	1	1	1	1
215	1.584	1	0.9999	1	0.7391	1	1	1	1	0.9965	1	1	1	1
216	1.591	1	0.9999	1	0.7506	1	1	1	1	0.9966	1	1	1	1
217	1.597	1	0.9999	1	0.7618	1	1	1	1	0.9967	1	1	1	1
218	1.604	1	1	1	0.7728	1	1	1	1	0.9969	1	1	1	1
219	1.611	1	1	1	0.7835	1	1	1	1	0.997	1	1	1	1
220	1.618	1	1	1	0.7939	1	1	1	1	0.9972	1	1	1	1
221	1.625	1	1	1	0.804	1	1	1	1	0.9974	1	1	1	1
222	1.632	1	1	1	0.8137	1	1	1	1	0.9977	1	1	1	1
223	1.639	1	1	1	0.8232	1	1	1	1	0.998	1	1	1	1
224	1.646	1	1	1	0.8324	1	1	1	1	0.9982	1	1	1	1
225	1.653	1	1	1	0.8412	1	1	1	1	0.9985	1	1	1	1
226	1.660	1	1	1	0.8498	1	1	1	1	0.9986	1	1	1	1
227	1.666	1	1	1	0.858	1	1	1	1	0.9987	1	1	1	1
228	1.673	1	1	1	0.8659	1	1	1	1	0.9987	1	1	1	1
229	1.680	1	1	1	0.8735	1	1	1	1	0.9986	1	1	1	1
230	1.687	1	1	1	0.8806	1	1	1	1	0.9987	1	1	1	1
231	1.694	1	1	1	0.8878	1	1	1	1	0.9988	1	1	1	1
232	1.701	1	1	1	0.8945	1	1	1	1	0.9991	1	1	1	1
233	1.708	1	1	1	0.9009	1	1	1	1	0.9996	1	1	1	1
234	1.715	1	1	1	0.907	1	1	1	1	1	1	1	1	1
235	1.722	1	1	1	0.9129	1	1	1	1	1	1	1	1	1
236	1.728	1	1	1	0.9184	1	1	1	1	1	1	1	1	1
237	1.735	1	1	1	0.9237	1	1	1	1	1	1	1	1	1
238	1.742	1	1	1	0.9287	1	1	1	1	1	1	1	1	1
239	1.749	1	1	1	0.9335	1	1	1	1	1	1	1	1	1
240	1.756	1	1	1	0.938	1	1	1	1	1	1	1	1	1
241	1.763	1	1	1	0.9422	1	1	1	1	1	1	1	1	1
242	1.770	1	1	1	0.9463	1	1	1	1	1	1	1	1	1
243	1.777	1	1	1	0.9501	1	1	1	1	1	1	1	1	1
244	1.784	1	1	1	0.9536	1	1	1	1	1	1	1	1	1
245	1.791	1	1	1	0.957	1	1	1	1	1	1	1	1	1
246	1.797	1	1	1	0.9602	1	1	1	1	1	1	1	1	1
247	1.804	1	1	1	0.9632	1	1	1	1	1	1	1	1	1
248	1.811	1	1	1	0.966	1	1	1	1	1	1	1	1	1
249	1.818	1	1	1	0.9686	1	1	1	1	1	1	1	1	1
250	1.825	1	1	1	0.971	1	1	1	1	1	1	1	1	1
251	1.832	1	1	1	0.9733	1	1	1	1	1	1	1	1	1
252	1.839	1	1	1	0.9754	1	1	1	1	1	1	1	1	1
253	1.846	1	1	1	0.9774	1	1	1	1	1	1	1	1	1
254	1.853	1	1	1	0.9793	1	1	1	1	1	1	1	1	1
255	1.859	1	1	1	0.981	1	1	1	1	1	1	1	1	1
256	1.866	1	1	1	0.9826	1	1	1	1	1	1	1	1	1
257	1.873	1	1	1	0.9841	1	1	1	1	1	1	1	1	1
258	1.880	1	1	1	0.9854	1	1	1	1	1	1	1	1	1
259	1.887	1	1	1	0.9867	1	1	1	1	1	1	1	1	1
260	1.894	1	1	1	0.9879	1	1	1	1	1	1	1	1	1

Table D.2 Cumulative containment failure probabilities (continued)

Node	North An.	Oconee	Palsades	Palo Verde	Point Bch	Prairie Is	Robinson	Robinson	Salem	San Onofre	Seabrook	Sequoyah	Sharon
Material	Re Conc.	Pre Conc.	Pre Conc.	Pre Conc.	Pre Conc.	Steel	Pre Conc.	Pre Conc.	Re Conc.	Pre Conc.	Re Conc.	Steel	Re Conc.
Cont. Type	Sub.	Dry	Dry	Dry	Dry	Dry	Dry	Dry	Dry	Dry	Dry	Ice	Dry
Design Pressure (psig)	45	60	60	80	80	41	42	42	47	60	60	10.8	45
Analysis Temp.	No Temp	No Temp	No Temp	No Temp	No Temp	No Temp	300 F	300 F	300 F	420 F	No Temp	200 F	300 F
Fit Type	Surry	Best Est.	Est Fit.	Best Est.	Best Est.	Best Est.	LN&B WB Fail	LN&B All Fail	Best Est.	LN&B	Best Est.	LN&B	Best Est.
PSIG	MPa abs												
20	0.239	0	0	0	0	0	0	0	0	0	0	0	0
21	0.246	0	0	0	0	0	0	0	0	0	0	0	0
22	0.253	0	0	0	0	0	0	0	0	0	0	0	0
23	0.260	0	0	0	0	0	0	0	0	0	0	0	0
24	0.267	0	0	0	0	0	0	0	0	0	0	0	0
25	0.274	0	0	0	0	0	0	0	0	0	0	0	0
26	0.281	0	0	0	0	0	0	0	0	0	0	0	0
27	0.287	0	0	0	0	0	0	0	0	0	0	0	0
28	0.294	0	0	0	0	0	0	0	0	0	0	0	0
29	0.301	0	0	0	0	0	0	0	0	0	0	0	0
30	0.308	0	0	0	0	0	0	0	0	0	0	0	0
31	0.315	0	0	0	0	0	0	0	0	0	0	0	0
32	0.322	0	0	0	0	0	0	0	0	0	0	0	0
33	0.329	0	0	0	0	0	0	0	0	0	0	0	0
34	0.336	0	0	0	0	0	0	0	0	0	0	0	0
35	0.343	0	0	0	0	0	0	0	0	0	0	0	0
36	0.350	0	0	0	0	0	0	0	0	0	0	0	0
37	0.356	0	0	0	0	0	0	0	0	0	0	0	0
38	0.363	0	0	0	0	0	0	0	0	0	0	0	0
39	0.370	0	0	0	0	0	0	0	0	0	0	0	0
40	0.377	0	0	0	0	0	0	0	0	0	0	0	0
41	0.384	0	0	0	0	0	0	0	0	0	0	0	0
42	0.391	0	0	0	0	0	0	0	0	0	0	0	0
43	0.398	0	0	0	0	0	0	0	0	0	0	0	0
44	0.405	0	0	0	0	0	0	0	0	0	0	0.0001	0
45	0.412	0	0	0	0	0	0	0	0	0	0	0.0001	0
46	0.418	0	0	0	0	0	0	0	0	0	0	0.0001	0
47	0.425	0	0	0	0	0	0	0	0	0	0	0.0002	0
48	0.432	0	0	0	0	0	0	0	0	0	0	0.0003	0
49	0.439	0	0	0	0	0	0.0001	0.0001	0	0	0	0.0005	0
50	0.446	0	0	0	0	0	0.0001	0.0001	0	0	0	0.0008	0
51	0.453	0	0	0	0	0	0.0001	0.0001	0	0	0	0.0012	0
52	0.460	0	0	0	0	0	0.0002	0.0002	0	0	0	0.0017	0
53	0.467	0	0	0	0	0	0.0002	0.0002	0	0	0	0.0026	0
54	0.474	0	0	0	0	0	0.0003	0.0003	0	0.0001	0	0.004	0
55	0.481	0	0	0	0	0	0.0004	0.0004	0	0.0001	0	0.0061	0
56	0.487	0	0	0	0	0	0.0005	0.0005	0	0.0001	0	0.0082	0
57	0.494	0	0	0	0	0	0.0006	0.0006	0	0.0001	0	0.0138	0
58	0.501	0	0	0	0	0	0.0008	0.0008	0	0.0001	0	0.0205	0
59	0.508	0	0	0	0	0	0.001	0.001	0	0.0002	0	0.0302	0
60	0.515	0	0	0	0	0	0.0012	0.0013	0	0.0002	0	0.0437	0
61	0.522	0	0	0	0	0	0.0015	0.0016	0	0.0003	0	0.0622	0
62	0.529	0	0	0	0	0	0.0018	0.002	0	0.0004	0	0.0867	0
63	0.536	0	0	0	0	0	0.0022	0.0024	0	0.0005	0	0.1185	0
64	0.543	0	0	0	0	0	0.0027	0.0029	0	0.0006	0	0.1582	0
65	0.549	0	0	0	0	0	0.0032	0.0036	0	0.0007	0	0.2066	0
66	0.556	0	0	0	0	0	0.0038	0.0043	0	0.0008	0	0.2636	0
67	0.563	0	0	0	0	0	0.0046	0.0052	0	0.001	0	0.3283	0
68	0.570	0	0	0	0	0	0.0054	0.0062	0	0.0012	0	0.3994	0
69	0.577	0	0	0	0	0	0.0064	0.0074	0	0.0014	0	0.4748	0
70	0.584	0	0	0	0	0	0.0074	0.0087	0	0.0017	0	0.5617	0
71	0.591	0	0	0	0	0	0.0086	0.0102	0	0.002	0	0.6272	0
72	0.598	0	0	0	0	0	0.01	0.012	0.001	0.0023	0	0.6965	0
73	0.605	0	0	0	0	0	0.0115	0.014	0.0029	0.0027	0	0.7633	0
74	0.612	0.0001	0	0	0	0	0.0132	0.0163	0.0053	0.0031	0	0.8198	0
75	0.618	0.0005	0	0	0	0	0.0151	0.0188	0.008	0.0036	0	0.8672	0
76	0.625	0.0012	0	0	0	0	0.0172	0.0217	0.0106	0.0042	0	0.9052	0
77	0.632	0.0024	0	0	0	0	0.0195	0.0249	0.0127	0.0048	0	0.9346	0
78	0.639	0.0039	0	0	0	0	0.022	0.0285	0.0146	0.0055	0	0.9564	0
79	0.646	0.0056	0	0	0	0	0.0247	0.0325	0.0167	0.0063	0	0.9719	0
80	0.653	0.0076	0	0	0	0	0.0277	0.037	0.0193	0.0072	0	0.9825	0
81	0.660	0.0096	0	0	0	0	0.0306	0.0418	0.0224	0.0081	0	0.9895	0
82	0.667	0.0117	0	0	0	0	0.0344	0.0472	0.0258	0.0092	0	0.9939	0
83	0.674	0.0138	0	0	0	0	0.0382	0.053	0.0296	0.0103	0	0.9966	0
84	0.680	0.0156	0	0	0	0	0.0422	0.0594	0.0337	0.0116	0	0.9981	0
85	0.687	0.0173	0	0	0	0	0.0465	0.0664	0.0384	0.013	0	0.999	0
86	0.694	0.0188	0	0	0	0	0.0511	0.0732	0.0437	0.0145	0	0.9995	0
87	0.701	0.0204	0	0	0	0	0.056	0.0821	0.0497	0.0162	0	0.9998	0
88	0.708	0.0222	0	0	0	0	0.0612	0.0908	0.0564	0.018	0	0.9999	0
89	0.715	0.0246	0	0	0	0	0.0667	0.1002	0.0636	0.0199	0	0.9999	0
90	0.722	0.0278	0	0	0	0	0.0725	0.1103	0.0715	0.022	0	1	0
91	0.729	0.032	0	0	0	0	0.0786	0.121	0.0799	0.0243	0	1	0
92	0.736	0.0371	0	0	0	0	0.085	0.1323	0.089	0.0268	0	1	0
93	0.743	0.0429	0	0	0	0	0.0918	0.1444	0.099	0.0295	0	1	0
94	0.749	0.0492	0	0.0001	0	0	0.0988	0.1571	0.1101	0.0323	0	1	0
95	0.756	0.0567	0	0.0001	0	0	0.1062	0.1704	0.1225	0.0354	0	1	0
96	0.763	0.0623	0	0.0001	0	0	0.1138	0.1844	0.1359	0.0387	0	1	0
97	0.770	0.0689	0	0.0001	0	0	0.1218	0.1991	0.1496	0.0423	0	1	0
98	0.777	0.0757	0	0.0002	0	0	0.13	0.2143	0.1639	0.046	0	1	0
99	0.784	0.0829	0	0.0002	0	0	0.1385	0.2302	0.1792	0.0501	0	1	0.0016
100	0.791	0.0906	0	0.0003	0	0	0.1474	0.2466	0.1958	0.0544	0	1	0.0039
							0.1564	0.2636	0.2124	0.0591	0	1	0.0056





Table D.2 Cumulative containment failure probabilities (continued)

Name	North An. Re Conc.	Oconee Pre Conc	Paisades Pre Conc	Palo Verde Pre Conc	Poiré Bch Pre Conc	Prairie Is Steel Dry	Robinson Pre Conc	Robinson Pre Conc	Salem Re Conc	San Onofre Pre Conc	Seabrook Re Conc	Sequoyah Steel 10.8	Shearon Re Conc	
Material														
Cont. Type														
Design Pressure (psig)	45	66	65	60	60	41	42	42	47	60	65	10.8	45	
Analysis Temp.	No Temp	No Temp	No Temp	No Temp	No Temp	No Temp	300 F	300 F	300 F	420 F	No Temp	200 F	300 F	
Fill Type	Surry	Best Est.	Est Fil.	Best Est.	Best Est.	Best Est.	LW&B WB Fill	LW&B AI Fill	Best Est.	LW&B	Best Est.	LW&B	Best Est.	
PSIG	MPa abs													
181	1.349	1	0.9952	0.9999	0.8018	0.9866	0.9673	0.8985	0.9996	1	0.997	0.0722	1	0.8104
182	1.356	1	0.9991	0.9990	0.8208	0.9801	0.9713	0.9022	0.9997	1	0.9975	0.078	1	0.8174
183	1.363	1	0.9990	0.9999	0.8386	0.9926	0.9746	0.9058	0.9997	1	0.9979	0.0842	1	0.8241
184	1.370	1	0.9999	0.9999	0.8552	0.9948	0.978	0.9093	0.9998	1	0.9983	0.0908	1	0.8305
185	1.377	1	1	0.9999	0.8707	0.9965	0.9809	0.9126	0.9998	1	0.9986	0.0978	1	0.8368
186	1.384	1	1	1	0.8851	0.998	0.9835	0.9159	0.9998	1	0.9989	0.1053	1	0.8429
187	1.391	1	1	1	0.8982	0.9991	0.9858	0.919	0.9999	1	0.9991	0.1133	1	0.849
188	1.398	1	1	1	0.9102	0.9997	0.988	0.922	0.9999	1	0.9993	0.1218	1	0.855
189	1.404	1	1	1	0.9211	1	0.9899	0.925	0.9999	1	0.9994	0.1307	1	0.8611
190	1.411	1	1	1	0.9311	1	0.9916	0.9278	0.9999	1	0.9995	0.1401	1	0.8671
191	1.418	1	1	1	0.9401	1	0.9933	0.9305	0.9999	1	0.9996	0.1499	1	0.8729
192	1.425	1	1	1	0.9481	1	0.9948	0.9332	0.9999	1	0.9997	0.1502	1	0.8784
193	1.432	1	1	1	0.9552	1	0.9962	0.9357	1	1	0.9998	0.1709	1	0.8836
194	1.439	1	1	1	0.9615	1	0.9975	0.9382	1	1	0.9998	0.1819	1	0.8885
195	1.446	1	1	1	0.9671	1	0.9988	0.9406	1	1	0.9999	0.1934	1	0.8931
196	1.453	1	1	1	0.972	1	1	0.9429	1	1	0.9999	0.2052	1	0.8973
197	1.460	1	1	1	0.9763	1	1	0.9451	1	1	0.9999	0.2173	1	0.9013
198	1.466	1	1	1	0.98	1	1	0.9472	1	1	0.9999	0.2298	1	0.905
199	1.473	1	1	1	0.9832	1	1	0.9492	1	1	0.9999	0.2427	1	0.9085
200	1.480	1	1	1	0.986	1	1	0.9512	1	1	1	0.2558	1	0.9119
201	1.487	1	1	1	0.9883	1	1	0.9531	1	1	1	0.2692	1	0.9151
202	1.494	1	1	1	0.9903	1	1	0.955	1	1	1	0.2829	1	0.9182
203	1.501	1	1	1	0.992	1	1	0.9567	1	1	1	0.2969	1	0.921
204	1.508	1	1	1	0.9935	1	1	0.9585	1	1	1	0.3111	1	0.9235
205	1.515	1	1	1	0.9947	1	1	0.9601	1	1	1	0.3266	1	0.9257
206	1.522	1	1	1	0.9957	1	1	0.9617	1	1	1	0.3403	1	0.9278
207	1.529	1	1	1	0.9965	1	1	0.9632	1	1	1	0.3552	1	0.9299
208	1.535	1	1	1	0.9972	1	1	0.9647	1	1	1	0.3704	1	0.9322
209	1.542	1	1	1	0.9977	1	1	0.9661	1	1	1	0.3857	1	0.9345
210	1.549	1	1	1	0.9982	1	1	0.9674	1	1	1	0.4013	1	0.937
211	1.556	1	1	1	0.9986	1	1	0.9688	1	1	1	0.4172	1	0.9396
212	1.563	1	1	1	0.9989	1	1	0.97	1	1	1	0.4332	1	0.9422
213	1.570	1	1	1	0.9991	1	1	0.9712	1	1	1	0.4496	1	0.9448
214	1.577	1	1	1	0.9993	1	1	0.9724	1	1	1	0.4661	1	0.9474
215	1.584	1	1	1	0.9995	1	1	0.9735	1	1	1	0.4829	1	0.95
216	1.591	1	1	1	0.9996	1	1	0.9746	1	1	1	0.5	1	0.9525
217	1.597	1	1	1	0.9997	1	1	0.9756	1	1	1	0.5173	1	0.9549
218	1.604	1	1	1	0.9998	1	1	0.9766	1	1	1	0.5348	1	0.9572
219	1.611	1	1	1	0.9999	1	1	0.9776	1	1	1	0.5523	1	0.9594
220	1.618	1	1	1	0.9999	1	1	0.9785	1	1	1	0.5699	1	0.9616
221	1.625	1	1	1	0.9999	1	1	0.9794	1	1	1	0.5874	1	0.9637
222	1.632	1	1	1	1	1	1	0.9802	1	1	1	0.6048	1	0.9657
223	1.639	1	1	1	1	1	1	0.981	1	1	1	0.6219	1	0.9676
224	1.646	1	1	1	1	1	1	0.9818	1	1	1	0.6387	1	0.9695
225	1.653	1	1	1	1	1	1	0.9826	1	1	1	0.6552	1	0.9712
226	1.660	1	1	1	1	1	1	0.9833	1	1	1	0.6711	1	0.973
227	1.666	1	1	1	1	1	1	0.984	1	1	1	0.6866	1	0.9746
228	1.673	1	1	1	1	1	1	0.9846	1	1	1	0.7016	1	0.9762
229	1.680	1	1	1	1	1	1	0.9853	1	1	1	0.7161	1	0.9777
230	1.687	1	1	1	1	1	1	0.9859	1	1	1	0.7302	1	0.9791
231	1.694	1	1	1	1	1	1	0.9865	1	1	1	0.7438	1	0.9805
232	1.701	1	1	1	1	1	1	0.987	1	1	1	0.757	1	0.9819
233	1.708	1	1	1	1	1	1	0.9876	1	1	1	0.7698	1	0.9831
234	1.715	1	1	1	1	1	1	0.9881	1	1	1	0.7823	1	0.9843
235	1.722	1	1	1	1	1	1	0.9886	1	1	1	0.7943	1	0.9855
236	1.728	1	1	1	1	1	1	0.9891	1	1	1	0.806	1	0.9866
237	1.735	1	1	1	1	1	1	0.9895	1	1	1	0.8174	1	0.9876
238	1.742	1	1	1	1	1	1	0.99	1	1	1	0.8284	1	0.9886
239	1.749	1	1	1	1	1	1	0.9904	1	1	1	0.8391	1	0.9895
240	1.756	1	1	1	1	1	1	0.9908	1	1	1	0.8494	1	0.9904
241	1.763	1	1	1	1	1	1	0.9912	1	1	1	0.8595	1	0.9912
242	1.770	1	1	1	1	1	1	0.9916	1	1	1	0.8694	1	0.992
243	1.777	1	1	1	1	1	1	0.9919	1	1	1	0.8789	1	0.9927
244	1.784	1	1	1	1	1	1	0.9923	1	1	1	0.8882	1	0.9934
245	1.791	1	1	1	1	1	1	0.9926	1	1	1	0.8973	1	0.9941
246	1.797	1	1	1	1	1	1	0.9929	1	1	1	0.9062	1	0.9947
247	1.804	1	1	1	1	1	1	0.9932	1	1	1	0.9148	1	0.9952
248	1.811	1	1	1	1	1	1	0.9935	1	1	1	0.9232	1	0.9958
249	1.818	1	1	1	1	1	1	0.9938	1	1	1	0.9313	1	0.9962
250	1.825	1	1	1	1	1	1	0.994	1	1	1	0.939	1	0.9967
251	1.832	1	1	1	1	1	1	0.9943	1	1	1	0.9465	1	0.9971
252	1.839	1	1	1	1	1	1	0.9945	1	1	1	0.9535	1	0.9975
253	1.846	1	1	1	1	1	1	0.9948	1	1	1	0.9602	1	0.9978
254	1.853	1	1	1	1	1	1	0.995	1	1	1	0.9664	1	0.9981
255	1.859	1	1	1	1	1	1	0.9952	1	1	1	0.9722	1	0.9984
256	1.866	1	1	1	1	1	1	0.9954	1	1	1	0.9776	1	0.9987
257	1.873	1	1	1	1	1	1	0.9956	1	1	1	0.9824	1	0.9989
258	1.880	1	1	1	1	1	1	0.9958	1	1	1	0.9867	1	0.9991
259	1.887	1	1	1	1	1	1	0.996	1	1	1	0.9905	1	0.9993
260	1.894	1	1	1	1	1	1	0.9962	1	1	1	0.9936	1	0.9994



IPE Fragility Curves

Table D.2 Cumulative containment failure probabilities (continued)

Name	South Tex	Bl. Luce	Summer	Surry	TMI-1	Trojan	Turkey	Vogtle	Waterford	Watts Bar	Wolf Crk	Zion
Material	Pre Conc	Steel	Pre Conc	Re Conc	Pre Conc	Pre Conc	Pre Conc	Pre Conc	Steel	Steel	Pre Conc	Pre Conc
Cont. Type	Dry	Dry	Dry	Sub.	Dry	Dry	Dry	Dry	Dry	Ice	Dry	Dry
Design Pressure (psig)	66	44	65	45	65	80	66	62	44	15	60	47
Analysis Temp.	300 F	No Temp	No Temp	No Temp	No Temp	No Temp	No Temp	No Temp	No Temp	200 F	No Temp	No Temp
FR Type	LN&B	Best Est.	Best Est.	1150	Onflow	Shut Down	Best Est.	Best Est.	LN&B	LN&B	3-Pr Bt	Best Est.
PSIG	MPa abs											
20	0.239	0	0	0	0	0	0	0	0	0	0	0
21	0.246	0	0	0	0	0	0	0	0	0	0	0
22	0.253	0	0	0	0	0	0	0	0	0	0	0
23	0.260	0	0	0	0	0	0	0	0	0	0	0
24	0.267	0	0	0	0	0	0	0	0	0	0	0
25	0.274	0	0	0	0	0	0	0	0	0	0	0
26	0.281	0	0	0	0	0	0	0	0	0	0	0
27	0.287	0	0	0	0	0	0	0	0	0	0	0
28	0.294	0	0	0	0	0	0	0	0	0	0	0
29	0.301	0	0	0	0	0	0	0	0	0	0	0
30	0.308	0	0	0	0	0	0	0	0	0	0	0
31	0.315	0	0	0	0	0	0	0	0	0	0	0
32	0.322	0	0	0	0	0	0	0	0	0	0	0
33	0.329	0	0	0	0	0	0	0	0	0	0	0
34	0.336	0	0	0	0	0	0	0	0	0	0	0
35	0.343	0	0	0	0	0	0	0	0	0	0	0
36	0.350	0	0	0	0	0	0	0	0	0	0	0
37	0.356	0	0	0	0	0	0	0	0	0	0	0
38	0.363	0	0	0	0	0	0	0	0	0	0	0
39	0.370	0	0	0	0	0	0	0	0	0	0	0
40	0.377	0	0	0	0	0	0	0	0	0	0	0
41	0.384	0	0	0	0	0	0	0	0	0	0	0
42	0.391	0	0	0	0	0	0	0	0	0.0001	0	0
43	0.398	0	0	0	0	0	0	0	0	0.0001	0	0
44	0.405	0	0	0	0	0	0	0	0	0.0002	0	0
45	0.412	0	0	0	0	0	0	0	0	0.0003	0	0
46	0.418	0	0	0	0	0	0	0	0	0.0004	0	0
47	0.425	0	0	0	0	0	0	0	0	0.0005	0	0
48	0.432	0	0	0	0	0	0	0	0	0.0006	0	0
49	0.439	0	0	0	0	0	0	0	0	0.0011	0	0
50	0.446	0	0	0	0	0	0	0	0	0.0015	0	0
51	0.453	0	0	0	0	0	0	0	0	0.002	0	0
52	0.460	0.0001	0	0	0	0	0	0	0	0.0026	0	0
53	0.467	0.0001	0	0	0	0	0	0	0	0.0035	0	0
54	0.474	0.0001	0	0	0	0	0	0	0	0.0045	0	0
55	0.481	0.0002	0	0	0	0	0	0	0	0.0058	0	0
56	0.487	0.0002	0	0	0	0	0	0	0	0.0073	0	0
57	0.494	0.0003	0	0	0	0	0	0	0	0.0092	0	0
58	0.501	0.0004	0	0	0	0	0	0	0	0.0115	0	0
59	0.508	0.0006	0	0	0	0	0	0	0	0.0142	0	0
60	0.515	0.0008	0	0	0	0	0	0	0	0.0173	0	0
61	0.522	0.0011	0	0	0	0	0	0	0	0.021	0	0
62	0.529	0.0014	0	0	0	0	0	0	0	0.0253	0	0
63	0.536	0.0018	0	0	0	0	0.0007	0	0	0.0302	0	0
64	0.543	0.0023	0	0	0	0.0015	0	0	0	0.0358	0	0
65	0.549	0.0029	0	0	0	0.0022	0	0	0	0.0421	0	0
66	0.556	0.0037	0	0	0	0.0029	0	0	0	0.0491	0	0
67	0.563	0.0046	0	0	0	0.0036	0	0	0	0.057	0	0
68	0.570	0.0057	0	0	0	0.0042	0	0	0	0.0656	0	0
69	0.577	0.007	0	0	0	0.0049	0	0	0	0.0754	0	0
70	0.584	0.0085	0	0	0	0.0056	0	0	0	0.0859	0	0
71	0.591	0.0103	0	0	0	0.0061	0	0	0	0.0974	0	0
72	0.598	0.0124	0	0	0	0.0067	0	0	0	0.1098	0	0
73	0.605	0.0148	0	0	0	0.0073	0	0	0	0.1232	0	0
74	0.612	0.0175	0	0	0.0001	0.0078	0	0	0	0.1375	0	0
75	0.618	0.0207	0	0	0.0005	0.0083	0	0	0	0.1527	0	0
76	0.625	0.0242	0	0	0.0012	0.0087	0	0	0.0001	0.1688	0	0
77	0.632	0.0281	0	0	0.0024	0.0091	0	0	0.0001	0.1859	0	0
78	0.639	0.0326	0	0	0.0039	0.0094	0	0	0.0001	0.2037	0	0
79	0.646	0.0375	0	0	0.0056	0.0097	0	0	0.0001	0.2224	0	0
80	0.653	0.0429	0	0	0.0076	0.01	0	0	0.0002	0.2419	0	0
81	0.660	0.0489	0.0358	0	0.0096	0.0102	0	0	0.0003	0.2621	0.0003	0
82	0.667	0.0554	0.0717	0	0.0117	0.0105	0	0	0.0004	0.283	0.0006	0
83	0.674	0.0625	0.1081	0	0.0138	0.0107	0	0	0.0006	0.3044	0.0017	0
84	0.680	0.0702	0.1447	0	0.0156	0.011	0	0	0.0008	0.3265	0.0028	0
85	0.687	0.0785	0.1809	0	0.0173	0.0113	0	0	0.001	0.349	0.0043	0
86	0.694	0.0875	0.218	0	0.0188	0.0116	0	0	0.0013	0.372	0.0064	0
87	0.701	0.097	0.2494	0	0.0204	0.0119	0	0.0002	0.0017	0.3953	0.006	0.0002
88	0.708	0.1072	0.2809	0	0.0222	0.0123	0	0.0006	0.0022	0.419	0.0079	0.0005
89	0.715	0.118	0.31	0	0.0246	0.0127	0	0.0012	0.0027	0.443	0.0102	0.001
90	0.722	0.1294	0.3376	0	0.0278	0.0132	0	0.002	0.0034	0.4672	0.0127	0.0016
91	0.729	0.1414	0.3656	0	0.032	0.0138	0	0.0028	0.0043	0.4916	0.0154	0.0024
92	0.736	0.1541	0.3968	0	0.0371	0.0145	0	0.0036	0.0053	0.5162	0.0184	0.0033
93	0.743	0.1672	0.4318	0	0.0429	0.0152	0	0.0045	0.0065	0.5408	0.0216	0.0043
94	0.749	0.181	0.4677	0	0.0492	0.0161	0	0.0054	0.0079	0.5655	0.025	0.0054
95	0.756	0.1952	0.5	0	0.0567	0.017	0	0.0062	0.0096	0.5902	0.0287	0.0064
96	0.763	0.21	0.5256	0	0.0623	0.0181	0	0.0077	0.0115	0.6149	0.0326	0.0074
97	0.770	0.2253	0.546	0	0.0689	0.0193	0	0.0084	0.0138	0.6394	0.0366	0.0084
98	0.777	0.2406	0.5636	0	0.0757	0.0207	0	0.0092	0.0164	0.6637	0.0409	0.0094
99	0.784	0.257	0.5811	0	0.0829	0.0222	0	0.0099	0.0193	0.6877	0.0454	0.0106
100	0.791	0.2735	0.6011	0	0.0906	0.0238	0	0.0101	0.0227	0.7113	0.05	0.0122
										0.7344	0.0548	0.0141

Table D.2 Cumulative containment failure probabilities (continued)

Name	South Tex	St. Luke	Summer	Surry	TMI-1	Trojan	Turkey	Vogtle	Waterford	Watts Bar	Wolf Crk	Zion	
Material	Pre Conc	Steel	Pre Conc	Re Conc.	Pre Conc	Pre Conc	Pre Conc	Pre Conc	Steel	Steel	Pre Conc	Pre Conc	
Cont. Type	Dry	Dry	Dry	Sub.	Dry	Dry	Dry	Dry	Dry	Ice	Dry	Dry	
Design Pressure (psig)	56	44	56	45	56	80	56	52	44	15	80	47	
Analyse Temp	300 F	No temp	No Temp	No Temp	No Temp	No Temp	No Temp	No Temp	No Temp	200 F	No Temp	No Temp	
FR Type	LnM&B	Best Est.	Best Est.	1150	Ononee	Best Est.	Best Est.	Best Est.	LnM&B	LnM&B	3-Pt R	Best Est.	
PSIG	MPa abs												
101	0.798	0.2903	0.625	0.0021	0.099	0	0.0296	0	0.0112	0.0265	0.7569	0.0566	0.0186
102	0.805	0.3074	0.6516	0.0042	0.1079	0.0002	0.0275	0	0.0126	0.0308	0.7788	0.0649	0.0194
103	0.811	0.3248	0.6786	0.0063	0.1171	0.0006	0.0295	0	0.0143	0.0356	0.7996	0.0702	0.0224
104	0.818	0.3423	0.7047	0.0084	0.1266	0.0013	0.0316	0	0.0163	0.041	0.82	0.0756	0.0254
105	0.825	0.3601	0.728	0.0105	0.136	0.0026	0.0338	0	0.0189	0.0469	0.8391	0.0811	0.0284
106	0.832	0.3779	0.75	0.0125	0.1456	0.0043	0.0361	0	0.0219	0.0534	0.8571	0.0868	0.0313
107	0.839	0.3959	0.7715	0.0145	0.156	0.0066	0.0385	0	0.0254	0.0606	0.874	0.0925	0.0343
108	0.846	0.4139	0.7924	0.0164	0.1678	0.0093	0.041	0	0.0295	0.0684	0.8897	0.0982	0.0375
109	0.853	0.432	0.8121	0.0183	0.1818	0.0125	0.0435	0	0.0339	0.0769	0.9041	0.1041	0.0409
110	0.860	0.45	0.8305	0.0202	0.1888	0.016	0.0461	0	0.0383	0.0861	0.9173	0.11	0.0447
111	0.867	0.4679	0.8481	0.0222	0.2194	0.0197	0.0487	0.0012	0.0425	0.0959	0.9292	0.116	0.049
112	0.874	0.4858	0.865	0.0244	0.2425	0.0239	0.0513	0.0024	0.047	0.1065	0.9398	0.1223	0.0538
113	0.881	0.5035	0.8815	0.0269	0.2664	0.0286	0.054	0.0036	0.0521	0.1178	0.9493	0.1283	0.0593
114	0.887	0.5211	0.8979	0.0297	0.2892	0.0339	0.0567	0.0049	0.0579	0.1298	0.9576	0.1373	0.0655
115	0.894	0.5385	0.9146	0.0331	0.309	0.0398	0.0593	0.0062	0.0646	0.1425	0.9649	0.1465	0.0726
116	0.901	0.5566	0.9314	0.037	0.3242	0.0462	0.0619	0.0075	0.0721	0.1569	0.9711	0.1573	0.0807
117	0.908	0.5725	0.9484	0.0415	0.3355	0.053	0.0645	0.0089	0.0805	0.17	0.9765	0.17	0.0897
118	0.915	0.5892	0.9655	0.0464	0.3444	0.0603	0.0671	0.0104	0.0897	0.1848	0.981	0.1849	0.1
119	0.922	0.6056	0.9828	0.0516	0.3526	0.0682	0.0698	0.0119	0.1	0.2002	0.9848	0.2023	0.1116
120	0.929	0.6215	1	0.0567	0.3616	0.0769	0.0719	0.0135	0.1113	0.2162	0.9879	0.2225	0.1248
121	0.936	0.6372	1	0.0617	0.3726	0.0866	0.0742	0.0154	0.1238	0.2327	0.9905	0.2458	0.1397
122	0.942	0.6525	1	0.0663	0.3863	0.0976	0.0766	0.0177	0.1374	0.2498	0.9925	0.2726	0.1563
123	0.949	0.6674	1	0.0711	0.4018	0.1097	0.0792	0.0208	0.1515	0.2674	0.9942	0.303	0.174
124	0.956	0.682	1	0.077	0.4187	0.1227	0.0825	0.0246	0.1659	0.2855	0.9956	0.3375	0.1931
125	0.963	0.6962	1	0.0847	0.4365	0.1363	0.0866	0.0299	0.1803	0.3039	0.9966	0.3764	0.2166
126	0.970	0.71	1	0.0942	0.4548	0.1507	0.0919	0.0363	0.1957	0.3226	0.9975	0.4199	0.2475
127	0.977	0.7234	1	0.1052	0.4731	0.1656	0.0986	0.0444	0.2132	0.3419	0.9981	0.4684	0.2822
128	0.984	0.7363	1	0.1177	0.491	0.1813	0.1069	0.0542	0.2338	0.3613	0.9986	0.5221	0.316
129	0.991	0.7489	1	0.1314	0.508	0.1978	0.1164	0.066	0.2571	0.3809	0.999	0.5804	0.3478
130	0.996	0.761	1	0.1463	0.5242	0.2152	0.1267	0.0796	0.2814	0.4007	0.9992	0.6414	0.3865
131	1.005	0.7727	1	0.1623	0.5402	0.2337	0.1372	0.0948	0.3051	0.4205	0.9995	0.7029	0.4168
132	1.011	0.7841	1	0.18	0.5562	0.2532	0.1474	0.1115	0.3285	0.4404	0.9996	0.7631	0.4565
133	1.018	0.7949	1	0.2002	0.5728	0.2735	0.1569	0.1295	0.3524	0.4604	0.9997	0.8199	0.4969
134	1.025	0.8054	1	0.2233	0.5903	0.2939	0.1657	0.1485	0.3774	0.4802	0.9998	0.8714	0.5367
135	1.032	0.8155	1	0.2501	0.6093	0.3141	0.1739	0.1685	0.4036	0.5	0.9999	0.9154	0.5768
136	1.039	0.8252	1	0.2812	0.63	0.334	0.182	0.1891	0.431	0.5196	0.9999	0.95	0.6188
137	1.046	0.8344	1	0.3163	0.6524	0.3537	0.1917	0.2103	0.4594	0.5391	0.9999	0.9739	0.6622
138	1.053	0.8433	1	0.3549	0.6762	0.3733	0.2049	0.2317	0.4887	0.5583	1	0.9886	0.7042
139	1.060	0.8518	1	0.3964	0.7012	0.3939	0.2213	0.2534	0.5188	0.5772	1	0.9954	0.7422
140	1.067	0.86	1	0.4402	0.7272	0.4163	0.2381	0.275	0.5507	0.5958	1	0.9994	0.776
141	1.073	0.8677	1	0.4858	0.7536	0.4368	0.2525	0.2966	0.5854	0.6141	1	1	0.8076
142	1.080	0.8752	1	0.5325	0.7809	0.4579	0.2654	0.3183	0.6215	0.632	1	1	0.8384
143	1.087	0.8822	1	0.5793	0.8082	0.4767	0.2845	0.3402	0.6556	0.6494	1	1	0.8666
144	1.094	0.889	1	0.6251	0.8354	0.5014	0.3174	0.3622	0.6853	0.6665	1	1	0.8899
145	1.101	0.8954	1	0.6696	0.862	0.5343	0.3501	0.3844	0.7147	0.6831	1	1	0.9066
146	1.108	0.9015	1	0.7087	0.8873	0.5694	0.3865	0.4068	0.7426	0.6992	1	1	0.9254
147	1.115	0.9073	1	0.745	0.9107	0.6026	0.4275	0.4295	0.7701	0.7149	1	1	0.9403
148	1.122	0.9128	1	0.7794	0.9317	0.6322	0.4515	0.4526	0.7962	0.73	1	1	0.9525
149	1.129	0.918	1	0.8142	0.9495	0.6598	0.468	0.4761	0.8201	0.7447	1	1	0.9616
150	1.136	0.9229	1	0.8509	0.9635	0.6878	0.4769	0.5	0.8419	0.7588	1	1	0.9685
151	1.142	0.9276	1	0.8857	0.9734	0.7159	0.4987	0.5244	0.8618	0.7724	1	1	0.9732
152	1.149	0.9321	1	0.9136	0.9798	0.7428	0.5221	0.5491	0.8804	0.7854	1	1	0.977
153	1.156	0.9363	1	0.9347	0.9835	0.7679	0.5247	0.574	0.8975	0.798	1	1	0.9809
154	1.163	0.9402	1	0.9505	0.9855	0.7917	0.5557	0.599	0.9131	0.81	1	1	0.9847
155	1.170	0.944	1	0.9624	0.9866	0.8142	0.5845	0.624	0.9267	0.8215	1	1	0.9875
156	1.177	0.9475	1	0.9719	0.9876	0.8352	0.6189	0.6489	0.938	0.8325	1	1	0.9892
157	1.184	0.9509	1	0.9801	0.9888	0.8541	0.7806	0.6734	0.9473	0.8429	1	1	0.9906
158	1.191	0.954	1	0.9873	0.99	0.8709	0.8074	0.6976	0.9549	0.8529	1	1	0.9922
159	1.198	0.957	1	0.9938	0.9913	0.8858	0.8342	0.7212	0.9614	0.8624	1	1	0.9937
160	1.204	0.9597	1	1	0.9926	0.8993	0.8544	0.7441	0.9672	0.8713	1	1	0.9952
161	1.211	0.9624	1	1	0.994	0.9117	0.8655	0.7663	0.9725	0.8799	1	1	0.9967
162	1.218	0.9648	1	1	0.9955	0.9232	0.871	0.7875	0.9771	0.8879	1	1	0.9979
163	1.225	0.9672	1	1	0.997	0.9335	0.8745	0.8079	0.9807	0.8955	1	1	0.9989
164	1.232	0.9693	1	1	0.9985	0.9426	0.8784	0.8274	0.983	0.9027	1	1	0.9996
165	1.239	0.9714	1	1	1	0.9503	0.8826	0.8461	0.9842	0.9095	1	1	1
166	1.246	0.9733	1	1	1	0.9569	0.8877	0.8638	0.9851	0.9159	1	1	1
167	1.253	0.9751	1	1	1	0.9625	0.8928	0.8807	0.986	0.9219	1	1	1
168	1.260	0.9768	1	1	1	0.9675	0.8981	0.8966	0.9872	0.9276	1	1	1
169	1.267	0.9784	1	1	1	0.9721	0.9035	0.9117	0.9884	0.9329	1	1	1
170	1.273	0.9799	1	1	1	0.9763	0.9089	0.9259	0.9897	0.9378	1	1	1
171	1.280	0.9812	1	1	1	0.9802	0.914	0.9391	0.9911	0.9425	1	1	1
172	1.287	0.9825	1	1	1	0.9836	0.9189	0.9515	0.9925	0.9468	1	1	1
173	1.294	0.9837	1	1	1	0.9865	0.9234	0.963	0.9939	0.9509	1	1	1
174	1.301	0.9849	1	1	1	0.9887	0.9274	0.9735	0.9952	0.9547	1	1	1
175	1.308	0.9859	1	1	1	0.9904	0.931	0.9832	0.9964	0.9582	1	1	1
176	1.315	0.9869	1	1	1	0.9917	0.9342	0.9919	0.9975	0.9615	1	1	1
177	1.322	0.9878	1	1	1	0.9929	0.937	1	0.9985	0.9645	1	1	1
178	1.329	0.9887	1	1	1	0.9942	0.9394	1	0.9992	0.9674	1	1	1
179	1.335	0.9895	1	1	1	0.9956	0.9416	1	0.9998	0.97	1	1	1
180	1.342	0.9903	1	1	1	0.997	0.9436	1	1	0.9724	1	1	1

Table D.2 Cumulative containment failure probabilities (concluded)

Home Aerial	South Tex Pre Conc	St. Lucie Steel	Summer Pre Conc	Surry Ra Conc.	TMI-1 Pre Conc	Trojan Pre Conc	Turkey Pre Conc	Vogtle Pre Conc	Waterford Steel	Watts Bar Steel	Wolf Crk Pre Conc	Zion Pre Conc	
Cont. Type	Dry	Dry	Dry	Sub.	Dry	Dry	Dry	Dry	Dry	Ice	Dry	Dry	
Design Pressure (psig)	56	44	66	45	55	80	56	5.	44	15	80	47	
Analysis Temp.	300 F	No temp	No Temp	No Temp	No Temp	No Temp	No Temp	No Temp	No Temp	200 F	No Temp	No Temp	
FE Type	LnM&B	Best Est.	Best Est.	1150	Onones	Best Est.	Best Est.	Best Est.	LnM&B	LnM&B	3-Pt fit	Best Est.	
PSIG	MPa abs												
181	1.348	0.991	1	1	1	0.9982	0.9454	1	1	0.9747	1	1	1
182	1.356	0.9916	1	1	1	0.9991	0.9471	1	1	0.9768	1	1	1
183	1.363	0.9922	1	1	1	0.9996	0.9487	1	1	0.9787	1	1	1
184	1.370	0.9928	1	1	1	0.9999	0.9502	1	1	0.9805	1	1	1
185	1.377	0.9933	1	1	1	1	0.9517	1	1	0.9822	1	1	1
186	1.384	0.9938	1	1	1	1	0.9533	1	1	0.9837	1	1	1
187	1.391	0.9942	1	1	1	1	0.9548	1	1	0.9851	1	1	1
188	1.398	0.9947	1	1	1	1	0.9564	1	1	0.9864	1	1	1
189	1.404	0.9951	1	1	1	1	0.958	1	1	0.9875	1	1	1
190	1.411	0.9954	1	1	1	1	0.9596	1	1	0.9886	1	1	1
191	1.418	0.9958	1	1	1	1	0.9612	1	1	0.9896	1	1	1
192	1.425	0.9961	1	1	1	1	0.9627	1	1	0.9906	1	1	1
193	1.432	0.9964	1	1	1	1	0.9643	1	1	0.9914	1	1	1
194	1.439	0.9966	1	1	1	1	0.9658	1	1	0.9922	1	1	1
195	1.446	0.9969	1	1	1	1	0.9674	1	1	0.9929	1	1	1
196	1.453	0.9971	1	1	1	1	0.9689	1	1	0.9935	1	1	1
197	1.460	0.9973	1	1	1	1	0.9703	1	1	0.9941	1	1	1
198	1.466	0.9975	1	1	1	1	0.9717	1	1	0.9947	1	1	1
199	1.473	0.9977	1	1	1	1	0.9731	1	1	0.9951	1	1	1
200	1.480	0.9979	1	1	1	1	0.9744	1	1	0.9956	1	1	1
201	1.487	0.9981	1	1	1	1	0.9757	1	1	0.996	1	1	1
202	1.494	0.9982	1	1	1	1	0.9769	1	1	0.9964	1	1	1
203	1.501	0.9983	1	1	1	1	0.9781	1	1	0.9967	1	1	1
204	1.508	0.9985	1	1	1	1	0.9792	1	1	0.997	1	1	1
205	1.515	0.9986	1	1	1	1	0.9803	1	1	0.9973	1	1	1
206	1.522	0.9987	1	1	1	1	0.9814	1	1	0.9976	1	1	1
207	1.529	0.9988	1	1	1	1	0.9824	1	1	0.9978	1	1	1
208	1.535	0.9989	1	1	1	1	0.9833	1	1	0.998	1	1	1
209	1.542	0.999	1	1	1	1	0.9843	1	1	0.9982	1	1	1
210	1.549	0.9991	1	1	1	1	0.9852	1	1	0.9984	1	1	1
211	1.556	0.9991	1	1	1	1	0.986	1	1	0.9985	1	1	1
212	1.563	0.9992	1	1	1	1	0.9868	1	1	0.9987	1	1	1
213	1.570	0.9993	1	1	1	1	0.9876	1	1	0.9988	1	1	1
214	1.577	0.9993	1	1	1	1	0.9883	1	1	0.9989	1	1	1
215	1.584	0.9994	1	1	1	1	0.989	1	1	0.999	1	1	1
216	1.591	0.9994	1	1	1	1	0.9897	1	1	0.9991	1	1	1
217	1.597	0.9995	1	1	1	1	0.9904	1	1	0.9992	1	1	1
218	1.604	0.9995	1	1	1	1	0.991	1	1	0.9993	1	1	1
219	1.611	0.9995	1	1	1	1	0.9915	1	1	0.9994	1	1	1
220	1.618	0.9996	1	1	1	1	0.9921	1	1	0.9994	1	1	1
221	1.625	0.9996	1	1	1	1	0.9926	1	1	0.9995	1	1	1
222	1.632	0.9996	1	1	1	1	0.9931	1	1	0.9995	1	1	1
223	1.639	0.9997	1	1	1	1	0.9936	1	1	0.9996	1	1	1
224	1.646	0.9997	1	1	1	1	0.9941	1	1	0.9996	1	1	1
225	1.653	0.9997	1	1	1	1	0.9945	1	1	0.9997	1	1	1
226	1.660	0.9997	1	1	1	1	0.9949	1	1	0.9997	1	1	1
227	1.666	0.9998	1	1	1	1	0.9953	1	1	0.9997	1	1	1
228	1.673	0.9998	1	1	1	1	0.9957	1	1	0.9998	1	1	1
229	1.680	0.9998	1	1	1	1	0.996	1	1	0.9998	1	1	1
230	1.687	0.9998	1	1	1	1	0.9964	1	1	0.9998	1	1	1
231	1.694	0.9998	1	1	1	1	0.9967	1	1	0.9998	1	1	1
232	1.701	0.9998	1	1	1	1	0.997	1	1	0.9998	1	1	1
233	1.708	0.9999	1	1	1	1	0.9973	1	1	0.9999	1	1	1
234	1.715	0.9999	1	1	1	1	0.9976	1	1	0.9999	1	1	1
235	1.722	0.9999	1	1	1	1	0.9979	1	1	0.9999	1	1	1
236	1.728	0.9999	1	1	1	1	0.9981	1	1	0.9999	1	1	1
237	1.735	0.9999	1	1	1	1	0.9984	1	1	0.9999	1	1	1
238	1.742	0.9999	1	1	1	1	0.9986	1	1	0.9999	1	1	1
239	1.749	0.9999	1	1	1	1	0.9989	1	1	0.9999	1	1	1
240	1.756	0.9999	1	1	1	1	0.9991	1	1	0.9999	1	1	1
241	1.763	0.9999	1	1	1	1	0.9993	1	1	0.9999	1	1	1
242	1.770	0.9999	1	1	1	1	0.9996	1	1	0.9999	1	1	1
243	1.777	0.9999	1	1	1	1	0.9998	1	1	0.9999	1	1	1
244	1.784	0.9999	1	1	1	1	1	1	1	1	1	1	1
245	1.791	0.9999	1	1	1	1	1	1	1	1	1	1	1
246	1.797	1	1	1	1	1	1	1	1	1	1	1	1
247	1.804	1	1	1	1	1	1	1	1	1	1	1	1
248	1.811	1	1	1	1	1	1	1	1	1	1	1	1
249	1.818	1	1	1	1	1	1	1	1	1	1	1	1
250	1.825	1	1	1	1	1	1	1	1	1	1	1	1
251	1.832	1	1	1	1	1	1	1	1	1	1	1	1
252	1.839	1	1	1	1	1	1	1	1	1	1	1	1
253	1.846	1	1	1	1	1	1	1	1	1	1	1	1
254	1.853	1	1	1	1	1	1	1	1	1	1	1	1
255	1.859	1	1	1	1	1	1	1	1	1	1	1	1
256	1.866	1	1	1	1	1	1	1	1	1	1	1	1
257	1.873	1	1	1	1	1	1	1	1	1	1	1	1
258	1.880	1	1	1	1	1	1	1	1	1	1	1	1
259	1.887	1	1	1	1	1	1	1	1	1	1	1	1
260	1.894	1	1	1	1	1	1	1	1	1	1	1	1

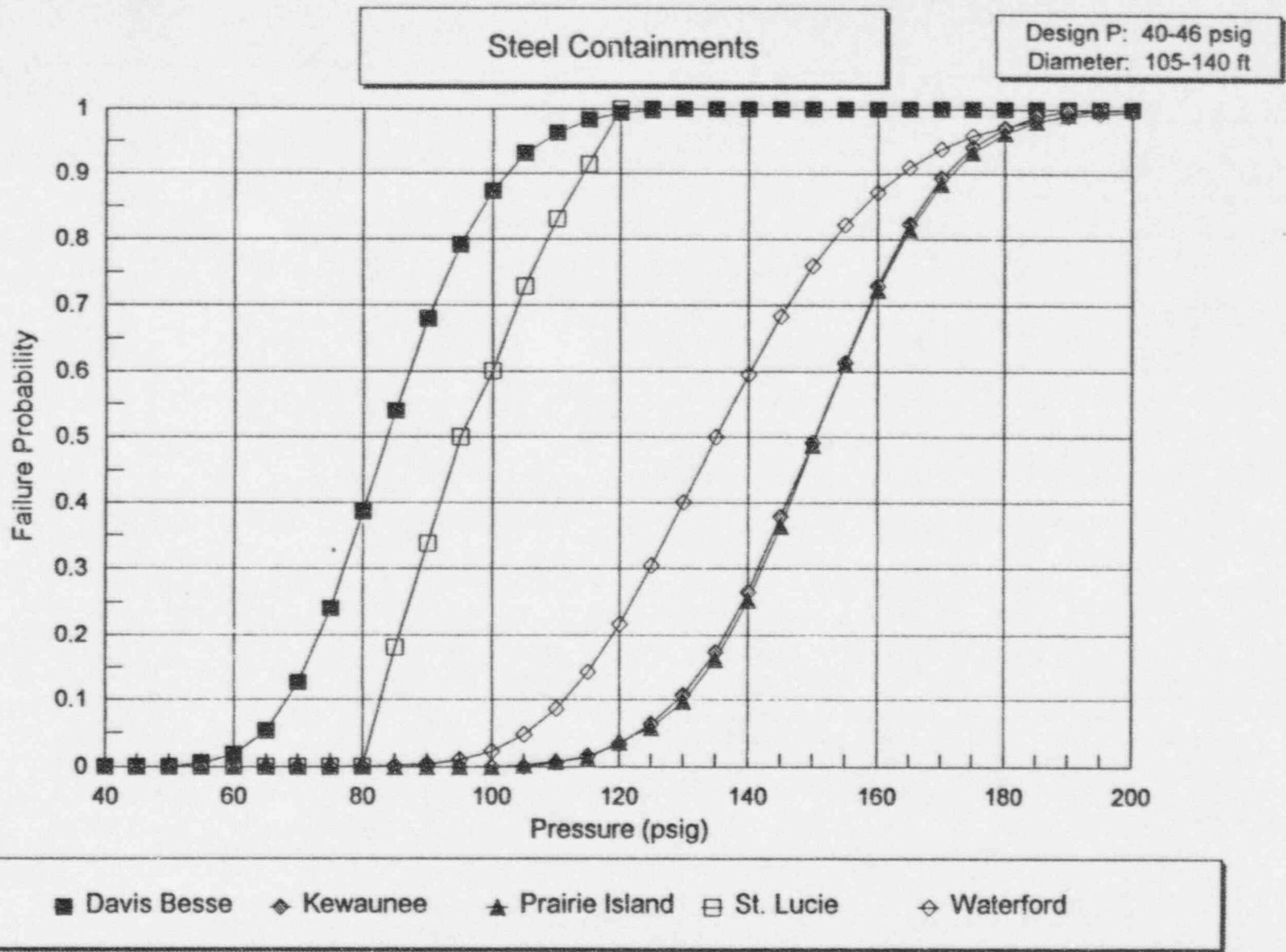


Figure D.1 Comparison of steel containment fragility curves (non-Ice Condenser type).



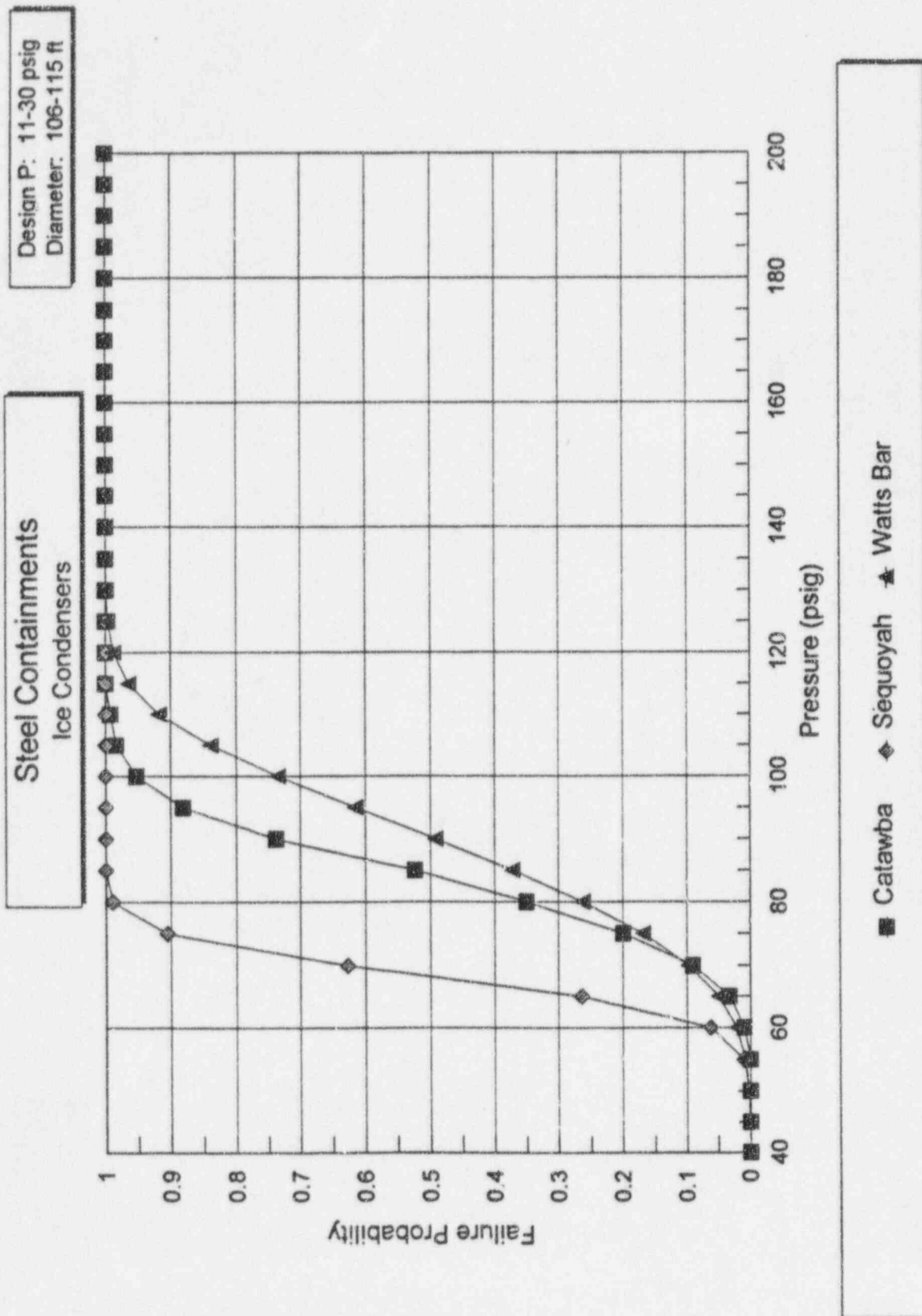
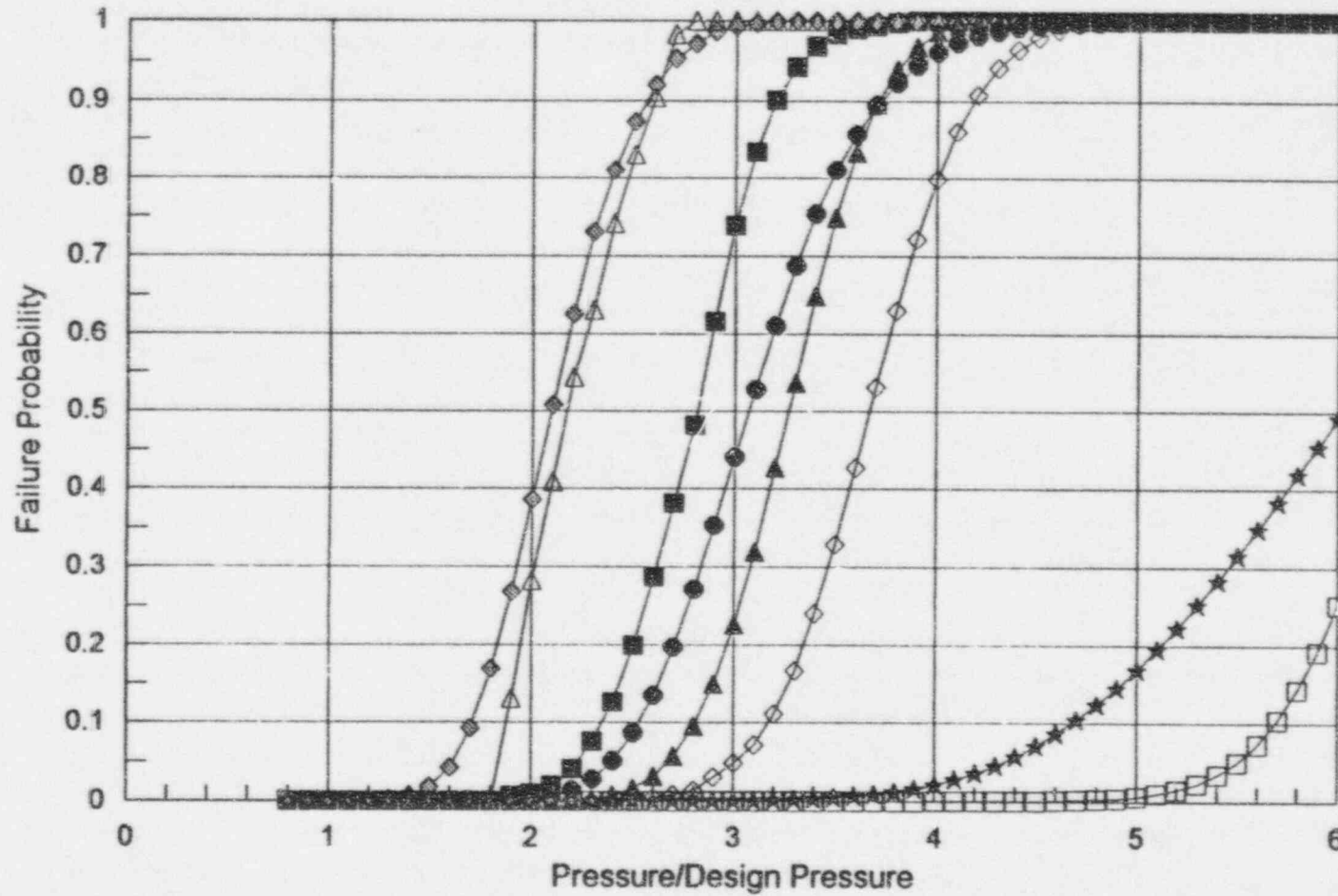


Figure D.2 Comparison of steel containment fragility curves (Ice Condenser type).



Steel Containments

Diameter: 105-140 ft



- |                  |               |             |             |
|------------------|---------------|-------------|-------------|
| ■ Catawba        | ◇ Davis Besse | ▲ Kewaunee  | □ Sequoyah  |
| ◊ Prairie Island | △ St. Lucie   | ● Waterford | ★ Watts Bar |

Figure D.3 Comparison of normalized steel containment fragility curves.

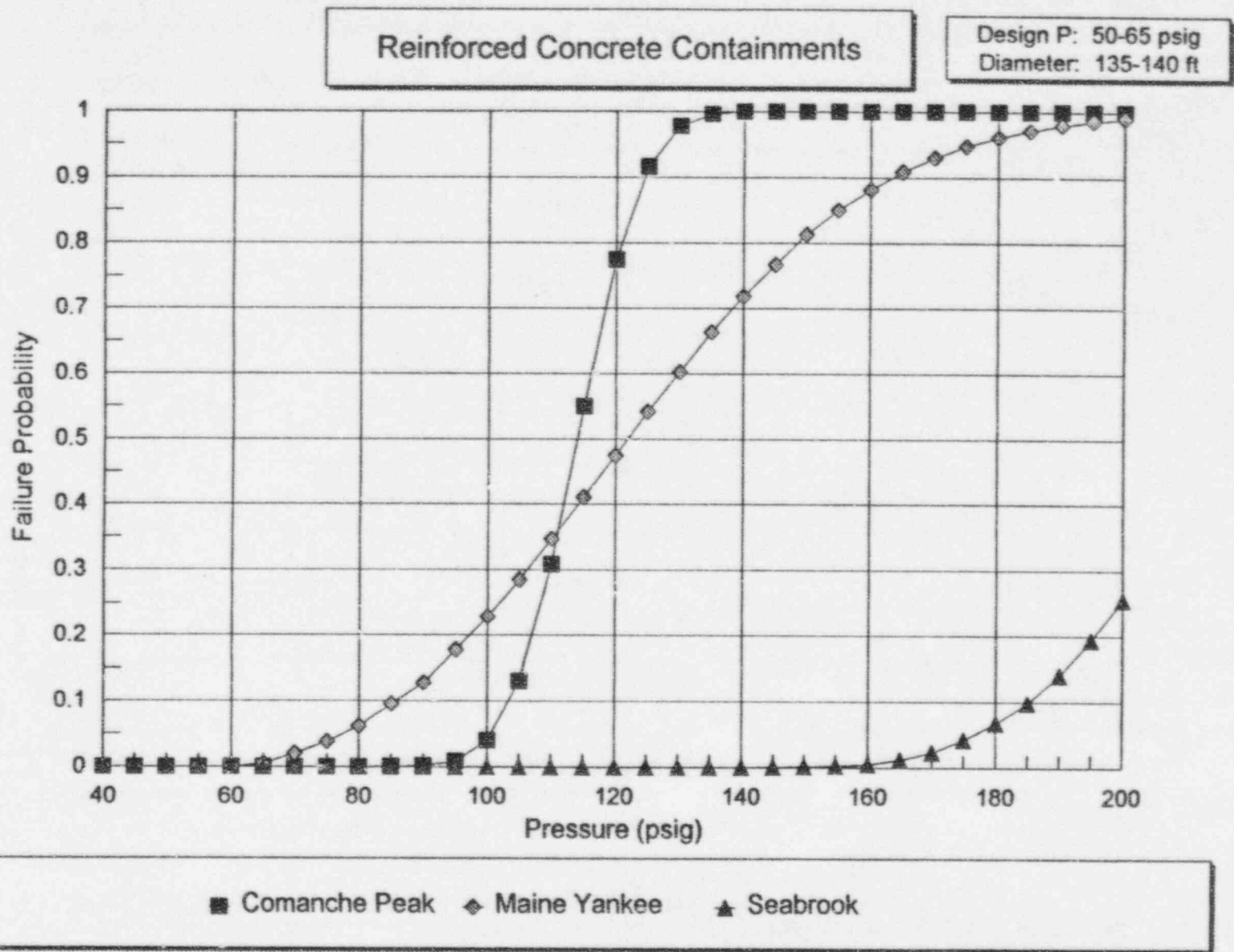
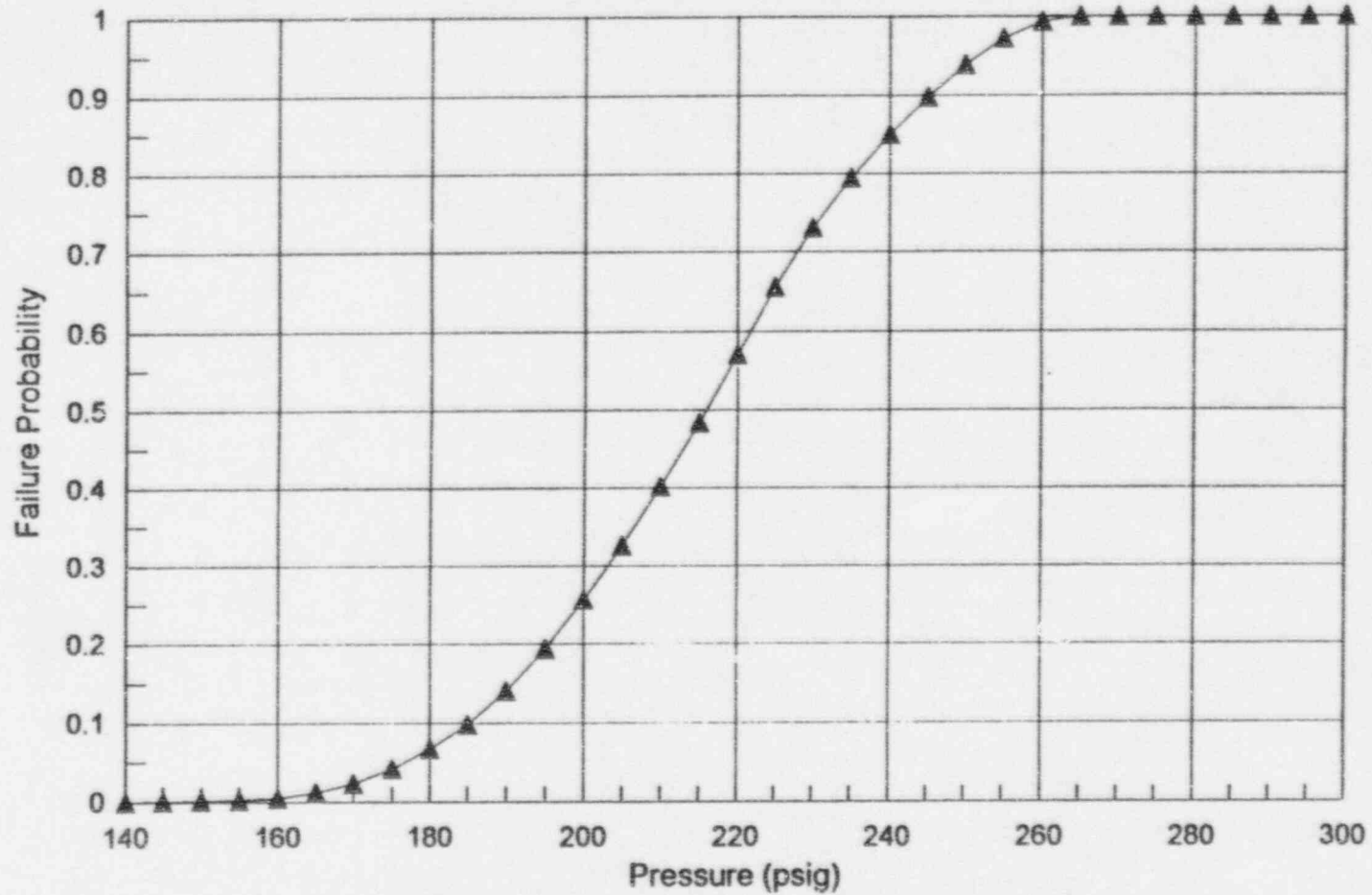


Figure D.4 Comparison of reinforced concrete containment fragility curves (higher pressure).

Reinforced Concrete Containments

Design P: 65 psig  
Diameter: 140 ft



▲ Seabrook

Figure D.5 Seabrook containment fragility curve.

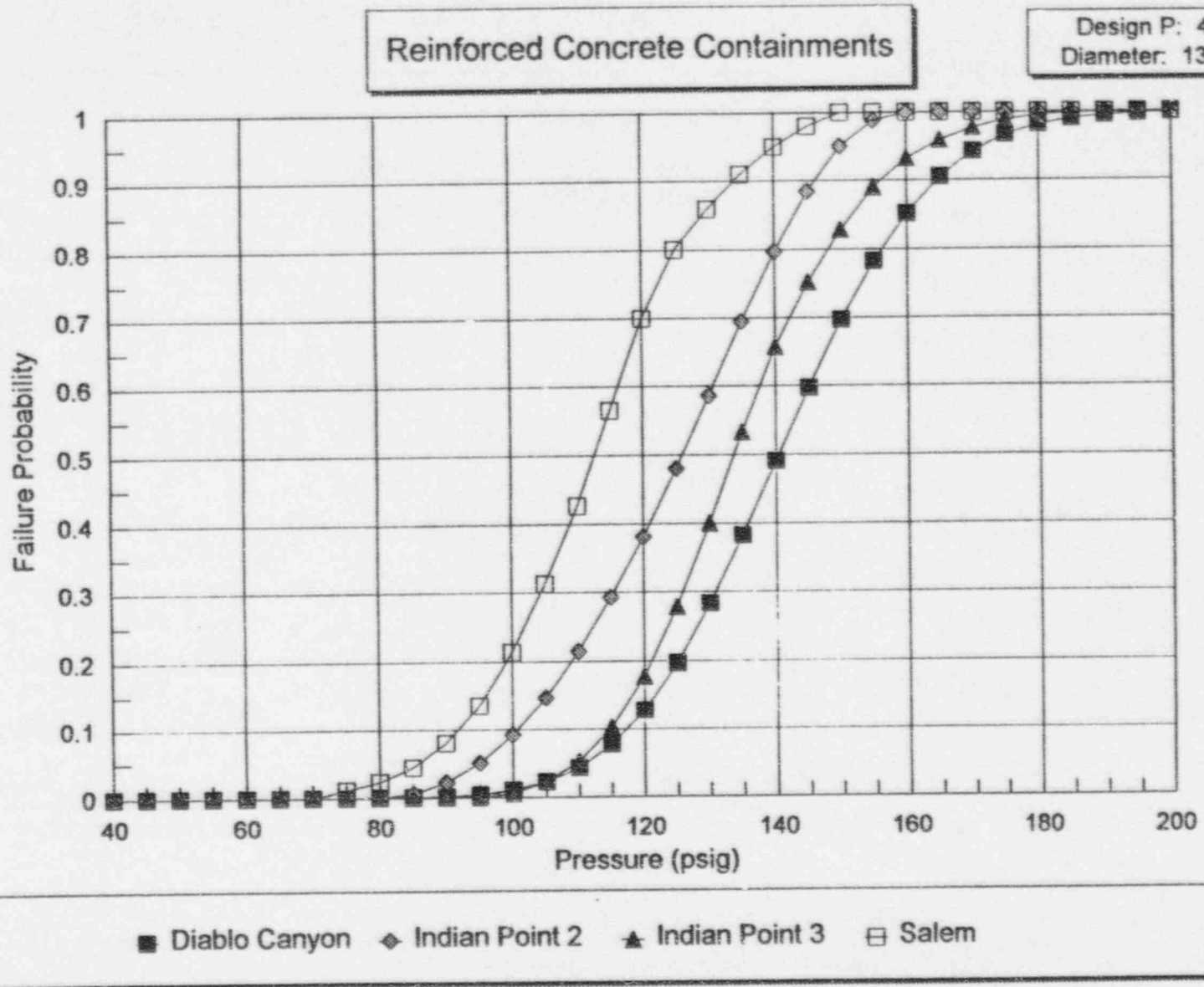


Figure D.6 Comparison of reinforced concrete containment fragility curves (medium pressure).

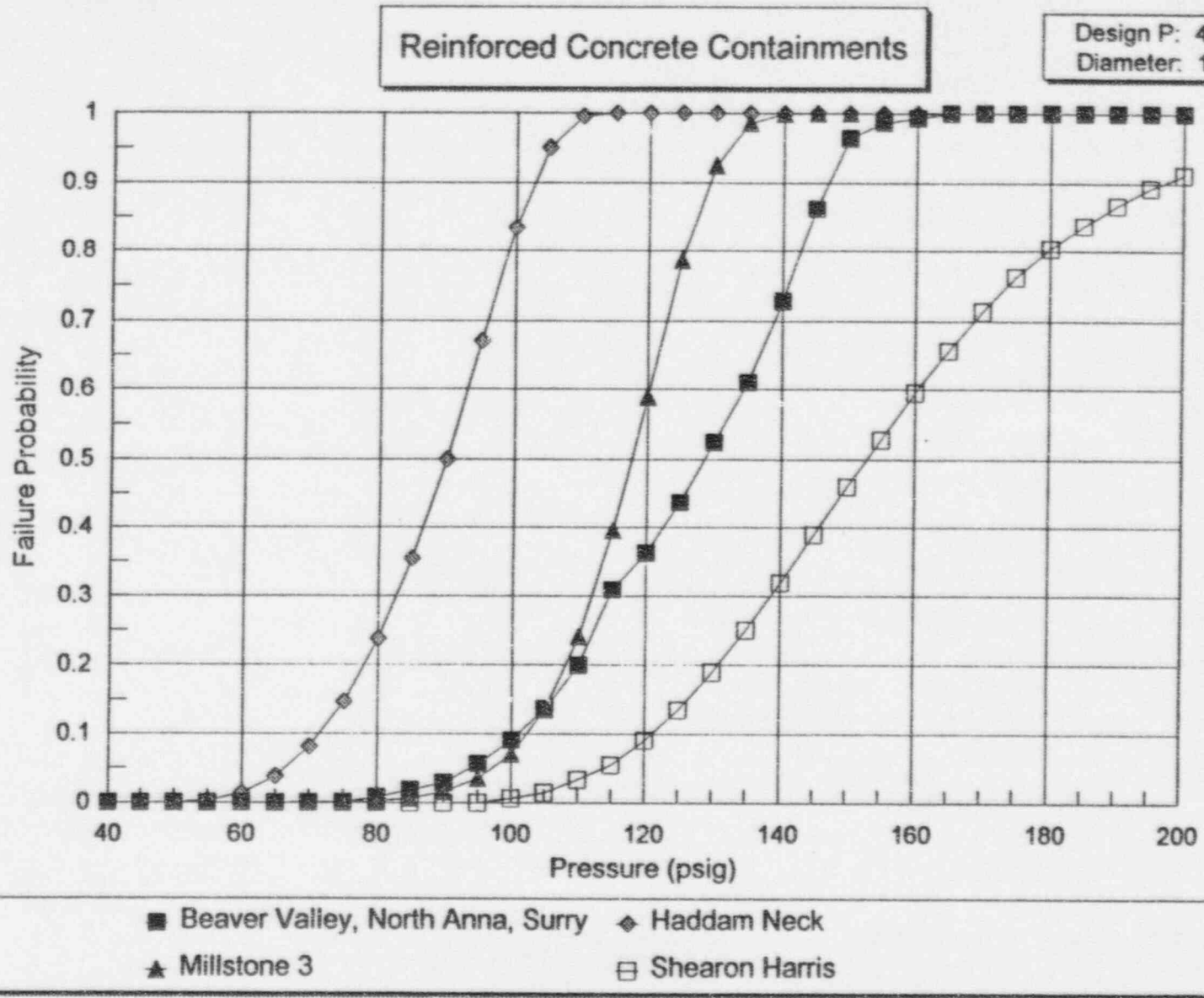


Figure D.7 Comparison of reinforced concrete containment fragility curves (lower pressure).



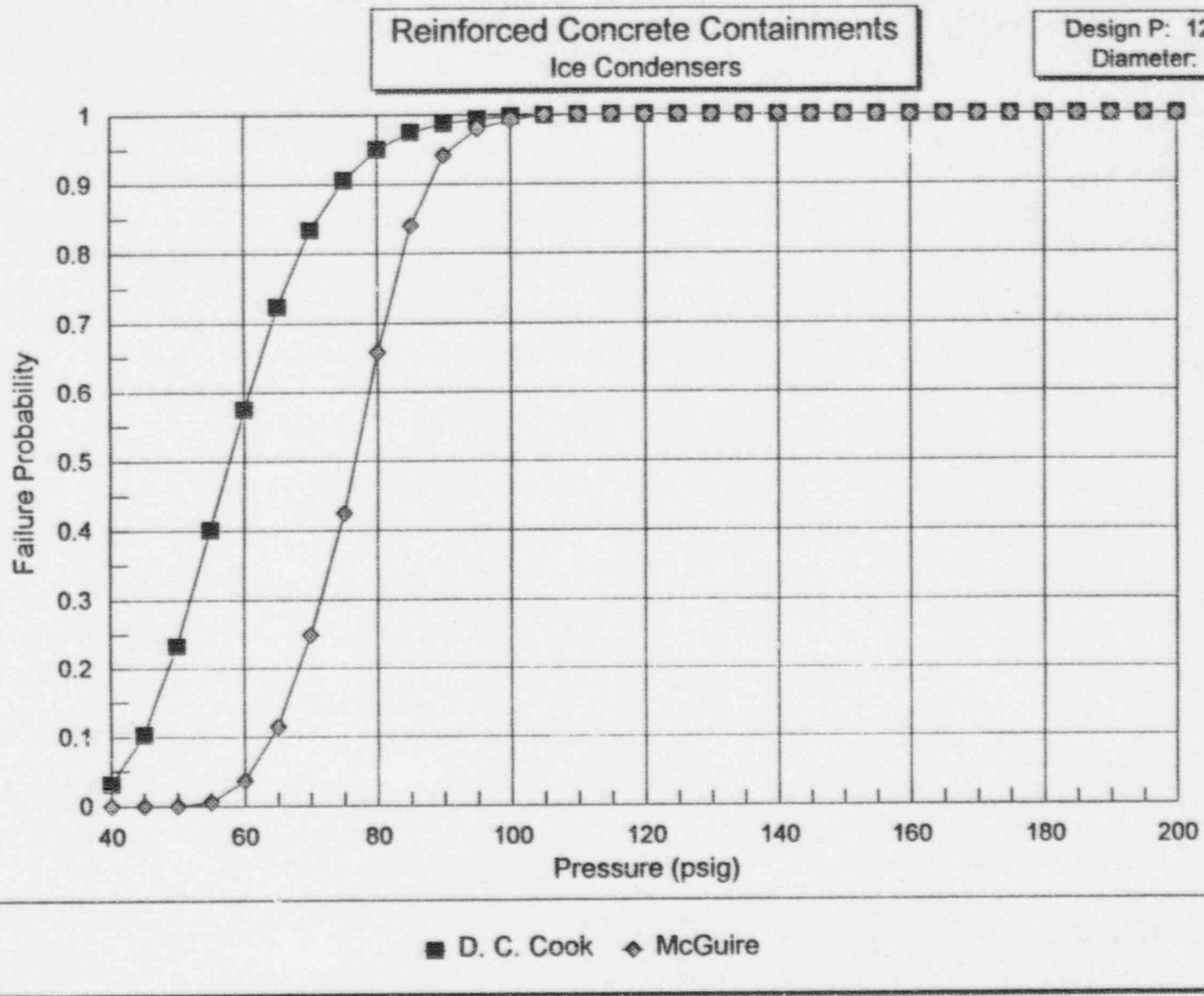
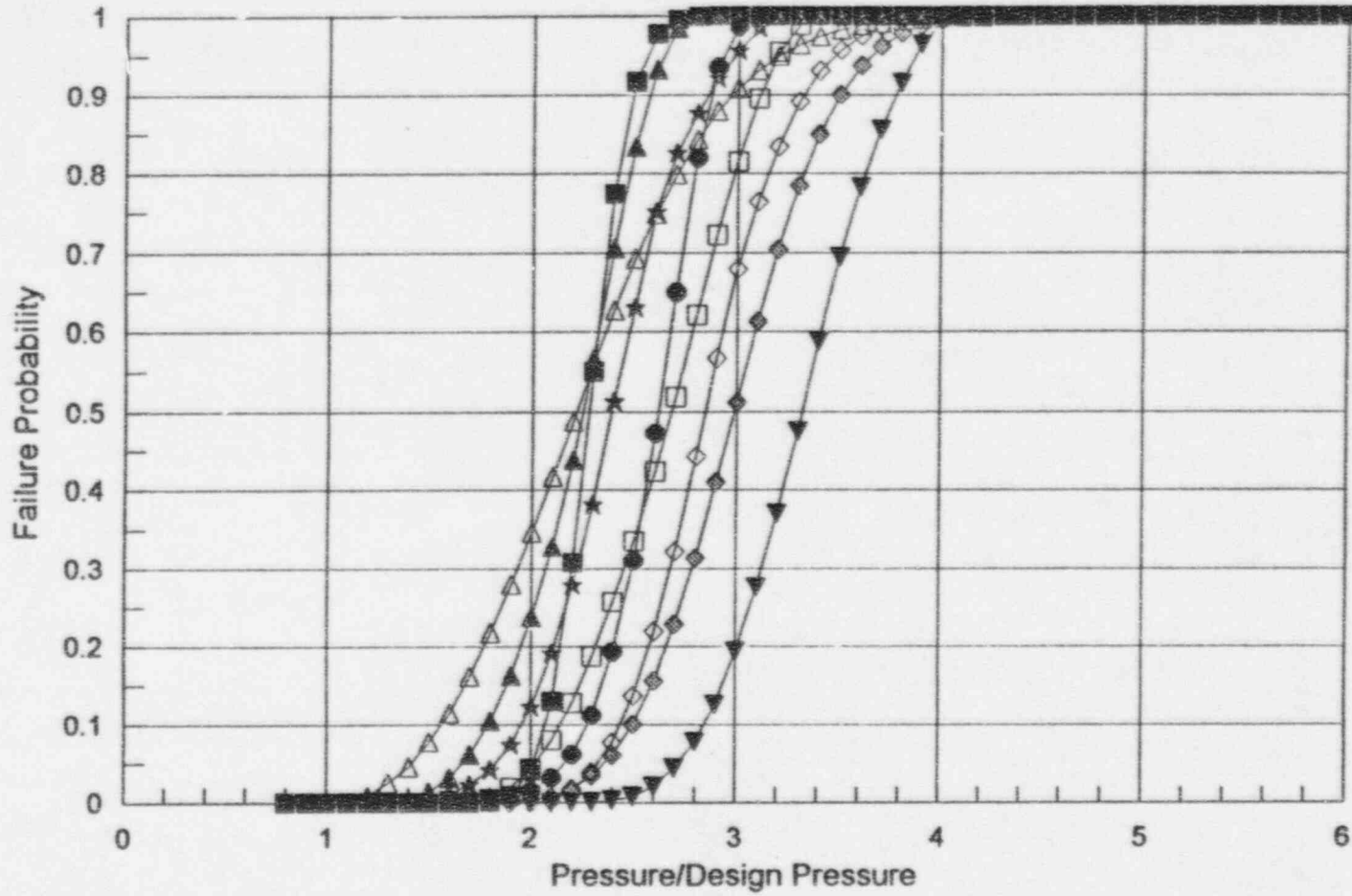


Figure D.8 Comparison of reinforced concrete containment fragility curves (Ice Condenser type).

Reinforced Concrete Containments

Diameter: 135-140 ft



- |                |                 |               |                |                |
|----------------|-----------------|---------------|----------------|----------------|
| ■ Comanche     | ◆ Diablo Canyon | ▲ Haddam Neck | □ Indian Pt. 2 | ◇ Indian Pt. 3 |
| △ Maine Yankee | ● Millstone 3   | ★ Salem       | ▼ Seabrook     |                |

Figure D.9 Comparison of normalized reinforced concrete containment fragility curves (larger).

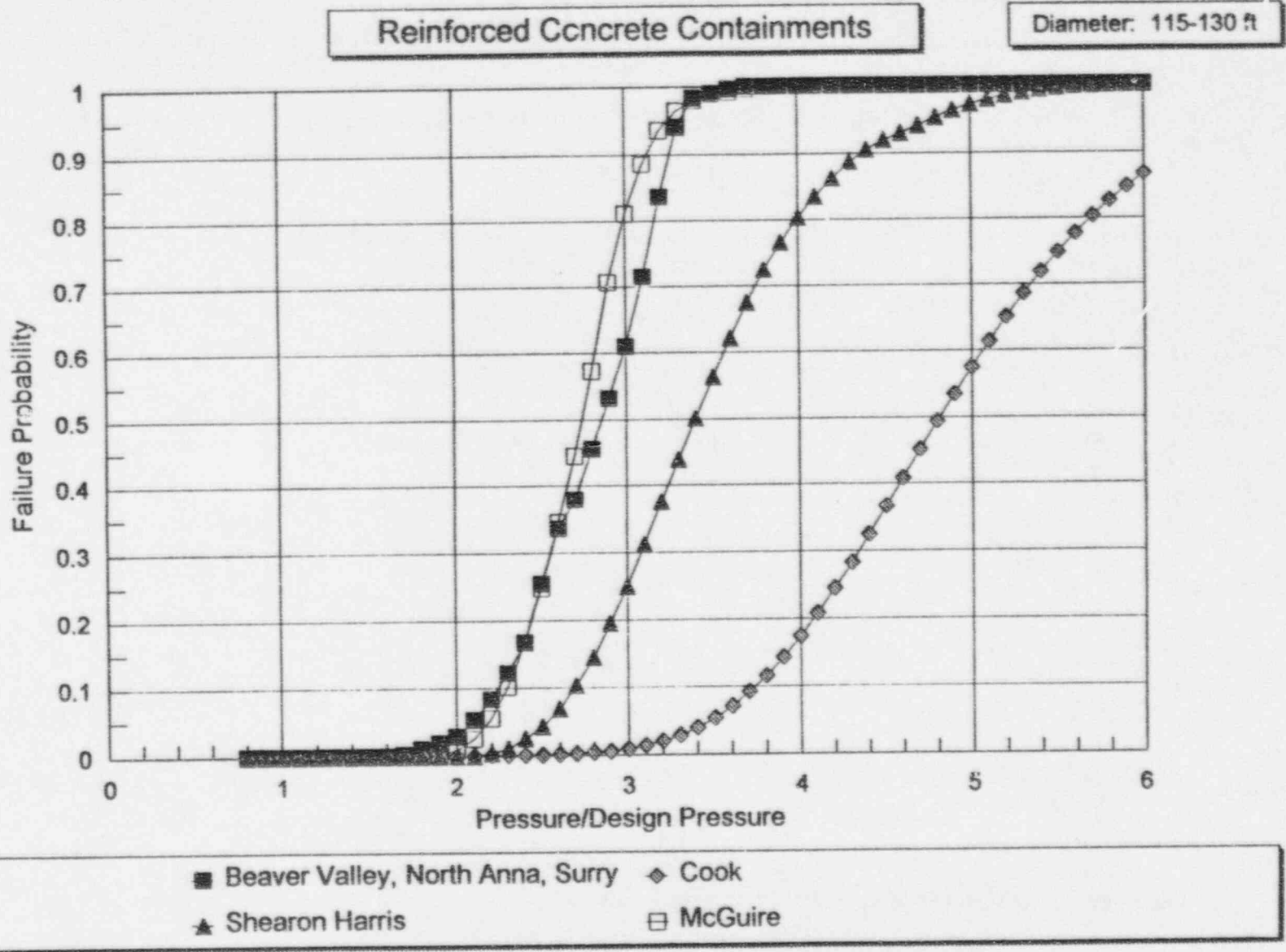


Figure D.10 Comparison of normalized reinforced concrete containment fragility curves (smaller).

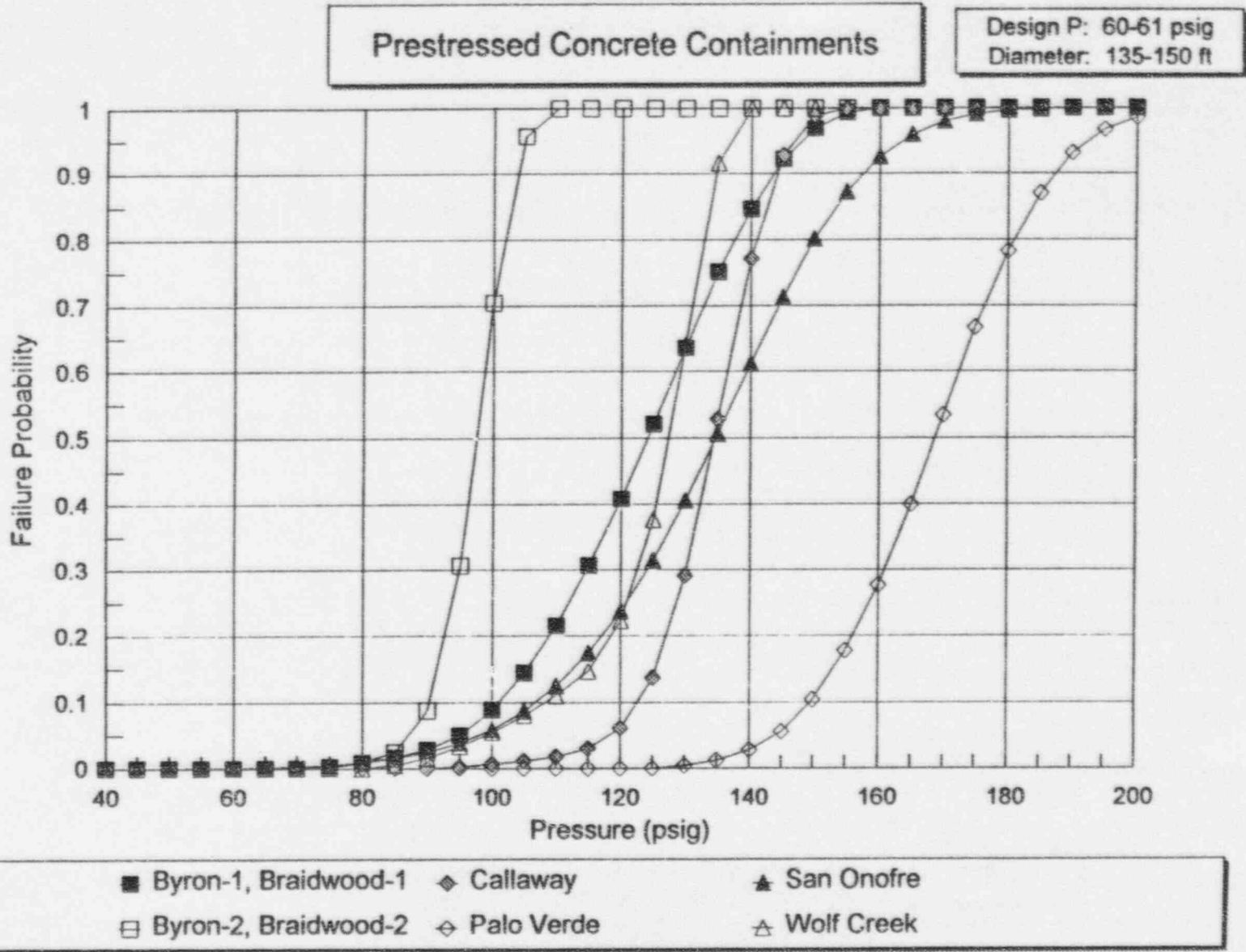


Figure D.11 Comparison of prestressed concrete containment fragility curves (higher pressure, larger).

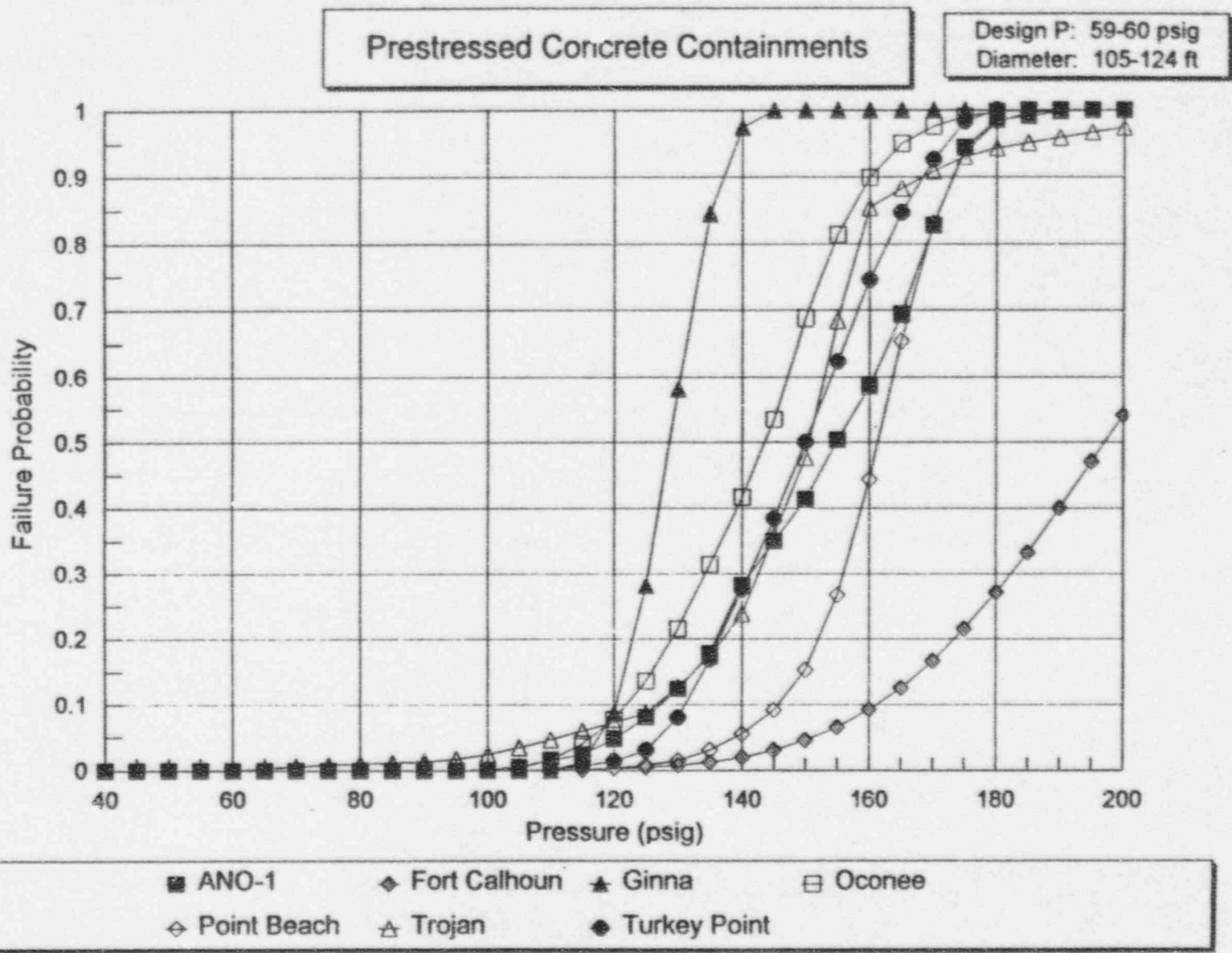
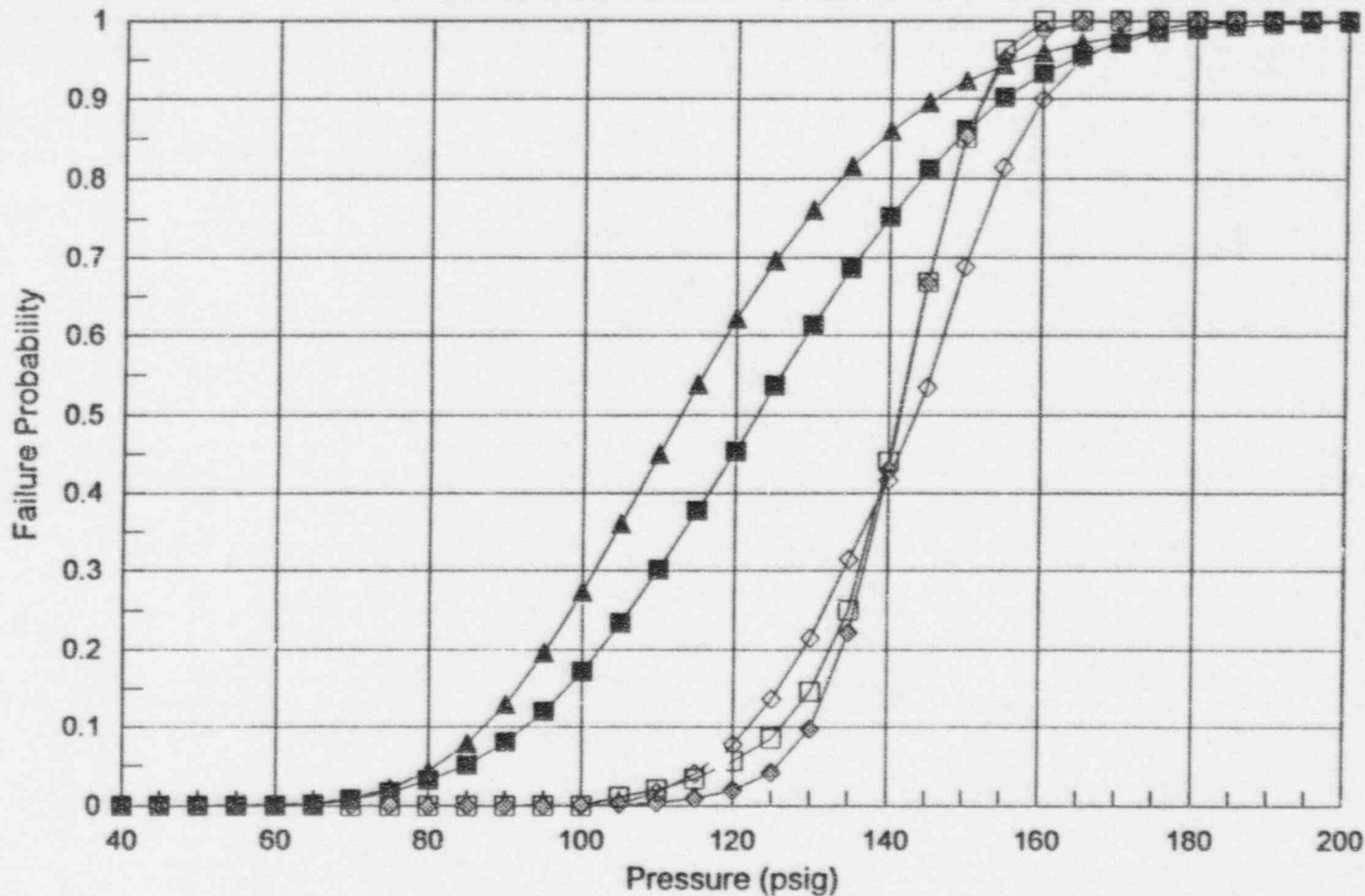


Figure D.12 Comparison of prestressed concrete containment fragility curves (higher pressure, smaller).



Prestressed Concrete Containments

Design P: 55-56 psig  
Diameter: 116-150 ft



■ Crystal River    ◆ Palisades    ▲ South Texas    □ Summer    ◇ TMI-1

Figure D.13 Comparison of prestressed concrete containment fragility curves (medium pressure).

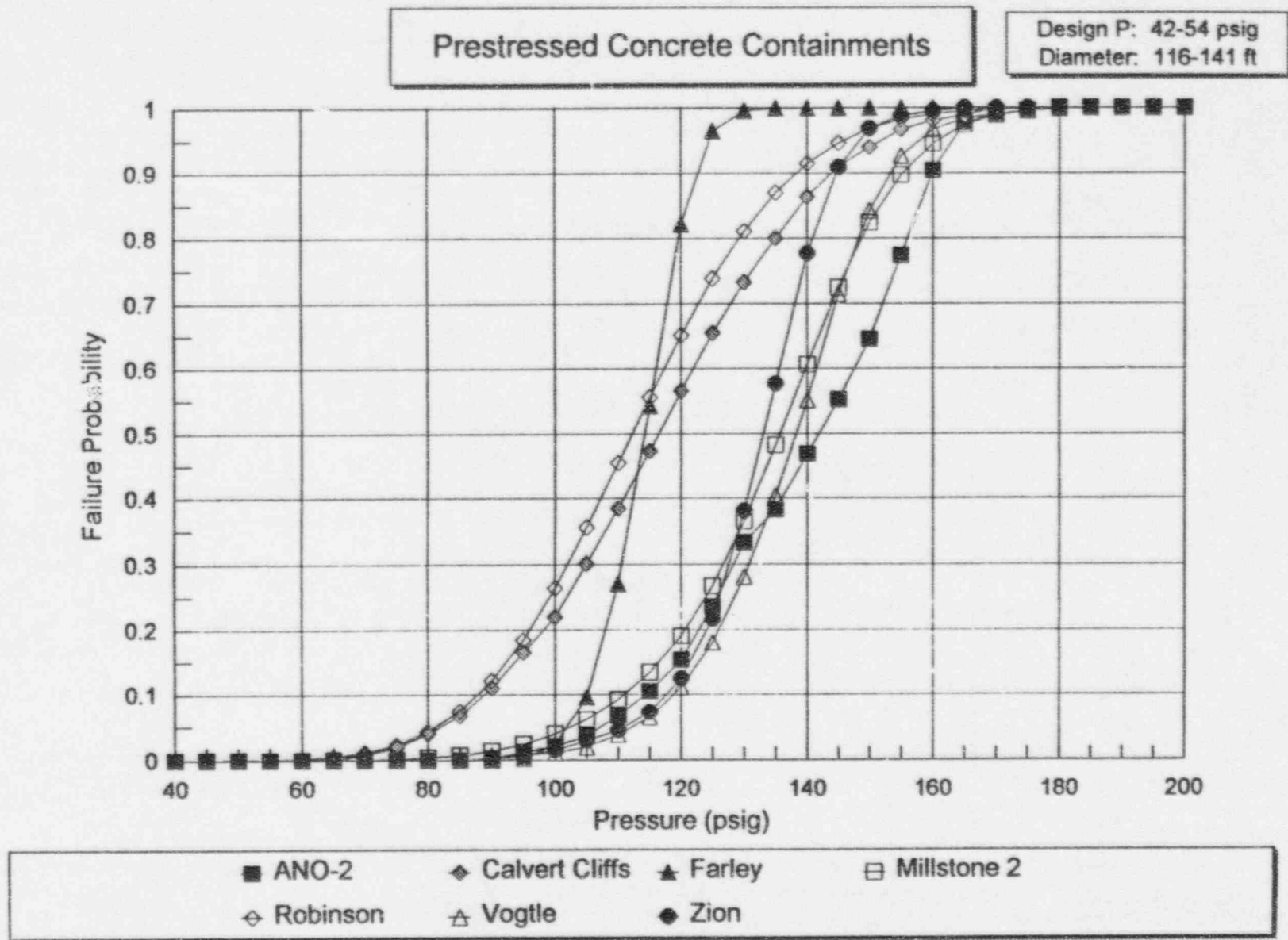
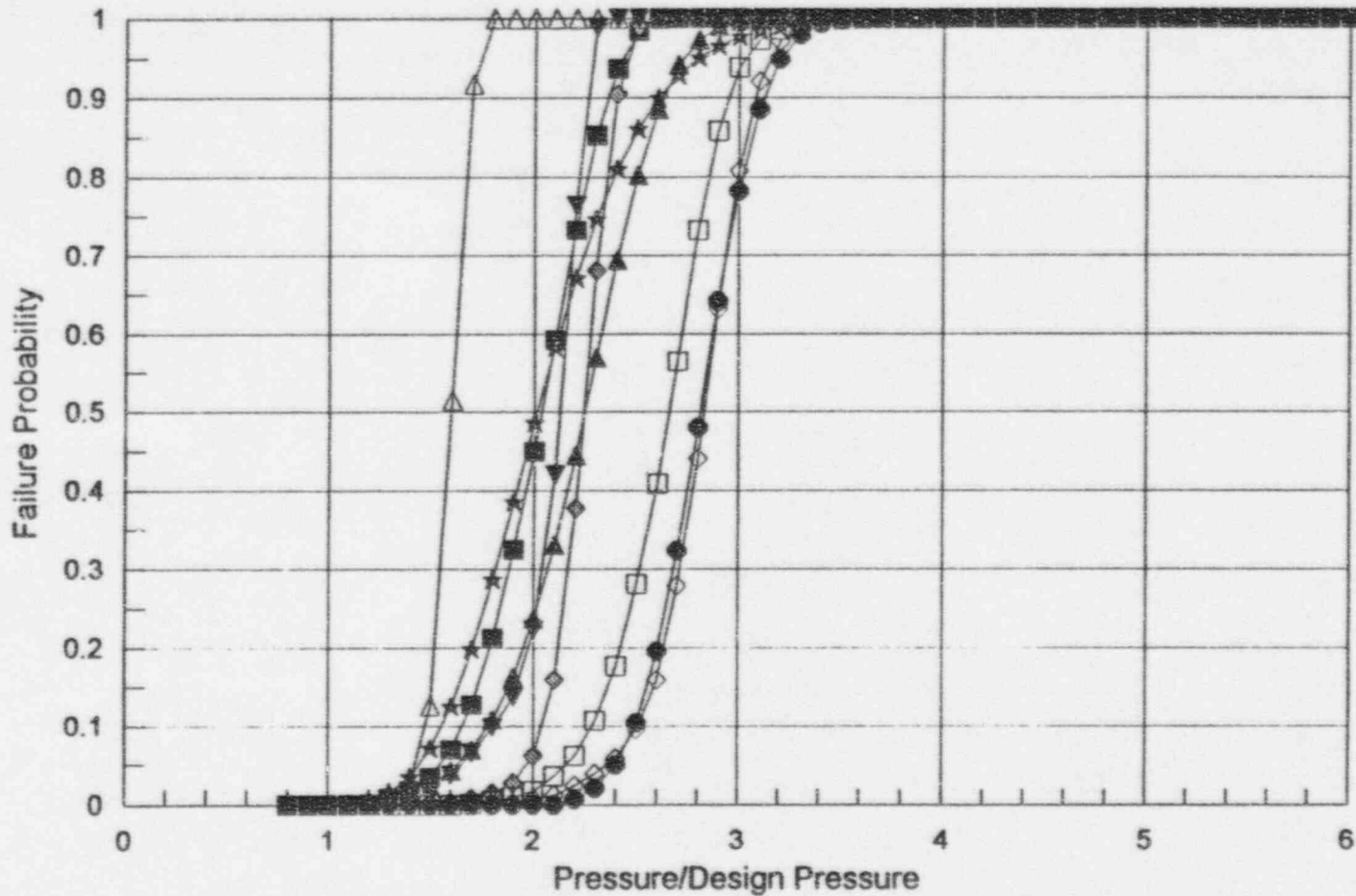


Figure D.14 Comparison of prestressed concrete containment fragility curves (lower pressure).

Prestressed Concrete Containments

Diameter: 135-150 ft



■ Byron, Braid.-1	◇ Callaway	▲ San Onofre	□ Vogtle	◊ Zion
△ Byron, Braid.-2	● Palo Verde	★ South Texas	▼ Wolf Creek	

Figure D.15 Comparison of normalized prestressed concrete containment fragility curves (larger).

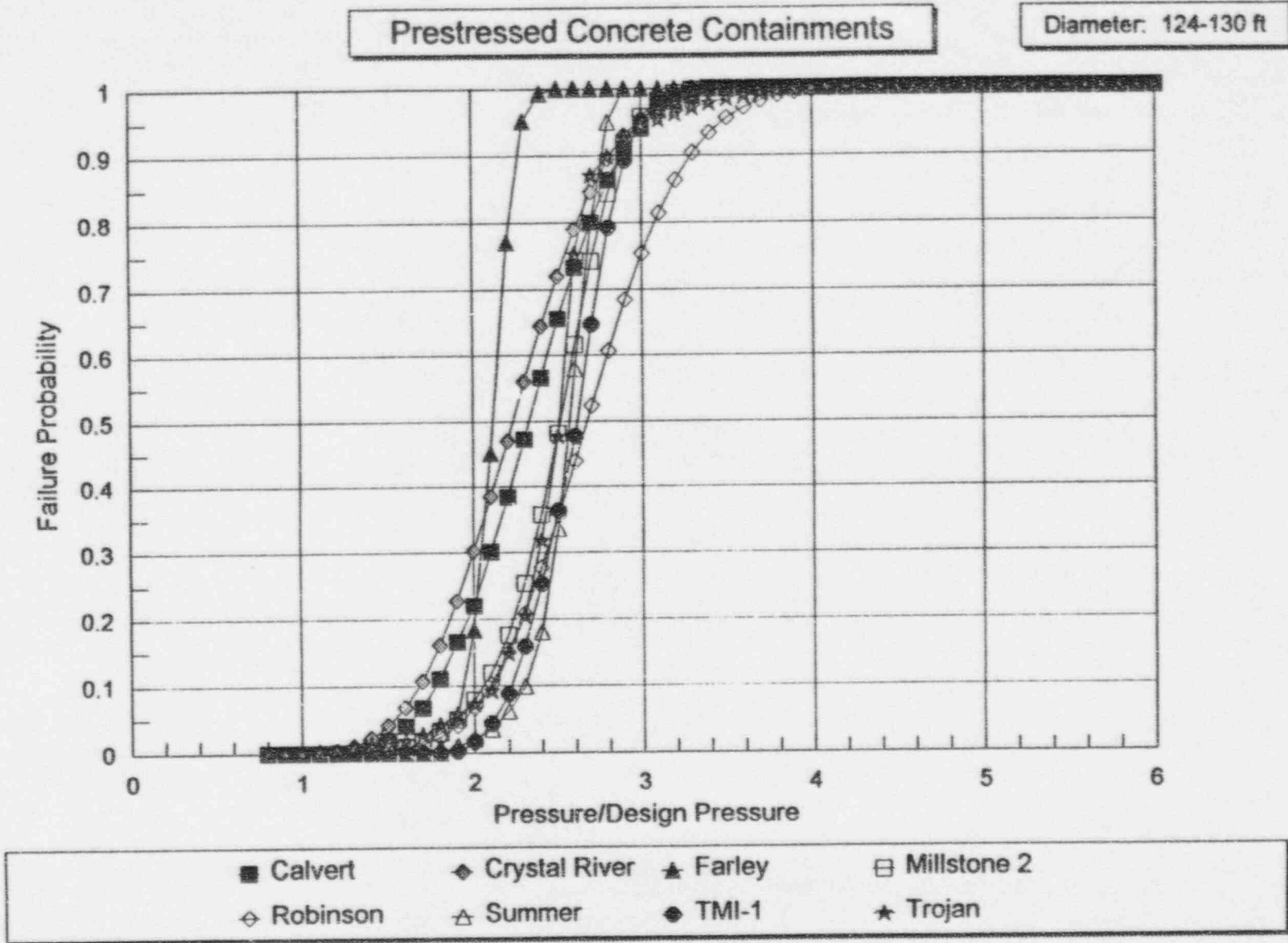


Figure D.16 Comparison of normalized prestressed concrete containment fragility curves (medium).

Prestressed Concrete Containments

Diameter: 105-116 ft

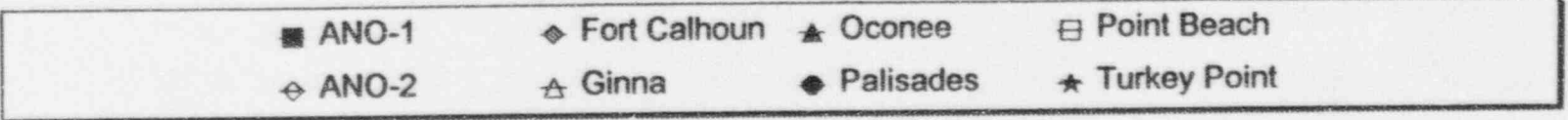
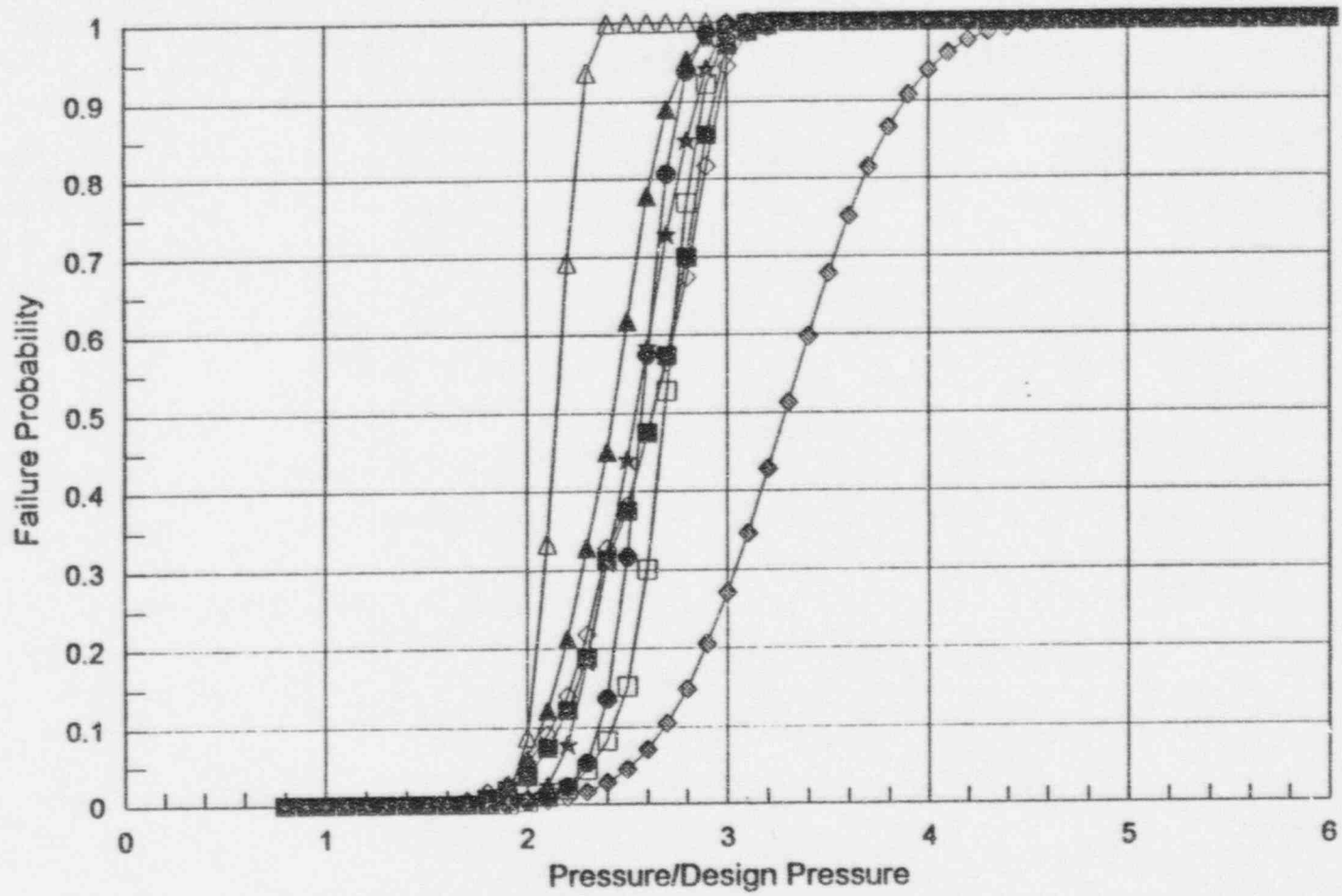


Figure D.17 Comparison of normalized prestressed concrete containment fragility curves (smaller).





**BIBLIOGRAPHIC DATA SHEET**

*(See instructions on the reverse)*

1. REPORT NUMBER  
(Assigned by NRC. Add Vol., Supp., Rev.,  
and Addendum Numbers, if any.)

NUREG/CR-6338  
SAND95-2381

2. TITLE AND SUBTITLE

Resolution of the Direct Containment Heating Issue for all  
Westinghouse Plants with Large Dry Containments or  
Subatmospheric Containments

3. DATE REPORT PUBLISHED

MONTH | YEAR

February | 1996

4. FIN OR GRANT NUMBER

J6027

5. AUTHOR(S)

M.M. Pilch, M.D. Allen, E.W. Klamerus

6. TYPE OF REPORT

Technical

7. PERIOD COVERED (Inclusive Dates)

8. PERFORMING ORGANIZATION - NAME AND ADDRESS (If NRC, provide Division, Office or Region, U.S. Nuclear Regulatory Commission, and mailing address; if contractor, provide name and mailing address.)

Sandia National Laboratories  
P.O. Box 5800  
Albuquerque, NM 87185-1137

9. SPONSORING ORGANIZATION - NAME AND ADDRESS (If NRC, type "Same as above"; if contractor, provide NRC Division, Office or Region, U.S. Nuclear Regulatory Commission, and mailing address.)

Division of Systems Technology  
Office of Nuclear Regulatory Research  
U.S. Nuclear Regulatory Commission  
Washington, DC 20555-0001

10. SUPPLEMENTARY NOTES

R.Y. Lee, NRC Project Manager

11. ABSTRACT (200 words or less)

This report uses the scenarios described in NUREG/CR-6075 and NUREG/CR-6075, Supplement 1, to address the direct containment heating (DCH) issue for all Westinghouse plants with large dry or subatmospheric containments. DCH is considered resolved if the conditional containment failure probability (CCFP) is less than 0.1. Loads versus strength evaluations of the CCFP were performed for each plant using plant-specific information. The DCH issue is considered resolved for a plant if a screening phase results in a CCFP less than 0.01, which is more stringent than the overall success criterion. If the screening phase CCFP for a plant is greater than 0.01, then refined containment loads evaluations must be performed and/or the probability of high pressure at vessel breach must be analyzed. These analyses could be used separately or could be integrated together to re-calculate the CCFP for an individual plant to reduce CCFP to meet the overall success criterion of less than 0.1. The CCFPs for all the Westinghouse plants with dry containments were less than 0.01 at the screening phase, and thus, the DCH issue is resolved for these plants based on containment loads alone. No additional analyses are required.

12. KEY WORDS/DESCRIPTORS (List words or phrases that will assist researchers in locating the report.)

direct containment heating  
high-pressure melt ejection  
risk  
Westinghouse Nuclear Power Plants

13. AVAILABILITY STATEMENT

Unlimited

14. SECURITY CLASSIFICATION

(This Page)

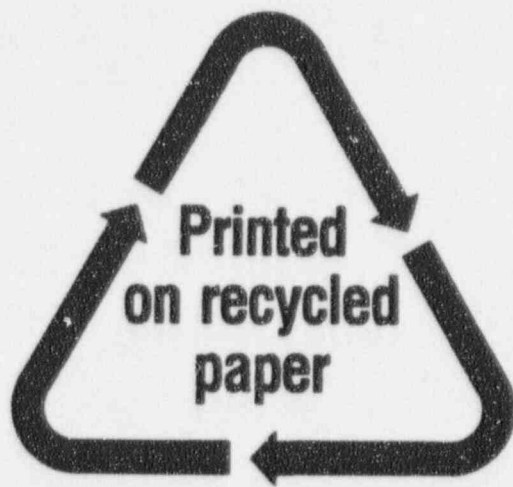
Unclassified

(This Report)

Unclassified

15. NUMBER OF PAGES

16. PRICE



Federal Recycling Program

UNITED STATES  
NUCLEAR REGULATORY COMMISSION  
WASHINGTON, DC 20555-0001

SPECIAL FOURTH-CLASS MAIL  
POSTAGE AND FEES PAID  
USNRC  
PERMIT NO. G-67

OFFICIAL BUSINESS  
PENALTY FOR PRIVATE USE, \$300

120555139531 1 1A1R3  
US NRC-OADM  
DIV FOIA & PUBLICATIONS SVCS  
TPS-PDR-NUREG  
2WFN-6E7  
WASHINGTON DC 20555